Progress in Energy and Combustion Science 90 (2022) 100995

Contents lists available at ScienceDirect

Progress in Energy and Combustion Science

journal homepage: www.elsevier.com/locate/pecs

Synthesis gas as a fuel for internal combustion engines in transportation

Amin Paykani [a,*], Hamed Chehrmonavari [a], Athanasios Tsolakis [b], Terry Alger [c], William F. Northrop [d], Rolf D. Reitz [e]

[a] School of Physics, Engineering and Computer Science, University of Hertfordshire, Hatfield, AL10 9AB, UK
[b] Department of Mechanical Engineering, School of Engineering, University of Birmingham, Birmingham B15 2TT, UK
[c] Automotive Propulsion Systems, Powertrain Engineering Division, Southwest Research Institute, TX, USA
[d] Department of Mechanical Engineering, University of Minnesota, 111 Church St. SE Minneapolis, MN, 55419, USA
[e] Engine Research Center, University of Wisconsin-Madison, 1500 Engineering Drive, Madison, WI 53705, USA

ARTICLE INFO

Keywords:
IC engine
Syngas
Fuel reforming
Combustion
Efficiency
Emissions

ABSTRACT

The adverse environmental impact of fossil fuel combustion in engines has motivated research towards using alternative low-carbon fuels. In recent years, there has been an increased interest in studying the combustion of fuel mixtures consisting mainly of hydrogen and carbon monoxide, referred to as syngas, which can be considered as a promising fuel toward cleaner combustion technologies for power generation. This paper provides an extensive review of syngas production and application in internal combustion (IC) engines as the primary or secondary fuel. First, a brief overview of syngas as a fuel is presented, introducing the various methods for its production, focusing on its historical use and summarizing the merits and drawbacks of using syngas as a fuel. Then its physicochemical properties relevant to IC engines are reviewed, highlighting studies on the fundamental combustion characteristics, such as ignition delay time and laminar and turbulent flame speeds. The main body of the paper is devoted to reviewing the effect of syngas utilization on performance and emissions characteristics of spark ignition (SI), compression ignition (CI), homogeneous charge compression ignition (HCCI), and advanced dual-fuel engines such as reactivity-controlled compression ignition (RCCI) engines. Finally, various on-board fuel reforming techniques for syngas production and use in vehicles are reviewed as a potential route towards further increases in efficiency and decreases in emissions of IC engines. These are then related to the research reported on the behavior of syngas and its blends in IC engines. It was found that the selection of the syngas production method, choice of the base fuel for reforming, its physicochemical properties, combustion strategy, and engine combustion system and operating conditions play critical roles in dictating the potential advantages of syngas use in IC engines. The discussion of the present review paper provides valuable insights for future research on syngas as a possible fuel for IC engines for transport.

1. Introduction

Worldwide, approximately 80% of useful energy, including high-quality heat, propulsion work, and electricity, is produced by combustion-driven processes using fossil fuels. The main detriments of the application of fossil fuels in IC engines are their contribution to global warming and environmental pollution, and therefore governments are encouraging the use of zero/low-carbon fuels in power and propulsion systems for achieving energy security and meeting emissions targets [1,2]. In the coming decades, both IC engine efficiency and fuel technology must improve and contribute to achieving carbon-neutral transportation [3]. Engine technology must also use fuels that minimize greenhouse gas (GHG) emissions on a well-to-wheel basis to meet worldwide emissions legislation [4]. The next generation of cleaner fuels is governed by several important factors, including the availability of the feedstock, production efficiency and environmental impact, distribution and storage, safety issues, integration and compatibility with engines, vehicle, and transportation systems – costs, regional variations, standardization and public acceptance [5,6]. In this regard, natural gas [7,8], hydrogen [9] and ammonia [10,11] and optimized engines [12] have recently drawn much attention from engine researchers to meet the future emission standards.

Hydrogen (H_2) has been considered as a viable energy carrier for fuel cells and future IC engines. The wide flammability range of hydrogen makes it suitable for engine operation over a wide range of air-fuel

* Corresponding author:
E-mail address: a.paykani@herts.ac.uk (A. Paykani).

https://doi.org/10.1016/j.pecs.2022.100995
Received 30 June 2020; Received in revised form 3 February 2022; Accepted 6 February 2022
Available online 18 February 2022

Nomenclature

Greek

λ	Air–fuel equivalence ratio
ϕ	Fuel–air equivalence ratio
γ	Ratio of specific heats
θ	Crankshaft angle
η	Efficiency

Abbreviations

AFR	Air fuel ratio
AHRR	Apparent heat release rate
AKI	Anti-knock index
ATDC	After top dead center
ATR	Autothermal reforming
BMEP	Brake mean effective pressure
BSFC	Brake specific fuel consumption
BTDC	Before top dead center
BTE	Brake thermal efficiency
CA	Crank angle
CDC	Conventional diesel combustion
CFD	Computational fluid dynamics
CFR	Cooperative fuel research
CHP	Combined heat and power
CI	Compression ignition
CN	Cetane number
CNG	Compressed natural gas
CO	Carbon monoxide
COV	Coefficient of variation
CR	Compression ratio
CRI	Common rail injector
D-EGR	Dedicated exhaust gas recirculation
DFBG	Dual fluidized bed gasifier
DF	Dual fuel
DI	Direct-injection
DISI	Direct injection spark ignition
DME	Dimethyl ether
DNS	Direct numerical simulation
EGR	Exhaust gas recirculation
EPA	Environmental protection agency
ERC	Engine research center
FTP	Federal test procedure
FT	Fischer–Tropsch
GA	Genetic algorithm
GDI	Gasoline direct injector
GHG	Greenhouse gas emissions
GIE	Gross indicated efficiency
GT	Gas turbine
GTL	Gas-to-liquid
HCCI	Homogenous charge compression ignition
HD	Heavy-duty
HE	Hydrous ethanol
HOME	Honge oil and its methyl ester
HRR	Heat release rate
HTHR	High-temperature heat release
HWFET	Highway Fuel Economy Test
ICE	Internal combustion engine
IDT	Ignition delay time
IGCC	Integrated gasification combined cycle
IMEP	Indicated mean effective pressure
ITE	Indicated thermal efficiency
LFS	Laminar flame speed
LD	Light duty
LFG	Landfill gas
LHV	Lower heating value
LPG	Liquefied petroleum gas
MAP	Manifold absolute pressure
MBT	Maximum brake torque
MES	Methane enriched syngas
MFB	Mass fraction burned
ML	Machine learning
MN	Methane number
NIMEP	Net indicated mean effective pressure
NOx	Nitrogen oxides
NTC	Negative temperature coefficient
NVO	Negative valve overlap
PG	Producer gas
POX	Partial oxidation
PPM	Parts per million
PRF	Primary reference fuel
PRIEMER	Premixed mixture ignition in the end-gas region
RCCI	Reactivity controlled compression ignition
R-EGR	Reformed exhaust gas recirculation
RG	Reformer gas
RMG	Reformed methanol gas
RON	Research octane number
SAC	Superadiabatic combustion
SAE	Society of Automotive Engineers
SEC	Specific energy consumption
SI	Spark ignition
SMR	Steam methane reforming
SOC	Start of combustion
Syngas	Synthesis gas
SZM	Single zone model
SwRI	Southwest Research Institute
TCR	Thermochemical recuperation
TFR	Thermochemical fuel reforming
TFS	Turbulent flame speed
THC	Total hydrocarbons
TIDR	Total inert dilution ratio
TWC	Three-way catalyst
UHC	Unburned hydrocarbons
WGS	Water–gas shift
WHR	Waste heat recovery
WOT	Wide-open throttle

mixtures, and the lean mixture operation can increase the fuel economy of the hydrogen-fueled engines. Moreover, its high diffusivity and flame speed result in a faster uniform fuel/air mixture and an improved combustion inside the cylinder [13,14]. The carbon-free structure of the hydrogen also makes it an excellent fuel for the clean and efficient operation of IC engines. Fig. 1 shows the energy density of various fuels based on lower heating values (LHV) compared to hydrogen. As can be seen, hydrogen has nearly three times the energy content of gasoline on a mass basis.

In contrast, hydrogen's high auto-ignition temperature (858 K) necessitates the use of a spark plug or a supplementary low auto-ignition temperature fuel. On the other hand, its low ignition energy increases the propensity of phenomena like pre-ignition, backfire and knock. NOx emissions can also be increased due to the higher combustion temperatures associated with hydrogen combustion in IC engines [15].

Hydrogen can be produced in various ways to be stored in a pressurized tank on-board in a vehicle aiming at improving both combustion and aftertreatment processes [17]. The comparison of hydrogen usage in

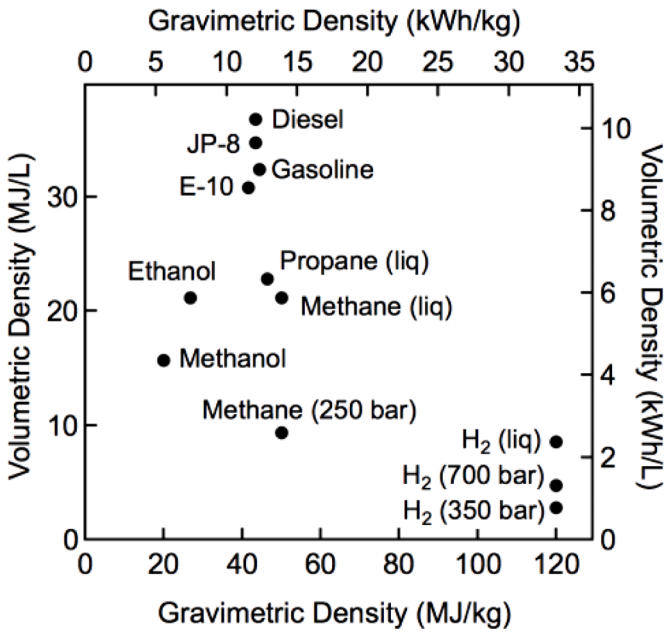

Fig. 1. Gravimetric and volumetric density of hydrogen and other fuels [16].

vehicles through on-board hydrogen production, hydrogen storage, and stationary power generation systems is summarized in Table 1. The low ignition energy and volumetric energy density make storage of hydrogen on-board a challenging task [18,19]. Hydrogen as a low-density fuel needs to be compressed at high-pressure tanks (350–700 bar) to allow an adequate driving range of more than 500 km with safety and cost to be the main challenging issues. Difficulties involved in the storage and transport of hydrogen still present barriers to the commercial use of hydrogen as a secondary or a main fuel for IC engines [19,20]. However, hydrogen is currently viewed as the most promising clean energy carrier of the future, and the hydrogen infrastructure is now rapidly expanding in many counties, both in the EU and outside. This has sparked research interest in the energy conversion technologies, particularly fuel cells that are capable of using hydrogen as the fuel [21].

While the merits of operating IC engines with varying concentrations of hydrogen have been well documented [25], the key challenges remain unresolved, including practical approaches to hydrogen production without sacrificing system efficiency and/or sufficiently addressing its adverse combustion properties [26]. Syngas is considered an intermediate step in the transition from carbon-based fuels to H_2-based fuels, since it is composed mainly of hydrogen (H_2) and carbon monoxide (CO). In IC engines, using syngas produced from on-board stored liquid fuels on vehicles can mitigate many of the hydrogen storage and combustion challenges [27–31], and this will be extensively discussed in the upcoming sections.

Table 1
Comparison of hydrogen usage in vehicles through on-board hydrogen production, hydrogen storage, and stationary power generation systems [22–24].

Transportation (on-board in vehicles)	Transportation (storage in vehicles)	Stationary power generation
• Ability to operate on H_2 partly • More complicated design • Less space required • Few safety concerns • Challenge with the catalyst activation under a wide range of temperature and reactants changes • Moderate cost • Fast response during transient operation is a challenge • Aesthetic issues	• Ability to operate on 100% H_2 • Simple design • More space required • Serious safety concerns • Challenge with hydrogen production, store and distribution • Highest cost • Fast response during transient operation	• Ability to operate on 100% H_2 • Simple design • No space problem • No safety problem • Hydrogen can be produced or can be used from the storage system • Lowest cost • Aesthetic issues are not important

1.1. What is syngas?

Syngas (an abbreviation for synthesis gas) can be derived by gasification processes from natural gas, heavy oil, biomass, and coal (carbon-containing fuels) for stationary application or by chemical processes from liquid and gaseous fuels for vehicular application, in which a complex and long-chain molecule converts to simpler molecules including H_2 (hydrogen), CO (carbon monoxide), and CH_4 (methane), CO_2 (carbon dioxide), H_2O (water vapor), and N_2 (nitrogen). Based on the process adopted and the type of feedstock used, end-products as a form of syngas will have varying compositions and heating values, thus different terms such as "*town gas*", "*wood gas*", "*water gas*", "*producer gas*", "*reformer gas*", "*power gas*", and etc. have been used in the literature. A possible range for the volumetric composition of syngas is shown in Table 2, indicating that it is comprised mainly of H_2 and CO. The preferred composition generally depends upon the purpose of syngas usage, feedstock, and production cost. For example, if the goal is hydrogen production by a biomass gasification process, much more cost and effort are needed for adequate purification than the reaction reforming process.

Syngas can also be produced through fuel reforming with steam and/or air using compact systems that can be located on-board a vehicle [27,33,34]. External on-board and in-cylinder fuel reforming techniques have been identified as possible pathways to produce syngas on-board in IC engines to improve efficiency and emissions [33]. The details of on-board fuel reforming and syngas production will be covered in section 4.

1.2. Syngas applications

Syngas can be used as an intermediate to create other attractive clean fuels such as ammonia (NH_3), dimethyl ether (DME), and methanol (CH_3OH) [35–39]. Another use of syngas is as a primary chemical building block in petrochemical and refining processes [40]. Syngas can be used in many different applications, including:

- Power generation in existing coal power plants [22]
- Combined heat and power (CHP) plants [41]
- Integrated gasification combined cycles (IGCC) [42]
- Fuel cells [43–46]
- Production of transportation fuels from gas-to-liquid (GTL) processes [47]
- Gas turbines [48–50]
- Directly as the primary or secondary fuel in IC engines [51]

Table 2
A possible range for syngas composition on a volume percent basis [29,32].

Species	Min	Max
H_2	8.6	61.9
CO	22.3	55.4
CH_4	0.0	8.2
CO_2	1.6	30.0
N_2+Ar	0.2	49.3
H_2O	-	39.8
H_2/CO	0.33	2.36*
LHV (MJ/m^3)	5.02	12.57

* The broad experimental studies of syngas-fed IC engines reviewed in sections 3 and 4 have been performed with simulated syngas whose H_2/CO ratio can go beyond this value, i.e., H_2/CO: 3/1 (by vol.).

1.3. Syngas production methods

Solid fuel (coal, biomass, wastes) feedstocks are sources for syngas production [52,53] by traditional gasification methods [54,55]. Also, liquid and gaseous feedstocks can be converted to syngas by non-gasification methods [56] that comprise one or a chain of reforming processes using the catalysts; such processes are expected to be viable in-situ methods of syngas production for automotive engines. In this section, only a brief review of different syngas production methods is presented since several comprehensive review papers [57,58] explain them in detail and emphasize the IC engine operation with gasification fuel [59,60] and non-gasification fuel [33].

1.3.1. Gasification processes

Biomass gasification converts a solid fuel into syngas which can be burnt in stationary gas turbines and IC engines. Gasification is a thermochemical process that converts a solid hydrocarbon feedstock like coal, petroleum coke, refinery residuals, biomass, and municipal solid waste, into syngas without consuming a large part of its heating value [58]. In gasification, the carbon-containing feedstock reacts with a gasifying agent like oxygen, steam, and air, which breaks down the mixture into syngas, as illustrated in Fig. 2 [54,57,61,62]. The type and design of the gasifier, gasification temperature, type and flow rates of the feedstock and oxidizing agents, and type and amount of catalysts [63], are the main parameters in influencing the gasification process and syngas production [64–70]. Oxygen as the gasifying agent produces syngas called "*medium syngas*," and if air is used, then it is called "*producer gas*" [71]; the following sub-section will clarify the terms used in the rest of the paper. Using gasification methods, in addition to H_2 and CO, other typical products including H_2O, CO, CH_4, unwanted tars, small amounts of NH_3, and H_2S are also produced. The relative amount of each species depends on the feedstock and the gasification process [57]. Modeling approaches for biomass gasification have been extensively reviewed in [72].

For syngas production, a typical solid fuel gasification system coupled to spark ignition and dual-fuel diesel engines is illustrated in Fig. 3 [73]. The system includes a gasifier, a gas clean-up and cooling system, a gas mixer, a starting blower, and the engine. The engine draws air from the gasifier during the intake stroke, through the cleaning system, and from the gas mixer where air is combined with the syngas [74]. For example, Marculescu et al. [80] used food processing industry waste for energy conversion, using gasification and an IC engine for power generation. The biomass used consisted of bones and meat residues sampled directly from the industrial line, characterized by high water content, about 42% in mass, and potential health risks. They reported that syngas with a composition of 19.1%CO, 17%H_2, and 1.6% CH_4 was produced.

New gasification concepts such as dual fluidized bed gasifiers (DFBG) [76], plasma gasification [77–80], and supercritical water gasification [81,82], have demonstrated the potential to improve syngas quality from biomass gasification. However, they are not of significant interest at present, and are more applicable for stationary power generation. Moreover, wood and solid fuels seem to be not effective for transport applications due to their low energy density. A further analysis on this topic is presented in section 3.

1.3.2. Non-gasification processes

Non-gasification processes include catalytic fuel reforming, where the parent fuel reacts with steam and/or oxygen in a heterogeneous process to produce syngas [27,83]; and non-catalytic processes like plasma-assisted reforming [84]. The three main global reactions in fuel reforming are partial oxidation (POX), steam reforming (SR), and auto-thermal reforming (ATR) [47,85], which will be explained in the following.

When a mixture of sub-stoichiometric oxygen and feedstock reacts to produce syngas, this self-sustaining chemical reaction is called "*partial oxidation (POX)*," It is an exothermic reaction. The complete combustion reaction forming CO_2 is restricted due to insufficient O_2 in the reactants [86,87]. In endothermic steam reforming (SR), a high-temperature mixture of fuel and steam is sent through a bed of catalyst. The heat required to drive the endothermic reaction is provided externally (e.g., electric heaters or combustion of fuel). The syngas stream from the steam reforming can then flow to a water gas shift (WGS) reactor, where additional steam converts CO to CO_2 and generates additional H_2 [88–91].

When both the POX and SR reforming reactions are combined in a single reactor, it is called autothermal reforming (ATR). Industrially, the ATR reactor is implemented in a refractory-lined pressure vessel with a combustion chamber, burner, and catalyst bed. In this reactor, a sub-stoichiometric environment oxidizes fuel, natural gas in most cases, with O_2. In the ATR reaction, POX provides heat for later SR reactions, thus controlling the exit temperature of the reactor. Endothermic dry reforming (DR) where the CO_2 is reacting with hydrocarbons feedstock to create H_2 and CO can also be employed [92–95]. The advantages and

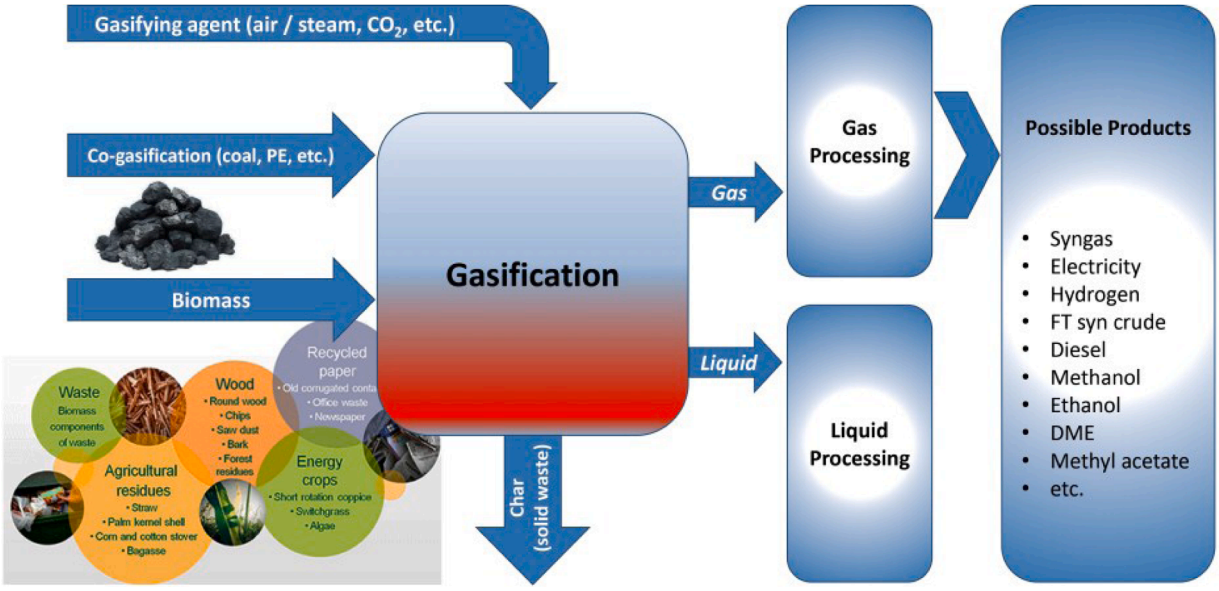

Fig. 2. Schematics of biomass gasification process [66].

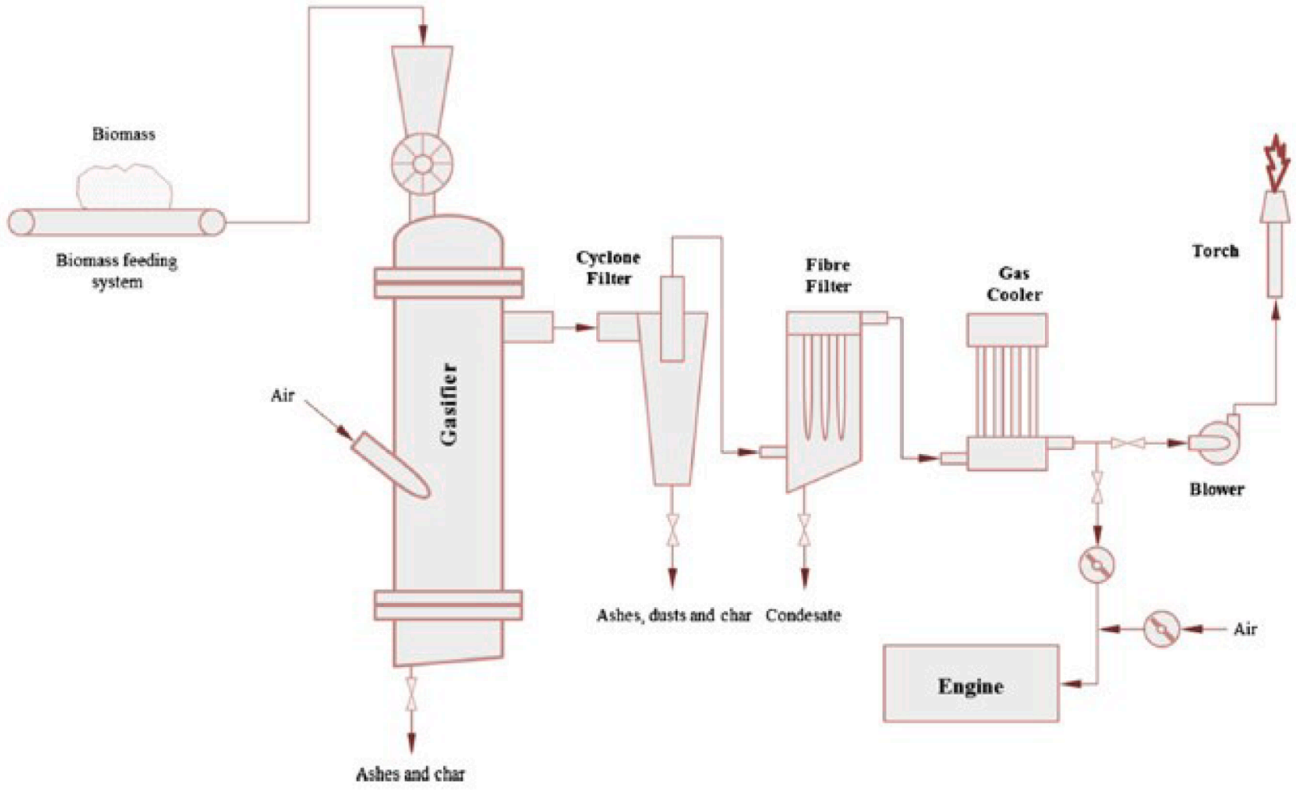

(a)

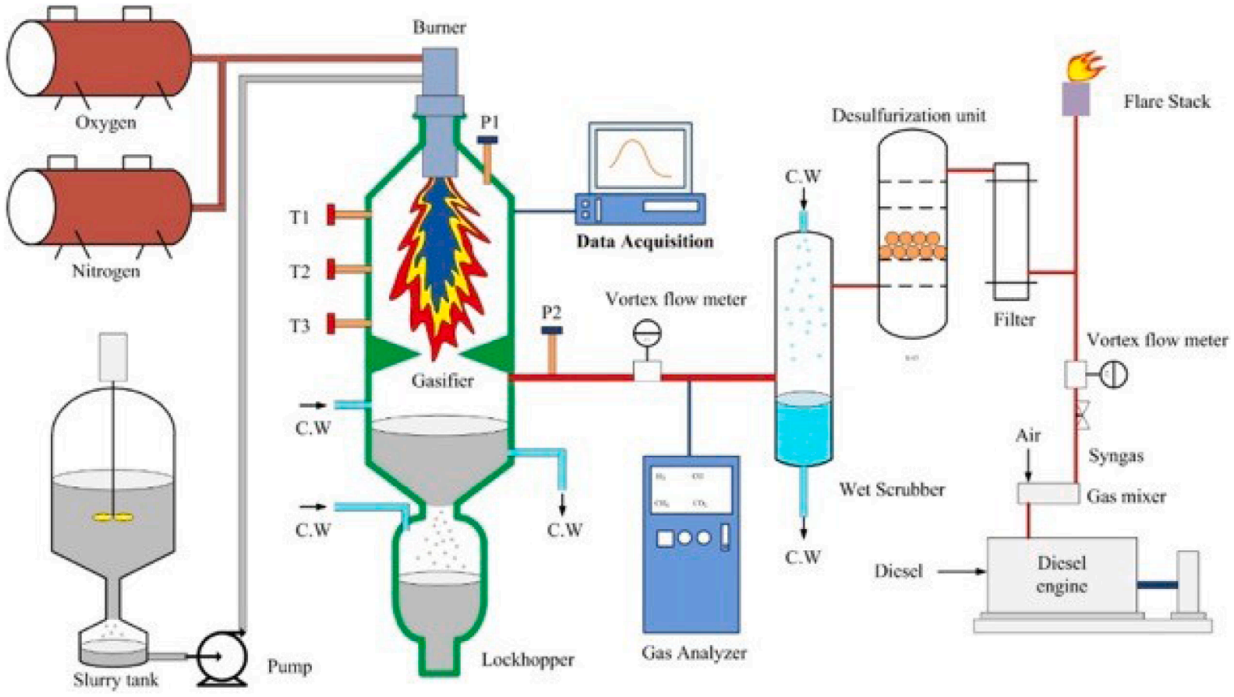

(b)

Fig. 3. a) Syngas production system for an SI engine (Reprinted from [73] with permission of Elsevier); b) diagram of the entrained-flow gasifier for power generation on dual-fuel diesel engine (Reprinted from [75] with permission of Elsevier).

disadvantages of these processes and the corresponding chemical reactions are summarized in Table 3 as main reforming reactions and in Table 4 as side reactions that may occur. These fuel reforming processes have been proposed for on-board hydrogen-rich gas production in vehicular applications, discussed in detail in section 4. Note that the goal is high hydrogen content; therefore, understanding the nature of these reactions aids us in deciding which reactions should participate in reforming processes within a designed reactor and which ones to avoid.

1.3.3. Syngas as an IC engine fuel

Syngas as an IC engine fuel can be utilized in power generation and transportation, produced mainly by gasification and reforming processes, respectively. As mentioned above, syngas names would be different based on composition and LHV, while the terminology we use throughout the current work can be seen in Fig. 4, taken from IC engine-relevant published works. It is worth noting that the figure does not encompass all viable routes for syngas production.

As seen in the first row of Fig. 4, producer gas (PG) or low heating value (LHV) fuel [59] is a gasification product with low LHV due to using air as the gasifying agent and, therefore, the presence of high N_2 content in products. With steam or oxygen or a combination of both utilized as the gasifying agent, the gasification product can be upgraded to fuel with a medium LHV. In general, the gasification process suffers from low thermal efficiencies ($\sim < 50\%$) due to the extra step of vaporizing the moisture contained in biomass and then from tar in the products [101]. Noting that in addition to gas constituents, tar and residue co-exist in the end-product of gasification, but their amounts reduce as high-temperature steam reforming is employed, as seen in Fig. 5. Thus, gasification fuel presumably creates concerns of NOx emissions (due to probably high N_2 content) and deposit formation in the combustion chamber, which should be considered when this fuel is being used as an IC engine fuel. Several IC engine related studies, particularly with SI engines, with gasification fuels have been investigated so far, which will be discussed in section 3.

In the second row of Fig. 5, reformate or reformer gas (RG) is a reforming reaction product, which often has high H_2 and CO contents with negligible N_2 and high heating value. RG can be economically produced with in-situ methods, which will be discussed partially in section 3 (sub-sections of 3.2.2, and 3.3) and comprehensively in section 4 (on-board fuel reforming technologies).

The overall purpose of using syngas as a primary or secondary IC engine fuel is to benefit from renewable energy sources and clean power conversion technologies without scarifying efficiency, power derating, and pollutant emission formation of engines fueled with syngas [102,103]. However, its advantages are dependent on the physicochemical properties of syngas (i.e., the amount of CO and H_2) (see section 2), the type of combustion engine (see section 3), and the fuel reforming technique used for on-board syngas production (see section 4).

1.4. Historical use of syngas as an engine fuel

The first application of syngas in vehicles was reported in the 1920s when German engineer Georges Imbert developed a wood gas generator for automobile use [104]. The gases were cleaned and dried, and then fed into the vehicle's combustion engine. Later, during World War II, shortages of petroleum fuels led to further development of wood gas vehicles [105,106]. By 1945 syngas was used for trucks, buses, agriculture, energy generation, and industrial machinery. After the end of World War II, the application of syngas was changed to integrated gasification combined cycles (IGCC) for stationary power generation. This could be due to less interest in syngas usage in IC engines related to the sharp drop in global oil price and intensified ambitions towards high power engines by increasing the anti-knock index (AKI) of gasoline fuel. The 1950s and 1960s are recalled as the "*Power Wars*" age [107]. The potential of syngas production and application in a low compression ratio SI engine fueled with a syngas-methane mixture was studied in 1956 by Szezich [108]. Later, further interest in biomass-based fuel application in engines was sparked by the oil crisis in the mid-1970s [109]. Simultaneously, in response to the oil price shocks, US Congress passed the first national standards for tailpipe-out emissions to increase miles per gallon (mpg) of passenger vehicles within ten years [110], which was the onset of adopting further stringent regulations for oil-based fuels. As already mentioned, by that time, syngas use was mainly limited to IGCC for stationary power generation [40,111,112], and as an intermediate to produce other biofuels [113,114].

On the other hand, fuel reforming has been used for producing syngas industrially for more than 70 years [115], but the concept of compact on-board reforming for engine applications dates back to the 1970s [116]. Investigations carried out in 1973–1975 in the US with a Chevrolet car with an engine equipped with a syngas generator demonstrated a decrease in petrol consumption by 26% when driving according to the Federal Drive Cycle CVS-3 [117]. On-board fuel reforming was first practically applied to a carbureted gasoline engine through a project named "*Boston Reformed Fuel Car*" by Newkirk and Abel [118], which had an on-board non-catalytic system operated at higher than $T = 1100\ ^\circ C$ for the steam reforming reactions of gasoline. Martin [119] at the University of Arizona demonstrated a better concept of this project using a catalyst to reduce the temperature of the steam reforming of gasoline to around $T = 620\ ^\circ C$. In the meantime, Houseman and Cerini [120] from the Jet Propulsion Laboratory (JPL) evaluated on-board hydrogen generation by adding partial oxidation reforming to steam reforming along with the catalyst to perform the whole reforming process for both hydrocarbon and alcohol feedstocks fueled SI engine. A series of works from Lindström and Sjöström [121–123] at the Royal Institute of Technology (Sweden) was seemingly the first investigation on directly using the recirculated exhaust gases as the primary heat supplier for driving the endothermic reactions of the steam reforming process and as species that can participate in the reforming process. At the University of Birmingham, Jones [124,125] evaluated the feasibility of this concept as exhaust-gas reforming in more detail by incorporating the exhaust gases and using the entire fuel feedstock in the reforming process. For more reading on this topic, there are two notable reviews in the literature [126,127], and additional discussions are provided in section 4.

The development of syngas-fueled IC engines was not commercialized because of the low lifespan of the catalysts and tightening of NOx emission standards. However, research on syngas as a potential fuel for IC engines in transportation has gained much interest in recent decades with advances in catalysts and the potential for on-board generation through waste heat recovery (WHR). An average of 30% substitution of fossil fuels by syngas has been proposed, based on extrapolating from the current EU Directives [128,129]. For further information, several review papers [27,51,59] and a book chapter [29] have been published on the historical and trends of syngas for power generation.

1.5. Scope and structure of the current review

There are many studies in the literature on the use of syngas in different types of IC engines, and it has been shown that syngas can be used as a renewable and alternative low-carbon fuel for both spark ignition (SI) and compression ignition (CI) engines [130–133]. However, there are still numerous subjects such as on-board syngas production and application in advanced combustion strategies that require further investigation and review. This work is focused on determining syngas' potential as a renewable IC engine fuel in transportation. To do this:

- Section 2 presents the fundamental physicochemical characteristics of syngas, which ultimately help us perceive the combustion behavior of syngas as an IC engine fuel under engine-relevant conditions. Due to the composition variability of syngas, various H_2/CO

Table 3
Advantages and disadvantages of the three main fuel reforming technologies [43,96-98].

Reforming process	Chemical formulaEnthalpy of reaction (kJ mole^{-1}) [1]	Characteristics	Advantages	Disadvantage
Steam Reforming (SR)	$C_xH_y + xH_2O \rightarrow xCO + \left(x + \frac{y}{2}\right)H_2$ $\Delta h_R = +1259$[1]	Endothermic	• Highest H_2 generation (H_2/CO ~ 3:1 by vol.)	• Highly endothermic • Low rate of hydrogen production • Need significant quantity of water • Complex system regarding working in high temperature • Careful thermal management (S/C ratio control) • Less fuel flexibility (only certain fuel)
Partial Oxidation Reforming (POX)	$C_xH_y + \frac{x}{2}O_2 \rightarrow xCO + \frac{y}{2}H_2$ $\Delta h_R = -676$[1]	Exothermic	• Simple system (absence of external heat and water) and compactness • Rapid start • Fast response to temperature and reactant changes • Not have thermal management issue • High fuel-type flexibility	• Lowest H2 generation • Lower heating value of reformate than base fuel • Catalyst's deactivation issues by Sulphur and coke depositions • Non-catalytic partial oxidation needs costly materials because it operates at very high temperatures
Autothermal Reforming (ATR)	$C_xH_y + zH_2O + \left(x - \frac{z}{2}\right)O_2 \rightarrow xCO_2 + \left(z + \frac{y}{2}\right)H_2$	Combination of exothermic and endothermic (thermally neutral)	• Simple System (lack of water and external heat requirements) • Compact • Quick to start	• H_2 and CO selectivity is small, because the device uses two different catalyst types • During load changes and start-up, careful control system is required to balance SR and POX

[1] With assuming that fuel is n-octane, and reactants and products are both at 273.15 K and 1 bar.

Table 4
Other side reforming reactions that may take place [99,100].

Reforming process	Reaction	Enthalpy of reaction(kJ mole^{-1})	Notes
Dry reforming (DR)	$C_xH_y + xCO_2 \rightarrow 2xCO + \frac{y}{2}H_2$	$\Delta h_R = +1588$[1]	Lower H_2 yield than SR (H_2/CO ~ 1:1 by vol.). Likely to happen at high temperature and low pressure.
Combustion (complete oxidation)	$C_xH_y + \left(x + \frac{y}{4}\right)O_2 \rightarrow xCO_2 + \frac{y}{2}H_2O$	$\Delta h_R = -5116$[1]	If enough O_2 is available.
Water-gas shift (WGS)	$CO + H_2O \rightleftharpoons CO_2 + H_2$	$\Delta h_R = -41$[1]	A route to CO purification and thus increased H_2 yield at low temperatures.
Methanation 1	$CO + 3H_2 \rightleftharpoons CH_4 + H_2O$	$\Delta h_R = -206$[1]	H_2 will be consumed to increase CH_4 yield.
Methanation 2	$CO_2 + 4H_2 \rightleftharpoons CH_4 + 2H_2O$	$\Delta h_R = -165$[1]	
Boudouard	$2CO_2 \rightleftharpoons CO_2 + C$	$\Delta h_R = -172$[1]	Undesired reaction in catalytic reforming
Thermal Decomposition	$C_8H_{18} \rightarrow CH_4 + C_7H_{14}$	Endothermic	May occur on the catalyst and increase CH_4 yield.
Hydrogenolysis	$C_8H_{18} + H_2 \rightarrow CH_4 + C_7H_{16}$	Exothermic	May occur on the catalyst and increase CH_4 yield.

[1] Assuming that the fuel is n-octane, and reactants and products are both at 273.15 K and 1 bar.

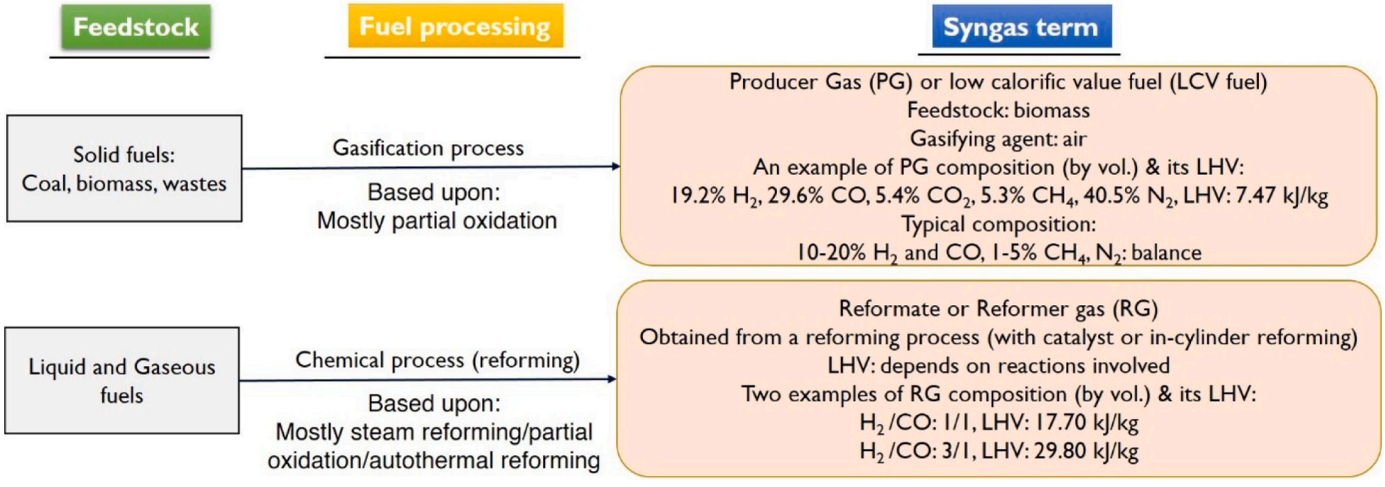

Fig. 4. Syngas terminology used in the current review paper.

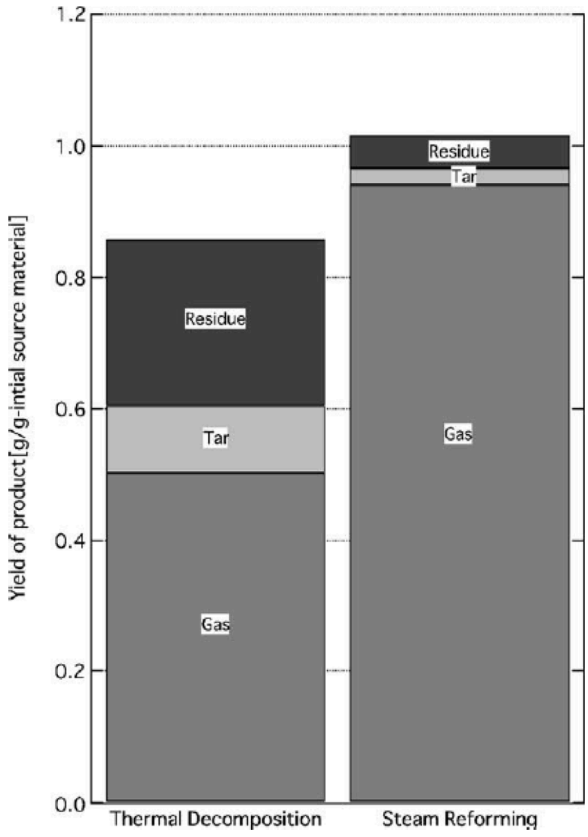

Fig. 5. Yield of product for biomass gasification with thermal decomposition and steam reforming (Reprinted from [101] with permissions of Elsevier).

mixtures are considered in the first place, then the effects of diluents are discussed.

- To better understand the effects of syngas on combustion, emissions, and performance of IC engines with conventional and advanced combustion strategies, section 3 reviews the syngas application in SI, HCCI and dual-fuel engines. In SI engine section, the power generation applications of the syngas-fueled engines are also included.
- The transition from syngas as an IC engine fuel to syngas as a transportation fuel requires producing and carrying the syngas on-board a vehicle, such that both fuel economy and engine efficiency can increase. We discuss all proposed on-board fuel reforming technologies compatible with IC engine in section 4 to achieve these goals, especially paying attention to waste heat recovery (WHR) from engine exhaust.
- The final section represents the summary and demonstrates suggestions to make a feasible future for syngas as a transportation fuel.

2. Fundamentals

2.1. Physicochemical properties of syngas relevant to engines

Table 5 lists the physicochemical properties of typical syngas mixtures compared to hydrogen, methane, biogas, and conventional fossil fuels. It is apparent that syngas has the highest laminar flame speed and widest flammability limits amongst all fuels after hydrogen, making it beneficial for application as a secondary fuel in IC engines, especially at low engine loads. It means that a wide range of stable operation (from rich to lean) could be achieved with syngas fuel, especially promoting the ultra-lean combustion in spark-ignition engines. The volumetric energy content is the main parameter determining the fuel injection system design and required storage tank for vehicular applications [134]. In the case of syngas use in IC engines, the fuel injection system size should be larger, or the injection duration should be longer.

Although there is no available data for the minimum ignition energy of syngas mixtures, it can be concluded that the high hydrogen content in syngas could facilitate cold starts and guarantee rapid ignition [135], considering the unwanted ignitions, specifically pre-ignition and backfire (see sub-section 3.1.1). A scarcity in data has also continued for the quenching distance, and a lower value means a more complete combustion [136], but with a higher heat transfer losses.

Detailed combustion characteristics of syngas mixtures for gas turbine engine-relevant conditions have already been reviewed by Lee et al. [137] and Jithin et al. [138]. In the following section, characteristics of the ignition delay times, laminar and turbulent flame speeds of syngas mixtures under engine-relevant conditions are reviewed and discussed with a focus on those aspects which have not been addressed carefully in previous reviews.

Table 5
Physicochemical properties of a typical syngas mixtures compared to other fuels [59,139-143].

Properties	Syn1[1] *	Syn2[1]*	Syn3[1]	Syn4[1]+	Syn5[1]+	Biogas	Hydrogen	Carbon monoxide	Methane	Gasoline	Diesel
Density [kg/m^3] [2]	0.54	0.67	0.68	1.05	1.04	1.11	0.0824	1.145	0.656	719.7	832
Molecular weight [kg/kmol] [2]	13.91	15	15.2		23.2	34.4	2.0	28	16.04	103	200
Stoichiometric air/fuel ratio [kg/kg]	5.3	4.58	7.23	1.4	2.07	5.67	34.2	2.5	17.2	14.7	14.7
Flammability limits [vol.% in air]	24-60	6.06-74.2	5.8-41.4	7-21.6	13.4-58	7.5-14	4-75	12.5-74	5-15	1.4-7.6	0.6-7.5
Flammability limit [ϕ]	0.2-7.2	-	-	-	-	-	0.1-7.5	0.3-6.8	0.4-1.6	0.7-4.3	1.0-6.5
Autoignition temperature [K]	980	873-923	873-923	898	898	923	858	882	813	550	589
Minimum ignition energy [mJ] [3]	-	-	-	-	-	-	0.02	-	0.28	0.24	-
Laminar flame speed [m/s] [3]	1.0	1.8	-	0.5	0.5	0.25	1.8-2.8	0.4	0.38	0.37-0.43	-
Adiabatic flame temperature [K] [3]	2584	2385	2400	-	2200	2145	2390	2214	2214	2580	-
Quenching distance [mm] [3]	-	-	-	-	-	-	0.64	1.6	2.1	2.84	-
Lower heating value [MJ/kg]	15.7	17.54	24.4	5	7.47	17.0	119.7	10.1	50.0	43.4	42.6
Volumetric energy content [MJ/m^3]	8.47	11.75	16.59	5.25	7.84	18.87	9.86	11.56	32.8	31235	35443

[1] Syn1:57/43:H_2/CO, Syn2:50/50:H_2/CO, Syn3:40/40/20:H_2/CO/CH_4, Syn4: 22.6/24.3/2.2/9.3/41.2:H_2/CO/CH_4/CO_2/N_2, Syn5: 19.6/29.6/5.27/5.41/40.56: H_2/CO/ CH_4/CO_2/N_2 and Biogas: 55.6/42.3/2.1: CH_4/CO_2/N_2 (by volume).
[2] at NTP: normal temperature (T=298.15 K) and pressure (p=1 bar). [3] at ϕ=1 (stoichiometry).
* A typical reformate, + A typical producer gas

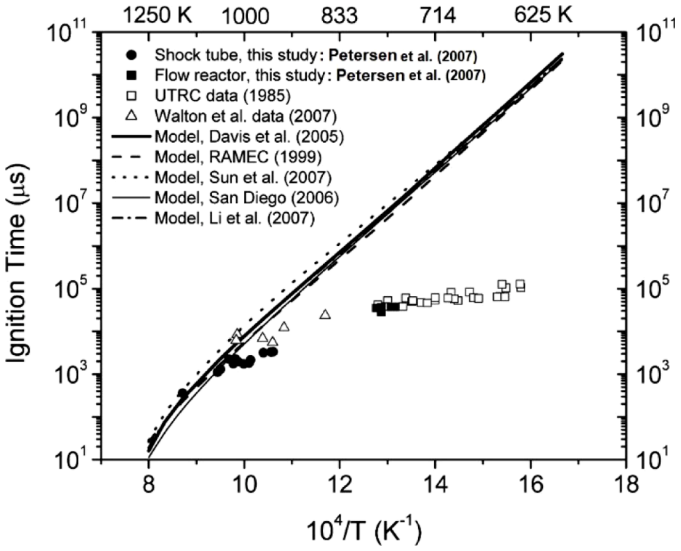

Fig. 6. Discrepancies of ignition delay times between five homogenous reactor models' predictions and three experimental datasets for syngas (H_2/CO: 50/50, by vol.)/air mixture at $\phi = 0.5$ and $p = 20.2$ bar (Reprinted from [156] with permission of Elsevier).

2.2. Ignition delay time (IDT)

The ignition delay times, IDTs, of syngas mixtures were measured in earlier studies mostly using a shock-tube apparatus confined to low pressure (up to 2.2 bar) and low-to-high temperature (up to 2850 K) conditions, which are less applicable to typical gas turbines and IC engines operating conditions [144–150]. The emergence of advanced integrated system technologies like syngas-fired IGCC as an alternative to conventional coal-fired power plants, together with reported discrepancies between measurements and reaction model predictions of IDTs of syngas mixtures (see Fig. 6), has provoked researchers to reproduce experimental measurements and refine the reaction kinetics for syngas oxidation at higher pressures and temperatures [151,152]. Thus, some later studies were conducted using rapid compression machines (RCM) [152–154] and shock-tubes [155,156] at higher pressures, suggesting that the observed discrepancies between measured and calculated IDTs at these pressures are due to not considering the overall activation energy correctly, HO_2/H_2O_2 chemistry dominance in the chain-propagation regime, and particularly the role of $CO + HO_2 = CO_2 + OH$ reaction. Those works were completely reviewed in [157,158].

Recently, in order to justify the observed discrepancies, Mansfield and Wooldridge [159] indicated two distinct ignition behaviors attributed to the strong (or spontaneous ignition which is referred to as spatially homogeneous ignition) and mild ignition (or deflagration ignition which is characterized by the onset of localized reaction sites) for a syngas, with a molar ratio of $H_2/CO = 0.7$, mixed with air (O_2/inert gas molar ratio = 1/3.76) at $\phi = 0.1$ and 0.5, $T = 870$-1150 K, and $p =$ 3-15.4 bar through high-speed imaging in RCM experiments. Two high-speed imaging frames of that work are depicted in Fig. 7, in which multiple localized flame-like structures can be seen on the right side. The authors [159] indicated that the ignition behavior is weakly affected by the molar ratio of H_2/CO, and, by comparison to other work [160], is not strongly dependent on the combustion device used, albeit strongly dependent on the initial thermodynamic state (i.e., pressure, temperature, and equivalence ratio). Also, they stated that the mild ignition behavior is not avoidable by reducing the equivalence ratio towards lean condition; however, the available chemical kinetics mechanisms used in the zero-dimensional (0-D) homogeneous reactor modelling would be capable of predicting the IDTs quite accurately.

As mentioned earlier, a review by Lee [137] evaluated IDTs of syngas mixtures at different H_2:CO ratios with different pressures ranging from 1.6 to 49 atm, by collecting data from Krejci et al. [161,162], Mathieu et al. [163], Vasu et al. [164], Keromnes et al. [165], Gersen et al. [166], and Mittal et al. [152], as shown in Fig. 8. Relying on this review and related works, the effects of various parameters on IDTs of syngas mixtures are summarized below:

Temperature and equivalence ratio (ϕ) effects:

While increasing the temperature shortens the IDT substantially, the IDT of the various compositions of H_2/CO syngas at lean equivalence ratios (ϕ) has a decreasing trend, but only at higher pressures, e.g., 49 atm, as seen in Fig. 8(h). Conversely, at lower pressures, e.g., 7.9 atm, the IDTs can have an increasing trend by reducing the ϕ, which is the case of Fig. 8(b).

Pressure effect:

The influence of pressure on IDT of 50:50 H_2:CO at $\phi = 1.6$, and at p = 8, 12, and 32 atm are shown in Fig. 9 (left). The complex behavior of IDT can be seen with altering pressure at different temperature regions. At high temperatures (>1250 K), higher pressures significantly shorten the IDT, while at intermediate temperatures (1110 K<T<1250 K), increasing pressure from 1.6 to 32 atm exhibits a mild decreasing and even increasing decreasing trend for IDT, which implies that a competition effect may exist. Actually, this was attributed to the pressure dependence of H_2 ignition [165], which is the competition between the

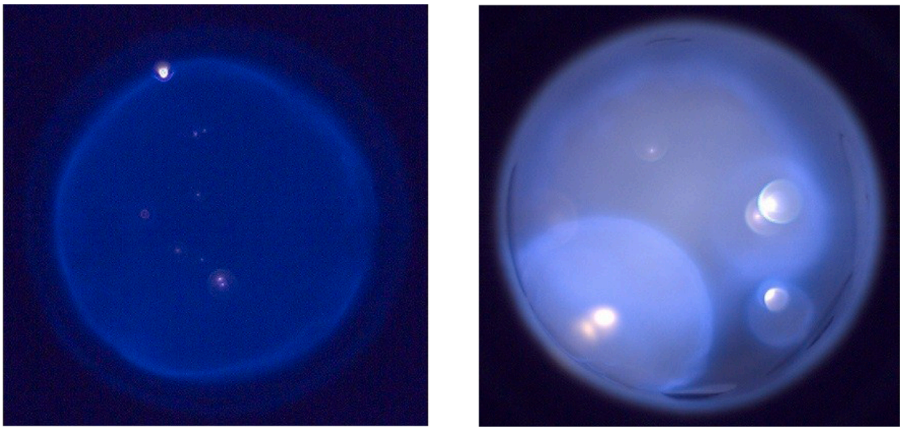

$\phi = 0.1$, $T = 1043$ K, and $p = 3.3$ bar $\phi = 0.5$, $T = 1019$ K, and $p = 9.3$ bar

Fig. 7. High-speed imaging of homogenous (left) and inhomogeneous (right) ignition behaviors of syngas, with a molar ratio of $H_2/CO = 0.7$, mixed with air (O_2/inert gas molar ratio of 1/3.76) illustrating uniform and non-uniform chemiluminescence (Reprinted from [159] with permission of Elsevier).

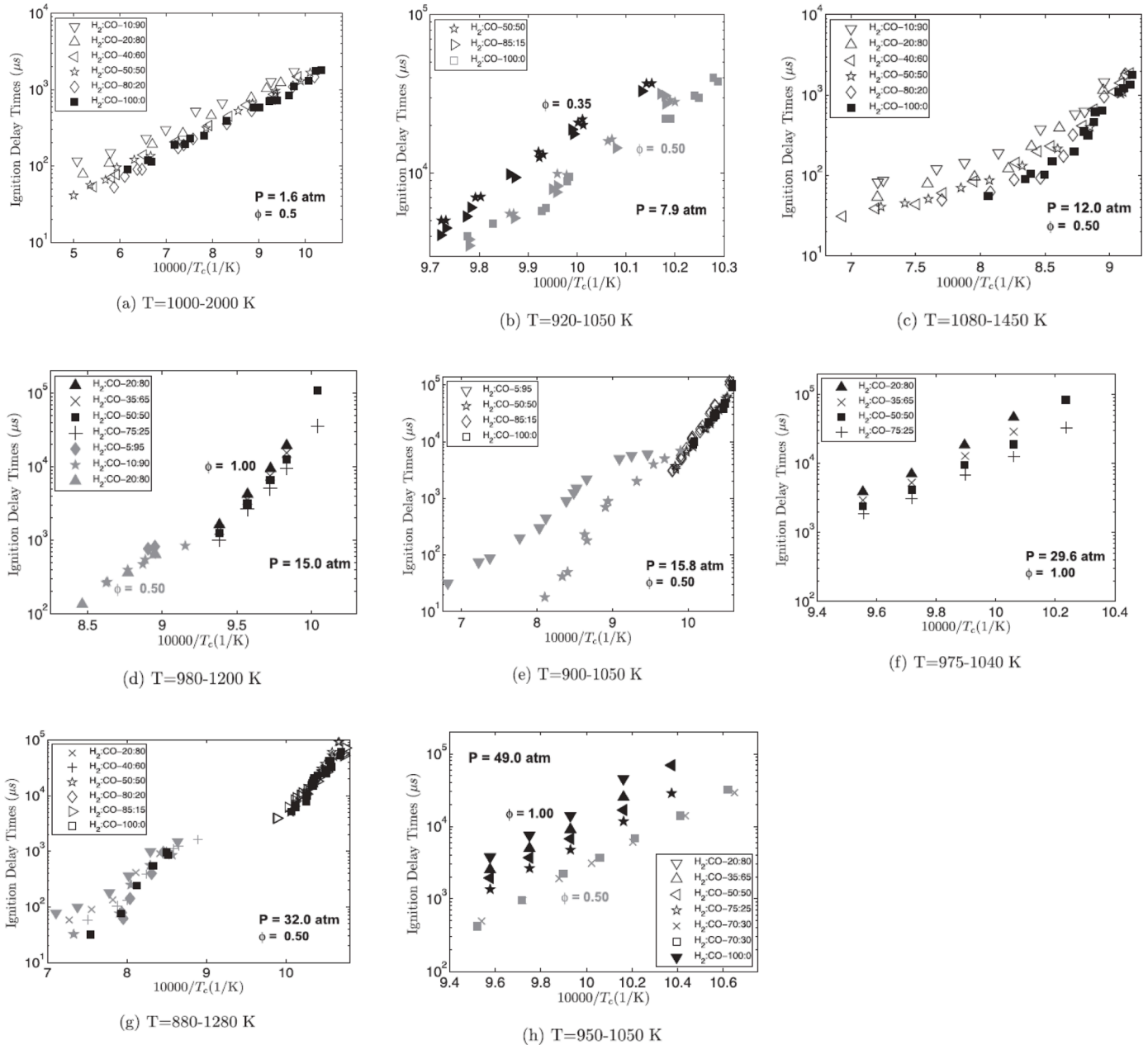

Fig. 8. Ignition delay times of different H_2:CO mixtures as a function of temperature at different pressures (Reprinted from [137] with permission of Elsevier).

chain branching reaction ($H + O_2 \rightarrow O + OH$) that dominates in the high-temperature region, and the pressure-dependent propagation reaction ($H + O_2(+M) \rightarrow HO_2(+M)$) that dominates in the low-temperature region. Moreover, the latter reaction is more favorable at high pressures and is also pressure-dependent, inhibiting the chain branching and resulting in longer IDT at elevated pressures, as seen in Fig. 9 (right).

CO effect:

Though the H_2-chemistry is dominant at low CO content, the CO has an inhibiting effect on the IDTs of H_2/CO fuel due to the decrease in activation energy. Lower activation energy can be detected in the high-temperature region, followed by a very steep increase at around T = 1000 K. The inhibition effect is much more prominent as pressure increases from ~15 to 30 bar; that is, the CO oxidation is retarded by increasing pressure. Beyond p=30 bar, the incremental variation in the inhibiting effect would be trivial. These mentioned trends can be seen in the labeled pictures of (a), (c), (e), and (g) in Fig. 8. For high H_2 concentration (i.e., CO < 60%), adding CO to H_2 did not lead to a significant increase in IDT, as shown by Gersen et al. [166] (see Fig. 8 (a)). Further discussions regarding the CO's inhibiting effect have been reported in [152,166].

CH_4 effect:

Under engine-relevant conditions, it has been reported [167–169] that the addition of H_2 has ignition-promoting effect in CH_4 mixtures, with substantially reduced IDT by replacing CH_4 with a 50% mole fraction of H_2, particularly at higher temperatures. For the purpose of IDT measurement in CH_4/H_2/CO/oxidizer mixtures, Gersen et al. [166] carried out experiments and calculations at $\phi = 0.5$ and 1, p = 20-80 bar, and T = 900-1100 K conditions using an RCM and the SENKIN code [170]. With the addition of CH_4 (> 50% by mole fraction) to the H_2/CO-oxidizer mixture, CO, with low mole fraction (≤ 30%), had no inhibiting effect on either IDTs of CH_4/H_2/CO or CH_4/CO, while CH_4 had this effect, particularly at high temperatures, as illustrated in Fig. 10 (a). In contrast to CO, CH_4 with an even low mole fraction (~ 6%) in the

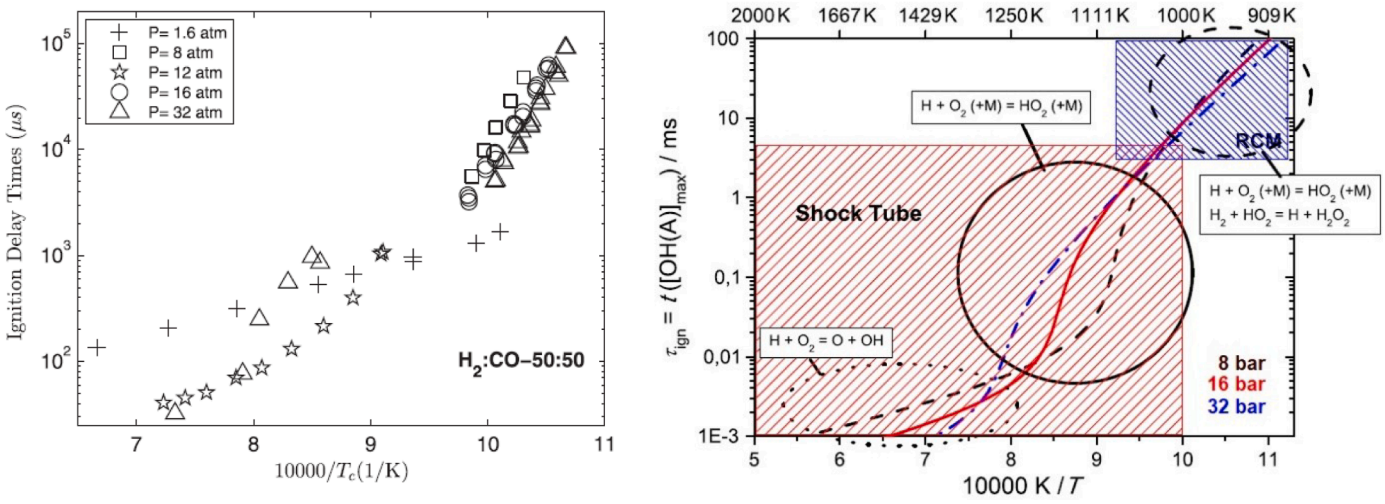

Fig. 9. Effect of pressure on the ignition delay times for 50:50 H_2:CO at $\phi = 0.5$ (left) and for a mixture of 0.7 H_2 + O_2 + 3.76 Ar (right) (Reprinted from [137,165] with permission of Elsevier).

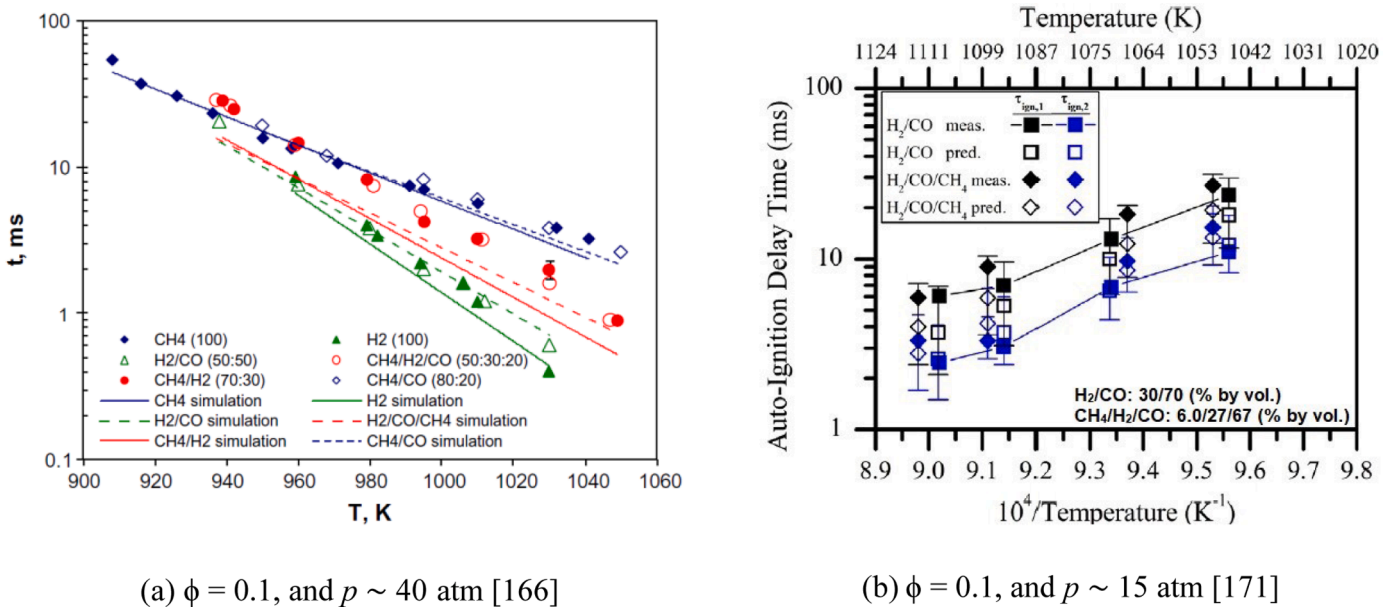

(a) ϕ = 0.1, and $p \sim 40$ atm [166]

(b) ϕ = 0.1, and $p \sim 15$ atm [171]

Fig. 10. Effect of CH_4 on ignition delay times of syngas (Reprinted from [166,171] with permission of Elsevier).
(a) ϕ = 0.1, and $p \sim 40$ atm [166]
(b) ϕ = 0.1, and $p \sim 15$ atm [171]

fuel showed an ignition-inhibiting effect due to OH consumption by CH_4 + OH = CH_3 + H_2O, as can be seen from Fig. 10 (b); noting that the ignition stage is depicted as a two-step ignition process, i.e., τ_{ign1} and τ_{ign2}, due to the presence of two separate regions of fast pressure increase on the recorded pressure-time history plot. This behavior has not been explicitly reported before [171] for syngas fuel mixtures. The experimental works measuring IDTs of syngas mixtures under engine-relevant conditions are summarized in Table 6.

There have been several correlations proposed in the literature for IDT calculation, which can provide a means to estimate syngas ignition properties in a simplified form, where detailed kinetic models are computationally expensive. Walton et al. [154] performed ignition studies of simulated syngas mixtures of H_2, CO, O_2, N_2, and CO_2 in an RCM. The IDT data spanned pressures between p = 7.1-26.7 bar, temperatures from T = 855-1051 K, equivalence ratios from ϕ = 0.1-1.0, oxygen mole fractions from 15% to 20% and H_2:CO ratios from 0.25 to 4.0 (molar basis). Regression analysis yielded the following best-fit to the data set:

$$\tau_{ign} = 3.7 \times 10^{-6} P^{-0.5} \phi^{-0.4} \chi_{O_2}{}^{-5.4} \exp\left(\frac{12500}{RT}\right) \quad (1)$$

In this correlation, τ_{ign} denotes the ignition delay time [ms], p pressure [bar], T temperature [K], φ the equivalence ratio, and χ_{O_2} the oxygen mole fraction. The experimental data were also in good agreement with model predictions based on the detailed mechanism proposed by Davis [151].

As a final note, it is also important to study ignition delay times of syngas blended with other gases such as CO_2, and H_2O, since syngas is not suitable as a sole fuel for some type of IC engines (as will be discussed in section 3). The effects of diluents like H_2O [163,173], CO_2 (negligible) [163], impurities (e.g., trimethylsilanol) [171] and NH_3 (negligible) [163] on IDT of syngas mixtures have been studied in only a few studies. It was suggested that H_2O has contradictory impacts on the IDTs under various pressures, increasing IDT at high pressures as

Table 6
Available experimental datasets for ignition delay times of syngas mixtures.

Year	Author(s)	Facility	Mixture (by vol.)	p (bar)	T (K)	ϕ (-)
2007	Mittal et al. [152,153]	RCM*	$H_2/CO/O_2/N_2/Ar$	15-50	950-1100	0.36-1.60
2007	Walton et al. [154]	RCM	$H_2/CO/O_2/N_2/CO_2$	7.1-26.4	855-1051	0.1-1.0
2007	Peterson et al. [156]	ST*	$H_2/CO/O_2/N_2/CO_2$	~ 20	943-1148	0.5
2012	Gersen et al. [166]	RCM	$CH_4/H_2/CO/O_2/N_2/Ar$	20-80	900-1100	0.5 & 1
2012	Krejci et al. [161]	ST	$H_2/CO/O_2/Ar$	1.5-32	960-2000	0.5
2013	Kéromnès et al. [165]	RCM & ST	$H_2/CO/O_2/N_2/Ar$	1-70	914-2220	0.1-4.0
2014	Mansfield and Wooldridge [159]	RCM	$H_2/CO/O_2/N_2$	3-15	870-1150	0.1-0.5
2015	Mansfield and Wooldridge [171]	RCM	$CH_4/H_2/CO/O_2/N_2$ + TMS**	5 & 15	1010-1110	0.1
2015	Ouyang et al. [172]	ST	$CH_4/H_2/CO/O_2/N_2/Ar$	5-10-15	1100-1700	0.5-1.0-2.0

* RCM: Rapid compression machine, ST: Shock tube.
** TMS: Trimethylsilanol which is added to syngas as impurity, 10-100 ppm.

HO_2/H_2O_2 reactions become more profound, thereby increasing the reactivity of the mixture [173]. Although substantial progress has been obtained in our awareness of IDT for H_2/CO syngas, there are still few studies to achieve a general description for a representative H_2/CO/diluents/(possible) impurities syngas under engine-relevant conditions.

2.3. Methane number (MN)

In the IC engine community, to isolate the knock propensity of the fuel from the specific engine design and condition, a practical measure was required to indicate the ability of a fuel to resist knock [174]. Due to this, octane number is defined, and some octane rating methods like the motor octane number (MON) have been established by ASTM for liquid fuels based on primary reference fuel blends, in which iso-octane-like fuel is assigned with ON (or MON) of 100 and n-heptane-like fuel with ON (or MON) of 0; which means fuels with high MON resist auto-igniting more than those with low MON. Extending this concept to gaseous fuels leads to the so-called methane number (MN), taken from the work done for the Austrian AVL Company through 1964-1969 [175]. The system rating of MN employs a reference fuel blend of methane and hydrogen, by which methane and hydrogen are given to MN of 100 and zero, respectively. CH_4-CO_2 mixtures were also considered as reference mixtures for MN beyond 100, defining 100 plus the volume of existing CO_2 for MON; for example, $20\%CO_2 + 80\%CH_4$ (by vol.) results in MON of 120 while $20\%H_2 + 80\%CH_4$ (by vol.) leads to MON of 80. Therefore, it is expected that an engine fueled with a syngas fuel having a higher CO_2 fraction leads to a rise in the upper limit of compression ratio (CR) without knock issue. More generally, once the MN number through this method is determined, regulating both spark timing and CR can be employed to avoid knock, applicable to an engine fueling with either 100% syngas or syngas blended with other gaseous fuels. To determine the MN, some researchers [176–179] have conducted their own procedure and compared it to developed MN programs, such as the AVL Methane program V3.20 [180] and the MWM MN program [181], which are partly looked at in the following.

Generally, the procedure for specifying the MN of tested fuel is basically a comparative basis in which unknown fuel is indirectly compared to a map of reference blends at the same CR via a curve; however, this subject is out of scope for the current review and can be found elsewhere [182,183]. As an alternative approach for indirectly comparing the tested fuels to reference blends, Malenshek and Olsen [182] conducted a direct comparison by developing a test procedure with a computer-controlled gas blending system, minimizing the effects of other uncontrolled variables besides CR, such as ambient temperature and atmospheric pressure, and producing maximum knock by sweeping the air-fuel ratio (rather than ϕ=1 for indirect comparison). Some results for a wide range of syngas composition are presented in Table 7.

Table 7
Measured MN for various test gases [182].

Test gas	H_2	CO	CH_4	CO_2	N_2	MN
Reformer gas	44.5	2.30	38.1	13.0	2.10	62.4
Coal gas	22.3	63.1	-	1.30	13.3	30.0
Wood gas or PG	39.2	23.5	8.50	26.4	2.40	61.4
Digester gas	-	-	60.8	37.8	1.50	139.1
Landfill gas	-	-	60.5	39.5	-	139.5

Experimental data, such as that represented in Table 7, were used in the literature to compare with the programs that estimate the MN of natural gas as a function of its composition. It was found that estimates can deviate considerably with respect to experimental data when syngas is considered as fuel [183]. These deviations are mainly caused by the various and high concentrations of carbon monoxide, and especially carbon dioxide (as a knock suppressor) and hydrogen (as a knock propagator) in syngas. The other reason, for example, for early version of AVL program was that carbon monoxide effects are not included [177]. Diaz et al. [177] carried out a comprehensive analysis of the auto-ignition tendency of binary mixtures of hydrogen and carbon monoxide diluted with carbon dioxide. They proposed a statistically validated second-order regression model to predict MN. Results revealed that increasing carbon dioxide concentration in the mixtures strongly increases the MN of the mixtures. A great fraction of H_2 and CO intensely reduces the MN, whereas the CO_2 or N_2 raise knock resistance and thus increase the MN [176]. Lechner et al. [184] showed that the classical methane number or the propane knock index[1] fail for the syngas compositions in practice. Based on a review of published fuel data, 31 gas mixtures were developed using a D-optimal statistical design consisting of H_2, CO, CH_4, CO_2, and higher hydrocarbons up to C_3. Additionally, pure methane, pure propane, pure hydrogen and a biogas mixture consisting of 60 vol% CH_4 and 40 vol% CO_2 were examined as reference fuels. Practically all syngas blends were more prone to knock than methane or biogas. Admixtures of higher hydrocarbons were found to substantially increase the knock propensity. This indicates the prominent role of higher hydrocarbons with regard to the knock propensity of fuel gases. Lean equivalence ratios, exhaust gas recirculation, and the addition of water vapor were effective measures to mitigate the risk of knock.

Under the MN determination, hydrogen should have the lowest resistance to knocking, which somehow is not true since some work has presented a research octane number (RON) of around 130 for hydrogen. Also, hydrogen and methane as reference fuels in the MN rating system have very different characteristics in flame speeds and ignition delays, in contrast to those in the ON rating system, which have similar flame speeds [185]. It was seen that the MN could be correlated to the adiabatic flame temperature and laminar flame speed, a high MN fuel having a low adiabatic flame temperature and long flame initiation period [176]. However, compared to H_2, propane (C_3H_8) has shown more knock tendency, which may stem from its lower auto-ignition temperature.

To summarize, there is still no comprehensive consensus to determine the knock propensity of gaseous, namely syngas fuels. The currently potential errors in the MN method, such as various operating

[1] The propane knock index is one of MN alternatives to index knock propensity of gaseous fuels.

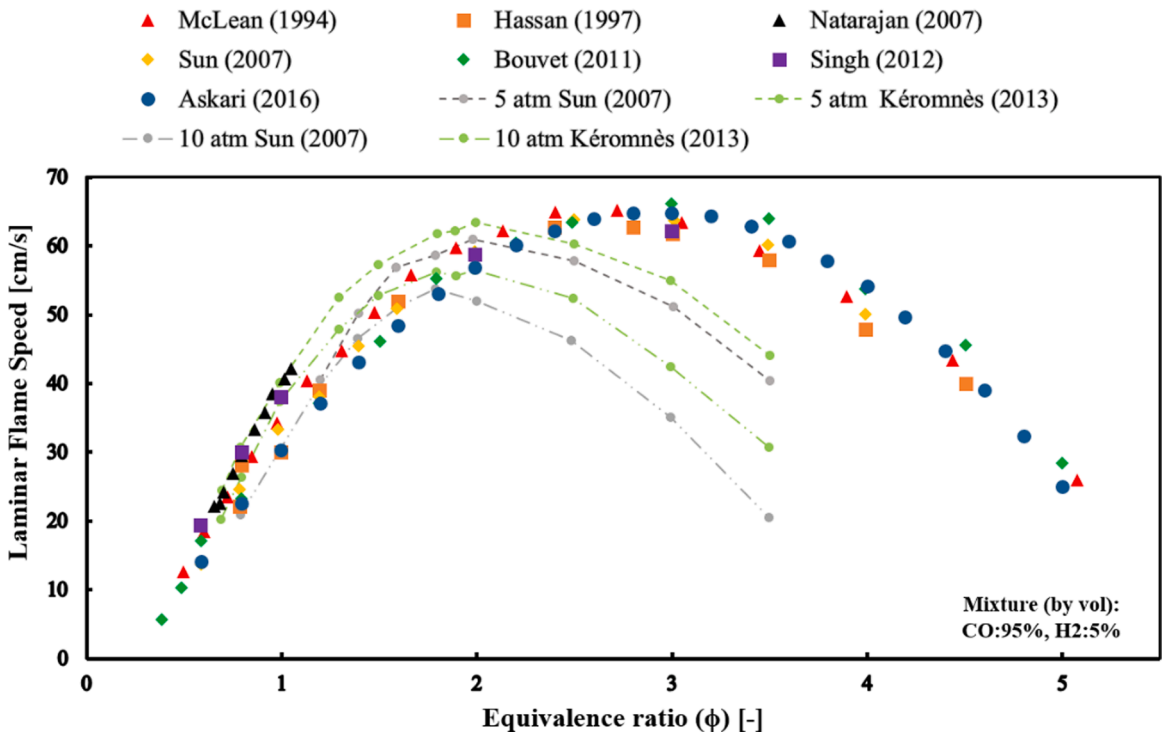

Fig. 11. Published measured data of laminar flame speeds for the model syngas mixture of H_2/CO: 5/95 with oxidizer (by vol.) at atmospheric (symbols), 5 and 10 atm (lines) (adopted and extended from [194] with permission of Elsevier, other references [165,188,189,192,193,195,196]).

engine conditions and heavy hydrocarbon presence in syngas, lead to keep investigating this matter.

2.4. Laminar flame speed (LFS)

Laminar flame speed is a crucial parameter, which results from the net effects of the diffusivity, exothermicity, and reactivity of the mixture [186], and has a strong dependency on pressure, temperature, mixture composition, and equivalence ratio [187]. The LFS of syngas-air mixtures at typical temperatures and pressures (NTP) conditions were extensively reported in [188–194], and Fig. 11 shows an example of published data for LFS of a syngas mixture (H_2/CO: 5/95 by vol.) at atmospheric and high-pressure conditions. As can be seen, a relatively decent consistency in measured LFS values can be observed among all data, with a maximum variance of 10 cm/s peak-to-peak, while the difference was seen to be larger as pressure increases.

Moreover, the discrepancies among measured LFS data are as high as 40 cm/s at fuel-rich conditions ($\phi > 2$) by increasing H_2 concentration by just 10%. Fig. 12 shows that the maximum LFS value increases approximately from 65 in Fig. 11 to 130 cm/s by substituting 20% of CO with H_2 in the syngas mixture. This can be attributed to the wide range of data sets used for extrapolation[2] (to eliminate stretch effects from data), the applied stretch extrapolation model, the chosen flame radius range, and the inhibiting effect of carbonyl compounds coming from the steel containers utilized to store the CO content of syngas. More information on fundamentals and technical possible sources of observed discrepancies and uncertainties are described in [187] and [197] for each distinct fuel-air mixture, and in [198] for spherically expanding syngas flames.

For the high-pressure operating condition, Sun et al. [196] were one of the first groups that conducted the LFS measurement of H_2/CO mixtures at pressures up to p=40 atm. They substituted nitrogen (N_2) with helium (He) to increase the Lewis number (L_e) of the mixture, minimizing flame-front instability[3] due to wrinkling and cell formation over the flame surface. It is also noteworthy that if the ignition energy supplied by the spark plug of a SI engine is not enough to drive the flame front to a minimum radius at which stretch effects are decreased, the propagating flame of a mixture with L_e>1 can extinguish [199]. Referring back to Fig. 11 and now to Fig. 13 (left) for pressures higher than p=10 atm, it is obvious that increasing initial pressure substantially reduces LFS, which is attributed to hydrodynamic instabilities due to decrease in flame thickness as seen in Fig. 13 (right). Some studies are available concerning the LFS of syngas mixtures at higher pressure [162, 165,194-196, 200,201]; most of them used helium rather than nitrogen.

High-H_2 syngas, the target fuel for IC engines, is more susceptible to flame front instabilities, taken from LFS of pure H_2-oxidizer mixtures [19]. Both thermal-diffusive and hydrodynamic instabilities are involved in amplifying the flame front's destabilization by affecting the Lewis number and flame thickness, respectively. So, as compared with CO, H_2 has a more dominant effect on flame stabilities [202]. To measure LFS of syngas with H_2/CO: 85:15% (by vol.) at elevated pressures up to p = 10 bar and lean conditions (ϕ = 0.5-0.6), which is relevant to IC engines with premixed charge, Goswami et al. [203] conducted experiments using the heat-flux method and then compared the resulting LFSs with those obtained from the available mechanisms [165,204-206] by kinetic modeling. They observed significant differences between experiment and modeling, attributed to the uncertainty in key reactions, and suggested that further studies are requisite to modify their rate

[2] To correctly determine the LFS, particularly in spherical propagating flame at elevated pressures, stretch effects due to flame curvature and flame unsteadiness should be subtracted from experimental data to avoid scattering the data. Stretch effects can be eliminated by using non- and linear extrapolation equations.

[3] Two common intrinsic flame instabilities have been pointed out within the present work, the thermo-diffusivity instability that is characterized by Lewis number and the hydrodynamic (as known as the Darrieus-Landau) instability, which is due to density jump across the flame-front, that is characterized by the flame thickness and thermal expansion ratio.

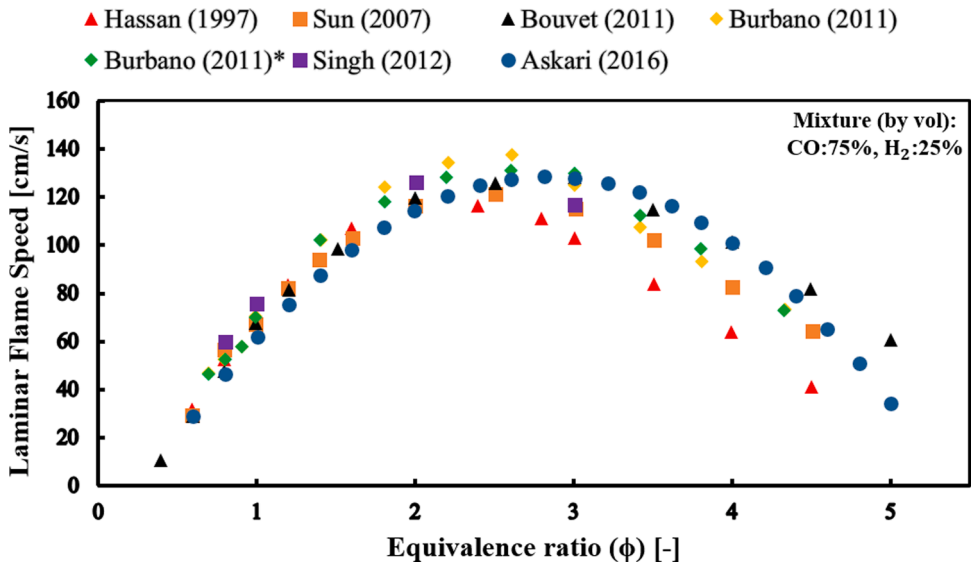

Fig. 12. Published measured data of laminar flame speeds for the model syngas mixture of H_2/CO: 25/75 with oxidizer (by vol.) at atmospheric (adopted from [194] with permission of Elsevier).

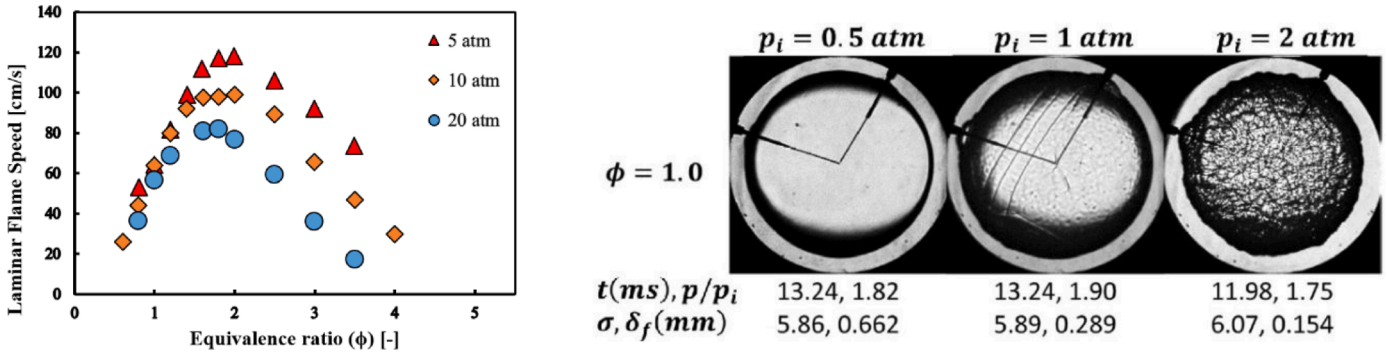

Fig. 13. Effect of pressure increase on laminar flame speeds of syngas diluted in helium (left) and flame front growth of syngas diluted in air with flame radius of 60 mm (right), for H_2:CO = 25:75 (by vol.) and at room temperature; p/p_i: pressure ratio, σ: thermal expansion ratio, andδ_f: flame thickness. (Reprinted from [137] with permission of Elsevier).

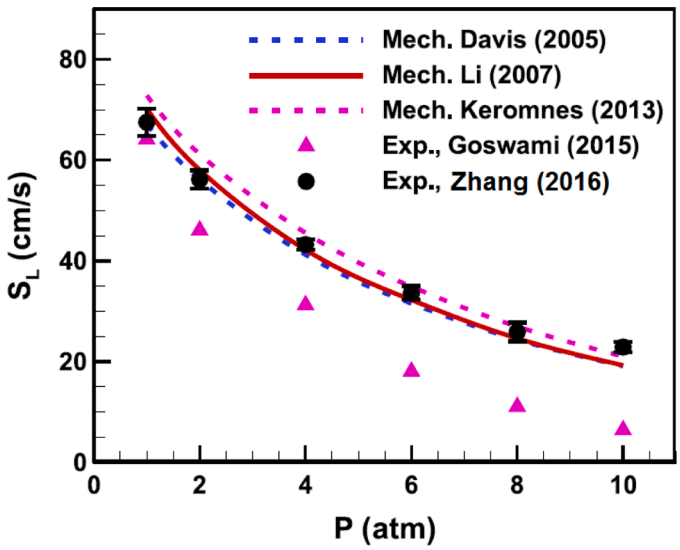

Fig. 14. Laminar flame speed of 85%H_2–15%CO/12.5%O_2–87.5%He mixture as a function of pressure (Reprinted from [207] with permission of Elsevier).

constants. Later, Zhang et al. [207] studied the LFS of the same lean high-H_2 syngas of the previous study [203] at elevated pressures but using the spherical flame method. Fig. 14 depicts that the measured LFS is seen to diminish monotonically as pressure increases, due to the fact that $S_L \sim p^{(n/2-1)}$ [197] and the overall order of reaction n is normally less than 2, due to the third body, inhibiting the $H + O_2 + M \rightarrow HO_2 + M$ reaction. As can be seen from Fig. 14, while mechanisms have better predicted the results of the latter study compared to that of the former study, the reason is unclear and needs additional study. In addition, the preferential diffusivity of high-H_2 syngas must be noted here due to the high mass diffusivity of H_2 [19], as it plays a vital role in the future of flame front structure [208]. Interestingly, at elevated pressures and lean conditions but lower H_2 content (35:65 H_2:CO mixtures), syngas laminar flames were determined [209] to be extremely unstable, resulting in cellular structures in the spreading flame front surface, where $S_L \sim p^{-0.15}$ having a fairly small reduction in pressure compared to lean methane flames where $S_L \sim p^{-0.50}$. As a result, it is challenging to measure the LFS of syngas-air mixtures free of flame instability effects without diluents. It is almost impossible to obtain accurate LFSs before the onset of flame instabilities at lean and elevated pressure conditions [210].

Based on the above discussions and Refs. [211,212], it is worth noting that lean high-H_2 syngas (H_2/CO) flames at elevated pressures tend to wrinkle and exhibit cellularity even at the early stage of kernel development. Such unstable cellular flames can be self-accelerated by

gradually increasing their frontal surface area, and, thus, this should be noted as a reason for knocking combustion in SI engines. Both intrinsic flame instabilities and the acceleration characteristic of the flame front, at decreased critical (minimum) flame radius, result in more difficulties in accurately measuring the LFS. Accordingly, Xie et al. [211] proposed an updated method, based on Bradley et al. [213], to obtain the LFS at various flame radii without the acceleration effect. Identification and characterization of self-acceleration of syngas flame are still in their infancy and an ongoing topic for research.

As H_2/CO mixtures do not represent real syngas and always refer to bottled gas or simulated gas, the effect of dilutions with CO_2, N_2, H_2O, at least on LFS of H_2/CO mixtures must be investigated by scrutinizing the thermal, chemical, and transport impacts of each of them. It has been separately reported in [195,200,202,214,215] that CO_2 decreases the flame temperature, thereby reducing the rate of H_2/CO oxidation and thus the LFS, which means the chemical effect of CO_2 is dominating. Han et al. [200] measured the LFS of H_2/CO (3/1, 1/1, and 1/3 by vol.) with CO_2 dilution for elevated pressures p=1, 4, and 10 bar and temperatures T=298, 375, and 450 K using the outward spherical flame propagation method, and indicated that increasing CO_2 dilution linearly decreases the LFS and directly affects the elementary reaction rates. A comprehensive study by Vu [202] revealed that CO_2- and N_2-diluted syngas-air flames are more sensitive to stretch effects than a He-diluted one because of the reduced Markstein number with increasing diluent concentrations. Also, from Fig. 15, it can be seen that the effective Lewis number (defined as a combination of fuel and oxidizer Lewis numbers) is reduced in both cases of CO_2 and N_2 dilution and will be more prone to thermo-diffusive instability at lean conditions; according to such trend, Parthap et al. [214] showed the minimum permissible quantity of the equivalence ratio to achieve flame stability would be shifted from 0.6 to 0.8 for increasing CO_2 concertation from 0 to 30%, respectively, for a H_2/CO: 1/1 (by vol.) mixture. A recent study [216] showed that for a diluted H_2/CO mixture, the flame would be more stabilized by increasing ϕ when the H_2 fraction is more than 50%. Also, it was shown that the flame instability of high-H_2 syngas (as H_2/CO mixture) scarcely varies with increasing CO_2 or N_2 dilution fraction compared to a high-CO syngas whose flame becomes more stable with rising dilution.

While decreasing LFS with both CO_2 and N_2 addition has been proven [217–222], syngas-air mixtures have higher LFS with N_2 dilution, which has a thermally dominant impact [222]. Therefore, increasing CO_2 dilution has a more substantial inhibiting effect on LFS due to its direct engagement in the chemical reactions through CO + OH ↔ CO_2 + H [214,223], and hence it is necessary to evaluate it with more caution in predicting syngas containing CO_2 by a reaction model.

The LFSs of H_2O diluted syngas-air mixtures have been explored by some researchers at atmospheric conditions using both stagnation [224] and spherical [193] flame methods, consistently concluding that H_2O addition will non- and monotonically reduce the LFS of CO- and H_2-rich syngas, respectively. For higher pressures up to p=10 bar, Santner et al. [225] found a monotonic drop in mass burning rate with increasing H_2O concentration for an equimolar H_2/CO syngas. Besides, they indicated that the inhibitory effect of H_2O addition would be increased with increasing pressure. In a research on CH_4 blended with H_2/CO, Zhou et al. [226] conducted measurements and numerical simulations at T_{in}=303 K, ϕ = 0.6–1.5 and p = 0.1–0.5 MPa with a wide range of bio-syngas (H_2/CO/CH_4) compositions. They experimentally determined and measured LFS of premixed bio-syngas/air flames under various compositions of fuel mixtures, as depicted in Fig. 16, in which αBasis, as a base for comparison, is set to H_2/CO/CH_4 = 40/40/20 (% by vol.) with constant mole ratios among species; and αH_2-60 equals H_2/CO/CH_4 = 60/26.6/13.3. It was observed that the Li mechanism [204] is well in line with the measured LFS of premixed bio-syngas flames, particularly under fuel-lean conditions. There is a slight difference between the expected findings and the experimental ones for

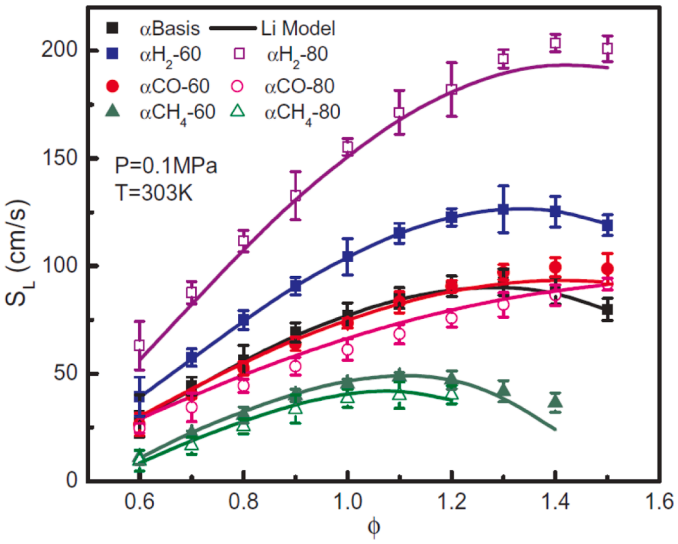

Fig. 16. Laminar flame speed of H_2/CO/CH_4/air mixtures at various compositions (Reprinted from [226] with permission of Elsevier).

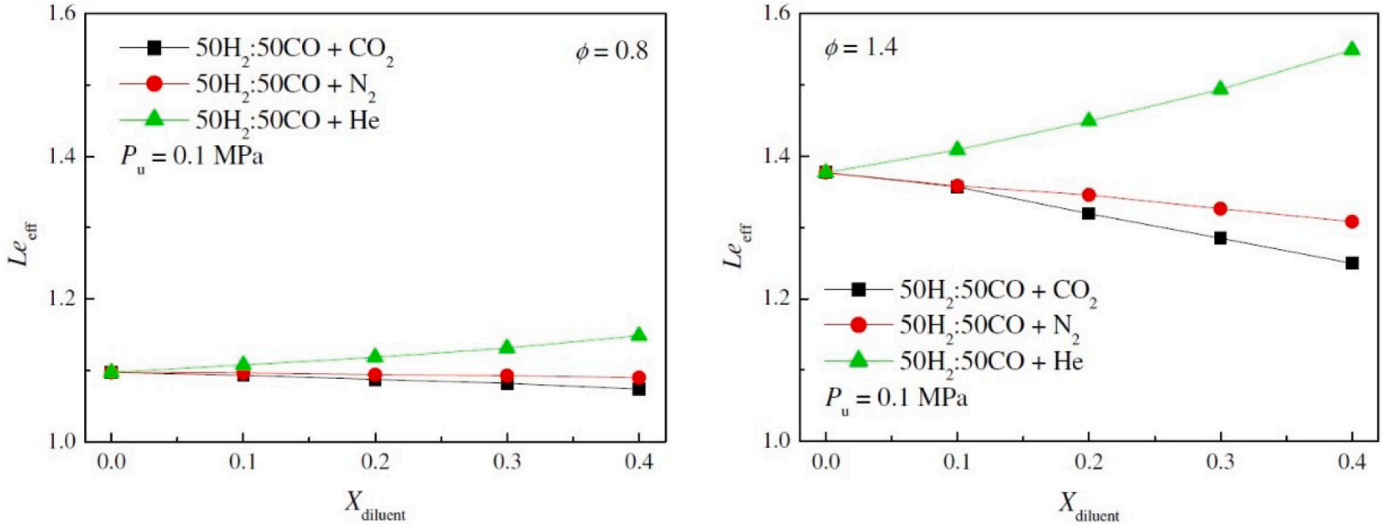

Fig. 15. Effective Lewis number at rich/lean conditions and room temperature with the (Reprinted from [202] with permission of Elsevier).

fuel-rich conditions.

It can also be seen in Fig. 16 that the peak value of LFS moves towards fuel-rich conditions with increasing H_2 content in the mixture due to the very high diffusivity of hydrogen [227], which has a severe, increasing trend with ϕ. Conversely, the addition of CH_4 to the mixture leads to shifting the peak value to the lean side with a quite large reduction in the quantity of LFS due to the inherent slower LFS of CH_4. Also, with an increase in CO fraction in the fuel, the LFS is not much influenced. The thermal and chemical kinetic analysis shows that the addition of CO has much more impact on the adiabatic flame temperature but plays a minor role in its chemical kinetic impact as opposed to the addition of H_2 [228]. The influence of H_2 addition to LFS is mainly due to its chemical effect at lean and stoichiometric conditions. However, with the addition of around 75% CO, the rise in laminar flammability is attributed to the high adiabatic flame temperature (thermal effect) [229].

The effects of inert gases like N_2, CO_2, and H_2O, and CH_4 on the laminar flame speeds of syngas, in the form of H_2/CO, were briefly reviewed here and are extensively discussed in [137,230]. The LFS of syngas in the form of producer gas (PG) have also been addressed in [231–235], which is the case of 100% syngas fueled IC engines in stationary applications. Monteiro et al. [234] investigated the impact of various compositions of PG generated through fluidized bed, updraft, and downdraft gasification on the LFS, using the spherical flame method. Fig. 17 illustrates that the LFS of two studied PG over a wide range of ϕ have a similar trend to those of syngas with high CH_4 content, although the maximum values are at stoichiometric conditions. Tippa et al. [236,237], concluded that PG combustion with higher H_2, CO, and N_2 fractions and comparatively lesser amounts of CH_4 and CO_2 are stable to preferential diffusion effects and predictable for minor changes in composition.

Other researchers have tried to determine the LFS of syngas blended with hydrocarbon fuels [238–240] and with exhaust gas recirculation (EGR) [241,242], which is the primary case in syngas fueled engines through reforming fuel on-board a vehicle, of which detailed discussions can be found in sections 3 and 4. For instance, Kwon and Min [238] calculated the LFS of syngas/iso-octane-air mixtures by a 1-D model under conditions relevant to SI engines. The EGR effect was also included using different fractions of burnt gas up to 0.5 in volume. The LFS of the studied mixtures were observed to be proportional to the initial temperature, LHV, the fraction of syngas in the fuel mixture and H_2 fraction in the syngas, and inversely proportional to the initial pressure, deviation of equivalence ratio from the stoichiometric condition, and the fraction of burnt gas. A few studies have also considered the combustion characteristics of syngas mixtures in premixed SI engines [73,243,244]. However, the extent of accuracy and reliability in the results of such studies are vastly dependent on the capability of the developed reaction mechanisms in predicting the LFS under desired simulation conditions.

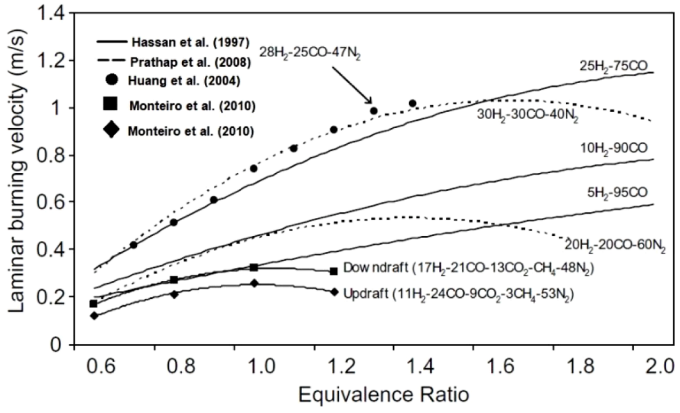

Fig. 17. Laminar flame speeds comparison between two producer gas generated by up- and downdraft gasification with H_2/CO [189], H_2/CO/N_2 [217, 231] mixtures (Reprinted form [234] with permission of Elsevier).

Finally, measured LFS data can establish correlations [245], which is a simpler and more convenient approach than detailed simulations with kinetic mechanisms, for easy use in estimating the LFS of syngas-based mixtures during engine combustion simulations [191]. However, those are only applicable to regions far away from stretch and ignition energy effects. An example of the kind of LFS correlation is given below, which is a function of equivalence ratio, temperature, and pressure [194]:

$$S_u = S_{u0}\left(1 + a(\phi - 1) + b(\phi - 1)^2\right)\left(\frac{T}{T_0}\right)^c \left(\frac{p}{p_0}\right)^d \quad (2)$$

where S_{u0} is the reference LFS at certain point ($\phi = 1$, $T_0 = 298.15$ K, $p_0 = 1$ bar), ϕ the equivalence ratio, T the temperature in K and p the pressure of the mixture in bar. The fitting coefficients, *a, b, c*, and *d* were obtained for different hydrogen concentrations using a nonlinear, least-squares method. This correlation is valid only for non-cellular laminar flames within the equivalence ratio range of $0.6 < \phi < 5$. The pressure and temperature ranges are a function of the equivalence ratio and hydrogen fraction.

Semi-empirical correlations are also available to predict the LFS of H_2/CO/air flames with N_2 and CO_2 dilution [246]. Although such correlations are preferred to comprehensive chemical kinetic models in terms of computational cost, they have been restricted to specific conditions, beyond which the predictions are inaccurate. This is because many earlier correlations were based on a small collection of experimental data, mostly carried out over a narrow range of engine operating conditions [73,191,196,238,245,247,248]. In addition, no flame speed correlation is available that allows the calculation of LFS for blends of syngas and gaseous fuels. For gaseous blends, blending has a non-linear effect on the LFS, resulting in complicated mathematical correlation equations to capture this behavior [249]. Therefore, the use of reaction kinetics calculations is preferred for the combustion study of syngas-fueled engines. With this in mind, data-driven machine learning (ML) algorithms [250], as a more recent solution, can be trained to overcome this issue based on a large dataset having high accuracy to anticipate the LFS of syngas with large fluctuations in their composition at various conditions. This approach also allows more researchers to participate in developing syngas-based combustion systems without requiring the in-depth knowledge that only qualified experts have.

In summary, instabilities induced by high H_2-containing syngas at elevated pressures make LFS measurements with reasonable accuracy impossible. In general, with an increase in pressure and concentration of H_2, the LFSs for premixed H_2/CO-oxidizer mixtures reduce and increase, respectively. Diluting syngas with N_2, CO_2, or H_2O decreases the LFS. The maximum flame speed occurs at fuel-rich conditions, while the maximum flame temperature occurs near the stoichiometric condition. Also, the LFS has shown a strong dependency on pressure, inlet temperature, and equivalence ratio. It was shown that extensive modifications in kinetic mechanisms should be taken into account. There is a broad experimental data collection available in the literature for the combustion of syngas with various concentrations of H_2:CO. Nonetheless, research on syngas mixed with other gases such as CO_2 and H_2O is still limited, and a few experimental data are available for the LFS of syngas mixed with CH_4 at elevated pressures [158,195,239,251]. New measurements with thorough uncertainty analysis on the LFS of syngas (H_2/CO + diluents) solely and blended with other fuels (like gasoline, diesel, etc.), which are of great interest in vehicular applications at elevated pressures and engine-relevant conditions, will help us to understand syngas combustion behavior properly.

2.5. Turbulent flame speed (TFS)

Like the LFS, the turbulent flame speed (TFS), S_T, is of interest and is

defined when the surface area of thin laminar flames interacting with the turbulent flow is increased. Unlike LFS that exclusively depends on mixture properties, TFS is also a function of turbulent flow, enclosed by the IC engine geometry. So, measuring TFS is sensitive to the experimental rig used, and it was confirmed [252,253] that it is an experiment-dependent variable. Turbulent spherical flames propagating inside the IC engine consume the unburned mixture when the flame-front enters to reaction zones, thereby determining the heat release rate. From an engine viewpoint, TFS is dependent on trapped-mass conditions, residual turbulence at trapping, and the mean piston speed, while processes such as auto-ignition, combustion, and heat conduction are also affected [254]. Generally, Lipatnikov and Chomiak [253] demonstrated that flame stretch and instability could significantly affect TFS, depending on the conditions and mixture properties.

Because of high stretch sensitivity due to the high mass diffusivity of H_2 content [255], the turbulent flame properties of model syngas (H_2/CO) mixtures are of great importance and interest. A few helpful experimental measurements on the H_2/CO-air mixtures have been carried out under elevated pressures, such as those by stabilized Bunsen-type flames [256–259] and centrally-ignited propagating flames [209,260]. The findings of several flame configurations suggested that the TFS of lean hydrogen flames are around a factor of two faster than those of hydrocarbon flames, although their magnitudes vary significantly for various flame geometries [29]. Regarding measuring the TFS of syngas-air mixtures in high-pressure environments, the two most discussed topics in the literature are:

1- The impact of pressure increase, fuel composition, flame-front sensitives, and Re_T on TFS.
2- Extracting S_T correlations from experimental data for a particular fuel-air mixture at specific conditions and generalizing them.

Herein, the turbulent Reynolds number is defined as $\mathrm{ReT} = (u' l_0)\nu$, where u', l_0 and ν are the turbulent intensity or root-mean-square (r.m.s) turbulent fluctuating velocity, the integral length scale, and the kinematic viscosity of the reactants, respectively. In the first topic, the influence of pressure, two scenarios have been reported to date. The first states that the TFS increases with increasing pressure due to the improvement of flame instabilities, at constant u' and l_0, regardless of the fact that Re_T also increases due to the inverse proportion of ν to pressure elevation. However, the second proved that TFS decreases, similar to LFS in a negative exponential behavior, with increasing pressure as the Re_T is held constant [260,261].

As instances of the first scenario, Liu et al. [209] studied TFS for 35:65 H_2:CO-air mixtures at $\phi = 0.5$ and 0.7 over an initial pressure range of p = 1–10 bar. They found that S_T increases with increasing pressure ($S_T \sim p^{0.15}$ for $\phi = 0.7$ and $S_T \sim p^{0.11}$ for $\phi = 0.5$) at a fixed r.m.s turbulent fluctuating velocity ($u' \approx 1.4$ m/s), often attributed to cellular instability promotion due to thinner flame thickness (hydrodynamic instability) [253,262]. At higher pressure up to 20 bar, Daniele et al. [257] mentioned that the S_T increase is because of diffusive-thermal instability co-acting with hydrodynamic impact. Additionally, it was demonstrated that increasing u'/S_L is much more effective in increasing S_T/S_L than increasing pressure, particularly in the weak turbulence regime. Besides the pressure influence, the increase of S_T/S_L with increasing hydrogen fraction in syngas (H_2/CO) mixtures was observed using OH-PLIF measurements in a work by Wang et al. [263], which resulted in the promotion of the intensity of flame front wrinkles due to amplified preferential diffusive-thermal instability. In addition to results consistent with prior studies, Venkateswaran et al. [264] displayed measured quantities of S_T for 90:10 H_2:CO that are around three times larger than for CH_4 blends, with the same S_L,u', and operating conditions. An important conclusion from the work of the same authors [255] was that fuel effects on S_T are not simply a low turbulence intensity phenomenon – it clearly persists over the entire range of turbulence intensities used in the measurements. It is believed that these fuel effects are due to the reactant mixture's stretch sensitivity, which has a strong effect on the positively strained leading points of the turbulent flame brush for non-zero Markstein length fuels [265].

The second topic was devoted to extracting S_T correlations for ease of use in combustion modeling. Regarding syngas-air mixtures at higher pressure than atmospheric, some of them are presented in Table 8.

However, such correlations are obviously incapable of capturing all sensitivities of the TFS. For example, Venkateswaran et al. [267] used S_T databases for negative Markstein length fuel blends, i.e., mixtures with small Lewis number like H_2-rich syngas- or H_2-air mixtures, and highlighted that it is challenging to distinguish the effects of time-scale, length-scale, and Re_T on these correlations. Thus, future works are needed with novel correlations in a more unified form.

As the final point of this section, the detailed experimental study on chemistry-turbulence interaction and instabilities of the flame front for simpler fuels like H_2 particularly, in turbulent flame combustion is next to impossible at this instant, while it is possible with the aid of the direct numerical simulation (DNS) [268]. An exciting subject addressed with DNS is the effect of preferential diffusivity on turbulent spherical syngas flames on the lean side of stoichiometric. This is due to the well-known behavior of lean hydrogen-air mixtures, which is a non-unity Lewis number fuel and differs from heavy hydrocarbon fuels. In an example study of three-dimensional DNS with detailed chemistry for lean 70:30 H_2/CO syngas at p = 4 bar, it was found [269] that thermo-diffusive instabilities have negligible impact on cellularity development of flame structures under high turbulence levels, though the flame acceleration and species diffusive flux are still influenced by the preferential diffusion. The same authors [270] showed how the interaction between equivalence ratio variation and instabilities could affect the heat release rate. Performing two-dimensional DNS for a turbulent expanding 50/50 H_2/CO syngas flame at $\phi = 0.6$ and atmospheric conditions, Bhide and Sreedhara [271] found heat release rate enhancement and a rise in flame speed for even a quiescent medium due to high mass diffusivity of hydrogen. Under greater turbulence levels, a further increase in HRR and a shift in the peak location of HRR towards low-temperature zones were also seen. The shifting trend was ascribed to atomic hydrogen species, and it disappeared at high pressure and temperature conditions. The differential diffusion effect (related to the different values of the species Le) was also observed to diminish when raising the CO fraction to 70%.

In conclusion, while noting that high-pressure turbulent combustion

Table 8
Some correlations based on measured data for the turbulent flame speed (S_T) of syngas-air mixtures at elevated pressures.

Author(s)	Correlation for S_T	Constants	Eq.
Daniele et al. (2011) [257] B	$\frac{S_T}{S_L} = a\left(\frac{u'}{S_L}\right)^{0.63}\left(\frac{l_0}{\delta_L}\right)^{-0.37}\left(\frac{P}{P_0}\right)^{0.63}\left(\frac{T}{T_0}\right)^{-0.63}$	P_0= 1 bar, T_0 = 1 K a = 337.5	(3)
Wang et al. (2013) [263] B	$\frac{S_T}{S_L} \propto a\left[\left(\frac{P}{P_0}\right)\left(\frac{u'}{S_L}\right)\right]^n$	For H_2/CO: 35/65 a = 3.8, $n \approx 0.42$	(4)
Shy et al. (2015) [260] S	$\frac{S_T}{u'} = aDa^b$	For lean H_2/CO: 35/65 with Le ≈ 0.76: a=0.12, b=0.5	(5)
Sun and Zhu (2020) [266] S	$S_T^0 = (1.325.X_{H_2} + 0.916).u' + 0.597.e^{2.X_{H_2}}$	-	(6)

Note(s): the Damköhler number is defined as $Da = (l_0/u')(S_L/\delta_L)$, where δ_L is the laminar flame thickness which is approximated by $\delta_L \approx \alpha/S_L$, and α is the thermal diffusivity of unburned mixture.
X_{H_2}: Hydrogen fraction in H_2/CO syngas.
B : Bunsen-type flame method,
S : Spherical-type flame method.

cannot be directly inferred from atmospheric turbulent combustion results [209], there is no consensus among published findings at higher pressures than atmospheric, nor even a general description for turbulent premixed syngas flames. There are also very few studies presenting the turbulent combustion of spherical (model) syngas flames compared to Bunsen-type flames. As in Daniele et al. [257] study under gas turbine-relevant conditions, there is a need to study turbulent spherical syngas flames with boundary conditions matched with those in an IC engine, also considering the dilution effect.

3. Syngas application in IC engines

3.1. Syngas in SI engines

Research on syngas application in SI engines has been focused on improving the fuel consumption (or fuel conversion efficiency) and engine-out emissions. All employed strategies that result in a more efficient SI engine[4] can be divided into two categories, along with the associated engine design modifications:

1- Improve stoichiometric operation with a combination of downsizing, boosting, and exhaust gas recirculation (EGR) strategies.
2- Move towards lean or ultra-lean operation through the intake charge dilution and advanced direct injection strategies.

The lean combustion concept in gasoline SI engines has allowed higher brake thermal efficiency due to reducing pumping and heat transfer losses, while keeping NOx emissions low because of lower peak combustion temperatures. However, ultra-lean combustion requires careful consideration in order to operate the engine beyond the lean limit or dilution limit. While a number of methods, including intake design improvement, advanced ignition systems, and EGR stratification, could address this, reformate containing hydrogen-rich gas can serve as an extender of lean and flammability limits of the engine. Additionally, since the choice of fuel directly affects the engine's lean limit, alternative fuels with reformate can also be used in SI engines. Also, synergies can emerge from syngas production via on-board fuel reforming and thermochemical energy recovery techniques. However, the focus of this section is to run SI engines with syngas as the primary fuel, which can only improve engine's efficiency by extending its lean limit.

3.1.1. 100% Syngas in carbureted and port fuel injection (PFI) SI engines

The majority of studies on 100% syngas-fueled SI engine have used carburetor or port fuel injection (PFI) technologies in power generation for two main reasons. First, the SI engine can integrate thermo- and biochemical processes in which feedstock can be supplied from viable, eco-friendly energy resources, e.g., biomass. Second, since the LHV of syngas is lower than that of typical fuels such as gasoline and natural gas, the engine output power and torque could drop by 20-40% with syngas operation, as reported in several published works [59,272,273]. This drawback makes using 100% syngas in SI engines via carburetor or PFI technologies unsuitable for vehicular applications. However, it is a good choice for stationary applications where some limited operating points can be optimized by MBT timing. Also, the engine-out emissions can vary by changing the ways of syngas production or adding some other species to syngas. A brief review of 100% syngas fueled SI engines for stationary and transportation applications is presented below.

Syngas composition variability can affect the level of extending the lean limit of engine combustion. Ando et al. [274] evaluated the performance of low-BTU gases produced from gasification and a two-step pyrolysis/reforming process in a small-scale naturally aspirated (NA) single-cylinder SI engine with variable compression ratio from 8.47 and 11.9 and an installed mixer instead of the original carburetor. The gas produced from gasification was hydrogen-rich, while that from the two-step pyrolysis was methane-rich. They found that both gases provided similar thermal efficiency compared to CNG. In addition, the hydrogen-rich gas was observed to show a wider stable engine operation range with the λ up to 2.0, and NOx and HC emissions were quite low for it compared to both CNG and the methane-rich gas. Bika [275] investigated the combustion characteristics and knock limits of a syngas-fueled SI engine with a variable compression ratio (CR=6:1-10:1). The fuels investigated were pure H_2, H_2/CO: 75/25, and H_2/CO: 50/50 (% by vol.). He reported that increase in the CO fraction increased the knock limit of syngas and advanced the ignition timing of MBT but did not affect the indicated efficiency up to H_2/CO: 50/50. In addition, the maximum heat HRR was observed with pure hydrogen. However, the compression ratio increase affected the peak pressure more than by the CO percentage increase. A maximum ITE of 32% was reported with H_2/CO: 50/50 at ϕ=0.6 and CR=10:1. The general conclusion was that the extended combustion duration with a higher CO percentage provides more knock resistance at a higher compression ratio.

As mentioned earlier, the power output of SI engines is usually derated during operation with 100% syngas. For instance, Mustafi et al. [272] studied a syngas fuel named "Powergas" that contained 44%H_2, 52% CO, and 4% N_2 produced from the Aqua-fuel process[5], to evaluate the performance and emissions with Powergas (15.3 MJ/kg LHV) in a variable CR Ricardo E6 single-cylinder SI engine and also compared it with those with gasoline at lean (ϕ = 0.81) and CNG at stoichiometric conditions (ϕ = 1.0). The Powergas indicated no superior performance relative to CNG and gasoline as the main fuel in the SI engine. They observed more than 20% decline in brake torque output and more than 100% increase in BSFC compared to gasoline and CNG at 1500 rpm and CR = 8.1:1, as seen in Fig. 18. Although the engine-out THC and CO emissions with syngas fueling were lower than those with gasoline and CNG, both CO_2 and NOx emissions were higher. Similar power losses have also been reported with syngas combustion in SI engines [272,274,276-280], especially at lower CR and closer to stoichiometric conditions and operating away from the MBT timing. Munoz et al. [276] also found around 50% reduction in power output of a carbureted SI engine with producer gas compared to gasoline, at CR=8.1:1.

Shah et al. [277] experimentally studied the performance of a single-cylinder SI engine with syngas produced from biomass gasification. The syngas was composed of 16.2–24.2% CO, 13–19.4% H_2, 1.2–6.4% CH_4, 9.3–13.8% CO_2, and the balance N_2 with an LHV of about 5.79 MJ/Nm^3. Based on the results obtained, the overall engine efficiency from the combustion of both syngas and gasoline fuels was found to be similar at the same maximum power output, albeit higher maximum power output was achieved by gasoline operation. CO was observed to be 30–96% lower with syngas than gasoline at each operating point due to the higher carbon content of gasoline fuel. In addition, the HC emission of syngas was negligible at less than 40 ppm in all operating conditions due to the presence of very less HC (1.2–6.4%) in the syngas used in this study. However, the main reason for HC reduction could be the increased H_2 content in the fuel mixture, which is responsible for promoting fast conversion of HCs [273]. It was also reported that NOx emissions in syngas operation were lower, about 54–94%, compared to gasoline operation. This was due to the lower cylinder temperatures as a result of the lower LHV of syngas. The operating fuel/air equivalence ratio (ϕ) in this study was not directly declared while appearing that the operation of a designed gasoline-based engine is stoichiometric for gasoline and is lean for

[4] Here we can consider two ways of reduced pumping losses (also referred to as either throttling or gas exchange losses) at low to part loads and/or decreased friction losses at high speeds while maintaining emissions low enough.

[5] Aqua-fuel technology transforms clean by-products like glycerin into renewable fuels for standard generators.

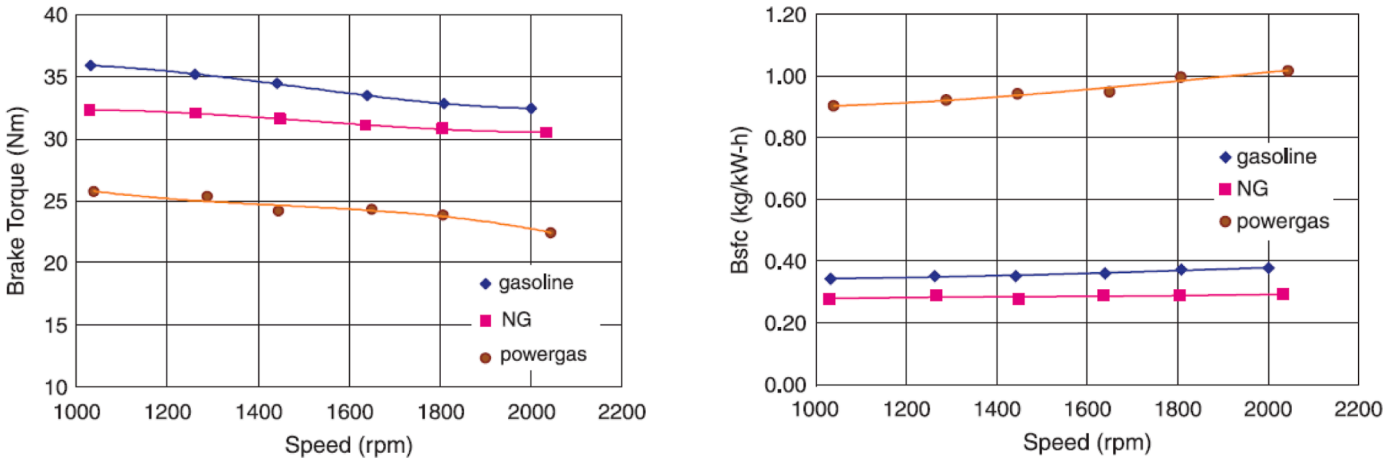

Fig. 18. Brake torque and BSFC versus engine speed at WOT and MBT timing and CR = 8:1 (Reprinted from [272] with permission of Elsevier).

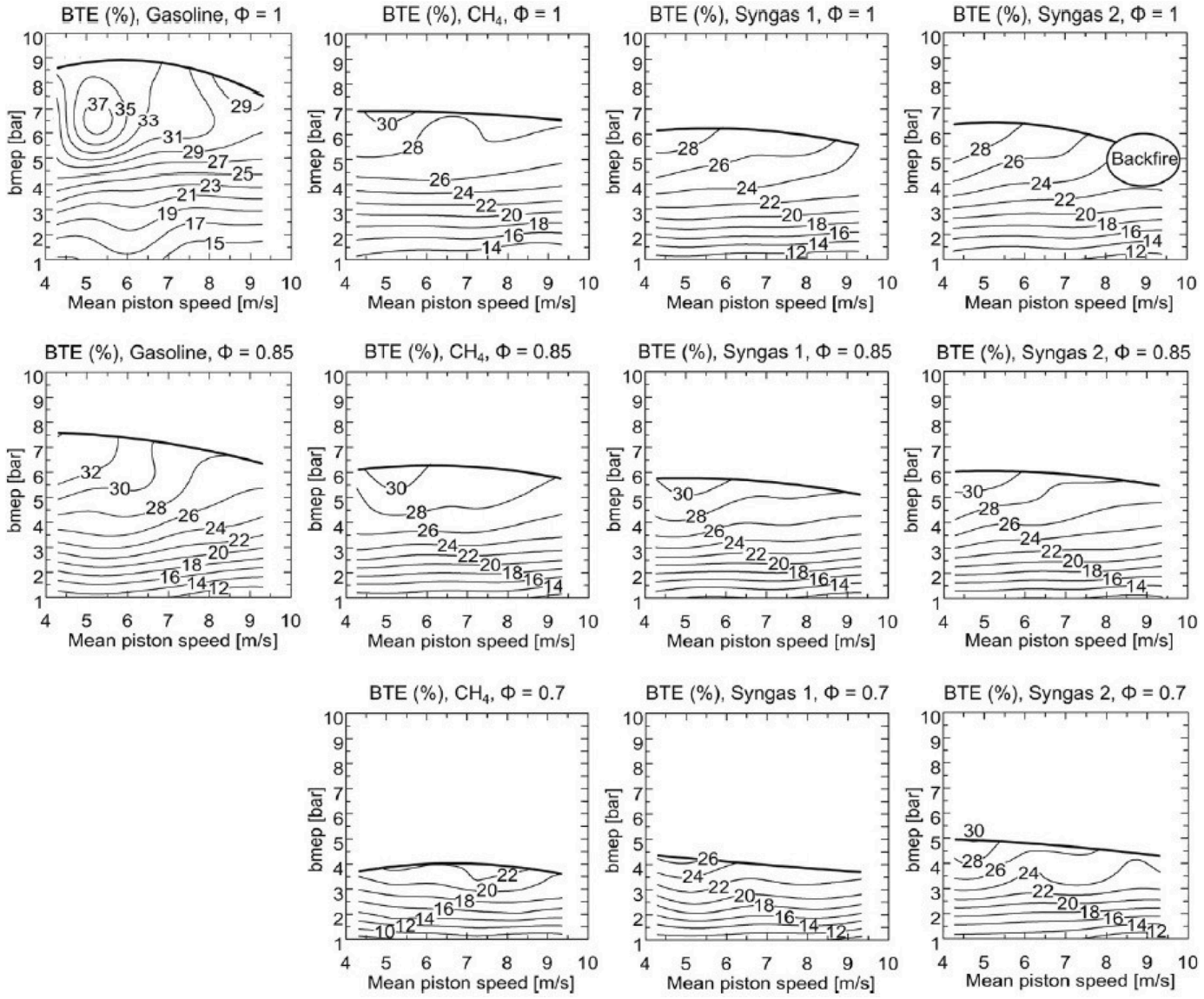

Fig. 19. Brake thermal efficiency contour maps for specified fuels at $\phi = 1$, 0.85, and 0.7 and a fixed ignition timing of 15° BTDC and CR = 10.7:1 (Reprinted from [281] with permission of Elsevier).

syngas. It is complicated to run a 100% syngas-fueled SI engine close to stoichiometric conditions (i.e., $\phi > 0.75$) because the retardation of ignition timing after the TDC is required due to hydrogen presence in the syngas composition (irrespective of unstable combustion possibility due to high hydrogen content in syngas). With this in mind, the following two studies are presented for fixed and varying ignition timings.

In a study intended for vehicular applications, Arroyo et al. [281] conducted an experimental study to compare the operation of a NA SI engine fueled with two different syngas cases and two typical gasoline and methane fuels, at $\phi = 1$, 0.85, and 0.7 in full and medium-loads over a wide range of engine speeds. Two syngas fuels produced from catalytic decomposition of biogas with molar composition of 23% H_2 and 23% CO, 26% CH_4, and 28% CO_2, with the LHV=14.095 MJ/kg as syngas #1, and 40% H_2, 39% CO, 11% CH_4, 10% CO_2, with LHV=16.525 MJ/kg as syngas #2, were tested. A considerable loss in BTE was observed in gaseous fueling cases at stoichiometric conditions; however, a slight increase in power occurred at ϕ=0.85, as shown in Fig. 19 (gasoline did not achieve stable combustion at ϕ=0.7). As the authors reported, the reason for higher NOx emissions was the increased H_2 and the decreased diluent contents, e.g., CO_2, in syngas composition. The established comparison with syngas #1, syngas #2, and methane showed that the high methane fraction of the syngas fuel accounts for the increased levels of HC emissions. The general increasing CO_2 trend of syngas cases with respect to gasoline and methane cases seen was due to the CO_2 content in syngas. Nevertheless, a fixed injection timing (15° BTDC) of gasoline used as a baseline for all cases in this study may result in a deviation from a realistic comparison.

In the case of varying ignition timing to achieve MBT, Ran et al. [282] conducted experiments to differentiate the performance and emissions of a NA PFI single-cylinder CFR engine operating on E10 (90% gasoline + 10% ethanol vol.), CNG (95% CH_4 vol.), ethanol (95% ethanol + 5% water vol.), and syngas (60% H_2 + 40% CO vol.) at an engine speed of 1200 rpm and CR = 8:1. The ϕ was in the range of 0.74-0.99, 0.63-0.98, 0.76-0.97, and 0.3-0.78 for fuels in the above-mentioned order. The high heat release rates and spark timing restricted the upper side of ϕ for syngas (see Fig. 20 (b)). Among tested fuels, syngas indicated the lowest net IMEP due to having the lowest volumetric efficiency and LHV. Generally, the volumetric efficiency of syngas and CNG due to their gaseous nature and lack of evaporative cooling effects is lower than for liquid fuels. Also, the stoichiometric air/fuel ratio of syngas is lower than CNG; therefore, extra mass fuel is injected for syngas fueling, resulting in more degradation of volumetric

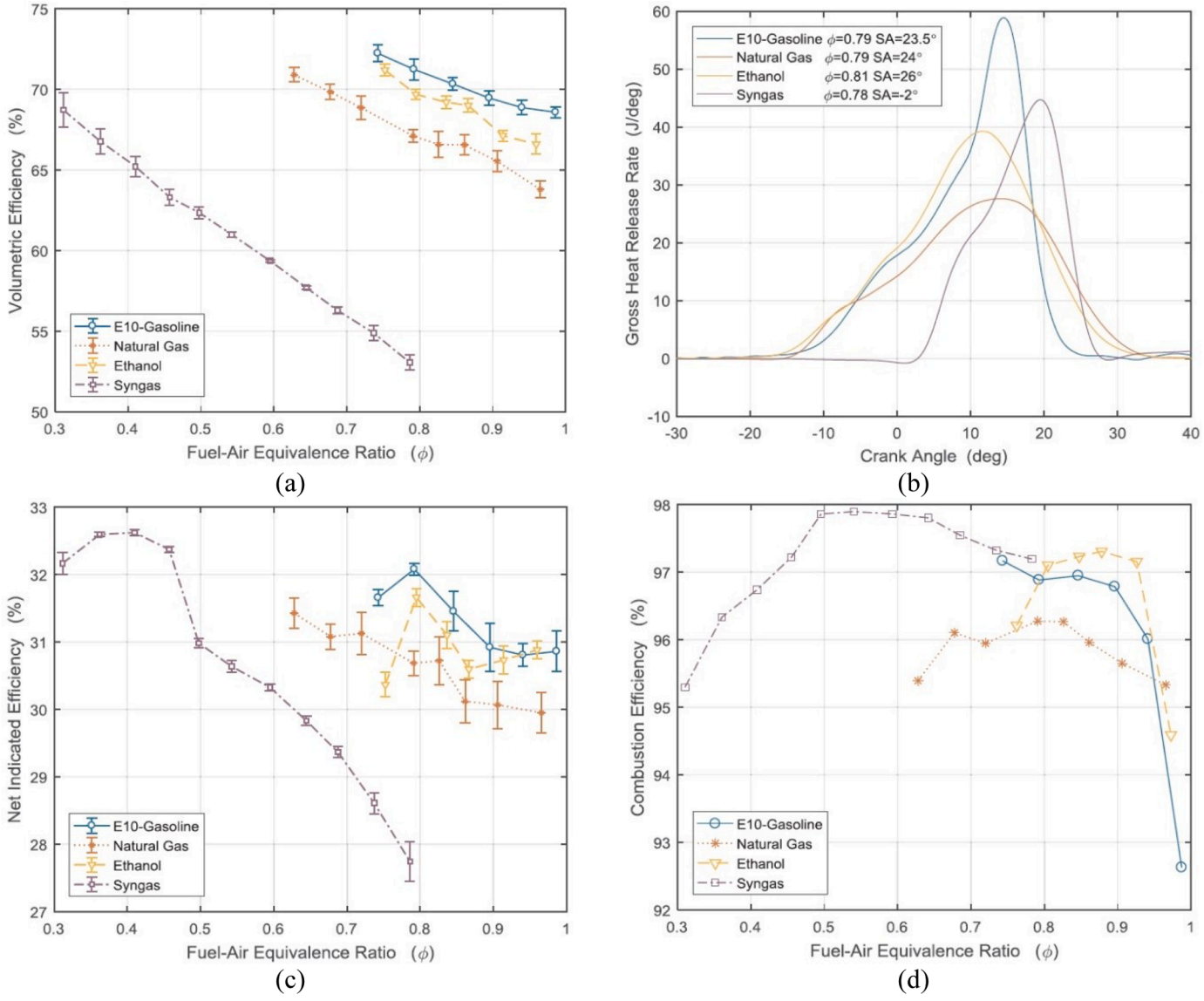

Fig. 20. Volumetric efficiency (a), gross heat release rate (b), net indicated efficiency (c), and combustion efficiency(d) for specified fuels at MBT timings and CR = 8:1 (Reprinted from [282] with permission of Elsevier).

efficiency, as can be seen in Fig. 20 (a). Moreover, the lowest $CA_{0\text{-}10\%}$ (flame development period) and $CA_{10\text{-}90\%}$ (rapid burn period) belonged to syngas because of the high laminar flame speed and high diffusivity of the H_2 content in syngas. However, the smaller quenching distance of H_2, which implies the flame could travel nearer to the cylinder wall, leading to higher heat loss, reducing the net indicated efficiency (Fig. 20 (c)) at closer stoichiometric conditions.

Another work [283] tried to draw a comparison between syngas, and biogas, biogas-syngas blend fueling cases in a NA SI engine at various MBT timings and at a fixed engine speed of 1500 rpm, using experiments and numerical simulations. The syngas used had a molar composition of 17% H_2, 15% CO, 4% CH_4, 15% CO_2, and the balance N_2 (HHV= 5.65 MJ/nm^3) and biogas had 65% CH_4, 35% CO_2 (HHV=25.83 MJ/kg). The corresponding ITE, NOx emissions, higher temperature, and maximum pressure derivative for both syngas and biogas fueling are shown in Fig. 21. As seen, all observed variables have a relatively distinct sensitivity to where ignition timing occurs, revealing that the previous work lacks a reasonable basis for comparison. Although the syngas fueled SI engine due to having high H_2, low CO_2, and presence of N_2 contents produces more NOx and has the highest temperature regions over the entire ignition timing sweep than the biogas one, lower NOx formation belongs to syngas, 3 g/kWh, rather than biogas, 7 g/kWh, at maximum MBT operation, where the maximum ITE happens (26° and 50° BTDC for syngas and biogas, respectively). Additionally, syngas fueling not only indicates 1.5% more ITE compared to biogas at maximum MBT, but also tends to maintain high ITE over the whole range of ignition timing in contrast to biogas, indicating the superior combustion characteristics of H_2 relative to CH_4.

3.1.2. 100% syngas in CI engines retrofitted to SI mode

To mitigate the power loss with syngas use in SI engines, Sridhar et al. [284,285] experimentally studied syngas combustion in a multi-cylinder SI engine modified from a diesel engine at varying CRs (11:5:1 to 17:1). Fig. 22 shows in-cylinder pressure traces at different CRs, which did not show any trace of knock for all the studied loads. Performance of the engine at higher CRs was smooth and proved that syngas use in the SI mode at higher CR is technically feasible. Homdoung et al. [286,287] also reported that for CRs as high as 17:1, the engine fueled with producer gas (PG, see section 1) could operate smoothly without knock risk. This was attributed to the faster burn rate due to the presence of H_2 in the PG. Although the maximum BTE for the PG engine was lower than the original diesel engine by about 3.5%, and the smoke density recorded in the diesel engine (1.5-12%) was much higher than that in the PG case (0-2%). Zero-dimensional (0-D) modeling was also employed to compare the brake power results obtained under a wide-open throttle (WOT) condition, and a good agreement was noticed

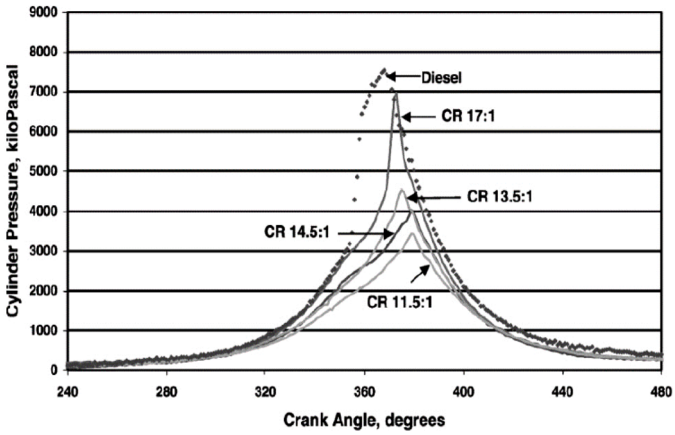

Fig. 22. In-cylinder pressure versus crank angle at different CRs (Reprinted from [284] with permission of Elsevier).

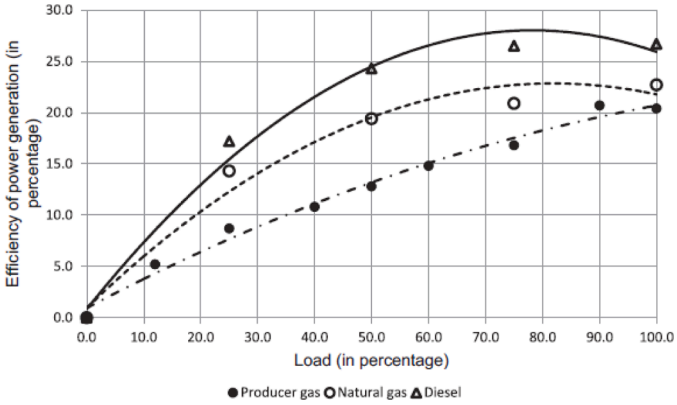

Fig. 23. Power generation efficiency of the syngas, diesel and natural gas engines at different loads (Reprinted from [289] with permission of Elsevier).

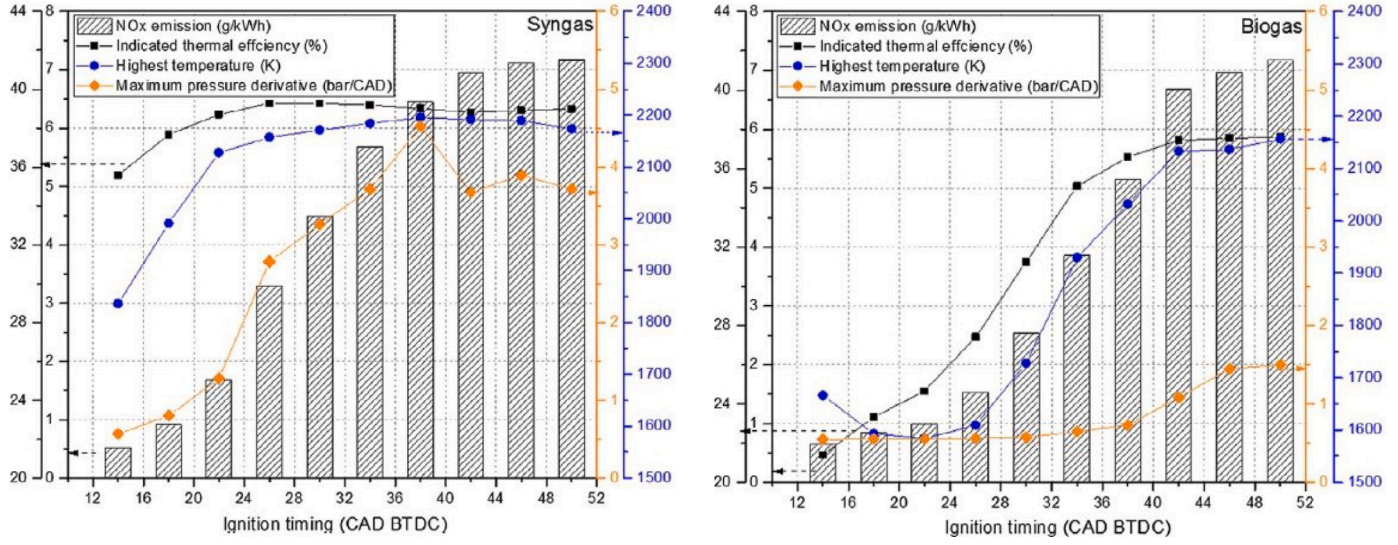

Fig. 21. The effects of ignition timing on other variables for syngas (left) and biogas (right) fueling, at CR= 12.9 and 1500 rpm (Reprinted from [283] with permission of Elsevier).

with experimental results [288].

Raman and Ram [289] studied the efficiency of a syngas-fueled engine at different loads. Fig. 23 illustrates the comparison of syngas, diesel, and natural gas engines in power generation efficiency at different load conditions. The maximum power generation efficiency of the diesel, natural gas, and syngas engine is 28%, 24%, and 21%, respectively. Again, a reduction in torque and power de-rating for the syngas engine was observed, but at a lower amount. The syngas engine operates at 21% power generation efficiency at the full load condition, which is about 20% and 10% less than that of the diesel and natural gas engines.

It can be mentioned that increasing the engine compression ratio through use of CI engines retrofitted to the SI mode is an efficient way to increase brake power. However, an average of 16% power loss can be observed in the gas mode compared to diesel operation at a comparable CR. Recently, Park et al. [290] demonstrated that high compression ratios and intake boosting could improve syngas (30% H_2, 25% CO, 45% CO_2) fueled SI engine power and efficiency. Engine operation with a high compression ratio of 17.1:1 was possible in the lean combustion mode owing to the low combustion temperature. The gross ITE in the lean combustion mode was 18.4% higher than that in the stoichiometric combustion mode, mainly because of a significant reduction in the heat transfer loss. However, the gross indicated power in the lean combustion mode was 25.6% lower than that in the stoichiometric combustion mode. In summary, stoichiometric operation using syngas was appropriate for a high-power engine generator, whereas lean operation using syngas is more suitable for a high-efficiency engine generator.

3.1.3. 100% Syngas in direct injection (DI) SI engines

Hagos et al. [291–293] were the first researchers to utilize syngas (50%H_2/50%CO) as the primary fuel in a direct-injection spark-ignition (DISI) engine, and then compared its combustion, performance, and emissions characteristics to those with CNG operation (as the baseline). It should be noted that besides overcoming the issues related to the volumetric efficiency of gaseous fuels, the backfire phenomenon is also being addressed by the DI ignition system. As well-known, implementation of gaseous injectors in comparison with liquid ones has its own difficulty in terms of injector geometry and engine-related characteristics such as the interaction between piston design[6] and the mixing process with late injection, injector width pulse, etc. An improvement to the previous work [272], as the authors stated, was a slight decrease in brake torque from ranging 20-30% to 14-19% at the same speed of 1500 rpm, due to eliminating issues attributed to volumetric efficiency penalty of delivering gaseous fuels at the intake. Despite the improvement, Hagos et al. [294] came across a limitation on the injection duration at late injection timings and higher BSFC with syngas fueling than CNG fueling. Thus, the engine operation was limited to near stoichiometric conditions, leading to a restriction in maximum brake power and a request for a bigger fuel tank. These all were attributed to the low LHV of syngas, which is lower than a fifth of LHV of CNG (see Table 5). To overcome this, in a series of works Hagos et al. [294–296] investigated enriching the syngas with methane (a higher LHV fuel) in a DISI engine. The new fuel was named methane enriched syngas (MES), consisting of H_2/CO/CH_4: 40/40/20 (% by vol.). It was found that the MES shortens the injection duration of syngas and extends the air/fuel stoichiometric ratio (λ) compared to CNG and syngas at the same engine speed. Furthermore, the MES improved the maximum BTE and the BSFC by 30.2% and 21.3%, with a little effect on the CO, NOx, and THC emissions [294] (see Fig. 24).

[6] Even by eliminating the physical processes associated with the spray of liquid fuel (droplet breakup to evaporation), a sufficient time for the charge mixing process at late injection is still needed because the shape of the piston head affects the charge distribution, which may result in an uneven air/fuel ratio in the chamber.

Following the work of Hagos [292], Fiore et al. [297] numerically investigated the effect of piston shapes and injection specifications on the performance and emissions of a syngas-fueled DI SI engine. The parametric study included three different piston bowl profiles and half-angles of injection of 30°, 45°, 52.5° and 60°. The SOI timing was also varied from 90° BTDC to 130° BTDC. They found that the Omega shaped profile can provide best performance, despite of maximum NOx emissions compared to the high clearance and low clearance combustion cups. The results were very sensitive to the injection angle and SOI, which affected the fuel distribution.

Particulate matter (PM) emission:

Compared to PFI engines, particulate matter (PM) emissions lead to a known big challenge in DISI engines, especially for ultrafine particles, which harmfully affect human health [298]. The sources of PM formation in DISI stem from mixture inhomogeneity because of a lack of time for fuel atomization and spray impingement, which depends on many factors, including operating engine conditions, air-fuel equivalence ratio, injection timing, spark timing, and fuel-specific properties [299]. While fueling a DISI engine with hydrocarbon-free gaseous fuels is seemingly expected to lead to lower particle emission, Thawko et al. [300] surprisingly showed a 170% increase in total particle concentration of reformate (H_2/CO_2:75/25 %by mole) fueling compared to gasoline at the same and fixed engine speed and load. The most likely reason for the high measured particle is attributed to the interaction between lubricating oil and high-pressure reformate jet, as the authors claimed. Due to its lower density, the required time for syngas fuel injection at high pressure is much longer than that for the liquid fuel. Besides, the small flame quenching distance of hydrogen content in syngas may result in the syngas flame traveling closer to the lubricated cylinder walls. Thus, the chance of lubricant participating in the combustion rises. In terms of particle size distribution, it was indicated that the nucleation mode (< 50 nm) is primarily responsible for the discrepancy in total particle number concentration between reformate and gasoline fueled DISI engines, as can be seen in Fig. 25 (right).

In contrast, Bogarra et al. [301] indicated that the addition of reformate (H_2/CO/CO_2/H_2O: 5/2.7/11/9.0 %vol.) plus EGR (called R-EGR, see Section 4.1) as supplementary fuel to gasoline in a gasoline direct injection (GDI) engine reduced the engine PM emissions even more than the addition of EGR only, as shown in Fig. 26. It was found that the reformate combustion can significantly decrease the PM emissions, however, the reduction was dependent on the PM nature. Reformate combustion was also found to remove soot cores more efficiently than the volatile PM. Moreover, fuel reforming technology did not show significant detrimental influence on the TWC operation for the studied conditions.

3.1.4. Syngas addition in SI engines

As mentioned earlier, a possible use of syngas in SI engines is as an additive to enrich or improve the performance of another fuel such as methane or a methane-rich biofuel (natural gas or landfill gas); and gasoline. Since syngas has a lower heating value than these two fuels, the improvement obtained by adding it is not really on the engine power but rather on the efficiency, combustion, and pollutant emissions. Concerning knock studies, Gerty and Heywood [302] experimentally investigated the performance of a knock-limited SI engine by considering the effects of relative air/fuel ratio, inlet boost pressure, compression ratio, and reformate added to the tested fuel-air mixtures. The tested fuels were: Unleaded test gasoline (UTG96, representing as gasoline or indolene fuel with octane number of 96), primary reference fuel (PRF, a mixture of iso-octane and n-heptane), and toluene reference fuel (TRF, a mixture of toluene and n-heptane). A bottled mixture, as reformate, of H_2/CO/N_2: 25/26/49 (% by vol.) was utilized to simulate the output of a POX fuel reformer (named Plasmatron, see subsection 4.1.1). The mixture was considered the replacement for a portion of the main fuel (gasoline), which then mixes with the gasoline in the intake manifold. Fig. 27 (a) shows the combustion retard, which was defined as

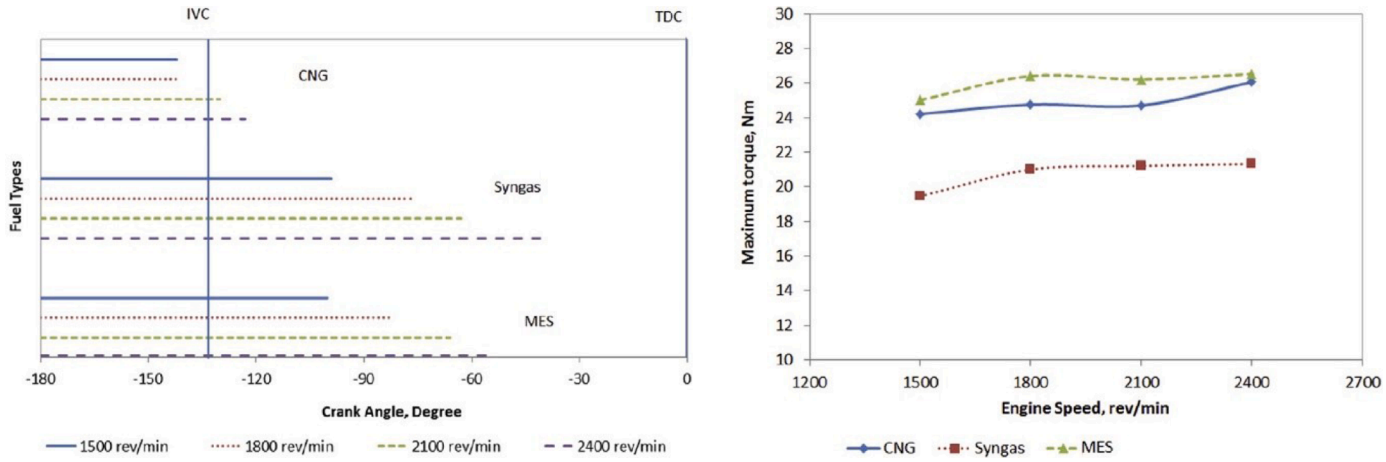

Fig. 24. Comparison of injection duration at maximum IMEP (left) and maximum brake torque vs. engine speed (right) for syngas, MES, and CNG at CR=14:1 (Reprinted from [294] with permission of Elsevier).

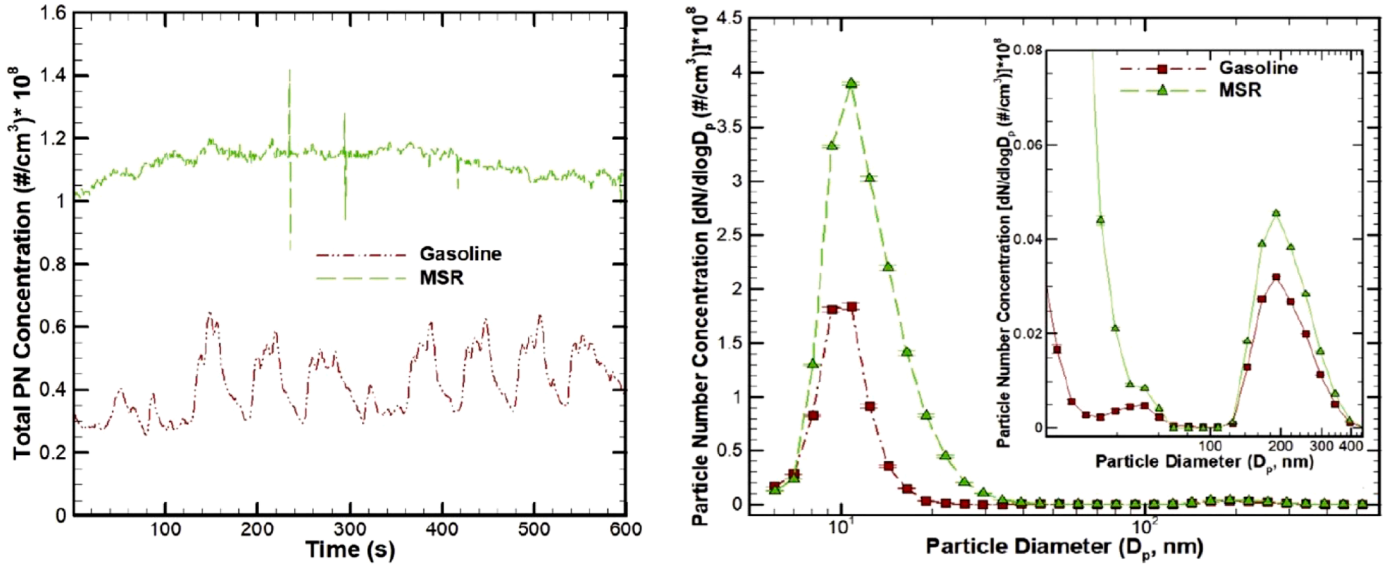

Fig. 25. Total PN vs. time (left) and total PN vs. particle diameter (right) comparisons between gasoline and methanol steam reforming (MSR) products as the fuel of a DISI engine at IMEP of 5 bar and engine speed= 2800 rpm (Reprinted from [300] with permission of Elsevier).

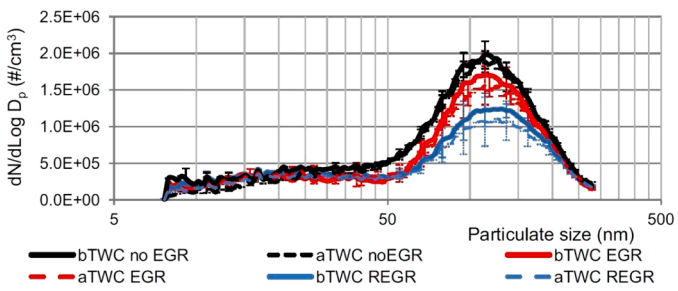

Fig. 26. Total PN vs. particle size comparison among no EGR, EGR, and REGR, as well as with after and before using the three way catalyst (TWC) operation (Reprinted from [301] with permission of Elsevier).

the combustion phasing disparity at the current state and the optimal one (i.e., MBT spark timing), as a function of reformate fraction. A reduction in combustion retard can be seen with increasing reformate fraction. The reduction with the addition of reformate for each fuel was normalized, as shown in Fig. 27(b). As can be seen, reformate addition was most effective when added to PRFs that are entirely composed of alkane hydrocarbons. The combustion retard needed to avoid knocking decreased by about 2° CA per 3% reformate fraction. When applied to TRF fuels composed of more than 20% n-heptane with octane numbers of 95 or lower, reformate addition was only marginally less effective than for PRF fuels. As the content of alkanes declined and the aromatic content increased, reformate addition seemed to be less successful for TRFs to the point where there was no value in reformate addition to pure toluene.

Using the same reformate and at low CR (9.8:1), a direct comparison between pure hydrogen and reformate additions showed that both of them could extend both peak efficiency and the lean limit of indolene combustion linearly [303,304]. On the contrary, at high CR (13.4:1), the reformate addition was no longer had a linear relationship, while pure hydrogen still indicated an obvious, proportional/linear extension of peak efficiency [305], as can be seen in Fig. 28 (left). The main reason for this behavior was due to the proportional extension of the location of the $\Delta\theta_{10-90\%}$=30°CA. However, no distinguishable curves were seen with increase of reformate, as shown in Fig. 28 (right).

Smith and Bartley [306] evaluated stoichiometric operation of natural gas + EGR and natural gas with syngas + EGR in a single-cylinder

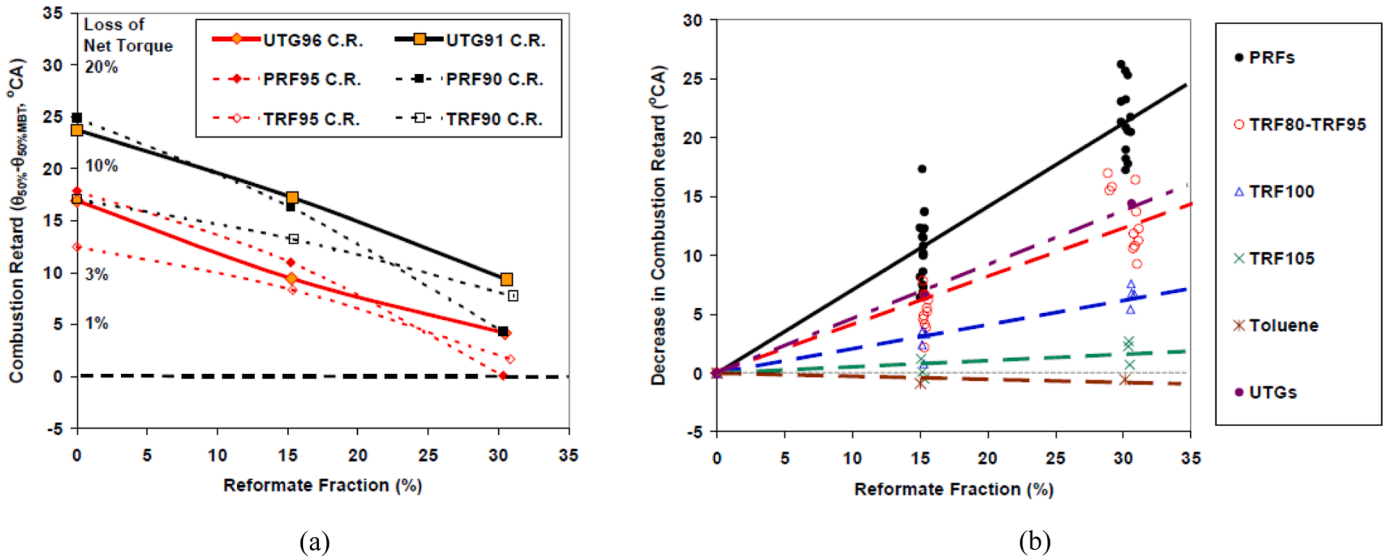

Fig. 27. a) Combustion retard to just avoid knock with increased reformate fraction for fuels with PRFs and TRFs; CR = 11.6:1, λ = 1.0, 1500 rpm, MAP for 40% boost (NIMEPMBT = 14.7 bar, 1.4 times un-boosted NIMEPMBT). b) Decrease of combustion retard with increased reformed fuel fraction at 1500 rpm, PRFs at λ = 1.0 (40% boost) and λ = 1.3, TRFs at λ = 1.0 (40% boost) and λ=1.3, and UTGs at λ = 1.3. Data is from all three compression ratios [302].

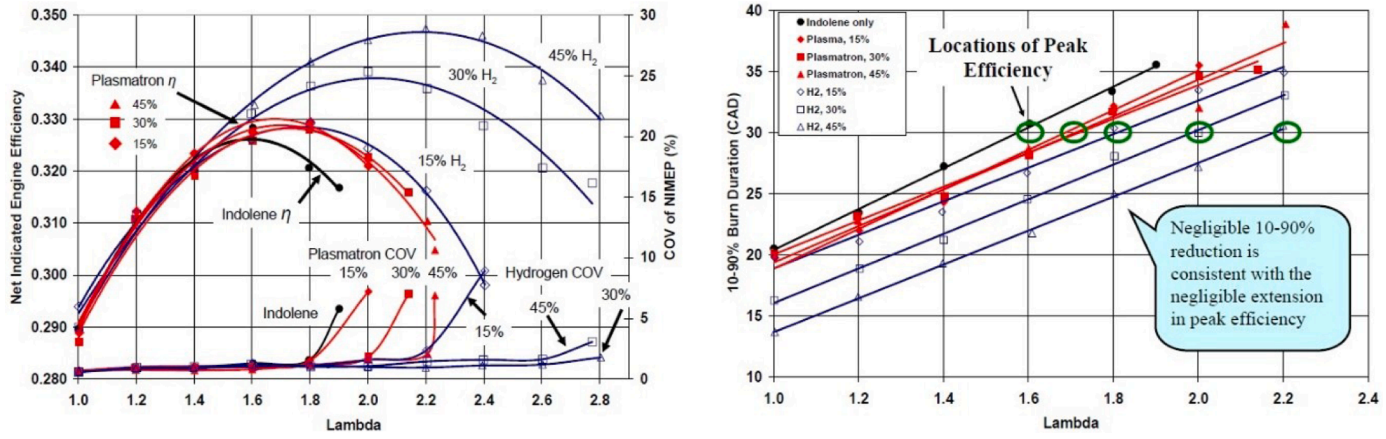

Fig. 28. Effect of air dilution on net indicated engine efficiency and CoV NIMEP (left) and on 10-90% burn duration (right) for various amounts of reformate (produced by Plasmatron) and pure hydrogen; at MBT, 1500 RPM, CR = 13.4:1, and NIMEP = 3.5 bar [305].

Caterpillar engine converted to SI operation. A 44% extension of EGR tolerance on a mass basis and a 77% reduction in raw NOx emissions for using syngas with natural gas were detected compared to the natural gas case. Cha et al. [307] experimentally investigated the operating characteristic of an SI engine for power generation upon mixing CH_4 and simulated syngas (H_2 and CO) in a diesel engine that was modified to run in the SI mode with a CR=13:1. Fig. 29 shows the fuel conversion efficiency versus NOx emissions for various fuel mixtures, where NOx emissions were elevated as fuel conversion efficiency increased. However, this increase was insignificant for syngas compared to H_2 or CO when added to CH_4-air mixtures at a ratio of 5% of the overall LHV. Since on-board fuel reforming methods can produce syngas as the primary fuel, this will be discussed in section 4.

A summary of the main research works published on syngas utilization in SI engine is presented in Table 9. Future study of 100% syngas-fueled SI engines can be followed in designing an appropriate injection system for gaseous fuel like syngas in DISI engines and applying advanced spark systems like multiple injections.

3.2. Syngas in HCCI engines

Research on syngas utilization in advanced combustion strategies has significantly increased due to its clean-burning properties and possible production from several paths. The homogeneous charge compression ignition (HCCI) engine is a low-temperature combustion (LTC) concept which combines the best features of SI and CI engines. The HCCI engine has shown the potential for higher efficiency and ultra-low NOx and soot emissions, however it has some drawbacks in terms of limited operating range, combustion control and excessive unburned products [319,320]. In this part, syngas-fueled HCCI combustion is analyzed in detail.

3.2.1. 100% syngas fueling

According to the finding of previously published papers, HCCI combustion with syngas has not shown superior performance over other fuels. It faces a similar barrier, such as the limited operating window and a need for regulating the intake temperature to control the combustion event. For instance, Stenlåås et al. [321] focused on HCCI combustion of 100% syngas, which was reformed methanol gas (RMG), a mixture of hydrogen and carbon monoxide in the volume ratio 2:1, and then

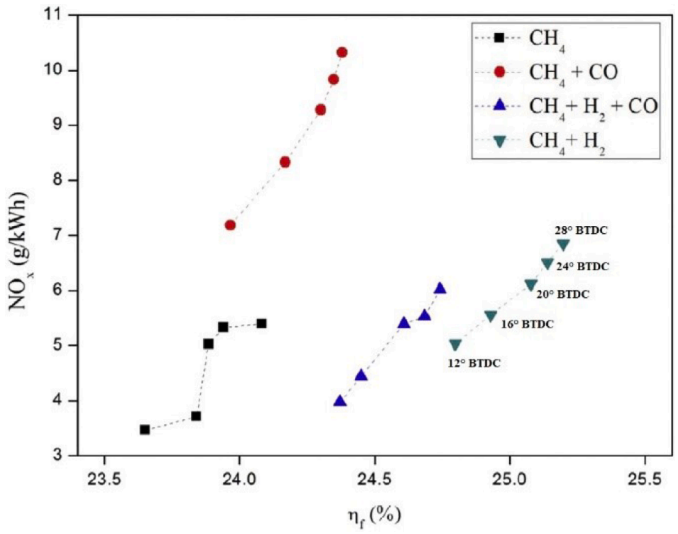

Fig. 29. NOx emissions versus fuel conversion efficiency for various components added to CH_4-air mixtures at different spark timings (Reprinted and modified from [307] with permission of Elsevier).

compared it to pure hydrogen fueling [322] in SI operating mode. They found that a higher temperature for RMG fueling than pure hydrogen was required to achieve the same combustion duration with HCCI mode. Both hydrogen- and RMG-fueled HCCI did not provide sufficient exhaust energy for the on-board reforming process by waste heat recovery. In summary, the operating mode based on 100% reformate was more favorable for SI mode operation.

Several years later, Bika et al. [323] measured the HCCI performance on 100% syngas fueling at two equivalence ratios, 0.26 and 0.30, and an engine speed of 1800 rpm, with a diesel engine converted to HCCI mode by adding PFI injection and intake air heating systems. Three compositions were considered: H_2=100%, H_2/CO=3/1, and H_2/CO=1/1 by volume. By increasing intake temperature, it was seen that the in-cylinder pressure, temperature, and heat release started to increase, and finally led to advancing the combustion phasing, which had combustion efficiency in the range of η_c = 83%-88%. Also, by altering the equivalence ratio towards leaner regions and increasing CO in syngas, the intake temperature was increased to maintain the best IMEP conditions.

With the aim of improving HCCI combustion and reduction of pollution emissions based on the syngas-air mixture, a few modeling studies [324,325] have been carried out to explore the effect of various species addition. Starik et al. [325] assessed the potential of the addition of a highly reactive species such as ozone or singlet delta oxygen (SDO) into an HCCI fueled with syngas (50%H_2/50%CO by volume). They noticed that the presence of 0.38% of O_3 mole fraction (=1% of SDO) in total oxygen could diminish the dependency on high intake temperature by accelerating and intensifying the ignition and combustion event, especially under the low load regime ($\varphi = 0.2$); this resulted in a 7-14% improvement of engine power output and up to a 15% reduction of both CO and NO emissions due to lack of excessO_2.

For better understanding of auto-ignition and combustion development in HCCI based on 100% syngas, Yamasaki and Kaneko [326] conducted an experimental and modeling study using mock syngas with varying compositions, ranging from 20% to 40% for H_2, 7-27% for CO, 20-40% for N_2, 10-30% for CO_2, and a 3% CH_4 by volume. An auto-ignition temperature of T=1100 K, almost similar to hydrocarbon fuels, was observed for syngas, governed by in-cylinder gas temperature and not by the fuel composition tested. It was also found that H_2 has a longer conversion time than CO during the combustion process, and combustion duration can be roughly determined by the volumetric ratio of H_2/ CO_2. For detailed analysis of the syngas combustion in HCCI combustion, Maurya et al. [327] used a stochastic reactor model (SRM) with a detailed chemical kinetic mechanism (32 species and 173 reactions) to numerically investigate syngas fueled HCCI combustion validated against previous experiments [323]. Within the SRM, a probability density function (PDF) was used to define the local (variable) and global (constant) physical parameters. For various engine operating conditions, simulations were performed by changing intake temperature, engine load, and speed at a constant compression ratio of 19:1, and the obtained operating window is shown in Fig. 30. The inclined hatched line represents operating conditions with a combustion efficiency of less than 80%. The area with PPRR > 5 MPa/ms is represented by the crossed hatched region, and the contour lines in the plot represent IMEP. Operating conditions with combustion efficiency higher than 80% and PPRR < 5 MPa/ms are considered as the operating area of the HCCI engine. It can be seen that increasing the intake temperature (or T_{ivc}, specified at intake valve closing) can help the operating range in the lean-side of stoichiometry, but at the expense of lowered IMEP due to decreased volumetric efficiency. At higher engine speed, suitable operating range has adversely shifted to a more bounded region that is highly sensitive to intake temperature and excess air (λ or air-fuel ratio). In this case, the chance of incomplete or vigorous combustion is severe. The maximum combustion efficiency of 98% is reported in the study.

While the abovementioned works have dealt with 100% syngas in the form of simulated reformate gas (with only H_2 and CO), there are a number of published works with producer gas generated from a biomass gasification process. Przybyla et al. [328] compared SI and HCCI fueled with low calorific producer gas under the same load; they reported that the syngas-fueled HCCI engine had extremely high CO and a lower indicated efficiency than SI, equaling a more than 10% loss in the base fuel's chemical energy. It is worth mentioned that the use of high intake temperature to control the combustion in syngas-fueled HCCI engines has been reported in previous works. Bhaduri et al. [329] employed high temperature strategy as a positive advantage over a syngas-fueled SI engine to introduce a novel concept of unprocessed syngas-fueled HCCI, which has tar contents and moisture. Because the intake temperature was set to around T=250°C, which is higher than the dew point of the tars, issues related to tar condensation were eradicated. According to the authors, moisture in syngas tends to delay combustion, while tars' effect was negligible. Nevertheless, such an intake temperature is not acceptable for vehicular applications, but the readers can refer to their later works [330–332] for in-depth information on this concept. We believe that a brief discussion of syngas impurities can also be useful here.

3.2.2. *Syngas addition*

Reformate as ignition controller:

The operating range of kinetically-controlled HCCI combustion is narrow due to lack of any direct control on ignition timing; this can lead to extremely high pressure rise rates corresponding to nearly constant volume heat release of a homogeneous air-fuel mixture in the combustion chamber at high loads (for low octane fuels), and poor combustion and misfiring at low loads (for high octane fuels). To mitigate this, various techniques such as intake charge preheating [333], EGR [334, 335], boosting [336,337], using two fuels with different reactivity (i.e., one has a high octane and the other has a high cetane number) [338, 339] have been proposed which proved to have a profound effect on control of ignition event. For more details about these techniques, one can refer to [340,341].

Syngas or reformate plays the role of the ignition-timing controller by either retardation (if it is the primary fuel with high octane number, e.g., syngas/diesel fueling case) or advancement (if used as the secondary fuel with higher combustibility characteristics, e.g., natural gas/syngas) of the main combustion, which leads to widening the load operating range of the HCCI engine. In the former case, syngas has two widespread effects on fuels, showing two stages of heat release such as diesel, n-heptane, and dimethyl ether (DME). These result in prolonged ignition delay times, and widened combustion duration (in other words,

Table 9
Summary of syngas utilization studies in SI engines.

Author(s)	Objective(s)	Syngas composition (% vol.)	Experimental info	Simulation	Finding(s)
100% Syngas in carbureted, port fuel injection (PFI), direct injection (DI) SI engines					
Mustafi et al. [272] (2006) [S]	A comparison study between 'Powergas', gasoline, and natural gas fueled SI engine	$H_2/CO/N_2$: 44/52/4.0 LHV= 15.3 MJ/kg	A 4-stroke, 1-cyl, SI engine, CRs= 8:1-11:1, rpm= 1000-2000, WOT, ITs = MBT timings	Engine simulation program ISIS	Compared to gasoline and CNG: 23-30% ↓ in brake torque, ↑NOx, ↑CO_2 while HC and CO were negligible.
Conte and Boulouchos [308] (2006)	Effect of RG addition on flame speed and flame front propagation in premixed, homogeneous charge gasoline engines	$H_2/CO/N_2$: 21/24/55 LHV= 5.3 MJ/kg	A 4-stroke, 2-cyl, PFI SI engine, CR= 8.7:1, rpm= 2000, BMEP= 2 bar, ITs = MBT timings	—	When the stability limit was met, combustion took place in a very similar way for different gasoline–RG blends.
Papagiannakis et al. [309] (2007)	Comparison between conventional natural gas (NG) and syngas fueled SI engine	$H_2/CO/CH_4/CO_2/N_2$: 19/29/6/8/38 LHV= 7.45 MJ/kg	A 4-stroke, 20-cyl, TC, SI engine, CR= 11:1, 1500 rpm	Two-zone thermodynamic model	↑syngas fuel concentration with ↑engine load: ↑peak cylinder pressure and an improvement of the engine efficiency. Compared to NG: ↑CO, ↑NOx emissions
Rakopoulos and Michos [310] (2008)	Development of a zero-dimensional, multi-zone combustion model for predicting the performance and NO emissions of a SI engine fueled with syngas	//	//	A zero-dimensional, multi-zone, thermodynamic combustion model	More reliable NO emissions prediction with multiple burned zones than single burned zone. Calculated NO were kept low at all engine loads (< 200 ppm) with lean combustion of syngas.
Shah et al. [277] (2010) [S]	Evaluation of syngas fueled SI engine-alternator and compared it with gasoline operation	$H_2/CO/CH_4/CO_2/N_2$: 13-19.4/16.2-24.2/1.2-6.4/9.3-13.8/balance LHV= 5.79 MJ/kg	A 4-stroke, 1-cyl, NA, SI engine, capacity= 5.5 kW	—	Lower power output (by about 1000 W), a significant ↑ in CO_2 (33-167%) but lower NOx (54-84%) and CO (30-96%) compared to gasoline operation
Arroyo et al. [281] (2013) [V]	Efficiency and emissions of a SI engine fueled with syngas, CH_4, and gasoline	Syn1: $H_2/CO/CH_4/CO_2$: 23/23/26/28 Syn2: $H_2/CO/CH_4/CO_2$: 40/39/11/10	A 4-stroke, 2-cyl, NA, SI engine, CR= 10.7:1, rpm= 2000-4500, loads= 50% and 100%, ϕ= 0.7-0.85-1, IT= 15°BTDC	—	Both syngas cases have ↑ CO_2 trend at all tested ϕ, and a ↓ BTE among others. Syn2 and CH_4 had the highest NOx and lowest CO, respectively.
Arroyo et al. [311] (2014) [V]	Combustion behavior of SI engine with syngas, CH_4, biogas, and gasoline	Syn1: // Syn2: // Biogas: CH_4/CO_2: 60/40	//	—	In all speeds and ϕ: CoV of IMEP: biogas>CH_4>syn1>gasoline>syn2. Maximum HHR and cylinder Pressure, highest NOx, and lowest HC belonged to syn2.
Arroyo et al. [312] (2015) [V]	Effects of IT and supercharging	//	//, various ITs= 11°-59° BTDC, intake boost= 1 to 1.3 bar	—	↑H_2, ↑CO, and ↓CO_2 contents: ↑advancement of IT retardation. Right ϕ and IT result in higher efficiencies than the gasoline. ↑boost pressure: ↓CO_2, ↓CO, ↑NOx, ~HC.
Hagos et al. [292] (2014)	First attempt at study on a direct-injected (DI) syngas fueled SI engine and compare it with CNG (baseline)	H_2/CO: 50/50 LHV= 17.54 MJ/kg	A 4-stroke, 1-cyl, DISI engine, CR= 14:1, rpm=1500-2400, ϕ= 0.67-1, a fixed SOI of 180° BTDC	—	Compared to CNG operation: ↓brake torque (14.2-19.6%) and ↓BTE (16.7%), and ↑BSFC. At higher loads: ↑NOx and ~CO. THC was negligible.
Hagos et al. [294] (2015)	Methane-enriched syngas (MES) in DISI engine	Syngas: // MES: $H_2/CO/CH_4$: 40/40/20 LHV= 24.4 MJ/kg	//	—	At all tested BMEP: BTE at 1500 rpm: CNG>MES>syngas. BTE at 2100 rpm: MES>CNG>syngas. BSFC at both rpms: syngas>MES>CNG. Little effect on CO, THC and NOx.
Hagos et al. [293] (2016)	Study of effect of injection timing on a syngas fueled DISI engine	H_2/CO: 50/50	//, SOIs= 120° and 180° BTDC	—	SOI= 120° compared to 180° BTDC: Better BTE, power, and BMEP at all engine speeds. With ↑speed, BTE started to ↓. THC, NOx, and CO all worsened.
Hagos et al. [295] (2017)	Effect of SOI timing on a DISI engine with 20% CH_4 augmented syngas	H_2/CO: 50/50 CH_4 augmentation: 20% (volume/volume)	//	—	Based on improved performance and emissions: the engine well-performed with SOI=180 but with SOI=120 just at lower speeds.
Hagos et al. [296] (2019)	Engine speed and A/F ratio (λ) effects on the CH_4 augmented H_2-rich syngas combustion in DISI engine	//	A 4-stroke, 1-cyl, DISI engine, CR= 14:1, rpm=1500-2400, ϕ= 0.3-0.8, SOI= 180° BTDC, WOT	—	With ↑λ: ↑CoV of IMEP in all speeds, ↑flame development and ↑flame propagation durations. All the durations were more sensitive to λ at lowest speed as compared to the other speeds.
Kan et al. [283] (2018)	Effects of IT, H_2 and CH_4 contents on SI engine fueled with syngas and biogas	$H_2/CO/CH_4/CO_2/O_2/N_2$: 17/15/4/15/0.14/48.86 Biogas: CH_4/CO_2: 65/35	A 4-stroke, 4-cyl, SI engine, CR= 12.9:1, rpm= 1500, ϕ=0.8, IT= variable	KIVA4-CHEMKIN	Under WOT and MBT operation: ITE (%): syngas (39) > biogas (37.5), NOx (g/kWh): syngas (3.3) < biogas (7.2) At advanced ITs: ↑H_2 (11-20% by vol.): was less sensitive to NOx change, than ↑CH_4 (55-88% by vol.).

(continued on next page)

Table 9 (*continued*)

Author(s)	Objective(s)	Syngas composition (% vol.)	Experimental info	Simulation	Finding(s)
Ran et al. [313] (2020)	The potential of lean SI combustion with E10, CNG, ethanol, and syngas.	H_2/CO: 60/40 LHV= 20.4 MJ/kg	A 4-stroke, 1-cyl, SI engine, CRs= 9:1-11:1, rpm= 1200, intake pressure= 0.75 bar, ϕ= 0.3-1, various ITs		With ↑CR: ↑engine efficiency and improved lean burn capability for all tested fuels. The leanest misfire limit (0.4<ϕ<0.7) was achieved with syngas with low NOx, low CO, and no THC.
100% syngas in CI engines retrofitted to SI mode					
Sridhar et al. [284] (2001)	Use of producer gas (PG) in engines at high CRs	H_2/CO/CH_4/CO_2/H_2O/N_2: 19/19/2/12/2/46 LHV= 4.5 MJ/kg	A 4-stroke, 3-cyl, NA, CI engine, CRs= 11.5:1-17:1, 1500 rpm, various ITs	—	Smooth combustion at CR=17:1. To achieve MBT, a retardation in spark timings is needed. Compared to diesel mode, at equal CR, the maximum power loss was 16% in SI mode with PG.
Sridhar et al. [131] (2005)	Develop a PG engine integrated with a biomass gasifier, with a new designed gas carburetor.	//	A 4-stroke, 3-cyl, NA, CI engine, CRs= 11.5:1-17:1 A 4-stroke, 12-cyl, TC, CI engine, CR= 12:1 A 4-stroke, 6-cyl, NA, SI engine, CR= 10:1	—	20 – 30% loss in power compared to diesel (baseline) case At CR =17:1 and maximum MBT: both NOx and CO were minimum.
Gamino and Aguillon [314] (2010)	Simulation of syngas combustion with a multi-spark ignition system	H_2/CO/CH_4/ CO_2/N_2: 6/25/5/11/53	—	2-D thermodynamic code and commercial CFD package, PHOENICS	A predictive model with capability to use in parametric studies of syngas combustion.
Ulfvik et al. [315] (2011)	Engine performance, efficiency and emissions of SI engine with PG and natural gas	H_2/CO/CH_4/CO_2/N_2: 30/20/1/15/34	A 4-stroke, 1-cyl, CR= 12.6:1, rpm= 1050, ITs= variable	—	Compared to NG: ↓NOx, ↓THC, and ↓maximum IMEP, ↑CO, wider the lambda range, with PG under comparable conditions.
Raman and Ram [289] (2013)	Comparison of PG engine with diesel and natural gas (NG) engines at various loads	H_2/CO/CH_4/CO_2/H_2O/N_2: 23/21/0.9/9.0/2.0/46.1	A 4-stroke, 6-cyl, NA CI engine, CR= 12:1, 1500 rpm, a fixed IT of 28° BTDC	—	At all loads: Overall efficiency: Diesel>NG >PG. Specific fuel consumption: PG>NG>PG. At full load the discrepancies were decreased.
Shivapuji and Dasappa [316] (2014)	The PG impact on overall engine performance with turbocharger (TC)	H_2/CO/CH_4/CO_2/H_2O/N_2: 19/19/2/12/2/46	A 4-stroke, 6-cyl CI engine, CR= 16.5 in CI mode and 10.5 in SI mode, 1500 rpm	zero-dimensional model	TC imbalance led to the highest power de-rating. The selection and optimization of TCs were described as the technique for recovering the loss of non-thermodynamic power.
Shivapuji and Dasappa [317] (2015)	Analysis of thermo-physical properties and experimental analysis of the proportion of fuel hydrogen on syngas fueled by SI engine	// – Effect of H_2 ratio	A 4-stroke, 2-cyl, SI research engine, CR= 11:1, 1500 rpm	CHEMKIN	↑H_2 part from 12.8% to 19.4% by vol.: ↑BTE ↑H_2 part up to 37.2% by vol.: ↑engine cooling load, ↓BTE, due to increasing the combustion stage
Cha et al. [307] (2015)	Study of a SI engine by adding syngas into CH_4, with a mixing ratio	H_2/CO: 50/50	A 4-stroke, 4-cyl, TC, CI engine, CR= 13:1, various ITs	—	↑Syngas mixing ratio (5%, 10%, and 15%): Combustion was improved, ↑fuel conversion efficiency, ↑NOx, and the rate of ↑ was non-linear. A/F and spark timings should be calibrated.
Homdoung et al. [286] (2015)	Effects of variable CRs, engine speeds and loads on the performance of a small engine operated on PG	H_2/CO/CH_4/CO_2/O_2/N_2: 8.5/30.5/0.35/4.8/6.3/49.55 8.5%H_2; 30.5% CO; 0.35% CH_4; 4.8% CO_2; 6.3%O_2 and 49.55%N_2	A 4-stroke, 1-cyl, CI engine, CRs= 9.1-17:1, rpm=1000-2000, load=20%-100%	—	The modified engine worked well at higher CRs with PG than with gasoline. Up to 23.9%, BTE was obtained. Rather to the original diesel: ↓BTE (11.3%), ↓engine's smoke density, ↑CO, with similar HC emissions.
Kim and Kim [318]	Feasibility assessment of hydrogen-rich syngas spark-ignition engine for heavy-duty long-distance vehicle application	H_2/CO/CO_2: 70/15/15	A 4-stroke, 1-cyl, CI engine, CRs= 15:1, rpm=1800	1-D multicylinder engine model in GT-SUITE	The vehicle with the syngas engine could travel for 152.6 km without refilling. The syngas bus exhibited lower fuel consumption than the equivalent CNG bus by 15%.

Denotations: ↑: increase, ↓: decrease, ~: nearly constant or insignificant, //: similar to above.
IMEP: indicated mean effective pressure, CR: compression ratio, ITE: indicated thermal efficiency, BTE: brake thermal efficiency, CoV IMEP: coefficient of variation of IMEP, TC: turbocharge, NA: naturally aspirated, IT: ignition timing, SOI: start of ignition, ϕ: the fuel/air equivalence ratio, WOT: wide open throttle, and MBT: maximum brake torque.

smoother combustion). This can be justified according to the following:

1- Dilution (or concentration) effect: O_2-deficiency happening by replacing O_2 with H_2 leads to weakening the low-temperature HR (LTHR or partial oxidation) stage of the fuel, which is a preparation step of combusting the in-cylinder mixture, resulting in lowering the hydroxyl (OH) concentration, and thus retarding the high-temperature HR (HTHR or combustion). It was shown that the magnitude of LTHR has a direct correlation with advancing or retarding the HTHR [342].

2- Chemical effect: OH generated from the first HR stage may be consumed by hydrogen (i.e., $H_2 + OH = H_2O + H$), suppressing chemical kinetics of the mixture before the combustion.

In the latter case, the strong thermal effect of syngas on high octane fuels like natural gas may result in rising the specific heat capacity of the mixture and increasing the compression temperature of in-cylinder charge eventually, depending on intake temperature. To highlight the thermal effect, valving strategies may be helpful without needing intake preheating. Eng et al. [343] reopened the exhaust valve during the

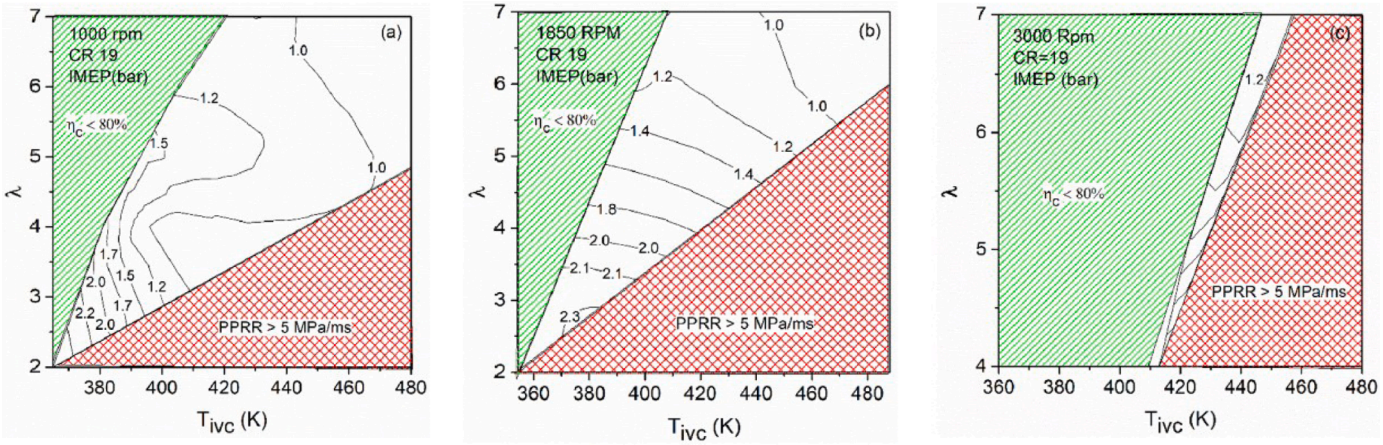

Fig. 30. Operating range for syngas fueled HCCI engine under various engine speeds at a constant compression ratio [327].

intake stroke to obtain more hot gases in the cylinder, i.e., exhaust re-breathing. The combustion chamber of an HCCI-mode engine fueled with iso-octane and partial oxidation gas (POX gas) added to the intake experiences a high quantity of internal residuals and thermal stratification; this causes the ignition timing to advance. Another technique is negative valve overlap (NVO), in which the residuals are trapped and recompressed, as described in section 4.

Dimethyl ether (DME) has some more interesting combustion characteristics than diesel (i.e., soot-free combustion and lower NOx emissions), but still faces challenges with regard to its physical properties (i.e., low viscosity, which leads to higher leakage and in turn engine durability concerns) [344]. Similar to syngas, DME can benefit from on-board fuel reforming in vehicles via a methanol-steam reforming process [345]. With these mentioned potentials for DME, and emerging dual-fueling strategies for achieving controllable HCCI combustion, Shudo et al. [346–351] conducted a number of experiments supported by chemical kinetics analysis, to run a single-cylinder SI engine converted to the HCCI mode fueled with DME and MRG (methanol reformed gas or syngas). Both fuels were produced from endothermic methanol steam reforming using engine exhaust gases, and then followed by methane dehydration for DME generation; with a single fuel tank required for liquid methanol, as seen in Fig. 31 (left). While using simulated reformate comprising 67% H_2 and 33% CO (by volume) in the experiments, they found that ignition of the second heat release (main combustion) and engine load could be controlled by altering the proportion of the MRG/DME ratio; by increasing the ratio, the overall system efficiency reached 49% and a 14% rise in engine efficiency over the baseline was obtained (see Fig. 31 (right)). This controllable HCCI concept was achieved due to delayed ignition and increased temperature before the main combustion, corresponding to the hydrogen content of the MRG. Similarly, they proposed this concept by storing a tank of DME and partial oxidation of it to produce DME reformed gas (DRG) [352].

They stated that this concept with HCCI combustion can result in high thermal efficiency over a wide operable window of equivalence ratio and high overall system efficiency, which is comparable to the fuel cell system. A brief summary of their work is given as follows:

1- Using an optimal compression ratio along with a suitable DME/MRG ratio (with increasing amount of MRG) resulted in a higher thermal efficiency for HCCI combustion, and a higher overall thermal efficiency can be achieved by using waste heat recovery (WHR) [346].
2- Higher compression ratio led to advanced ignition timing, but with higher heat transfer (cooling) loss [346] due to the small quenching distance and fast burning velocity of hydrogen content in MRG (syngas) [353].
3- While both H_2 and CO have influence on retarding the second stage HR, the role of H_2 is much more intense due to having a larger effect on first stage HR by consuming the OH radical [347]. Also, combustion of hydrogen during LTHR is controlled by $H + O_2 \rightarrow OH + O$ and less reactive HO_2 [349]. CO_2 also caused a slight retardation [348].
4- Despite larger amounts of H_2 being useful for ignition control effects, H_2 has a lower effect on WHR.
5- Highest overall thermal efficiency was expected from thermal decomposition [350] and highest output would be from steam reforming, which resulted in MRG with higherH_2 content.

A collection of works [354–356], which have studied use of a catalytic reforming reactor in the exhaust stream of a natural gas HCCI engine, have shown that hydrogen-rich gas could be a substitute for intake preheating for the same emitted NOx, greatly benefiting low engine loads. These works have been expanded to form on-board fuel reforming strategies, which are called reformed exhaust gas recirculation (R-EGR), as described in the next section. Those works concluded that employing

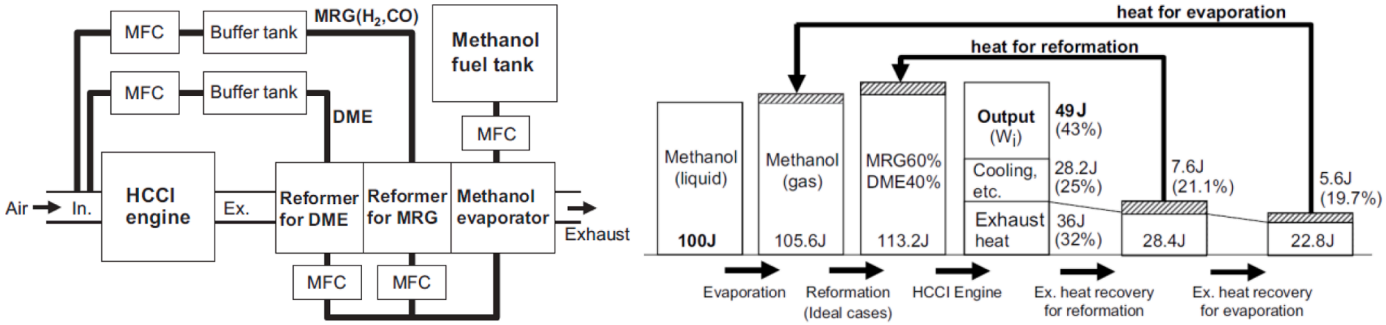

Fig. 31. Schematic of proposed concept (left) heat balance of this concept (right) (Reprinted from [349] with permission of Elsevier).

on-board fuel reforming products to extend the lower load-limit, along with using the supercharging and high internal EGR technologies for increasing the upper load-limit could be a solution for extending the entire operating window of HCCI engines fueled with natural gas or gasoline [357].

At the University of Alberta, a series of research works have been experimentally conducted to capture the effect of reformer gas (RG) blending on the base fuels, including high-octane primary reference fuels (PRF) [358], low-octane PRF [359], natural gas [360,361], n-heptane [361,362], and iso-octane [361] in a variable compression ratio, single-cylinder CFR engine operated in the HCCI mode. The effect of varying RG blend fraction ($\frac{m_{RG}}{m_{RG}+m_{base\_fuel}} * 100$) was studied, while intake temperature, air-fuel ratio, and EGR were kept constant. For low-octane PRF, such as PRF0 (i.e., 100% n-heptane) and PRF20 (i.e., 20% iso-octane and 80% n-heptane), it was observed, in conformity with the above discussion, that increasing values of RG replacement leads to a retarded and prolonged combustion event even after TDC [359]. As a reported case, 20% of RG replacement delayed the start of combustion (SOC) by about 14 CAD (3 ms) and lengthened the combustion duration by 50%, and increased the indicated power and thermal efficiencies by 17% and 12%, respectively. This remarks that combustion can be controlled by syngas without using other strategies like preheating the intake charge, adjusting dilution level or EGR, and by using valving strategies, which do have slow response or penalty in engine power. They also applied a similar procedure to high-octane PRF [358], PRF80 and PRF100, except by increasing CR and intake temperature (from 100°C to 140°C). Fig. 32 displays representative in-cylinder pressure traces and their corresponding heat release. As can be seen, the peak in-cylinder pressure and pressure rise rate were reduced by increasing the RG, with peak pressure shifting from approximately TDC to approximately 10° ATDC. RG substitution effectively smoothed combustion by retarding the combustion phasing towards a more efficient timing for HCCI combustion, and by widening the combustion duration. Replacing RG did not impact NOx emissions but increased CO and HC marginally, therefore, with a slight decrease in combustion efficiency. The indicated fuel conversion efficiency was slightly increased, because the combustion phasing was better than the baseline case. It was found that 40% of RG blended in a PRF80 fuel (by mass) has an octane number as close as PRF100, but with totally different combustion characteristics. Thus, the calculated octane number is not a good indicator of the characteristics of HCCI combustion.

Later in 2008, the same researchers [361] examined the effects of varying simulated RG compositions on HCCI combustion timing with natural gas, iso-octane, and n-heptane. The RG compositions chosen had H_2/CO ratios of 3/1 (H_2/CO=75/25 %by volume) and 1/1 (H_2/CO=50/50 %by vol.). The first and latter are a typical output of natural gas steam reforming and gasoline partial oxidation in an on-board fuel reformer, respectively. Fig. 33 reveals the impact of two selected RG compositions on ITE and SOC for selected fuels. For iso-octane, both compositions retarded the combustion timing similarly (i.e., +1.5 CAD per each 10% of RG); which implies that iso-octane may behave more sensitively to the thermal effect than the chemical effect of the H_2 content in RG. Also, at the same IMEP, the RG 75/25 moved the mixtures towards the richer region compared to the RG 50/50, which was operated at the leaner condition. Fig. 33(a) shows the ITE with the expanded rich-limit of RG75/25 decreased, presumably due to increased heat transfer losses. For natural gas, both compositions advanced the combustion timing with no obvious discrepancy by increasing the specific heat ratio and compression temperature of the mixture. The supporting modeling studies showed that the thermal effect is dominant, and the chemical effect arising from the various compositions used has an insignificant effect. Also, ITE with RG75/50 is increased due to H_2 properties in extending the lean limit of the mixture (see Fig. 33(c)).

For n-heptane, both compositions retarded the combustion timing by suppressing the LTHR stage (see Fig. 33(e)), in which H_2 indicates a stronger effect than CO (see Fig. 34). Indicated efficiency of the RG 75/25 fueling decreased after reaching an RG fraction of 10%, staying away from optimal combustion phasing of n-heptane, with more retardation (see Fig. 33(b)).

Thus, it is evident that RG with emphasis on the H_2 content acts as an LTHR inhibitor (chemical effect) due to its participation in low temperature oxidation for fuels having two-stage heat releases like n-heptane, PRFs, and DME. In this regard, Gou et al. experimentally [364] and numerically [365] studied the thermal, chemical, and dilution effects of hydrogen enrichment on HCCI fueled with n-heptane. Recently, based on numerical validation against experimental data acquired from the work of Hosseini and Checkel [358,359], multi-zone modeling studies with detailed chemical kinetics and with artificial inert species have been carried out to assist in the fundamental understanding of the chemical, dilution, and thermal effects of RG blending on the base fuels during the HCCI combustion [363,366-370]. For n-heptane [370] and low-PRF fuels [368], the dominance of the chemical effect among other

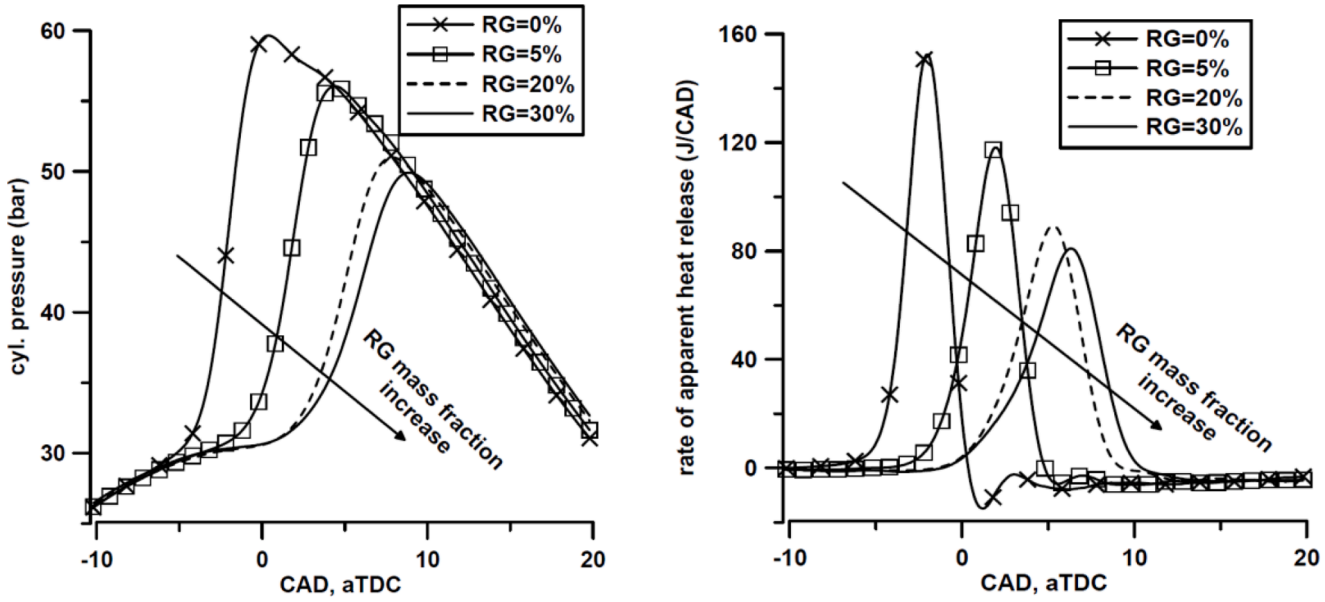

Fig. 32. Effect of reformer gas on in-cylinder pressure traces and heat release rates with PRF80 at CR = 14.4:1 and EGR = 33% [363].

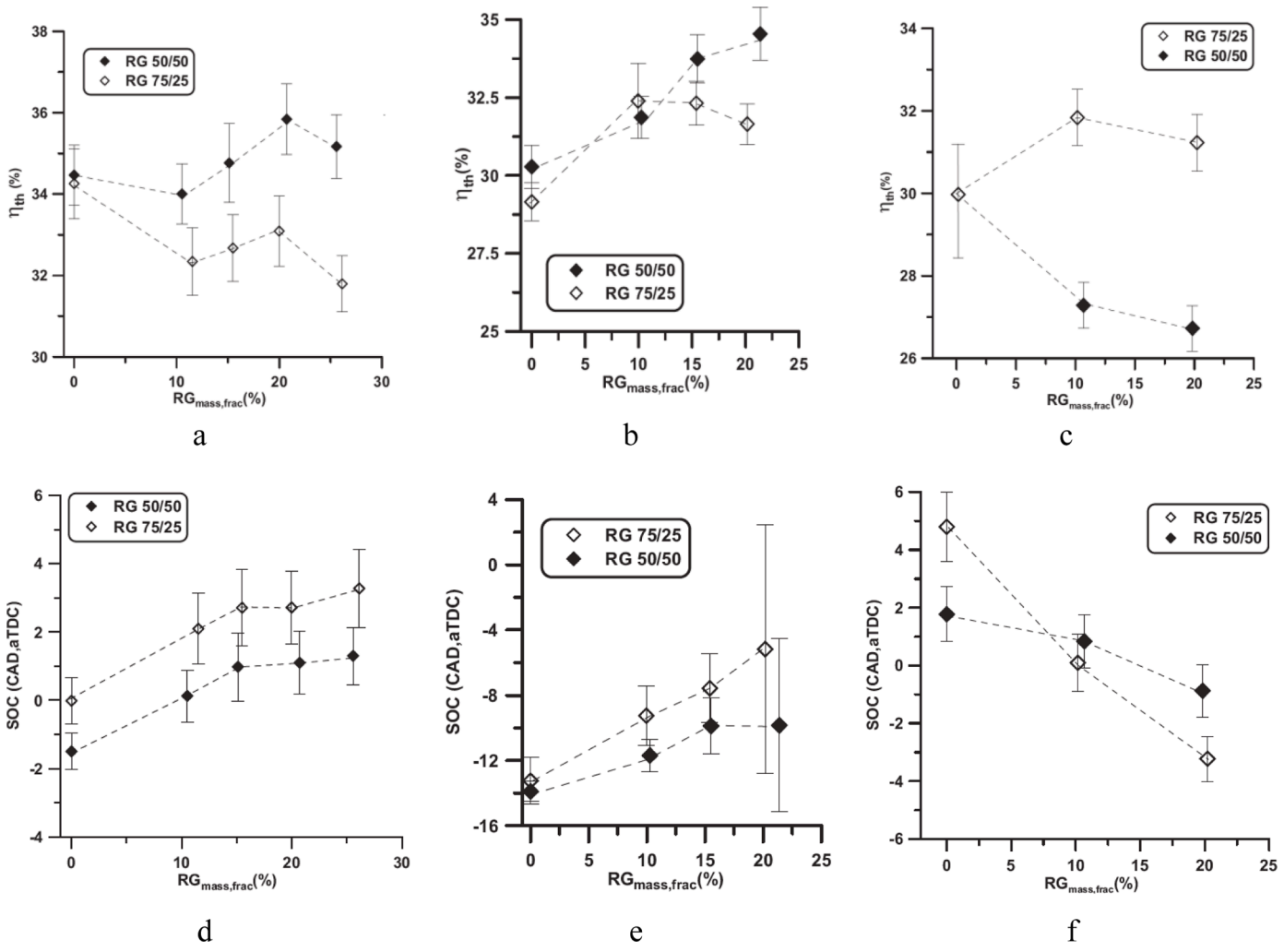

Fig. 33. Effect of RG composition on ITE and start of combustion of HCCI combustion of iso-octane (a & d), n-heptane (b & e), and natural gas (c & e) [361].

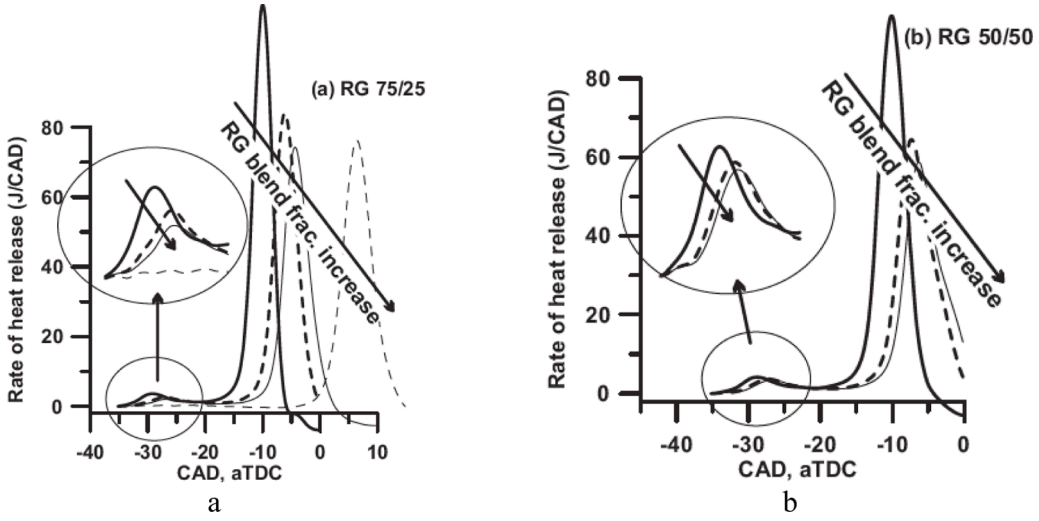

Fig. 34. Heat release of HCCI combustion of n-heptane for: (a) RG 75/25 and (b) RG 50/50 [361].

effects on retarding the SOC was confirmed, mostly due to H_2 presence in low-temperature oxidation reactions during the negative coefficient temperature or NTC (period between LTHR and HTHR). For high PRF fuels, the dilution effect increases by increasing the PRF number [368].

Table 10 summarizes the main syngas works on HCCI engines published in the literature. Syngas as a primary fuel of an HCCI engine has serious obstacles such as its lower combustion efficiency than 90%, high CO emissions, and excessive dependency on intake preheating and high

Table 10
Summary of syngas utilization studies in HCCI engines.

Author(s)	Experiments/Simulation	Main fuel	Fuel addition (% by volume)	Objective(s)	Finding(s)
Syngas addition (Bold ones showed retarding effect on SOC), others showed advancing effect on SOC)					
Shudo and Ono [346] (2002)	1-cyl SI converted to HCCI, CR= 8.3, 9.7, 12.4, 15.8, rpm= 1000, T_{intake}= at room temp.	**Dimethyl-ether (DME)**	A model gas for methanol reformed gas (MRG): H_2/CO: 67/33	Using onboard generated DME and MRG by waste heat recovery to control HCCI combustion timing	Combustion ignition timings were controlled by DME/MRG ratio. With ↑ CR: HRR advances and cooling loss increases
Peucheret and Wyszynski [354] (2004)	A modified 1-cyl SI, CR= 12.0-14.5, T_{intake}=140°C-230°C	Natural gas (NG)	10% of Reformate was added into intake. $H_2/CO/CH_4/CO_2/O_2/N_2$: 10/0.3/0.4/9.0/0.8/79.5	A solution to: High auto-ignition of NG fueling needs a high compression ratio (CR) and high intake temperatures at low load	Proposed an onboard catalytic exhaust gas fuel reforming strategy for NG HCCI engine. Stable combustion Lower intake temperature requirement ↓ NOx ↑ HC ↑ CO.
Hosseini and Checkel [360] (2006)	1-cyl CFR, CR= 16.0, 17.0, 18.5, rpm= 470, 700, T_{intake}= 140°C	CNG	Reformer gas (RG) was introduced to the intake charge (0-60% replacement with the main fuel by mass) H_2/CO = 3/1	A solution to: Pure NG-fueled HCCI with knock severity, high NOx and low performance	By ↑ RG replacement fraction: Expanding the operating window to very lean range: ↓ Knock ↓ NOx ↑ CO ↑ Combustion eff.
Hosseini and Checkel [358] (2007)	1-cyl CFR, CR= 14.4, 16.0, rpm= 700, T_{intake}=140°C	**PRF80 (20% n-heptane, 80% iso-octane) PRF100**	RG (0-40% replacement by mass) RG1: H_2/CO = 3/1 RG2: H_2/CO = 1/1	A solution to SI at part load: RG effects on high octane fueling in an engine with dual SI/HCCI modes (improving HCCI operating at part load)	By ↑ RG replacement fraction: Expanding and shifting the engine operating window towards ultra-lean: ↓ Maximum cylinder pressure ~ NOx ↑ HC ↑ CO ↓ Combustion efficiency.
Hosseini and Checkel [359] (2007)	1-cyl CFR CR= 9.5, 11.5, rpm= 700, T_{intake}= 100°C	**PRF0 PRF20**	RG (0-40% replacement by mass) H_2/CO = 3/1	A solution to high emissions of diesel engines: RG effects on low octane fueling in an effective HCCI	By ↑ RG replacement fraction: Expanding the engine operating window on the rich side: ↓ Peak cylinder pressure and PRR ↑ IMEP ↓ CoV IMEP ↑ Engine power ~ NOx ↑ HC ↑ CO.
Hosseini and Checkel [361] (2008)	1-cyl CFR, CR= 14.4, rpm= 800, T_{intake}=100°C	**iso-octane**	H_2/CO = 3/1 H_2/CO = 1/1	Thermal and chemical effects of RG blending	At high initial temperature: Thermal effect dominates (advancing the combustion phasing). At moderate temperature: Chemical effect dominates (retarding the combustion phasing). Overall: insignificant effect on combustion
Hosseini at al. [371] (2009)	1-cyl CFR CR= 11.8, rpm= 800, T_{intake}= 110°C	**n-heptane**	RG blending (0-40% replacement by mass) RG1: H_2/CO = 3/1 RG2: H2/CO = 1/1	A solution to: Knock propensity at high load	With RG blend fraction of 10%: 4.4° CA retardation in SOC, ↑ H_2content was more effective in retarding, ↑IMEP by 0.25 bar, ↑ITE by 2.8%
Voshtani et al. [372] (2014)	Single-zone and multi-zone thermodynamic-kinetic models, based on [360]	NG	RG1: H_2/CO = 3/1 RG2: H_2/CO = 1/1	RG enrichment effects on a HCCI combustion engine operating with NG.	Both chemical and thermal effect advance the SOC, but dilution retards that. chemical > dilution > thermal H2 and CO in RG at low and high amount of RG have strong responsibility of altering SOC.
Zheng et al. [373] (2014)	Zero-dimensional (0D) and three-dimensional (3D) combustion models	**DME**	DME reformed gas (DRG) produced by REGR strategy: H2/CO: 66.7/33.3	Effect of REGR on HCCI fueled with DME	REGR (EGR + DRG): can delay ignition time, allowing main combustion closer to TDC, minimizing negative compression work. Compared to EGR-only: ↓HC, ↓CO.
Neshat et al. [368] (2016)	Multi-zone model and semi detailed chemical-kinetic mechanism	**PRFs**	(0-30% replacement) H_2/CO = 1/1	Effect of RG blending on HCCI combustion of PRFs	By RG addition: ↓ H abstraction reactions rate ↑ decomposition fuel time ↓ LTHRR peak. ↑ PRF number: ↑ dilution ↓ chemical effect. ↓ NOx ↑ HC ↑ CO
Reyhanian and Hosseini [370] (2018)	Multi-zone model with detailed chemical-kinetic mechanism + an artificial inert species method	NG **iso-octane normal-heptane**	H_2/CO = 3/1	Understanding of various effects of RG addition, with composition of RG in HCCI combustion	Thermal effect: SOC was advanced for all fuels. Chemical effect: SOC was advanced with NG and iso-octane and retarded with n-heptane, mainly due to H2. Dilution effect: SOC was retarded for all fuels.
Kozlov et al. [374] (2018)	2D CFD simulation At ϕ= 0.2, 0.4	**iso-octane**	H_2/CO = 2/1	Combustion and emission characteristics of HCCI operating on iso-octane/syngas	Ignition timing and combustion duration were retarded and decreased, respectively, especially at ϕ= 0.2.

(*continued on next page*)

Table 10 (*continued*)

Author(s)	Experiments/Simulation	Main fuel	Fuel addition (% by volume)	Objective(s)	Finding(s)
					↑ NOx at ϕ= 0.4 ↓ HC ↓ CO at ϕ= 0.2
100% syngas fueling (%vol)					
Achilles et al. [375] (2011)	Modified, 1-cyl truck/bus engine, CR= 22.5:1, 1050 rpm, T_{intake}=80-180°C for NG, T_{intake}=75-145°C for PG	PG: $H_2/CO/CH_4/CO_2/N_2$: 30/20/1.0/15/34	—	Comparing producer gas (PG) and natural gas (NG) in HCCI engine	PG as compared to NG fueling: Wider ϕ range, faster combustion, more smooth and stable, ↓maximum IMEP, ↓intake temperature requirement, ↓THC, and ↑CO emissions.
Bika et al. [323] (2012)	1-cyl engine, CR=21.2:1, 1800 rpm, T_{intake}=60-90°C	RG 1: H_2/CO: 75/25 RG 2: H_2/CO: 50/50	—	Studying HCCI engine with two different syngas compositions at ϕ=0.26 and 0.3	↑CO fraction in RG: ↑auto-ignition temperature, ↑intake temperature requirement, ↓combustion efficiency (83-88%). At low load and high intake temp.: ↑↑heat transfer to wall.
Przybyla et al. [328] (2016)	SI engine with CR=8.2, HCCI engine with CR=20, T_{intake}=132-153°C	$H_2/CO/CH_4/CO_2/N_2$: 10.1/24.9/2/5.2/57.8	—	Fueling of SI (ϕ=1) and HCCI (ϕ=0.5) engines with low heating value PG	ITE: SI>HCCI by about 3.5%, Energy loss in exhaust based on chemical energy of the fuel: HCCI (10%) > SI (2%). The SI efficiency can be easier than HCCI optimized.
Bhaduri et al. [329] (2015)	Air cooled mono-cylinder HCCI engine CR= 12, rpm=1500, T_{intake}=230-270°C	H_2:CO ratio from 30:70 to 55:45%	—	Proposing a novel tar-tolerant HCCI engine in response to various syngas compositions (with water and tars)	Moisture in syngas: water's damping effect on chemical reaction rate, delay in combustion (positive effect). Tars in syngas: ↑LHV of syngas, but their effect on the combustion phasing were negligible.
Bhaduri et al. [330] (2016)	Air cooled mono-cylinder HCCI engine CR= 12.2, rpm=1500, T_{intake}=250°C	$H_2/CO/CH_4/CO_2/N_2$: 15-25/15-25/1-3/8-15/balance	—	Testing the stability of the engine in response to the naturally occurring random variations in the syngas composition	Over a 24 h test: high ITEs of 33%-39%, a low IMEP of about 2.5 bar, and a relatively high NOx (due to ammonia in the syngas) were observed.
Bhaduri et al. [376] (2017)	Air cooled mono-cylinder HCCI engine CR= 12.2, rpm=1500, T_{intake}=250°C	$H_2/CO/CH_4/CO_2/N_2$: 18/22/1.0/11/48	—	EGR effect on a tar tolerant HCCI engine	↑EGR from 0% to 25%: ↑IMEP from 2.5 bar to 3.3 bar, via damping maximum pressure rise and allowing higher ϕ.
Starik et al. [377] (2017)	Zero-dimensional single-zone thermochemical model	H_2/CO: 50/50	—	Improvement of combustion in a syngas fueled HCCI engine by adding ozone or excited oxygen molecules	Ignition can be accelerated before TDC, thus ↓intake temperature. At the same IT, 1% of SDO in total oxygen may ↑ the power by 7-14% compared to the base case with higher intake temperature.
Jamsran et al. [378] (2021)	1-cyl 126TI-II series, Doosan Infracore, CR= 17.1, rpm= 1800, T_{intake}=140°C-140°C-230°C	H_2:CO:CO_2: 30/2545 30/15/55 15/25/60 15/15/70	—	Investigate the combustion and emissions of an HCCI engine with various syngas compositions	↑ intake temperature and boosting: Low-calorific syngas (15% H_2, 15% CO, and 70% CO_2 3.34 MJ/Nm^3) can be auto-ignited

Denotations: ↑: increase, ↓: decrease, ~: nearly constant or insignificant, //: similar to above.
IMEP: indicated mean effective pressure, CR: compression ratio, ITE: indicated thermal efficiency, BTE: brake thermal efficiency, CoV IMEP: coefficient of variation of IMEP, TC: turbocharge, NA: naturally aspirated, IT: ignition timing, SOI: start of ignition, ϕ: the fuel/air equivalence ratio, WOT: wide open throttle, and MBT: maximum brake torque.

compression ratios, hindering it from progress in vehicular engines. In contrast, syngas as a fuel additive can support the HCCI combustion of other fuels to push its operating window to a broader range with attainable high thermal efficiency comparable to that of SI combustion. Briefly, syngas addition can be regarded as a means of extending the lean- or the rich-side of the operating equivalence ratio of HCCI combustion fueled with low- and high- octane fuels, respectively.

3.3. Syngas in dual-fuel engines

Stable combustion of a premixed syngas-air mixture is problematic in CI engines due to the low reactivity and high auto-ignition temperature (> 500 °C) of syngas [59]. Also, more stringent diesel engine emissions regulations have directed research towards further development of advanced combustion engines. Meanwhile, dual-fuel operation [379–381] with a premixed fuel and pilot-injected diesel has shown interesting advantages in terms of efficiency and emissions over conventional diesel combustion (CDC). Similar to compressed natural gas (CNG) and liquefied petroleum gas (LPG) [382], syngas is also a good candidate for the premixed fuel in dual fuel mode owing to its variable composition, flexible feedstocks, and possibility of on-board production on a vehicle [383,384]. In this part, syngas utilization in dual-fuel combustion is analyzed and reviewed in detail.

3.3.1. Diesel/syngas engine performance and emissions

Several studies have been focused on using syngas in dual-fuel concepts, where diesel is directly injected into the cylinder as a pilot fuel to initiate the ignition, while syngas is introduced into the intake port as a premixed fuel. Syngas application in diesel engines as a secondary energy carrier has been considered to be a promising alternative method mainly for emissions reduction. In the early stages of the research, efforts were dedicated to clarifying and distinguishing dual-fuel combustion from CDC, which led to the recognition of two-stage combustion for dual fueling at higher engine loads. Specifically, Garnier et al. [385]

established a predictive model to determine the ignition delay and combustion of a syngas/diesel CI engine, based on an empirical model and three Wiebe functions (for pilot-fuel, gaseous-fuel, and diffusive combustions) calibrated with experimental data. After that, some experiments were conducted to characterize syngas/diesel dual-fuel combustion in terms of engine performance and emissions by varying syngas compositions. Sahoo et al. [386] evaluated the dual-fuel concept using syngas with a H_2/CO ratio = 1/1 by volume in a single-cylinder diesel engine at a constant 1500 rpm and injection timing of 23° BTDC by altering the load from 0 to 100%. Compared to the diesel-only mode, a lower BTE with a peak reduction of 21% at 80% load, increased exhaust gas temperature (50-100°C), increased CO and HC emissions for all engine loads were observed; however, both NOx emissions and peak cylinder pressure were decreased. Also, by varying H_2/CO's volumetric ratio during various loads [387], the maximum HC, CO, and CO_2 emissions and minimum BTE occurred with 100% CO; however, the opposite behavior was observed with 100%H_2 [388]. Moreover, from the second law efficiency point of view, the same authors [389] concluded that a syngas/diesel CI engine's theoretical performance favors higher load (beyond 40% load) over lower loads, where the exergy destruction increases due to the heat transfer losses, see Fig. 35 (right).

Bika et al. [390] experimentally assessed the cycle efficiency of a single-cylinder syngas/diesel engine for four diesel substitutions of 0% (diesel-only baseline case), 10%, 20%, and 40%, at two net IMEPs of 2 and 4 bar, see Fig. 35 (left). Bottled gases of H_2 and CO with varying proportions (H_2/CO: 100/0, 75/25, 25/75, and 0/100 by %volume) were used to simulate syngas. Compared to the diesel baseline case, they displayed lowered efficiencies at both loads (10-25% for 2 bar and 5-17% for 4 bar IMEP), presumably attributed to the unburned syngas discharged in the exhaust stream. Moreover, NOx emissions were increased for all syngas proportions at 4 bar IMEP.

So far, syngas/diesel dual fuel operation findings have shown a common trend of efficiency degradation particularly at low- and part-engine loads with the decrease in combustion efficiency being due to increased H_2 and CO. Wagemakers and Leermakers [382] reviewed the comparison of dual fueling of diesel with various gaseous fuels like CNG, LPG, syngas, and hydrogen. They reported that all gaseous fuels could reduce soot emissions except for syngas. As a consequence of the dual fuel mode for diesel substitution, methane demonstrated better performance than syngas. The drawbacks generally reported from engines operating on gaseous fuels/diesel at part loads are excessive HC and CO emissions, and high fuel consumption, resulting in lower combustion efficiency and low thermal efficiency [391]. Also, a recent review on natural gas (NG)/diesel engines reported the same trend with up to a 2.1% fall in engine power and low BTE at low-to-part engine loads, while a maximum rise of 3% at high loads would be attainable compared to the diesel engine [392]. The only reported solution to the stated problems was to increase the H_2 content of the syngas, while the pilot injection strategy has not received much attention. It is also worth noting that higher efficiency with H_2/diesel dual operation than diesel-only operation has been obtained when H_2 is injected directly within the cylinder [393,394]. Antunes et al. [393] indicated fuel efficiencies of 34% for H_2/diesel and 43% for H_2-only compared to 28% for the diesel-only case.

At Okayama University, a group has conducted research on dual-fuel operation [395–402] with different producer gas generated by biomass gasification (BMG) and coke-oven gasification (COG) in a supercharged, single-cylinder diesel engine. They reported performance and emissions characteristics of a dual fuel syngas/diesel engine considering the effect of pilot injection. Their key findings are summarized below:

- The effect of injection pressure and amount of pilot fuel (diesel): Smoke emissions were increased with increasing amount of injected diesel, while decreasing with increasing injection pressure (i.e., 2 mg/cycle with 400 bar has the same measured smoke with 10 mg/cycle with 800 bar) [395].
- The effect of pilot-injection strategy with timings ranging from 4 to 12 °BTDC, injection pressures of 40, 60 and 80 bar, pilot quantities of 2 to 10 mg/cycle: 80 MPa with 3 mg/cycle was optimal for best performance [396].
- The lowest energy content PG used showed the lowest level of NOx emissions and smoke-free operation with smooth combustion [398].
- The effect of varying hydrogen content in PGs from 13.7% to 20% by volume: High hydrogen content in syngas led to a wide operating

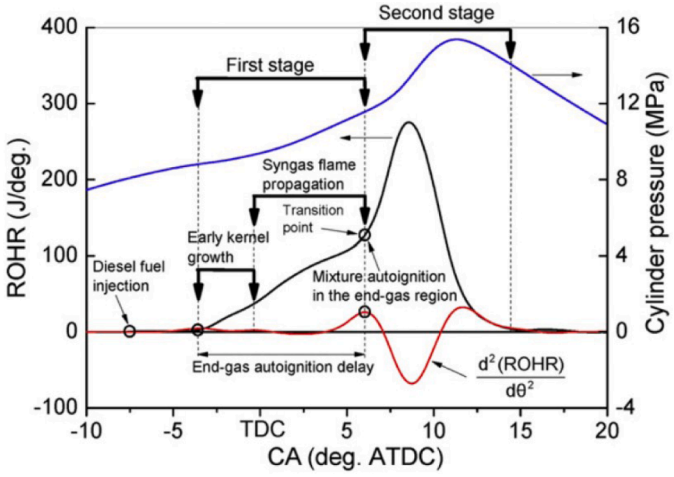

Fig. 36. Premixed mixture ignition in the end-gas region (PREMIER) combustion concept (Reprinted from [401] with permission of Elsevier).

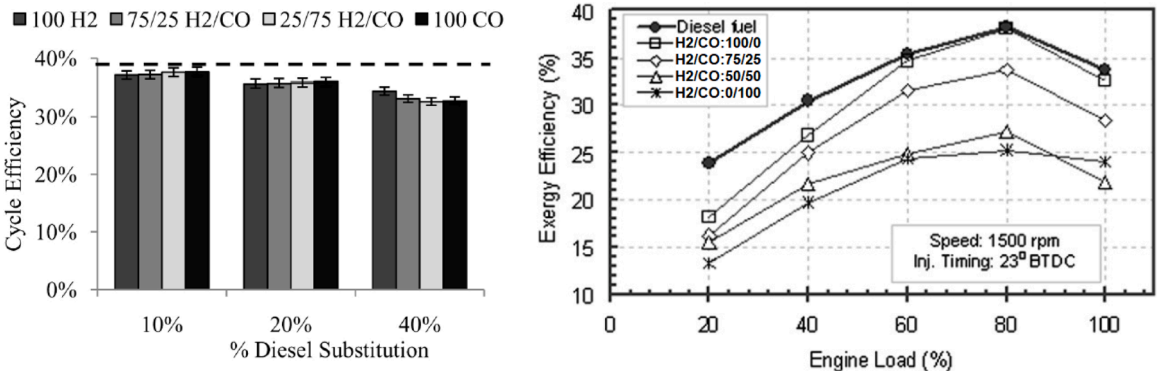

Fig. 35. Comparison of cycle efficiency vs. diesel substitution at 4 bar IMEP (left) [390] and exergy efficiency vs. engine load (right) [389] for various H_2/CO volumetric ratio (Reprinted with permission of Elsevier).

range (i.e., equivalence ratio) and high thermal efficiency; however, increased NOx emissions [397].

Following this work, Azimov et al. [403] suggested a novel combustion strategy with inspiration from the knock event in the end-gas regions of SI engines. The natural gas engine with a homogenous air-fuel mixture could be controlled; when natural gas combusts with the flame front supported concurrently by pilot-injected diesel fuel, which has already been ignited. They called it premixed mixture ignition in the end-gas region (PREMIER) combustion; also, shifting from diffusion combustion to flame front combustion for syngas/diesel dual-mode was reported in [404]. With the proposed combustion strategy illustrated in Fig. 36, the effect of H_2 and CO_2 content in syngas on the performance and emission of a syngas/diesel engine was investigated under lean operating conditions [401]. PREMIER combustion was observed primarily when the amount of pilot fuel used was minimal. Additionally, they [401] stated that an increase in syngas's hydrogen content shortened the main combustion period and caused the mean combustion temperature, IMEP, and efficiency to increase. They also found that diesel could not be substituted completely, or syngas could not be used as a single fuel in the diesel engine.

Some other researchers [396,405-409] have explored the feasibility of the dual-fuel concept with syngas generated from various sources by either gasification like producer gas or on-board reforming processes like reformer gas. Dohle et al. [409–411] performed a series of experimental studies to investigate the combustion characteristics of a dual-fuel diesel engine fueled by three cases of H_2, PG, which was generated from rice husk, and PG in combination with H_2 (PG + H_2) as a secondary fuel. Fig. 37 (left) shows the thermal efficiency variations with five different combinations of gaseous fuel replacement at 13%, 40%, and 80 % engine loads. Again, up to 30% load, a decrease of BTE was found due to the poor combustion characteristic of low calorific producer gas even in combination with H_2 at low loads. While by increasing the total mass quantity of fuel through increasing the engine load, the combustion of the dual fuel mode improved due to the higher flame velocity and diffusivity of gaseous fuels compared to diesel. As compared to H_2/diesel and PG/diesel cases (see Fig. 37 (right)), H_2 would augment more stability in the flame of the H_2+PG/ diesel case, presumably attributed to the high stability of H_2-air flames while the PG flames tend to become unstable. Nevertheless, the increase in H_2 from a certain amount (here, 40% of H_2 in PG/H_2 mixture) resulted conversely in the destabilization of the flame, which may be attributed to a decrease in the Markstein length [412]. At higher loads, much oxygen was consumed by PG/H_2 while hydrocarbon fuel received not enough oxygen; thus, a reduction in BTE would be sensible.

Fig. 38 depicts the variation in emissions at 80% load conditions for the three cases, with PG/H_2 ratio of 60:40. Because of the low pilot quantity, HC emission is high with gaseous fuel replacement at higher engine loads. As noted above at higher loads, larger gaseous fuel substitutions, which replace some of the air during the intake stroke, can lead to increased utilization of oxygen and the reduction of oxygen available for further combustion of the pilot diesel fuel, thus raising the HC level. Higher CO emissions implies that incomplete combustion and burning of lubrication oil take place, together with the lower heating value of PG, CO-containing PG (lower mean effective pressure), lower adiabatic flame temperature, and lower over-mixing. For the PG case, the drop in NOx may be due to the lower adiabatic flame temperature of PG and the absence of nitrogen in the PG, as well as a more uniform temperature distribution achieved with the gaseous fuel-air mixture, allowing the number of high-temperature regions around the diesel flame to decrease.

The summary of relevant literature that has been reviewed so far indicates:

1- Feasibility of syngas/diesel among gaseous fuels/diesel as a good choice for dual-fuel operation: according to all cited work here, while it has no beneficial aspects in terms of engine performance, and even also emissions, it performs well at low and part loads.
2- The influence of syngas compositions confirmed that increasing the H_2 content of the syngas has considerable merit in combustion improvement.
3- Modifying the pilot injection strategy can be a promising way of extending the prospects of the dual-fuel mode with syngas.

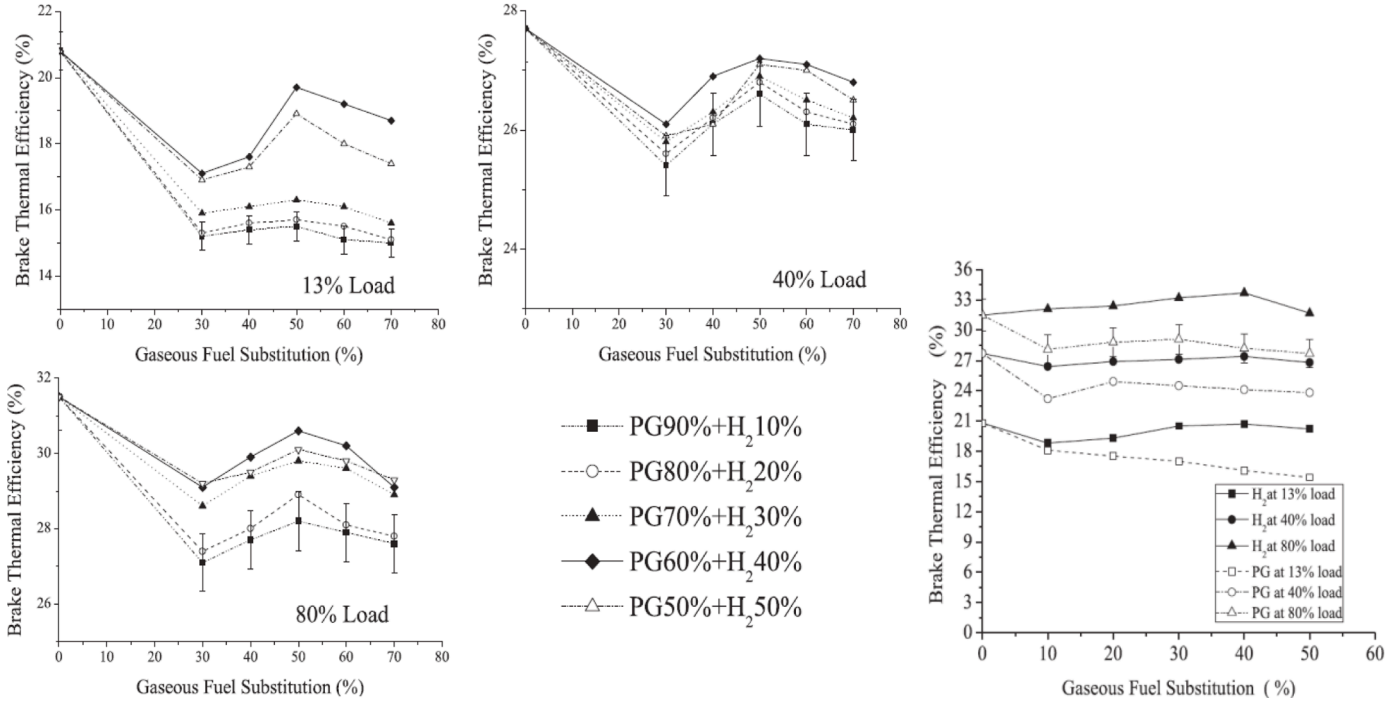

Fig. 37. Brake thermal efficiency for PG+H_2/diesel mixtures (left) and for H_2/diesel and PG/diesel (right) at different loads (Reprinted from [409] with permission of Elsevier).

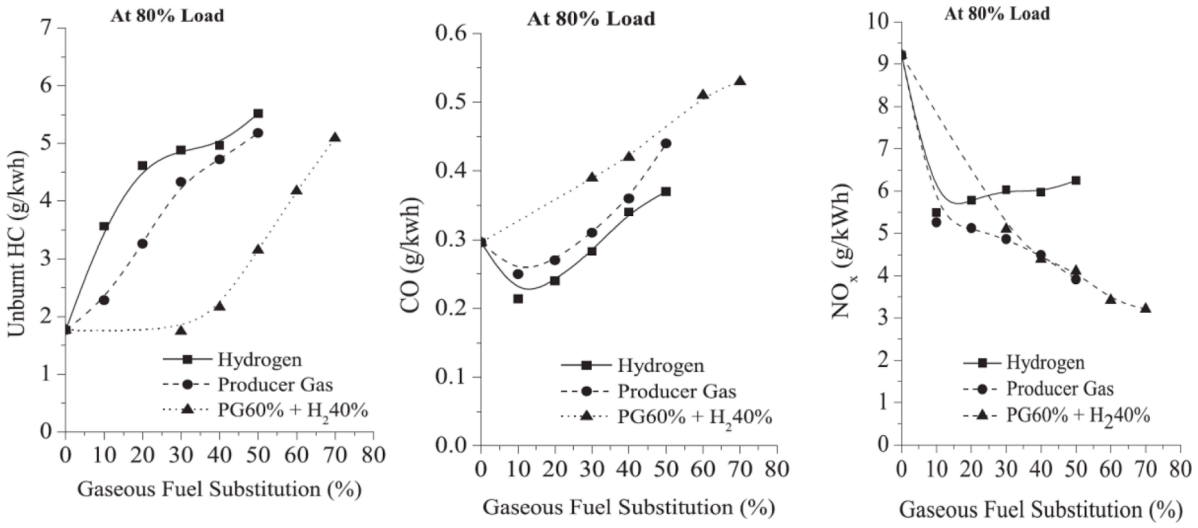

Fig. 38. UHC, CO and NOx emissions at 80% load for different Diesel+PG+H_2 mixtures (Reprinted from [409] with permission of Elsevier).

4- This concept's flexibility with a broad range of synthetic gases derived from varying sources has led to more attention in research.

The pilot injection strategy of Roy [396], is regarded as a means of controlling the in-cylinder reactivity and combustion phasing. By introducing two fuels having different reactivity (i.e., low and high reactivity) with a pair of separate injections for the high-reactivity fuel within the cylinder control can be achieved. This concept has been presented by Kokjohn et al. [413], who named it reactivity-controlled compression ignition (RCCI). In terms of commercialization, RCCI [380,381,414,415] is under more investigation for single-fuel operation, where high reactivity like diesel as the parent fuel, can be converted into a low-reactivity fuel by suitable in-situ on-board fuel reforming [34, 416-424].

Rahnama et al. [34] investigated the effects of reformer gas, hydrogen, and nitrogen on the combustion characteristics of a heavy-duty RCCI engine fueled with natural gas/diesel. The impact of the introduction of syngas (up to 5%vol) at medium load engine operation was also investigated. As shown in Fig. 39, by adding syngas, peak pressure, combustion, and gross indicated efficiency values significantly increase, but after a certain point, the gross efficiency drops due to improper phasing in combustion and heat release during the compression stroke. With respect to emissions, the introduction of syngas increases NOx emissions due to the higher temperature induced by the higher adiabatic flame temperatures of carbon monoxide and hydrogen. It also decreases soot emissions, due to the higher temperature of combustion resulting from the hydrogen content of the syngas, which allows soot oxidation. It is also confirmed in a recent study by Zhong et al. [425] that hydrogen in syngas promotes NOx emission but suppresses soot emission. Even though HC and CO emissions at medium load operation are relatively low, syngas addition slightly reduces HC emissions and increases CO emissions due to the syngas CO content, as depicted in Fig. 40. In another work, Rahnama et al. [418] numerically studied the effects of reformer gas composition (3% syngas enrichment of intake air) on the combustion and emission characteristics of a natural gas/diesel RCCI engine at a low load condition. They observed that with increasing CO fraction in the syngas, peak pressure, ringing intensity, and pressure rise rate increased significantly. Using a mixture with a higher CO content, a shorter ignition delay and combustion time and advanced CA50 were achieved. These were interesting results but was attributed to the lower cylinder temperatures as a result of using lower intake temperatures with high-H_2 syngas.

Chuahy and Kokjohn [416] were the first to experimentally examine the effect of varying syngas composition on a single-fuel RCCI fueled

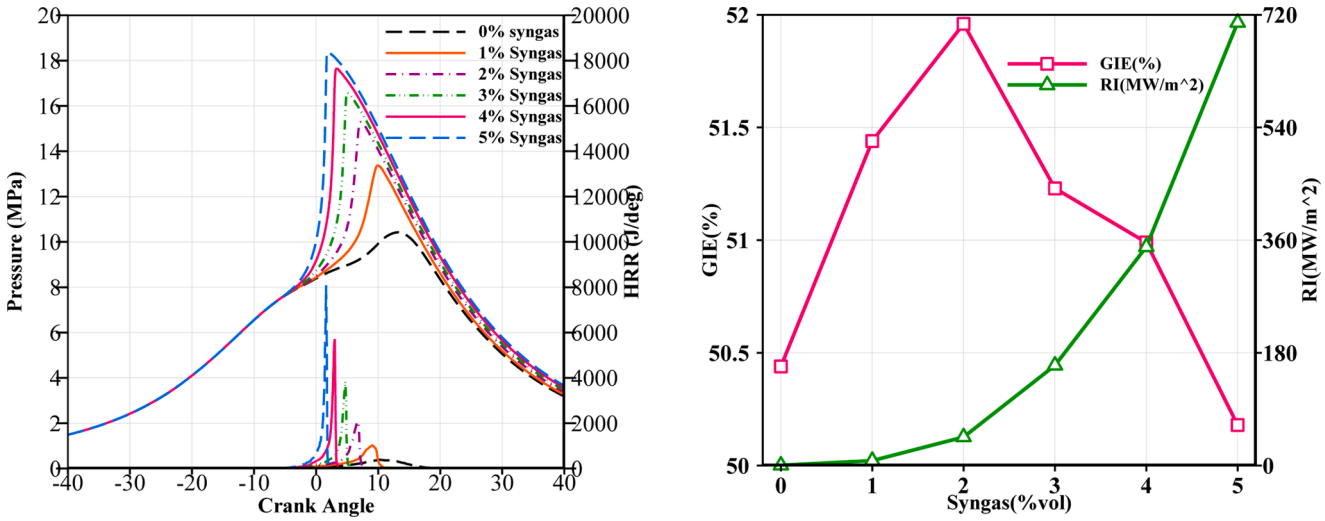

Fig. 39. Syngas addition effects on cylinder pressure and HRR, gross indicated efficiency and ringing intensity at 9 bar IMEP for a natural gas/diesel RCCI engine (Reprinted from [34] with permission of Elsevier).

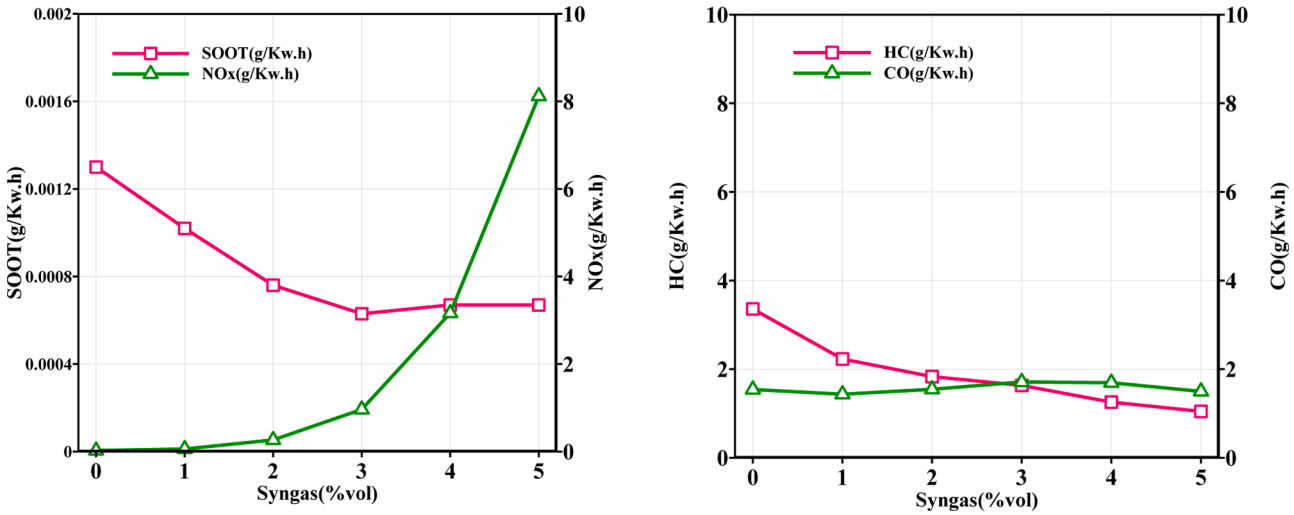

Fig. 40. Effect of syngas addition on engine emissions at 9 bar IMEP (Reprinted from [34] with permission of Elsevier).

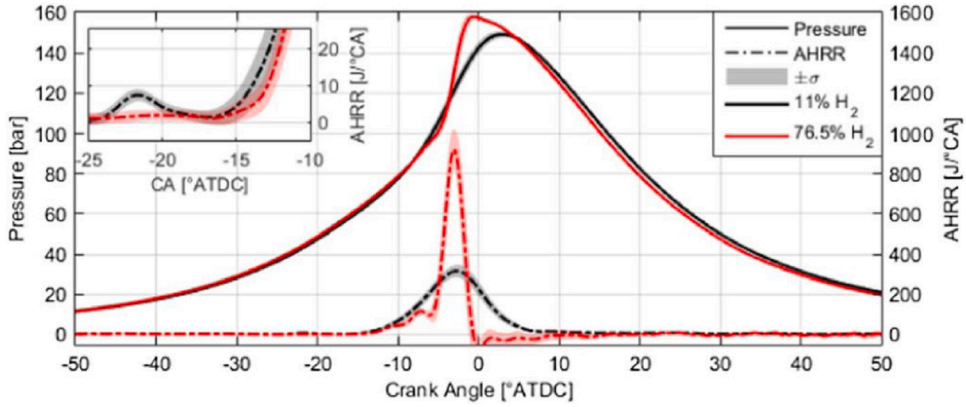

Fig. 41. In-cylinder pressure and heat release rate of a single-fuel RCCI fueled with diesel and syngas with lowest and highest H_2 content (Reprinted from [416] with permission of Elsevier).

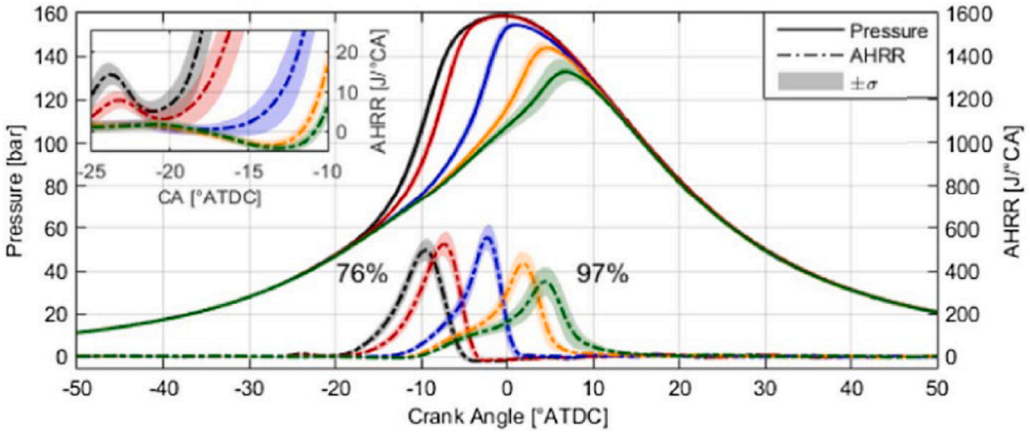

Fig. 42. In-cylinder pressure and heat release rate of a single-fuel RCCI fueled with diesel and syngas, with various syngas replacement (Reprinted from [416] with permission of Elsevier).

with diesel and simulated reformed diesel (50% H_2 and 50% CO by mole); it was done by keeping both the fuel energy level (4100 J/cycle) and the combustion phasing (at -0.3° and 0.5° ATDC for 0% and 40% EGR, respectively) constant by adjusting the injected diesel mass. The authors indicated that syngas with high H_2 content suppresses the low-temperature heat release (LTHR) stage and shortens the duration of high-temperature heat release (HRHR) or combustion with rising its peak, as seen in Fig. 41. They pointed out that by keeping the combustion phasing constant, increasing the H_2 content in syngas has an identical effect on the engine's gross indicated efficiency. Moreover, as shown in Fig. 42, the effect of syngas replacement by energy on the combustion phasing was shown that excessively high syngas has HTHR

with two distinct stages and higher cyclic variability, represented by shaded regions, which is ± standard deviation.

In light of the integration of single-fuel RCCI with varying fuel reforming reactions, work by Chuahy and Kokjohn [417] has shown that reformate generation from all reactions, including steam reforming, partial oxidation, and auto-thermal, have the capability of raising the net indicated efficiency of the engine by 4% compared to that of conventional diesel. The steam reforming case had the highest system efficiency if exhaust energy recovery was enabled. Further, it was reported [426] that the engine-reformer system with endothermic reforming has comparable efficiency to a conventional diesel engine at equal tailpipe-out NOx and negligible soot emissions; lower hydrogen to carbon ratios allows to achieve more engine-reformer efficiency.

By utilizing a thermally integrated R-EGR reactor (see the next section), single-fuel RCCI operation in a light-duty diesel engine was achieved by Hwang et al. [427]. Data were collected over a range of EGRs and main diesel injection timings at a constant fuel flow rate. The analysis indicated that RCCI is achievable with low efficiency in reactor conversion as long as reformate produced has reasonably small reactivity compared to diesel. The results also showed that while operating the reformer at a lower equivalence ratio resulted in higher hydrogen production, ignition was significantly delayed at achievable diesel injection timings. This work showed that while single-fuel RCCI is possible using an R-EGR diesel engine design, more research is required to optimize the system in order to reach the efficiency and emission rates achieved by dual-fuel RCCI engines.

3.3.2. *Biofuels/syngas engine performance and emissions*

Vegetable oils such as honge, rice bran, and neem oils have been investigated for their suitability as diesel engine fuels [428] due to being renewable, non-toxic, and biodegradable. Many researchers have performed tests on CI and dual-fuel engines with different vegetable oils at different operating condition. Banapurmath et al. [429–432] studied the combustion characteristics of a CI engine operated on the dual-fuel mode with PG as the premixed fuel and honge oil and its methyl ester (HOME) as the injected fuels (liquid pilot fuels). Fig. 43 represents heat release rate comparisons for the dual-fuel mode at optimum injection timings for the selected fuel combinations. It was observed that the premixed burning phase associated with a higher heat release rate is significant with diesel–PG dual-fuel mode leading to the higher thermal efficiency of diesel–PG operation. Furthermore, the diffusion burning process indicated under the second peak was higher for honge oil-PG and HOME-PG than diesel-PG dual fuel operation, which is in agreement with the effects of the viscosity of vegetable oils on the fuel spray and reduced air entrainment and lower fuel-air mixing rates. Higher exhaust temperatures and lower thermal efficiency were noticed with

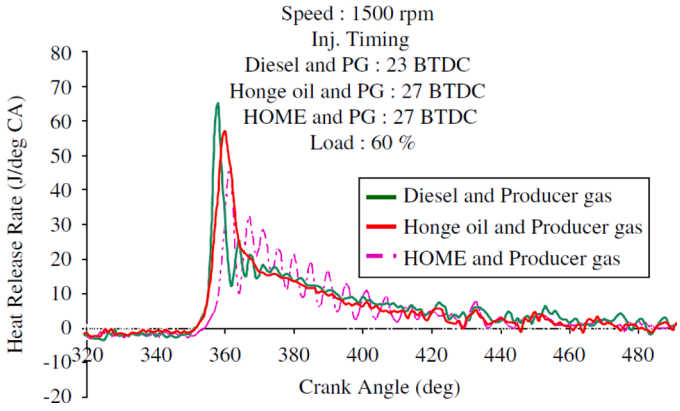

Fig. 43. HRR for honge oil–producer gas and honge oil methylester–producer gas at optimum injection timings (Reprinted from [429] with permission of Elsevier).

honge oil–PG due to the significantly higher combustion rates during the later stages. However, HOME–PG operation showed improvement in heat release rate compared to neat honge oil–PG dual-fuel operation.

Yaliwal et al. [51,433-438] increased the fuel efficiency of a single-cylinder, dual-fuel DI stationary diesel engine using HOME-Bioethanol (BE) blends, such as HOME+5% bioethanol (BE5), HOME+10% bioethanol (BE10) and HOME+15% bioethanol (BE15). Fig. 44 depicts in-cylinder pressure versus crank angle for diesel-PG, HOME-PG, and HOME+ bioethanol-PG combinations at a load level of 80%. The cylinder pressure was determined to depend on the combustion rate, the type of combinations of fuel utilized, and how much of the fuel is involved in the rapid combustion cycle. Lower cylinder pressure was observed for the combination of HOME –PG and HOME+ bioethanol – PG compared to the combination of diesel–PG, due to the combined impact of the lower heating value of the blends and PG and the longer ignition delay due to inadequate mixing with the slow-burning nature of the PG. Nonetheless, for the BE5–PG combination, a significantly higher in-cylinder pressure was observed compared with the combinations of HOME–PG, BE10-PG, and BE15–PG. This may be attributable to the BE5 blend's improved spray properties. Furthermore, when PG is present, a higher blend of bioethanol with HOME lowers the energy content for dual-fuel operation.

Overall, experimental work on the dual-fuel engine utilizing BE5-PG operation resulted in up to 4-9% increased BTE with reduced HC, CO emissions, and slightly equivalent NOx emissions compared to HOME-PG, BE10-PG, and BE15-PG modes. However, the overall performance of BE-PG operation was lower compared to diesel-PG operation.

Later in 2018 [439], the same group compared the performance, combustion, and emission characteristics of a single-cylinder, DI stationary diesel engine operated in dual fuel mode with a combination of HOME and the gaseous fuels CNG, HCNG, and PG. The combined effect of poor mixture preparation, longer ignition delay, lower heating value, and adiabatic flame temperature (1800 K) and slowing burning velocity nature of the PG (50 cm/s) resulted in the lower peak pressure and lowered rate of pressure rise for HOME–PG operation compared to HOME–CNG/HCNG operation.

Carlucci et al. [440–442] studied the improvements in dual-fuel biodiesel-producer gas combustion seen at low loads through pilot injection splitting. Utilizing a common-rail injection, single-cylinder research diesel engine fitted with a high-pressure common rail injection system controlled in dual-fuel mode, they measured changes resulting from splitting of the liquid fuel injection. In this case, the inducted gaseous fuel was a synthetic PG, while biodiesel was utilized as the pilot fuel. The experimental campaign was split into two parts, running on engine speed at 1500 rpm. First, only one pilot injection of constant fuel quantity (11 mm^3/cycle) was used, the rail pressure was set at 500 or 1000 bar, while the quantity of gaseous fuel produced in the cylinder was varied on three stages. Second, splitting pilot injection was shown to be an efficient way to increase the efficiency of fuel conversion and to reduce the levels of all polluting emissions compared to the single pilot strategy. Based on the comprehensive experimental tests, a dwell ranging from 10 to 30 degrees of crank angle combined with a first injection timing varying from 35 to 20 degrees of crank angle BTDC allowed the highest fuel conversion efficiency and the lowest emission levels. The injection pressure was verified to be a significant factor affecting the development of combustion, while the gaseous mass inducted in the cylinder determined a side effect in terms of oxygen depletion. Eventually, pilot injection splitting proved to be an efficient way to boost the combustion of gaseous fuel under low load (lean mixture) conditions in the dual-fuel system. Kan et al. [443] simulated the combustion and emission performance of three dual-fuel strategies for utilizing the syngas and biodiesel produced from the biomass wastes, namely syngas-biodiesel, hydrogen-enriched syngas-biodiesel and DME-biodiesel in a compression ignition engine using the KIVA-CHEMKIN code. It was found that syngas-biodiesel and hydrogen-enriched syngas-biodiesel cases can improve the combustion

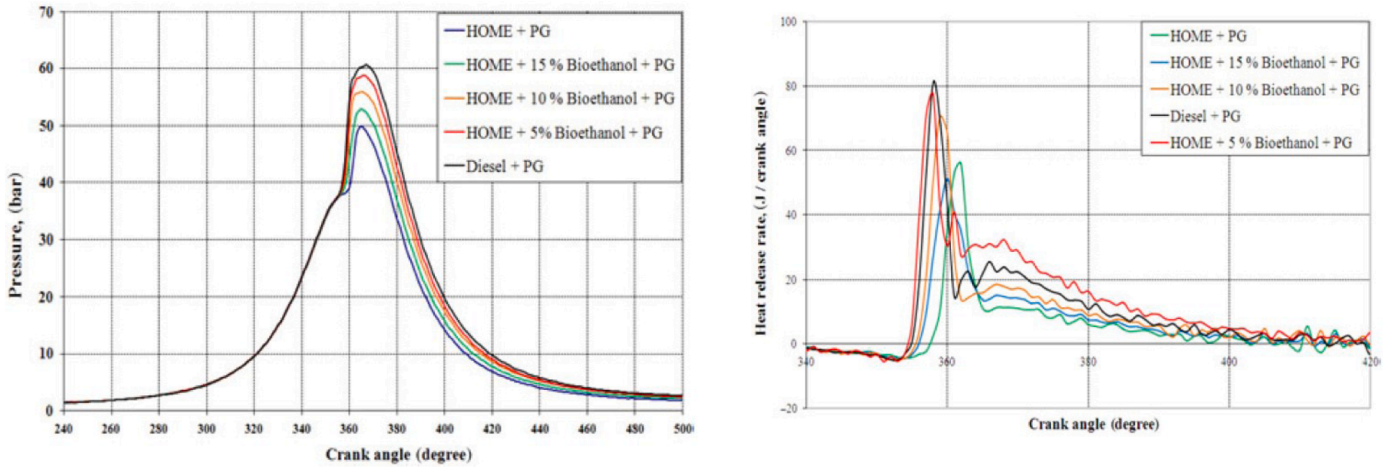

Fig. 44. In-cylinder pressure and HRR versus crank angle for different HOME/bioethanol blend–PG combinations at the 80% load condition [433].

and had higher indicated power at high engine loads of 50% and 100%. The DME-biodiesel case was advantageous for the combustion at 10% load comparing to the other two cases. With the increase in fuel supplement ratio, the soot emission generally showed a decreasing trend at all engine loads for all three strategies.

Table 11 summarizes the main syngas combustion works on dual fuel engines published in the literature.

3.4. Syngas contaminants in IC engines

There are two sources of contaminants leading to deposit formation after running the engine with syngas fuels:

1- Impurities that originate from the production method,
2- Changing syngas composition during the storage process.

Impurities in biomass feedstocks and partial gasification lead to contaminants in syngas, which are mainly classified as tars, PM, alkali, nitrogen (NH_3), Sulphur (H_2S), halides, and trace elements [451]. These contaminants are responsible for downstream problems in the gasifier, such as corrosion, clogging, and catalyst deactivation [61,452-455]. Syngas produced from biomass gasification should be refined to remove condensable tars prior to using it as a fuel for IC engines [456]. Syngas impurities affect engine performance for all types of IC engines, but there are few studies in the literature on this. Bhaduri et al. [329,331,376] developed a tar tolerant system, wherein syngas with tar contamination was used as a fuel for an HCCI engine where intake temperatures were set to be above the tar dew point to prevent condensation of tars. They noticed that the moisture content of the syngas adversely affects combustion efficiency. In addition, the results demonstrated that the introduction of tars leads to an increase in the LHV without affecting the timing of combustion for neat syngas operation. In another work, Bhaduri et al. [330] carried out experiments using an impure and hot biomass syngas burned in an HCCI engine without the intermediate cooling and tar purification steps to test the engine's stability in response to naturally occurring random variations in the syngas composition. Minimal tar deposits were found due to the use of a low tar gasifier after 24 h of operation (see Fig. 45). Besides, brown discoloration from some deposits was observed on the piston and cylinder heads, which was attributed to the regular oil-related deposits.

In the second case, Hagos et al. [457] ran a DISI engine with various syngas compositions free of tar and periodically checked the fuel injector, spark plug, piston, cylinder head, and valve seats during the engine shutdown. Deposit formation was visibly observed on the surface of the injection tip, turning the color glow red, as can be seen from Fig. 46 (left). While a similar deposit color was also seen in other engine components, as shown in Fig. 46 (right), such deposits have never been found when running the engine with CNG, hydrogen, or a combination of them. It was pointed out that producer gas with light tar compounds as fuel has less impact on the deposit formation [458], although neither the effect of engine hours running nor the effect of syngas composition on the deposit quantity were investigated. The deposit characterization revealed that reacting the CO content in syngas with the metallic wall of storage tanks at high pressure may result in metallic carbonyl contaminants such as iron pentacarbonyl ($Fe(CO)_5$) in the syngas, which in turn participates in the engine's combustion. Before deposit formation, as mentioned in section 2.4, these components also affect the ignition delay and laminar flame speed of the whole combustion process. Besides, such metallic carbonyl could be generated during syngas production via gasification. Consequently, extra attention should be paid to the design of syngas production and storage systems.

4. Syngas from on-board fuel reforming in IC engines

A study by Yang et al. [459] reported that syngas could be stored under pressures as high as p=83 bar and temperatures of T = -15°C to 45°C. However, with on-board syngas production, the storage-related issues such as the demand for a large storage tank due to the low energy density of the syngas and the syngas contaminants (see Section 3.4) can be eliminated. This section provides a comprehensive overview of previous research on on-board fuel reforming and syngas production in IC engines. Regarding the vehicular applications, the fuel reforming process can be achieved either inside cylinders (i.e., in-cylinder fuel reforming) or outside the engine cylinders (i.e., external fuel reforming). In-cylinder reforming methods are a preventive measure to achieve a more efficient engine by increasing thermal efficiency, reducing energy content in the engine's exhaust stream. In contrast, external reforming methods are a corrective one to a lower engine efficiency by capturing the exhaust gas energy via placing a WHR device (reformer) in the exhaust stream. Both methods are considered as thermochemical recuperation (TCR) technologies [460–462], which can be more efficient than thermomechanical methods [463] such as turbo-compounding and bottoming cycles because the energy transfer is not bounded by isentropic expansion and Carnot efficiency. Additionally, there is no significant modification needed in the design of production engines. Fig. 47 shows the schematic of the mentioned techniques by classification, and they are reviewed in detail in the following sections.

4.1. External fuel reforming

4.1.1. Intake fuel reforming

Engine intake on-board fuel reforming involves all methods in which

Table 11
Summary of syngas combustion research in the dual fuel engine mode.

Authors	Research objectives	Syngas composition	Experiments	Simulations	Main results
Reformer gas (RG)/diesel dual fuel CI engine					
Bika et al. [390] (2011)	Cycle efficiency comparison between RG-diesel dual case and diesel-only case, at 2 and 4 bar IMEP	RG1: 100%H_2; 0% CO RG2: 75%H_2; 25% CO RG3: 25%H_2; 75% CO RG4: 0%H_2; 100% CO	4-stroke, 1-cyl Yanmar L100V CI engine, CR= 21.2:1 rpm= 1825	—	Cycle efficiency: 10-25%, 5-18% lower than the diesel-only for 2 and 4 bar IMEP, respectively. NOx: ~ for 2 bar, ↑ for 4 bar with increasing diesel substitution.
Sahoo et al. [387] (2011)	Effect of load level on the performance of the RG-diesel and diesel (baseline) operation with varying H_2/CO content	RG1: 100%H_2; 0% CO (119.81 MJ/kg) RG2: 75%H_2; 25% CO (23.09 MJ/kg) RG3: 50%H_2; 50% CO (14.81 MJ/kg) RG4: 0%H_2; 100% CO (10.12 MJ/kg)	4-stroke, 1-cyl Kirloskar CI engine CR= 17.5:1 rpm= 1500	—	Maximum diesel replacement = 72.3% for RG1. At almost all loads: Ignition delay: diesel < RG4 < RG3 < RG1, RG2 HC: RG1 < diesel < RG2 < RG3 < RG4 CO: RG1 < diesel < RG2 < RG3 < RG4 NOx: RG4 < RG3 < RG2 < diesel < RG1
Sahoo et al. [389] (2011)	Second-law analysis of RG-diesel operation under varying load conditions	//	//	—	At higher loads: ↑ Combustion temperature and pressure; ↑ cumulative work availability; ↑ exergy efficiency. At 80% loads: max. ITE for RG 1-4: 19.8, 18.3, 16.1, 15.7% At lower loads: Opposite of higher loads due to poor combustion.
Christodoulou and Megaritis [444] (2014)	RG-N2 mixture effects on an high speed direct injection (HSDI) diesel engine's emissions and performance at various speeds	60%H_2; 40%CO	4-stroke, 4-cyl Ford Puma CI engine CR= 18.2:1 rpm= variable	—	With introducing RG+ N_2 mixture: ↓ NOx and smoke emissions over a large engine operating conditions; ↑ Engine speed: ↓ overall rate of pressure rise. Engine is more fuel efficient with neat diesel.
Rahnama et al. [34] (2017)	The effects of H_2, RG and N_2 (by direct injection) on combustion, emissions and load limits of a heavy-duty natural gas/diesel RCCI engine	H_2:CO – 0-100% variation in hydrogen fraction	—	3-D simulations using CONVERGE CFD	Extending high load by adding N_2: ↑ combustion phasing delay,↓ ringing intensity Extending low load by adding H_2 and syngas: ↑combustion efficiency At medium load with adding syngas: ↑ NOx, ↑ ringing intensity, ↑ pressure rise rate.
Chuahy and Kokjohn [416] (2017)	Effects of RG composition on a single-fuel RCCI engine at constant fuel energy and combustion phasing	50%H_2; 50%CO H_2 is variable from 10% to 80% by mole	4-stroke, 1-cyl Caterpillar C15 CI engine CR= 16.9:1 rpm= 1300	Constant volume ignition delay calculation by ChemkinPRO	By replacing CO with H_2: ↑ Charge reactivity, ↓ combustion duration, ↓ magnitude of low temperature heat release. ↑Soot with increasing fuel reforming.
Hariharan et al. [421] (2020)	Study on single-fuel RCCI with diesel and reformed diesel by catalytic partial oxidation	H_2:3%, CO:11%, CO:3.4%, N_2:78.15%, CH_4:1.35%, C_2H_4:2.9% (2.3 MJ/kg)	4-stroke, 1-cyl Ricardo Hydra CI engine CR= 15.5:1 rpm= 1200	3-D simulations using CONVERGE CFD	In comparison to gasoline/diesel and natural gas/diesel RCCI: Comparable thermal efficiency with ↓NOx, ↓THC, and good controllability, but at ↑CO and ↑CO2.
Producer gas (PG)/diesel dual fuel CI engine					
Roy et al. [397] (2009)	Performance and emission comparison of a supercharged dual-fuel diesel engine fueled by PG with varying H_2 content	PG 1: 13.7%H_2; 22.3%CO; 1.9% CH_4; 16.8%CO_2 and 45.3%N_2 PG 1: 20%H_2; 22.3%CO; 1.9% CH_4; 16.8%CO_2 and 39%N_2	4-stroke, 1-cyl CI engine, CR= 16:1, rpm=1000 Pilot injection timing= variable	—	Smooth and smoke-free, two-stage combustion was obtained. High H_2-content PG compared to low H_2-content PG: ↑12% at engine power ↑operable range of φ (from 0.52-0.68 to 0.42-0.79) ↓combustion duration by 4-5° CA ↓HC and CO by 10–25%.
Azimov et al. [401] (2011)	PG composition effects on a dual-fuel engine with PREMIER combustion at various equivalence ratios	7 different composition, H_2 varying between	4-stroke, 1-cyl CI engine, CR= 16:1, rpm=1000	—	↑ H_2 content: ↑ Combustion temperatures, ↑ IMEP, ↑efficiency, ↓ CO,↓ HC, but ↑ NOx.

(*continued on next page*)

Table 11 (*continued*)

Authors	Research objectives	Syngas composition	Experiments	Simulations	Main results
		13.7-56.8%. PG was from cock-oven and biomass gasification			↑ CO_2 content up to 34% in gas (just at a certain level): ↓ Combustion temperatures, ↓ IMEP, ↓efficiency, ↓ maximum pressure rise rate, ↓ NOx. COV_{IMEP}< 4% at various φ for all types of fuel.
Dhole et al. [409] (2014)	Effect of H_2, PG, and H_2(40%)+PG (60%) as secondary fuels on combustion parameters of a dual fuel diesel engine	21.6%H_2; 23 %CO; 2.1%CH_4; 10.2% CO_2 and 43.1%N_2 (6 MJ/kg)	4-stroke, 4-cyl, Turbocharged, Ashok Leyland ALU WO4CT engine CR= 17.5:1, rpm= 1500	—	At all loads and gaseous fuel substitutions: BTE: PG < PG+H_2 < H_2 Mean cylinder temperature: H2 < PG < PG+H_2 HC: PG+H_2 < PG < H_2 CO: H2 < PG < PG+H_2 Lowest NOx: for H_2 at 20% for PG at 80% load.
Rinaldini et al. [445] (2017)	Exploring the potential of using both Diesel fuel and syngas in a current turbocharged diesel engine	9.4%H_2; 22.4%CO; 3.4%CH_4; 5.4%CO_2 and 59.4%N_2 (4.65 MJ/kg)	4-stroke, 4-cyl VM Motori CI engine , CR= 17.5:1, rpm=3000	—	No need to significantly alter the standard stock engine design. ↑ Engine brake efficiency up to 5%. The use of syngas: ↓ Diesel oil consumption, ↑ quality of combustion.
RG or PG/biodiesel dual fuel CI engine					
Balakrishnan and Mayilsamy [446] (2014)	CR effects on CI engine performance with biodiesel and PG in mixed fuel mode	12.31%H_2; 10.13% CO; 1.48%CH_4; 14.58%CO_2 and 58.8%N_2 (3.56 MJ/m^3)	4-stroke, 1-cyl Modified Kirloskar AV1 engine CR= 5:1 to 20:1, rpm= 1450-1600	—	With ↑ CR: ↑ BTE and decrease ↓brake-specific energy consumption. At higher possible CR: ↓emissions, due to the well-mixed fuel with no engine modifications. The CR is limited by the ignition delay, noise pollution, and engine vibration to a maximum of 18.
Balakrishnan et al. [447] (2015)	Investigation on a CI engine fueled with 4 cases: Diesel (D) – D/PG - vegetable oil methyl ester (biodiesel or BD) – BD/PG	//	//	—	Maximum BTE: D:28.5%, BD:29.9%, D/PG:27.2%, BD/PG:26.8% Ignition delay: dual-mode > single-mode, BD/PG < D/PG by 13.6°. Smoke: BD/PG < D by 16%. The ICE could operate without any modifications with all fuel modes.
Carlucci et al. New(2014)	Study on splitting pilot injection to improve of dual-fuel biodiesel-PG combustion at low loads	20%H_2; 20%CO and 60%N_2	4-stroke, 1-cyl Modified Kirloskar AVL model 5402 engine CR= 17.1:1	—	By splitting the pilot injection: ↑ Fuel conversion efficiency, ↓ THC and ↓ CO. ↑ Dwells between two injections: Two-phase HRR was clearer. NOx showed an increasing-decreasing behavior.
Carlucci et al. (2017)	Investigate on pilot biodiesel injection parameters and strategy on the biodiesel-PG dual-fuel combustion	//	4-stroke, 1-cyl AVL model 5402 engine CR= 17.1:1, rpm= 1500	—	Highest fuel conversion efficiency and lowest emissions: Dwell with a range of 10-30° CA + first injection in the range of 20-35° BTDC. The injection pressure reported to be a major factor.
Yaliwal et al. [434] (2014)	Honge oil methyl ester (HOME) and PG fueled dual-fuel engine operated with varying CRs	15-19%H_2; 18-22% CO; 1-5%CH_4; 4% HO_2 and 45-55%N_2 (5-5.6 MJ/m^3)	4-stroke, 1-cyl Kirloskar CI engine, CR= variable (15:1, 16:1, 17.5:1)	—	↑ CR from 15 to 17.5: ↑ BTE by 39.1%, ↓ exhaust gas temperature by 26%, ↑ peak pressure by 9.65%, ↓ smoke by 20.5%, ↓ CO by 44.5%, ↓ HC by 30.2%, ↑ NOx by 24.4%. At various CRs, lower BTE was seen with HOME/PG than diesel/PG. More improvement by turbocharging was suggested.
Yaliwal et al. [436] (2016)	Combustion chamber and nozzle geometry effects on a diesel engine performance operated on HOME/PG dual-fuel mode	//	4-stroke, 1-cyl Kirloskar CI engine, CR= 17.5:1	—	↑ Injection pressure, ↑ hole number with ↓ hole size could result in efficient preparation of mixtures. With re-entrant combustion chamber + optimized nozzle geometry: ↑BTE by 4-5%, ↓ smoke by 19%, ↓ CO by

(*continued on next page*)

Table 11 (*continued*)

Authors	Research objectives	Syngas composition	Experiments	Simulations	Main results
					17.64%.
Yaliwal et al. [448] (2021)	Influence of producer gas and dairy scum oil methyl ester (DiSOME) on the thermal efficiency and emission character of a compression ignition engine under dual and HCCI mode	//	//	—	Diesel and DiSOME based DF mode of operation: ↑BTE by 4.01% and 6.4%; ↓ HC by 7.4% and 9.6% ↓ CO by 8.5% and 13.4% ↑NOx by 26.4% and 23.6% respectively than the operation with HCCI mode at 80% load.
Costa et al. [449] (2017)	Highlight the main influences on the combustion process related to the use of syngas and the effects of different biomass moisture contents on power output and main pollutants emission	18.58%H_2; 21.77% CO; 1.03%CH_4; 10.35%CO_2 and 48.28%N_2	—	3D engine model with the AVL Fire™	↑ Percentages of syngas: ↓ Combustion efficiency but ↑thermal efficiency. With syngas addition: ↓ NO formation ↑ CO and ↑ soot as compared to the case of pure use of biodiesel.
Krishnamoorthi et al. [450] (2020)	Experimental and numerical study on syngas/diesel and syngas/B20 (20% biodiesel)	50%H_2; 50%CO	4-stroke, 1-cyl direct injection, naturally aspirated KIRLOSKAR TV1 diesel engine CR = 15:1	3-D simulations using CONVERGE CFD	As compared diesel-only: Syngas/diesel with an inj. timing of 19° BTDC: Slightly ↑ BTE, ↓ NOx by 22%, ↓PM by 77%. Syngas/B20 with a pre-inj. at 50° BTDC and main inj. at 18° BTDC: Maximum BTE of 24%, ↓NOx by 29%.

↑: increase, ↓: decrease, ∼: approximately constant, //: similar to above.
IMEP: indicated mean effective pressure, CR: compression ratio, ITE: indicated thermal efficiency, BTE: brake thermal efficiency, BTDC: before top dead center, φ: air-fuel equivalence ratio, COV_{IMEP}: coefficient of variation of IMEP, and UHC: unburned hydrocarbon

(a) (b)

Fig. 45. (a) Tar deposits on a component of the check valve; (b) piston showed no deposits, but small impurities were found in the oil rings (Reprinted from [330] with permission of Elsevier).

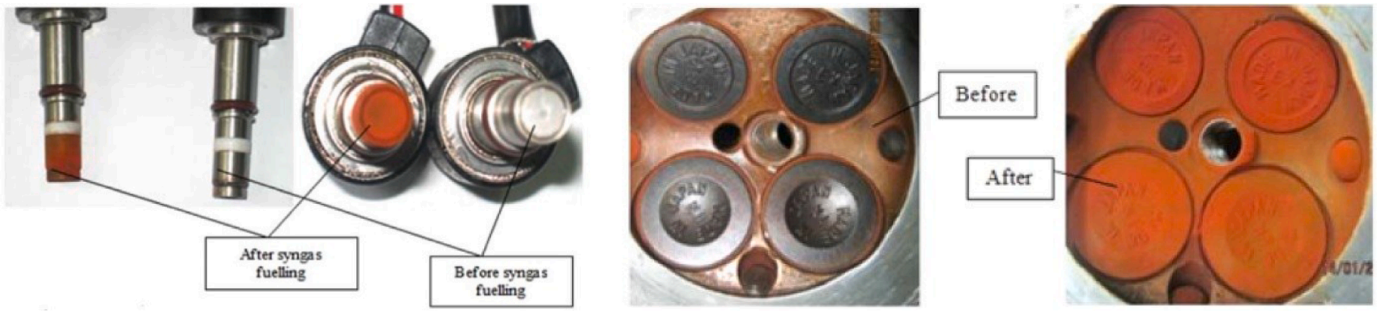

Fig. 46. Injector tip (left), cylinder head and valve seat (right) after and before syngas fueling [457].

fuel for the reformer is supplied from the engine's main fuel, and no relationship exists between the reformer and engine exhaust in terms of heat recovery, and the main purpose is not only to improve the combustion process, but also to improve the aftertreatment system performance at particular operating conditions. For example, on-board reformers have been employed to reduce HC and CO emissions during cold start and warm-up periods of a SI engine. Isherwood et al. [464] integrated a multi-cylinder SI engine with an electrically-heated prototype POX reactor to produce reformate as replacement of gasoline fuel during cold-start, and then observed time-averaged reductions in HC

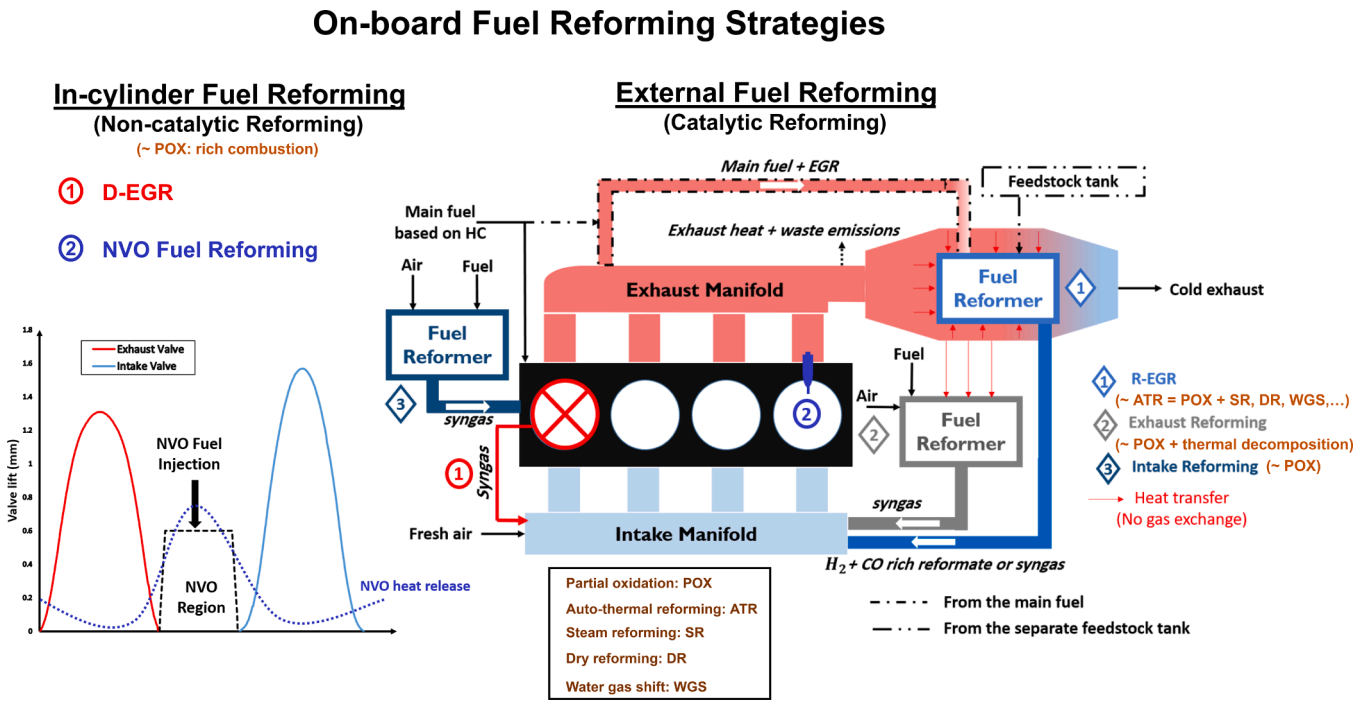

Fig. 47. Schematic layout of current on-board fuel reforming strategies.

and CO by about 80% and 40%, respectively. Kirwan et al. [465], at Delphi automotive, also established an intake-side, external POX reformer to convert a fraction of gasoline at rich conditions to reformate by catalytic reforming; then, the reformate was split into separate injections, a portion into the cylinder and the rest into the exhaust stream, resulting in a reduction of both engine-out and tailpipe emissions during cold-start. Another study [466] proposed an on-board water electrolysis system to reduce fuel consumption of the SI engine fueled with ethanol and gasoline at the idle condition.

The most significant way of producing reformate from this category is partial oxidation because of its inherently fast start-up and shut-down, rapid response to transient loads, and high hydrogen production, but at the expense of a drop in the reforming process efficiency, which should be offset by the increased engine thermal efficiency. Overall, enhancement in engine-reformer efficiency was reported for motorcycle applications assisted with plasma converter [467,468].

Briefly, although these on-board reforming processes could be operated independently of the engine condition (as a positive point), the complexity and extra costs bring additional issues. It is worth noting that developments in the aftertreatment systems following the adoption of more stringent emission standards are in progress.

Plasma reforming:

Plasma-assisted fuel reforming is a technique to generate hydrogen-rich gas on-board the vehicle by supplying a small fraction of the main fuel stream to a device where fuel and air are converted to a stream containing the syngas by POX process, and then mixed with the main intake air/fuel charge for SI and HCCI combustion improvements or directly applied to exhaust aftertreatment systems for a NOx trap [469] or for diesel particulate filter (DPF) regeneration [470], as demonstrated in Fig. 48. The device, which was initially developed and tested by Bromberg et al. [471,472] at the Plasma Science and Fusion Center (PSFC) of Massachusetts Institute of Technology (MIT) and they called it "Plasmatron", can be categorized into thermal and non-thermal plasma reformers, depending on how electrical power input transfers from the electric field to plasma components including electrons, ions, neutral gases to form and maintain plasma [473].

In thermal plasma reformers, the plasma energy input supplied by a DC source creates a small region with an extremely high temperature (in the range of 5000 to 10000K) to heat the electrons and the other plasma components, such that temperatures reach thermal equilibrium. While

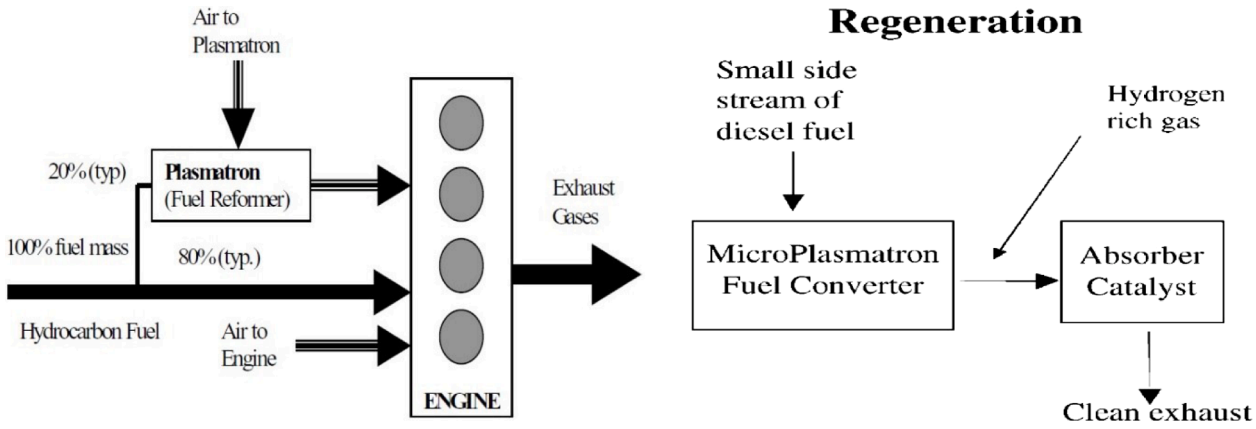

Fig. 48. Thermal (left) and low current (non-thermal) (right) Plasmatron fuel converters (Reprinted from [470] with permission of Elsevier).

the provided high-temperature environment, along with created plasma heating, boost the slow reaction rates associated with POX reactions, irrelevant inert species (such as N_2) are also heated, meaning that much-unused energy is wasted through this non-selective way. On the other hand, in non-thermal plasma reformers, only the electrons have very high temperatures; however, the other components are relatively cold (near room temperature) and capable of absorbing and storing energy to efficiently produce locally highly reactive species to perform fuel reforming at low temperatures. Due to this behavior acting as a catalyst, many researchers believe that non-thermal plasma reforming has inherent catalysis effects that are fundamentally yet unknown [84].

Rabinovich et al. [474] developed a high current (>10 A), thermal compact Plasmatron reformer to convert various fuels, namely biofuels, gasoline, and diesel, into H_2-rich gas, and also integrated it with an SI engine fueled with methane [475] and gasoline [476] to investigate engine performance, NOx emissions, and engine-reformer interactions. They succeeded to potentially apply the compact Plasmatron to IC engine, resulting in substantial NOx emissions reductions but at the expense of the high power requirement, the high overall engine-reformer efficiency cost, and possibly lower electrode lifetime [477]. Besides, as seen in Fig. 49(left), they needed two or more channels in which water flows for electrode cooling prohibit electrodes from erosion.

To overcome thermal compact Plasmatron-related issues, the same authors developed a low current (<120 mA) version of that through the non-thermal plasma generation mechanism, as indicated in Fig. 52 (right) [470]. A wide range of fuels such as heavy hydrocarbons, alcohols [478], and renewable fuels [479] can be used with different types of non-thermal plasma reformers.

It's worth noting that due to developing an understanding of plasma-chemistry interaction mechanisms, the role of plasma, specifically the non-equilibrium one, in combustion enhancement by assisting ignition and flame stabilization has been drawing more attention than the low-temperature fuel reforming application in recent years. For instance, microwave non-equilibrium plasma could enhance an ignitor such as the spark plug of SI engines to initiate a sufficiently large flame kernel, which in turn causes lean limit extensions by maintaining nearly constant combustion variability by increasing the air-to-fuel ratio, in addition to the observed improvements in fuel consumption and CO emissions. This is beyond the current review's scope, but in this regard, two critical and comprehensive reviews have been published [480,481]. Several studies were also conducted to mimic the Plamsatron-generated reformate in gasoline engines through simulated gases using bottled gas [305,482,483] with a typical reformate composition consisting of 25% H_2, 26%CO, and 42%N_2, which indicated an improvement of about 12% in engine efficiency at partial loads.

In short, plasma-assisted reformers have shown vastly superior characteristics compared to traditional catalytic reformers, including fast response, rapid startup, fuel flexibility, size requirements, and absence of sulfur and soot as bi-products. Nevertheless, they deteriorate the vehicle's overall power output by about 2%, as the engine must provide the electrical power. Additionally, they are immature for IC engine applications since plasma technology is still being under development.

4.1.2. *Exhaust gas fuel reforming*

Since in an IC engine approximately about 30% of the fuel's energy is lost through hot exhaust gases, utilizing a part of these hot gases for providing heat and the reactants required, along with a portion of engine fuel for an exhaust gas fuel reformer placed inside the EGR loop, can result in reformate having higher enthalpy than the base fuel, as seen in Fig. 50. Reformate mixed with the rest of the EGR (in total, reformed exhaust gas recirculation or R-EGR) is fed back to the intake manifold to run the engine similar to a dual-fuel (the base fuel + R-EGR (EGR + Reformate)) engine. The same concept with varying configurations has been investigated by several researchers, as seen in Fig. 50. Because of using a catalyst to convert the fuel, it is also called on-board catalytic reforming.

Catalyst considerations:

The catalyst formulation determines the catalyst activity and resistance to deactivation due to carbon deposition, and reformer design affects catalyst temperature; therefore, both influence reformer performance and reformate product. An earlier work [489] on an R-EGR reformer with a gasoline SI engine exhibited poor performance at moderate temperatures (T=600-650 °C) as compared with values predicted by thermodynamic equilibrium, resulting in a low concentration of hydrogen (2-5%). This low fuel conversion was mostly attributable to the inactivity of the catalyst that was however not specified in that study. Recent works by Gomez et al. [490,491] showed that high activity of precious metal catalysts, e.g., 1 wt% rhodium (Rh) supported on zirconia, can bring yields near equilibrium for a given fuel conversion rate by preventing methanation reactions at typical exhaust temperatures of a gasoline engine. The study revealed that increased fuel conversion occurred with higher catalyst mass and temperature (see Fig. 51). A 10% drop was also observed in hydrogen production when increasing pressure from p=1 to 1.3 bar. In a current configuration, the exhaust gas reformer is placed after the TWC in the exhaust gas system [492], and achievable hydrogen and CO yields were in the range of 5-10%.; another current (and more complex) layout [487] is that the reformer is positioned close to the exhaust manifold, as will be discussed

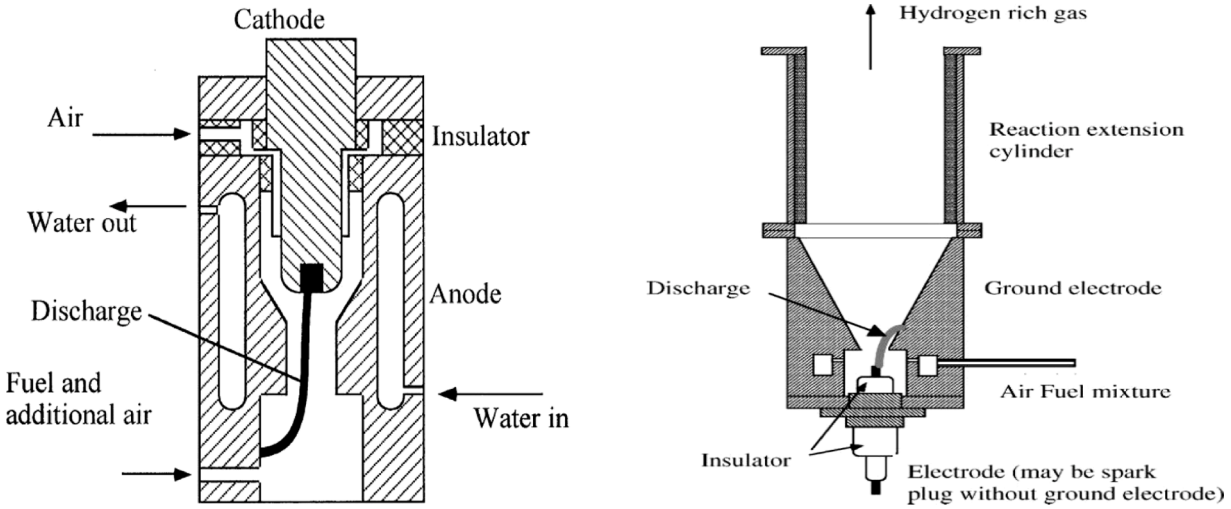

Fig. 49. Thermal (left) and low current (non-thermal) (right) Plasmatron fuel converters. (Reprinted from [470] with permission of Elsevier).

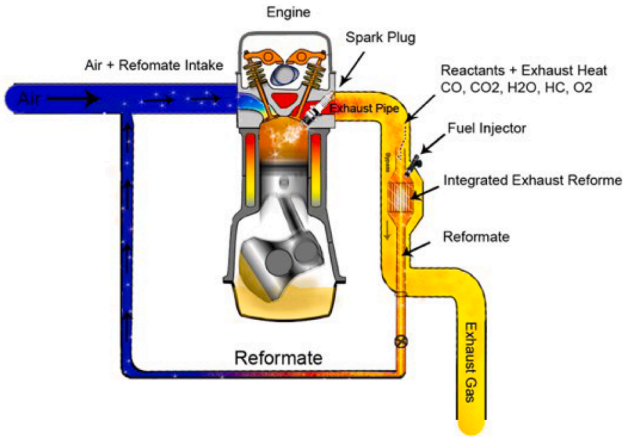

R-EGR (University of Birmingham) [484]

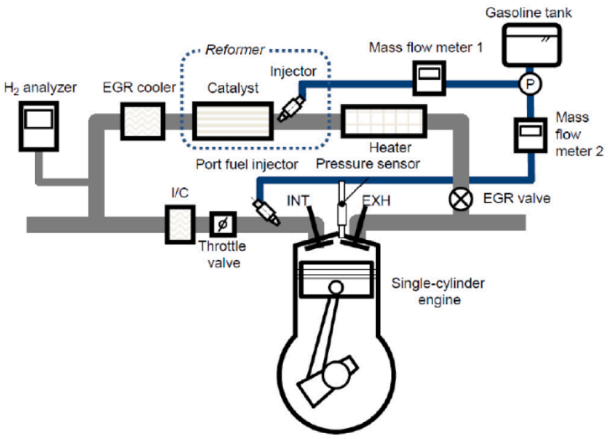

On-board fuel reformer (Nissan Motor Co.) [485]

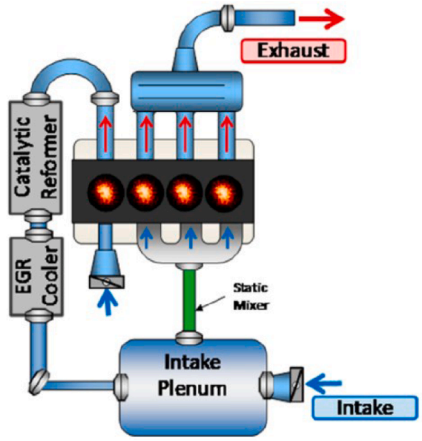

Catalytic EGR−loop reforming strategy (ORNL) [486]

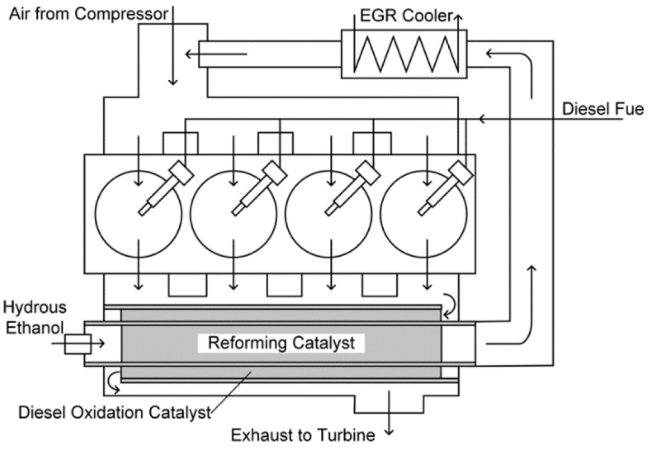

Integrated steam reforming (ISR) reactor (University of Minnesota) [487]

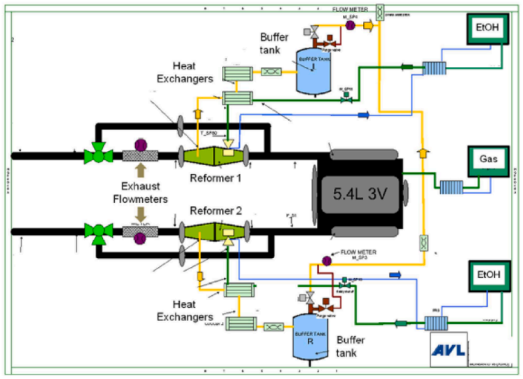

Shoebox reformer design (Monsanto Company) [488]

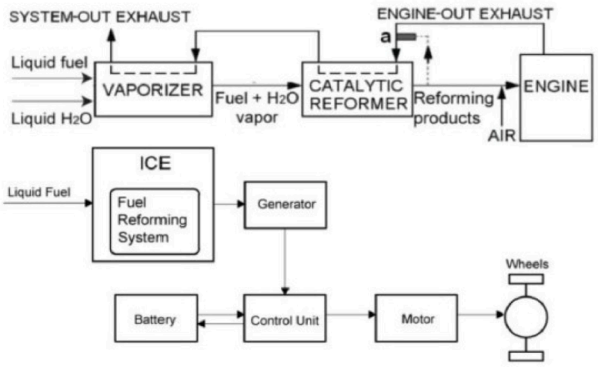

Vehicle hybrid propulsion system with onboard methanol reforming (TIIT) [24]

Fig. 50. Schematic of various integrations of on-board exhaust gas fuel reformer in IC engines adapted from literature.
R-EGR (University of Birmingham) [484]
On-board fuel reformer (Nissan Motor Co.) [485]
Catalytic EGR−loop reforming strategy (ORNL) [486]
Integrated steam reforming (ISR) reactor (University of Minnesota) [487]
Shoebox reformer design (Monsanto Company) [488]
Vehicle hybrid propulsion system with onboard methanol reforming (TIIT) [24]

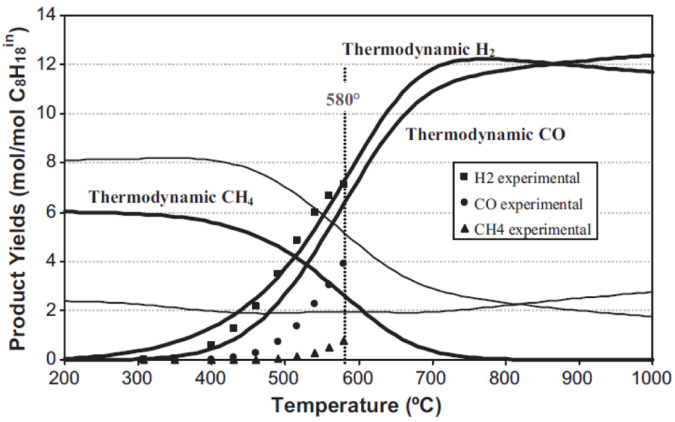

Fig. 51. Thermodynamic and experimental product yields as a function of temperature for iso-octane fuel and REGR conditions; experimental data were obtained during an increase of 10 °C/min and at $p = 1.3$ bar. (Reprinted from [490] with permission of Elsevier).

in the following. In general, optimized heat transfer from exhaust gas stream to catalyst with minimized heat loss positively affects hydrogen and CO yields, and this can be addressed with an appropriate reformer design and a fitting place of the reformer relative to the engine. However, before all of these, the engine operating conditions decide what will happen inside the reformer.

Thermochemical recovery:

The engine provides heat and reactants (oxidizer or steam) for evaporating liquid fuel and initiating reactions involved in the reforming process. The exhaust gas stream contains CO_2 (for dry reforming), H_2O (for steam reforming), and O_2 (for partial or complete oxidation); each of them can initially react with the engine fuel with a proper catalyst. Thereafter, CO supplied by incomplete combustion from the engine or by the product of preceding primary reactions can react with steam not yet consumed to perform the water-gas shift (WGS) reforming reaction as a means of minimizing CO, which may be considered as a CO clean-up strategy for the catalyst [116,493], similar to that for avoiding poisoning of fuel cell anodes [494]. Finally, methanation reactions may take place to consume available hydrogen in reformate, decreasing the potential H_2 yield.

Understanding which of the reactions has a significant share in the reforming process depends on the temperature and composition of the engine exhaust gas, which directly relies on the engine operating conditions. Efficient TCR with a high heating value reformate occurs when all reactions are eventually net endothermic; therefore, the target is to maximize endothermic reforming reactions, primarily dry and steam reforming. Nevertheless, the low temperature of the exhaust at low engine loads cannot drive endothermic reactions alone; thus, in this case, partial and complete oxidation reactions are useful to provide the heat required to achieve the reforming process and the likelihood of tailpipe-out emission reduction, with the possibility of heat loss. Hence, the exhaust gas fuel reformer may act like an auto-thermal reformer (ATR) without needing a separate water tank and air supply system. Recently, Tartakovsky and Sheintuch [33] thoroughly reviewed this concept and we would recommend to refer to this paper for more information.

IC engine considerations:

Incorporating the exhaust gas fuel reformer at various engine operating points at different combustion modes, including CI [495–502], SI [484,489], HCCI [356,498,503], and partially premixed compression ignition (PCCI) [504] to produce R-EGR reformate has been widely investigated at the University of Birmingham over the last two decades; and more recently with a gasoline direct injection (GDI) engine reported in [100,492,505-510].

A series of studies on diesel engines integrated with a prototype exhaust gas fuel reformer (see Fig. 52 (left)) has been done with precious metal catalysts. Tsolakis et al. [496] employed this reformer whereby direct catalytic reforming of diesel is performed with the exhaust gas of a single-cylinder diesel engine operating at part load. They achieved up to 16% hydrogen content in the R-EGR products for a reformer inlet temperature of T=290°C. They also indicated that the use of R-EGR shifted the traditional NOx-smoke trade-off curve to lower values and lowered the incremental slope of smoke as compared to conventional EGR, as depicted in Fig. 52 (right). The same author [499] externally heated a diesel oxidation catalyst (DOC) Pt/AL_2O_3 at the temperature of T=250°C (same condition as the engine running at 1800 rpm and 25% load) and then added R-EGR products to the engine intake manifold with reduced diesel fuel injected in order to maintain the engine condition constant at low load. They found that poor use of gaseous fuel (diesel combustion was still predominant) occurred with 20% R-EGR addition due to increased fuel consumption (i.e., a higher BSFC in g/kWh); while improving gaseous fuel oxidation with 30% R-EGR addition lowered BSFC due to approaching the stoichiometric air-fuel mixture by reducing O_2 concentration in the cylinder and the higher intake temperature. Note that all these engine tests were achieved with simulated R-EGR bottled gas replaced with a part (or entire) of EGR.

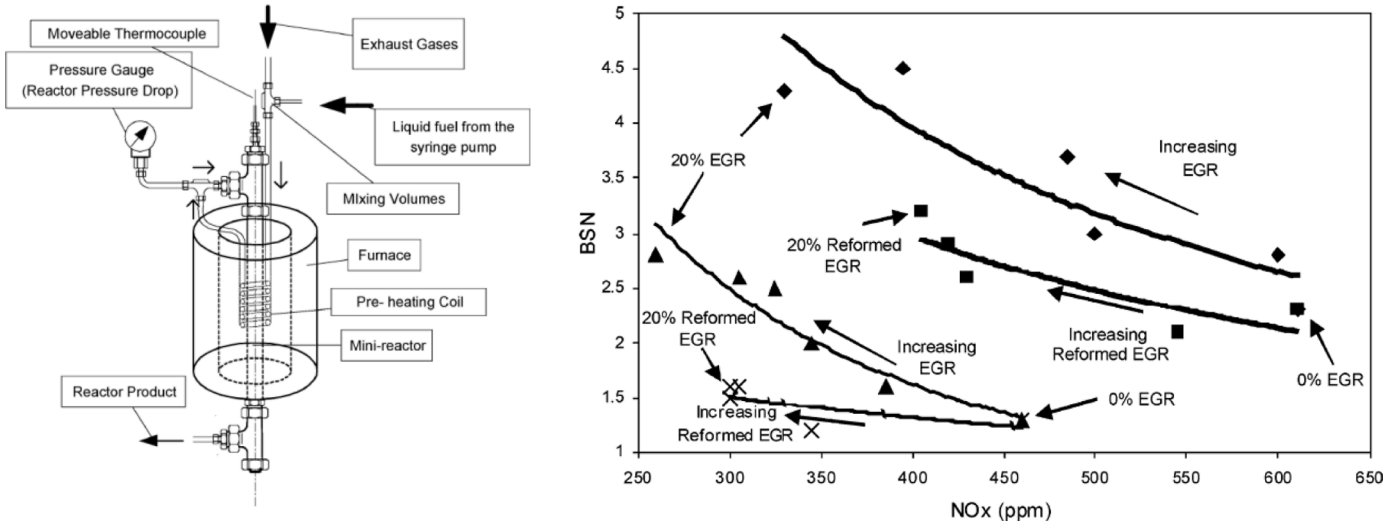

Fig. 52. Schematic of liquid fuel reforming system (left) and effects of EGR (0–20%) and R-EGR (0–20%) on the NOx and Bosch smoke number (BSN), both upper and both lower curves pertain to 6.1 and 4.6 bar IMEP, respectively, and 1500 rpm (right) (Reprinted from [495,496] with permission of Elsevier).

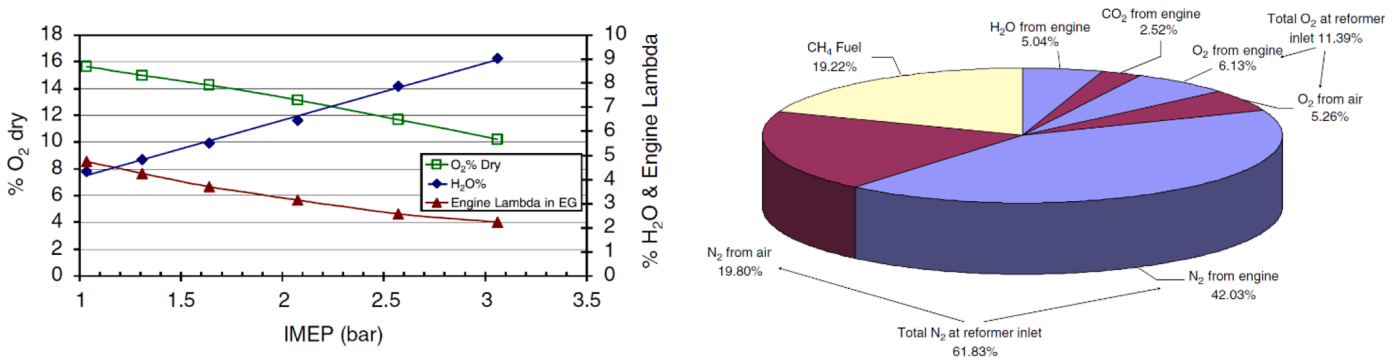

Fig. 53. Variation of oxygen and water contents of exhaust gas with IMEP (left) and reformer inlet composition for production of a 10.4% (vol.) H_2 in R-EGR (right). (Reprinted from [356] with permission of Elsevier).

Yap et al. [356] introduced a closed reforming loop system in the inlet of the exhaust manifold of a natural gas HCCI engine to perform methane (base fuel) reforming at low temperatures (~ 300°C) corresponding to lean operation. Since hydrogen yield varies with engine operating load (see Fig. 53 (left)), they suggested that a part of the exhaust gas can be displaced by extra O_2 content from the incoming fresh air (see Fig. 53 (right)) to maintain the hydrogen production target of 10% (by vol.) from 1 to 3 bar IMEP. Recently, another study [511] also reported that the adverse effect of highly endothermic conditions ($\phi_{catalyst}$ >7) on the suppression of high reformate yields could be counteracted by adding a small quantity of O_2, reaching 15% H_2 (by vol.).

In general, if the steam reforming process reduces the reformer temperature sufficiently, the possibility of inactivating the entire reforming process must be considered. Therefore, the addition of O_2 contained in the incoming fresh air as an option affords partial oxidation reforming to prevent inactivity of reforming process at low temperature and high reformer equivalence ratio (near to stoichiometric and higher engine loads) conditions. Interestingly, despite stressing on pure O_2 to provide a large amount of H_2 in fuel cells [512], just fresh air is sufficient due to the need for a small amount of H_2 for IC engine applications.

The effects of water added into the exhaust gas fuel reformer on hydrogen yield and conversion efficiency of catalytically diesel reforming were also investigated by Tsolakis et al. [497]; at T=290°C reformer inlet temperature, H_2 in the reformer product was obtained up to 15% more than with reformer operating without supplying water, due to presence of WGS reactions and then CO consumption in the reforming process. While heat losses from oxidative reactions can be mitigated by water addition, however, endothermic nature of WGS can lead to a reduction in overall engine-reactor efficiency.

Full scale engine-reformer integration:

A problem with aforementioned works was that the reformer and IC engine was not considered as a fully integrated system. As described in Fennel et al. [100,492], for the first time, a full-scale prototype gasoline reformer consists of a stack of five metallic catalyst plates loaded by 3.3% Pt/ 1.7% Rd was integrated with a modern TC, multi-cylinder GDI engine, by installing the reformer after TWC. A high pressure EGR loop was used to introduce a fraction of engine exhaust gas as the feed gas into the reformer and then the produced reformate was inducted into the intake manifold of the engine. Initially, they showed R-EGR benefits over the baseline and conventional EGR in GDI engine, in terms of engine efficiency, NOx and PM emissions, due to extension of the dilution limit [505,506]. Secondly, it was shown that temperature distribution and generally performance of the reformer have a great dependency on the exhaust temperature and mass flow rate of the feed gas. At high temperature conditions (> 650°C), both efficiencies of engine and reformer process were improved up to 8% and being more than 100%, respectively, indicating an improvement in the base fuel enthalpy. At lower temperatures (~ 600°C), engine efficiency increased up to 4%; but in contrast, reformer efficiency was less than 100%, meaning some energy is lost in the base fuel (gasoline) during the reforming process [507]. Finally, they offered that the downsizing strategy and using a boost device with GDI engine would be favorable for exhaust gas fuel reforming because operating IMEPs of engine will be shifted to the higher loads, resulting in increasing the exhaust gas temperature.

Ashida et al. [485,513] used a 4 wt% Rh/Al_2O_3 catalyst reformer installed in the external EGR line of a SI engine (see Fig. 50, under the label of 'On-board fuel reformer') for catalytic steam reforming of injected gasoline in the presence of high-temperature EGR gas, without any additional O_2. They initially observed an H_2 production close to the calculated equilibrium concentration, but later catalyst deactivation almost started appearing within 5 hours, affecting the catalyst's durability [514]. Thus, steam reforming only will potentially face the challenges of catalyst activity and durability in R-EGR strategy. Similarly, Brookshear et al. [515] at Oak Ridge National Laboratory (ORNL) incorporated a 2 wt% Rh/Al_2O_3 catalyst into the EGR loop of a multi-cylinder, stoichiometric SI engine. That work was followed by Chang et al. [511] to characterize the catalytic reforming performance using equilibrium modeling and experiments with iso-octane fueling. They firstly showed that reformer temperature, O_2 mole concentration, H/C ratio of the fuel, and equivalence ratio of the catalyst are all key factors for determining the reformate products. Findings at a quasi-state-state condition revealed that the highest H_2 yield (15% vol.) (Fig. 54-A) for O_2 catalyst flow rate of 12 g/min (and higher) has coincided with maximum water consumption (Fig. 54-D) in the range of4 < $\varphi_{catalyst}$ < 7, suggesting the strong presence of SR or WGS reactions. Moreover, for$\varphi_{catalyst}$ > 5, CO began being consumed (Fig. 54-B), and then H_2/CO captured higher values, meaning that the WGS would predominate at lower catalyst temperatures (Fig. 54-C).

Hwang et al. [516] were the first researchers who introduced a thermally integrated Rh/Pt catalyst reformer with a diesel engine to mitigate heat losses to the environment by mounting the reformer inside the exhaust manifold system. In this way, much more heat is readily accessible to the exhaust fuel reformer; thus, the primary candidate for catalytic reactions will be steam reforming. While the study showed the capability of producing high concentrations of hydrogen (as much as 10% indicating high conversion efficiency), the on-board reforming system indicated a decrease in overall engine efficiency due to a fuel energy penalty for diesel at conditions with low reformer equivalence ratio ($\varphi_{reformer}$~1.5). Hence, a thermally integrated reforming system with a high reformer equivalence ratio (lower dependency on POX reactions) demonstrated improvement in both engine and reformer conversion efficacies. Completely eliminating POX in the reformer along with using water contained in the fuel, like hydrous ethanol as the secondary fuel to provide a source of water for SR, is a solution to boost TCR effect; in this regard, the same authors [487] developed their proposed reformer and called it integrated steam reforming (ISR) (see Fig. 50, under the label of 'Integrated steam reforming (ISR) reactor') to

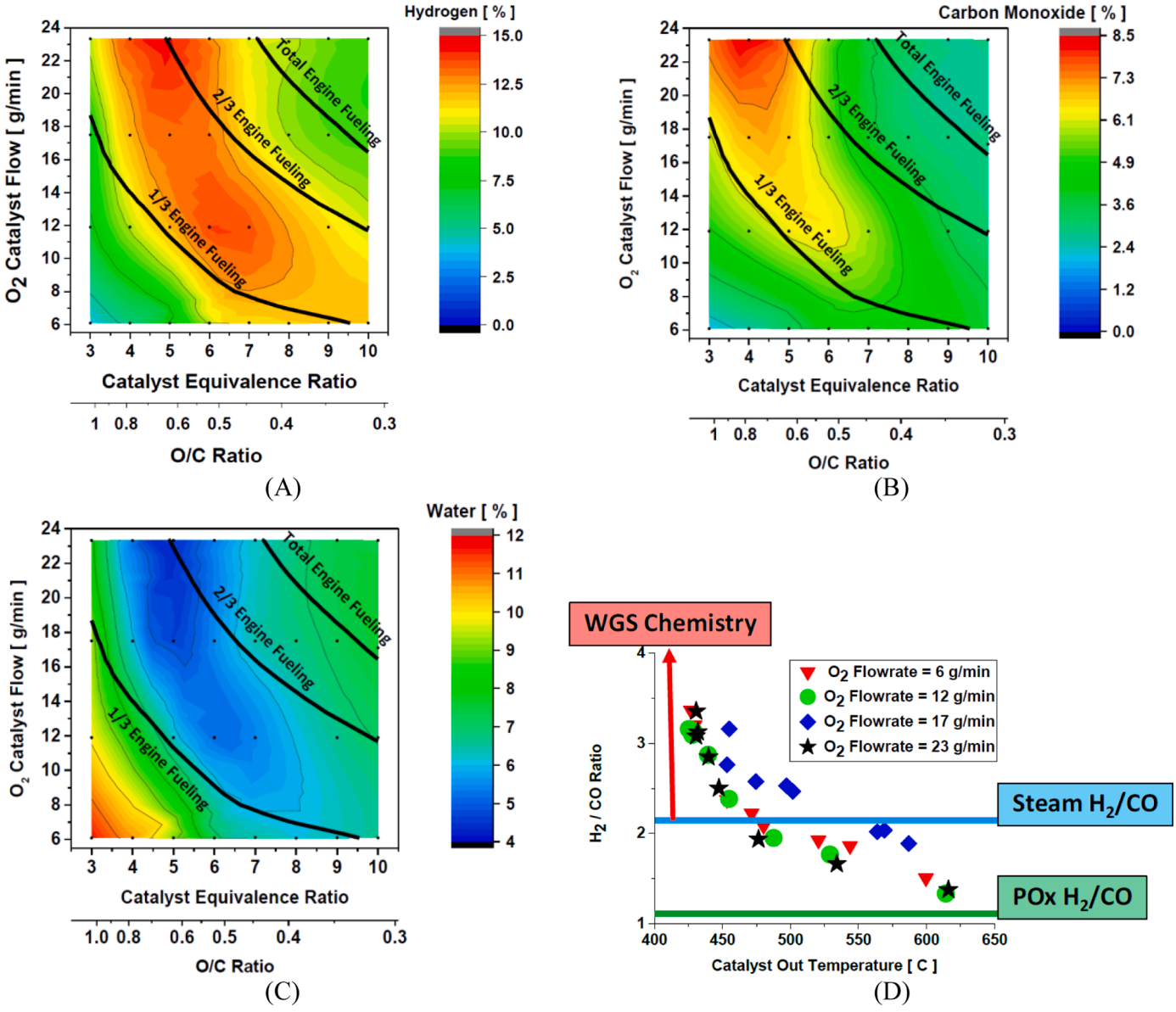

Fig. 54. Concentration of H_2 (A), CO (B), and H_2O (C) as function of $\Phi_{catalyst}$ and O_2 catalyst flow rate at the outlet of the catalyst, and correlation of H_2/CO ratio and the catalyst-out temperature (D) [511].

enable diesel engine dual-fuel (diesel/syngas) operation. It was shown that the heating value of the fuel increased by 23% at 100% conversion.

Reforming fuel type:

It has been reported that the reformer and catalyst designs should be optimized exclusively for each type of reforming fuel in the REGR-assisted IC engine application. For instance, Tsolakis et al. [517] compared the reforming of ultra-low sulfur diesel (ULSD) with ultra-clean gas-to-liquid (GTL) fuels for a single-cylinder diesel engine. They showed decreased methanation reactions, which ends with CH_4 present in the reformed products with GTL fueling. Thus, results in higher hydrogen generation and fuel conversion compared to ULSD reforming. These advantages of such fueling can result in reformer compactness improvement and catalyst cost-benefit.

The feasibility of R-EGR with renewable fuels such as biodiesel was shown in the earlier stages of research in a CI engine [495], and later with renewable oxygenated fuels like bioethanol and rapeseed methyl ester (RME) in both CI and HCCI engines [356,503,504,518]. Tsolakis et al. [519] indicated that both of them have higher reforming efficiency (as defined by low heating values of products over the fuel input) and H_2 production compared to ULSD, especially at lower reformer inlet temperatures (~290°C). Thus, reforming process efficiency has a strong reliance on reforming fuel type. For CI engines, other fuels such as biogas [501,520,521] are also used to upgrade into reformate through exhaust gas reforming.

SI engine fueled with bioethanol was investigated for the first time by Leung et al. [484] for R-EGR; the activity of a precious-metal catalyst containing 1%Rh – 2%Pt (by mass) on 30% (by mass) ceria-zirconia for all expected reaction routes of bioethanol reforming during exhaust gas reforming were observed, except for the WGS reaction. Their results predicted that the overall reforming process is oxidative, increasing fuel heating value by 6% while increasing it up to 20% with less O_2 present in the exhaust. Researchers at AVL and Monsanto Co. [488,522,523] designed a compact lightweight, exhaust gas ethanol reformer, called "shoebox", with a copper-nickel powder catalyst to combine with a multi-cylinder SI engine fueled with ethanol or E85 (see Fig. 50, under the label of 'Shoebox reformer design'), with the objectives of reducing HC emissions during cold start and improving part-load dilution. They initially observed that mixing 50% of (simulated) reformate, known as

the "low-temperature ethanol reformate" due to low temperatures requirement (300-350°C), with E85 enables diluted engine operation, leading to a 10-17% and 20-25% rise in brake thermal efficiency as compared to stoichiometric E85 and gasoline baselines, respectively [522]; mixing 25-40% of real ethanol reformate in E85 increased the efficiency by 10-12.3% at part load and idle conditions, as well as HC emission reduction [523]. Ji et al. [524] placed an ethanol steam reformer loaded with the copper catalyst inside a multi-cylinder SI engine fueled gasoline. Note that deionized water and ethanol were the feedstock of SR, meaning that the engine exhaust was just the source of heat, not reactants. They reported around 4.5% improvement in indicated thermal efficiency with 2.43% of reformate (by vol.) in the total intake gas. Also, the exploration of suitable catalyst formulation for exhaust gas-driven ethanol steam reforming (ESR) of a single-cylinder SI engine is discussed in [525]. Unlike the TCR goal, catalytic partial oxidation (CPOX) of ethanol over Pt, Pt-Palladium (Pd), and Pt-Rh catalysts at typical diesel exhaust temperatures up to 400°C have been experimentally carried out as a viable pathway of producing reformate for the automotive exhaust gas aftertreatment systems [526,527]. For instance, it has been reported that for the CPOX of ethanol over a Pt-Rh on alumina at a constant reformer inlet temperature of 300°C, that oxygen/ethanol (O/E) molar ratio has a key role in the determination of ethanol conversion, reaction temperature, H_2 generation, and selectivity towardH_2, such that the maximum H_2 would be produced at a higher O/E ratio than that predicted by equilibrium, for a given ethanol concentration.

Hydrous ethanol (HE) or wet ethanol has considerable saving energy rather than anhydrous ethanol, (as typical alcoholic engine fuel) in terms of not only eliminating the water removal requirement, but use of water content for assisting steam reforming. It has been claimed that HE distillation and dehydration account for about 50% consumption of total base ethanol energy [484]; thus, HE has higher overall energy cycle than anhydrous ethanol. HE as standalone fuel for IC engines may result in poor performance due to incomplete combustion and severe charge cooling effect of water [528]. Li [529] indicated the feasibility of 150 proof HE (i.e., 75% ethanol with 25% water volume content) as exhaust reformer fuel of SI engine fueled with gasoline; the HE conversion peaked at approximately 675 K using a copper-based catalyst. Also, Hwang et al. [487] catalytically converted a 150 proof HE over a Pt-Rh catalyst into a secondary fuel (with a 23% increase in heating value) for a diesel engine coupled to an exhaust reformer. Nevertheless, ethanol production is confined to certain regions such as Brazil and North America.

Methanol has been the primary fuel in reforming applications for many years because it requires a slightly lower reforming temperature than ethanol due to having no C-C bonds. This makes it candidates for 100% reforming such that its resultant reformate would be as standalone fuel for the IC engines [33]. In this regard, Tartakovsky et al. [530–535] conducted a series of studies on on-board methanol steam reforming (MSR) with a high-pressure TCR system and then introducing it with direct injection into the IC engine. Results from a DISI engine fed with 100% methanol SR products as engine fuel showed an 18-39% improvement in the indicated efficiency and a reduction of 73-94%, 90-95%, 85-97%, and 10-25% in NOx, CO, HC, and CO_2 emissions, respectively compared to gasoline within a wide range of engine loads. Lia and Horng [536] employed the exhaust heat of a 4-cylinder SI engine to drive MSR reactions over a CuO–ZnO/Al_2O_3 catalyst at a controlled reforming temperature of 300°C; a maximal methanol conversion of 93% and the molar flow rate of produced H_2 by about 1.34 mole/min for a steam to carbon (S/C) ratio of 1.2 were reported. More recently, Nguyen et al. [537] numerically examined the efficiency of a REGR-assisted SI engine fueled with methanol and then compared it with ethanol counterpart, considering only steam and dry reforming reactions for both fuels. As illustrated in Fig. 55, steam reforming of ethanol with H_2/CO products (EtOH-CO) and with H_2/CO_2 products (EtOH-CO_2) have higher engine-cycle efficiency than methanol steam

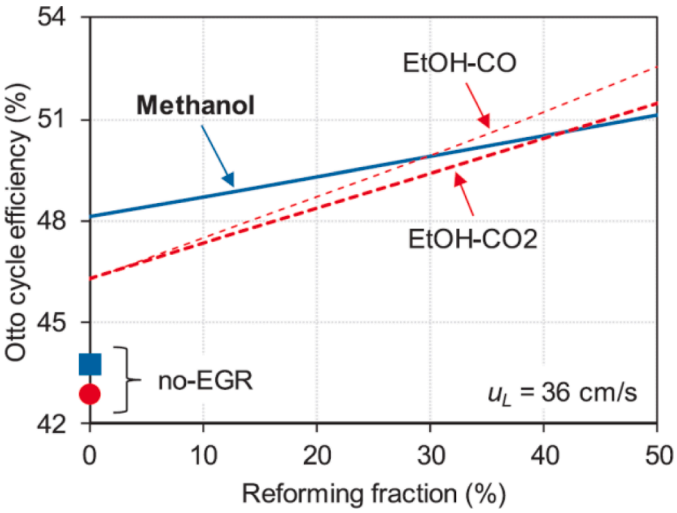

Fig. 55. The maximum Otto cycle efficiency of methanol, ethanol-CO_2 and ethanol-CO at the same combustion stability limit (Reprinted from [537] with permission of Elsevier).

reforming (MSR), at a higher reforming fraction. On the figure's y-axis, two lower cases indicate no EGR and no reforming usage, and the top of those relate to an EGR limit of 25% without reforming.

As another renewable fuel, ammonia, an affordable hydrogen carrier [538], can be converted into reformate which is free of COx. Earlier, ammonia in the form of urea was applied on catalytic after-treatment systems of heavy-duty diesel engines to reduce NOx [539]. Then, exhaust reforming of ammonia, which needs ~ 500°C for decomposing [540], with a diesel engine that provided 100-400°C was investigated through the auto-thermal (i.e., NH_3-ATR) process and using a ruthenium (Ru)-Al_2O_3 catalyst [541]. It was observed that the H_2 production was in the range of 2.5-3.2 l/min with the O_2/NH_3 ratio from 0.03 to 0.175 with a fixed NH_3 feed flow of 3 l/min; and when the small amount of produced reformate was added to the intake air (representing as 5% replacement of diesel fuel), a substantial reduction was obtained in CO, CO_2, and THC emissions. In a more recent study [542], exhaust reforming of ammonia at higher exhaust temperatures of a GDI engine (450-550°C) over an Rh-Pt/Al_2O_3 catalyst was evaluated by two cases of direct catalytic conversion of ammonia (a portion of exhaust used) and ammonia decomposition (only exhaust heat used) to produce H_2-N_2 products. They showed that 30 and 32% improvements were achieved in the case of extracting exhaust heat and using exhaust gas, respectively.

In summary, ethanol and methanol as suitable reforming feedstocks can facilitate catalyst reforming at lower temperatures, mainly due to having a simpler structure than the complex long-chain hydrocarbons. Another advantage is that they are soluble in water and can be premixed to contain appropriate molar steam-to-carbon ratio for reforming. Pure steam reforming of alcohols can be accomplished using waste heat in a TCR reactor due to their ability to be reformed at engine exhaust-relevant temperatures. The temperature needed for reforming HC fuels is at least about 550°C while for methanol and ethanol is typically in the range of 250-300°C. However, because of methanol's toxicity, it is less desirable than ethanol for reforming.

Conclusion:

With the assumption of a proper catalyst reformer choice and appropriate integration with the IC engine:

- At close to stoichiometric conditions and high engine loads: more provided heat and steam to drive predominantly endothermic reactions (steam and dry reforming) increase the heating value of the base fuel and afford a high TCR effect. In the case of low temperatures (<700°C), fresh air addition is an option to maintain catalyst activity by providing more heat from POX or combustion reactions

within the reformer. The overall process can be either exothermic or endothermic; depending upon catalyst temperature and reforming fuel type.

- At lean conditions and low engine loads: higher oxygen concentrations in the engine exhaust stream are accessible to the reformer but at lower temperatures. A high achievable conversion efficiency, which yields high reformate concentrations in the range of 10-15% for both H_2 and CO, can be demonstrated. In this case, the risk of combustion occurrence exists due to the possibility of complete fuel oxidation. POX reactions may increase the reformer temperature exceedingly until the catalyst burns out or deactivation takes place.
- Moreover, in an engine operating map, transients from low to high loads impose controllability issues due to variations in local reformer equivalence ratio (O_2 availability). Hence, there is a continuous balance to manage between high fuel enthalpy achievement and high reformate production (high fuel conversion) across all engine speed/load conditions.

According to the literature, stoichiometric exhaust at higher temperatures (i.e., modern SI engines) is the priority to fully take advantage of exhaust gas reforming in terms of heat recovery benefits; and for overall lower exhaust temperature, and proven feasibility of renewable oxygenated fuels such as methanol and ethanol with R-EGR suggest the need for more research in this area, despite having more cost relative to in-cylinder reforming strategies.

4.2. In-cylinder fuel reforming

4.2.1. Negative valve overlap (NVO) reforming

Negative valve overlap fuel injection or NVO fuel injection (initially referred to as activation injection) was suggested [543] as a chemical extender for homogenous combustion by injecting fuel into the remaining exhaust gas (called residuals, iEGR or residual gas fraction) between two timings of early exhaust valve closing and late intake valve opening. This technique offers control of the activation energy of the main combustion reactions by potentially providing an in-cylinder environment prone to ignite, as shown in Fig 56.

On the other hand, the absence of any direct control of in-cylinder fuel processing in a typical HCCI engine will lead to a narrower engine operating range due to the possibility of misfiring at low-load and severe high-pressure rise rates at high load. Urushihara et al. [545] recognized the concept of shifting the chemical composition of the fuel in the high-temperature residual gases and then recompressing during the exhaust stroke, and called it the fuel reforming process. They tested various patterns of direct fuel injection to explore the effect on expanding the operating range of a gasoline-fueled HCCI engine at low load. They represented an optimal direct fuel injection strategy in which a small amount of the fuel is injected during the NVO exhaust stroke while the rest is injected during the intake stroke, representing a split injection ratio. HCCI with NVO fuel reforming has been drawing a great deal of attention for several years [546–548]. The usefulness of this technique was also investigated in other low temperature combustion

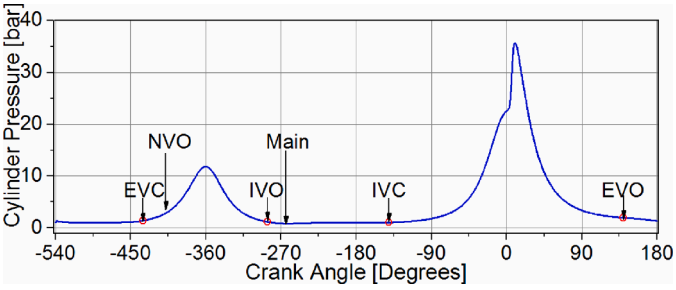

Fig. 56. Cylinder pressure versus crank angle degrees for NVO fuel injection and LTGC combustion, including valve events [544].

(LTC) modes, such as in partially premixed combustion (PPC) [549].

In the case of the SI engine, low-temperature combustion modes such as HCCI and spark assisted compression ignition (SACI) have been used to switch the stoichiometric mode of a traditional SI engine to an effective dilution mode, presenting a higher fuel economy than before; however, they encounter a narrower load range for the HCCI engine along with TWC deficiency. As a solution, employing NVO fuel reforming in stoichiometric SI engines has recently drawn attention, resulting in extending the dilution limit at low and maybe part engine loads. For instance, Chang et al. [550] explored the effects of sweeping the start of injection (SOI) timing, from 300 to 420 CAD $BTDC_{firing}$, during a fixed NVO period of 80 CAD and varying the NVO periods dilution limit in a stoichiometric SI engine fueled with E10 (baseline engine fuel) at BMEP=3 bar and engine speed of1800 rpm. At a fixed NVO period of 80 CAD, while the maximum peak heat release rate with lowest CoV of IMEP belonged to the SOI=380 CAD $BTDC_{firing}$ case, the volumetric efficiency remained unaffected by the swept NVO SOI, which means that no variation was seen in BMEP. Also, an extended dilution limit was seen with a total EGR rate of 32%, and a 22% reduction in BSFC as compared to the reference engine version, in the case of TDC injection (SOI=360 CA$BTDC_{firing}$) and 80 CAD NVO.

A comparison between symmetric NVO and PVO strategies has been conducted by Rodriguez and Cheng [551], which resulted in NVO benefits at low load by 7% improvement in fuel consumption due to reduced pumping losses. At part load, IMEP can increase up to 6 bar by combining symmetric NVO with optimized EVO timing to minimize losses of the blowdown process; which means that the PVO strategy is superior to the NVO strategy at part-load of a SI engine. More recently, the possibility of using NVO fuel reforming in a gasoline/diesel dual fuel engine [552] and RCCI engine fueled with natural gas(NG)/diesel has been proposed and evaluated through the simulation based on a developed in-house code [553]. The low-load efficiency of NG/diesel RCCI with NVO reforming was better than a lean strategy and EGR baselines by 5.5% and 3%, respectively, due to increased combustion efficiency and despite NVO's increased pumping losses.

NVO fuel reforming effects:

Thermal and chemical effects corresponding to the NVO fuel reforming process directly influence the main combustion; hence, these effects must be identified individually. Retained and recompressed exhaust enthalpy during the NVO period can raise the overall charge temperature and this increases the specific heat ratio (γ) of the charge. Moreover, NVO fuel injection, and the corresponding reactions and heat release, produce reformate, which itself has a high specific heat ratio ($\sim$1.40), which further enhances the overall γ of the charge prior to the subsequent main-combustion event. As an outcome, increased thermal efficiency can be expected. On the other hand, NVO-reformate products can reduce the mixture's overall ignition delay and expedite the mixture's chemical kinetics (i.e., a mixture with higher reactivity than the base fuel), which leads to improved stabilization of the main combustion and low-load limit of the engine. Here, temperature and available oxygen in the residuals during NVO link both effects together.

Song et al. [554] noticed that there is a competing effect between thermal and chemical effects by performing simulations on a gasoline HCCI engine operating at various equivalence ratios from 0.6 to 1 with NVO pilot injection, which resulted in optimum oxygen availability (equivalence ratio) for successfully reducing ignition delay. At lean conditions (high oxygen concentration) and near-stoichiometric (low-oxygen concentration), exothermic reactions and endothermic reactions (from fuel pyrolysis) will become dominant, respectively. Szybist et al. [555] pointed out that a large amount of reformate and other short-chain hydrocarbons could be obtained in the low-O_2 environment. Reported oxygen concentrations from documents are in a range of 2–4 % during the NVO period.

Due to the complexity of measuring in-cylinder temperature, especially at the IVC of an engine cycle with NVO fuel reforming, several thermodynamic-based predictor models have been developed, relying

on temperature measurements at the exhaust port during the exhaust event (blowdown and recompressing). For instance, Fitzgerald et al. [556] developed an algorithm to isolate the thermal effect of NVO fuel reforming on iso-octane HCCI combustion from the chemical effect through calculating cycle temperature. In a later work they found [557] that chemical effects are dominant in late NVO fueling, because the early exothermic reactions due to the presence of ethylene and formaldehyde (reformed NVO species) offsets the cooler charge at IVC (thermal effect), and the main combustion remains advanced similar to the early fueling case. But, thermal effects have prominent role in early NVO fueling, with higher fuel conversion efficiency (~ 80-90%) as compared with the late fueling case. As an overall conclusion, NVO heat release depends on the mass and injection timings of the NVO fuel and oxygen availability.

For better understanding of fuel reforming chemistry, kinetics, and the evolving reactive species, various sampling approaches in conjunction with gas analyzers have been implemented experimentally to characterize the NVO-period reformate [558,559]. In this regard, researchers at the Sandia National Laboratories (SNL), Oak Ridge National Laboratories (ORNL), and the University of Minnesota had valuable relevant contributions [544,560-568]. Through these studies the effect of molecular structure of the NVO-fuel [565] on NVO fuel reforming were explored for various fuels. The related ensemble-averaged in-cylinder pressure and heat release rate profiles during the NVO period are shown in Fig. 57. For ethanol fueling, the exothermic heat release resulted in the highest peak bulk-averaged in-cylinder temperature among the fuels. As shown, for most fuels the lack of sufficient heat release reveals that the fuel-injected was mainly converted into reformate. Later modeling work by the same authors [567] used a detailed kinetic mechanism for iso-octane in a stochastic reactor model (SRM) that examined the NVO reforming process. This work found that endothermic and exothermic reactions are mainly balanced for most fuels, limiting obvious heat release as found using in-cylinder pressure analysis. The modeling work also suggested that the in-cylinder mixture gradient during NVO reforming was responsible for producing reactive species, in addition to the main syngas components, such as allene, acetaldehyde, and acetylene, which were partially responsible for improved reactivity in the main low-temperature gasoline combustion (LTGC) ignition event. The significance of the NVO-fuel type also was reported by another work [560], in which hydrogen fraction of NVO-reformate was less than 1.5% with iso-octane and more than 8% with methanol fueling.

Moreover, pathways to get more fuel decomposition (more reactivity) during NVO [566], and the impacts of NVO-reformate on engine performance [544] have been discussed. For instance, it was reported that more fuel decomposition was achievable with longer chemistry residence times and lower spray impingement on piston surface (i.e., an advanced NVO SOI).

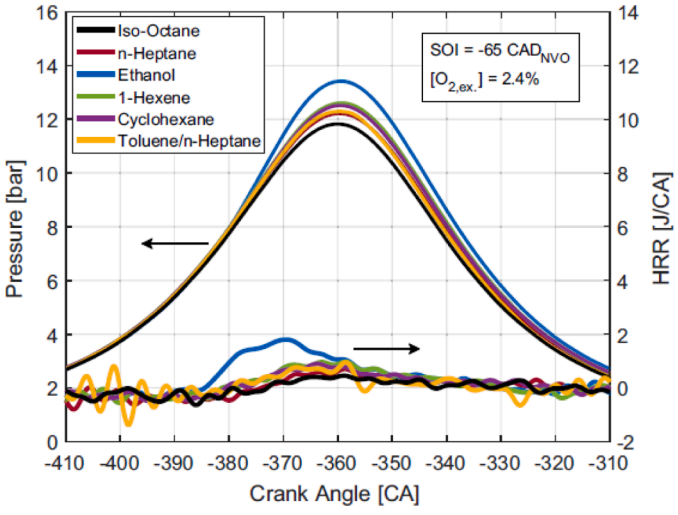

Fig. 57. In-cylinder pressure and heat release rate versus crank angle during the NVO period for various fuels (Reprinted from [544] with permission of Elsevier).

As an energy recovery method:

NVO fuel reforming can be regarded as a thermochemical recuperation process in which waste exhaust thermal energy converts to more accessible chemical energy for the main combustion; the injected fuel during the NVO period uses the heating provided from trapped and recompressed exhaust residuals left from the previous cycle to drive endothermic reactions, resulting in the reformate having higher overall energy content. However, heat transfer and pumping losses are two main source of losses which come from the trapped and recompressed NVO-gasses, and mixing of the NVO-period charge with the cooler intake charge, respectively. Adjusting a combination of fueling rate, fuel injection timing, and available oxygen concentration during NVO period, such that the recovered energy compensates for the losses, and the reformate species maximize at that combination is an important topic. Ekoto et al. [563] modeled a single-cylinder, LTGC engine with a NVO fuel reforming technique as a closed system (from EVC to IVC) undergoing thermodynamic processes to perform energy analysis for two fuels of ethanol and iso-octane. In comparison with iso-octane fueling, ethanol produced higher NVO-apparent heat release (AHR) despite its higher evaporative cooling effect, but with lower recovered energy due to its fast ignition chemistry. Among the findings, it has been reported that approximately 70% of usable energy recovery, which was defined as the sum of AHR and recovered fuel energy, is achievable in NVO in-cylinder fuel reforming for gasoline-like fuels with low (or zero) toluene content. As a result, a higher NVO global equivalence ratio by either reducing the NVO-period oxygen concentration or increasing fueling rates leads to a larger fraction of recovered fuel energy. Additionally, large NVO fuel injection and NVO-SOI advancement resulted in the highest overall-cycle thermodynamic efficiencies, all of which depended on NVO-fuel type (fuel chosen for the NVO reforming process).

Conclusions:

To sum up, NVO fuel reforming is a direct-injection fuel method that assists the NVO technique (a valving strategy) to address problems of undesirable combustion in the SI engine and misfiring at low load in the HCCI engine fueled with low reactivity fuels by changing the chemical and thermal effects, and consequently, the reactivity of the in-cylinder combustible mixture by reforming the base fuel. Application of NVO fuel reforming to control combustion phasing and as an extender of the low-load HCCI/LTGC and stoichiometric SI engines by providing more stabilized combustion has been successfully proved. However, the resultant NVO-reformate has shown great sensitivity not only to in-cylinder conditions, but also heavily to the NVO-injection strategy, which is varied by the selected fuel. Therefore, this sensitivity leads to complex interactions that must be considered to result in an overall optimum charge to favor the main combustion. Demonstrating this on-board fuel reforming technique with a combustion mode like RCCI, developing suitable kinetic mechanisms, and achieving the best fuel energy recovery in terms of appropriate in-cylinder thermal management might be attractive research topics for the future.

4.2.2. Dedicated exhaust gas recirculation (D-EGR)

Exhaust gas recirculation (EGR) is well-known as an effective technique of SI engine efficiency improver and NOx reducer; however, there are some severe impediments for EGR, including limited dilution and combustion instability at a higher EGR rate (10-20%). Developing concepts aiming at higher engine efficiency led to the idea of combining the EGR with the fuel reformation through dedicated cylinder(s) to perform in-cylinder partial oxidation reactions associated with rich combustion.

The idea of using one or some of the cylinders of a multi-cylinder engine as a fuel reformer (or a reactor) to perform the fuel reforming

process was first introduced by Meyers and Kubesh [569] at the Southwest Research Institute (SwRI), where they studied a lean natural gas-fueled SI engine with an assigned rich-burn cylinder to produce the EGR, primarily consisting of hydrogen and carbon monoxide. The work resulted in an efficient lean-burn SI engine with more combustion stability and thermal efficiency, called the "hybrid rich-burn/lean-burn engine." The idea was then further developed into forming an engine technology termed dedicated exhaust gas recirculation or D-EGR [570] from the sequential works at SwRI. In this technology, while the dedicated cylinder(s) runs beyond stoichiometric (i.e., rich combustion), the rest of the cylinders can operate at nearly stoichiometric conditions to properly comply with the three-way catalyst after-treatment system in SI engines. The dedicated cylinder's exhaust stream, containing not only the inert species (i.e., typical EGR products) but also the reactive constituents (i.e., reformate), is entirely separated from the exhaust manifold and redirected to the intake manifold to serve as the only EGR for the entire engine, as demonstrated in Fig. 58. The D-EGR concept from various aspects to its demonstration in modern engine technology will be discussed in the following.

D-EGR / TFR concept:

In the first practical attempt, Alger and Mangold [572] reconfigured a 2.4 L gasoline engine to dedicate one of its four cylinders for only EGR production of the entire engine by a fixed rate of 25% (by vol.). Prior to metal engine experiments, they calculated the concentration of reformate relative to the air-to-fuel (A/F) ratio variations from stoichiometric to rich, by measuring the gasses in the D-EGR cylinder exhaust (see Fig. 59). Then, they investigated the effects of the D-EGR products on the engine performance for the various engine speed/load combinations. The results obtained showed substantial improvements in thermal efficiency and emissions at both high and, in particular, low loads when the D-EGR cylinder steadily undergoes rich combustion up to about an equivalence ratio of 1.2 ($\varphi_{D-EGRcylinder} = 1.2$) and the other cylinders run at fixed stoichiometric conditions($\varphi_{othercylinders} = 1$). Fig. 60 shows the low-load results in which fuel consumption, stability in terms of CoV IMEP, and emissions have been improved over the baseline case. Also, it was observed that the total burn duration decreased significantly by reducing the early stages of kernel formation near the spark plug (i.e., 0-2% MFB duration), resulting in increased in-cylinder temperature and elevated NOx emissions, but still lower than the baseline.

Later, Zhu et al. [573] from Shanghai Jiao Tong University employed the analogous concept to D-EGR, named the thermochemical fuel

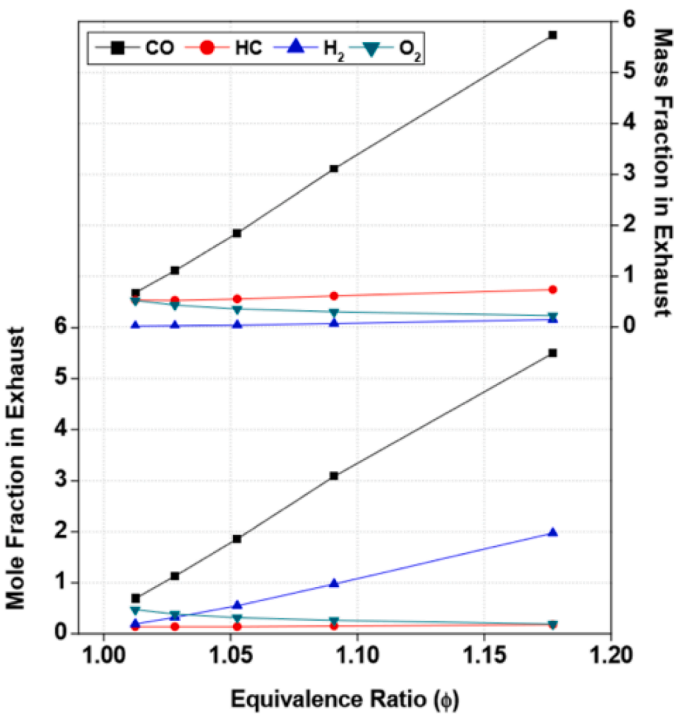

Fig. 59. Calculated exhaust species (mass and mole fractions) for different levels of enrichment by performing a chemical balance in the D-EGR cylinder exhaust [570].

reforming (TFR) concept (see Fig. 61 right). Initially, they applied it to a turbocharged, 4-cylinder SI engine specifically designed for natural gas fueling with stoichiometric operation to exhibit the potential benefits of the TFR concept over conventional EGR. Moreover, they defined the term in-cylinder TFR to evaluate the in-cylinder thermochemical process, in which a higher in-cylinder TFR would result in a greater amount of H_2 and CO and lower unreformed CH_4 fraction in the exhaust gas of the TFR cylinder (the cylinder dedicated to the TFR process). At a fixed speed of 1500 rpm and the same ignition timing of 20° BTDC applied to all cylinders, they performed a line of experimental works coupled with laminar flame calculations using CHEMKIN to evaluate in-cylinder TFR

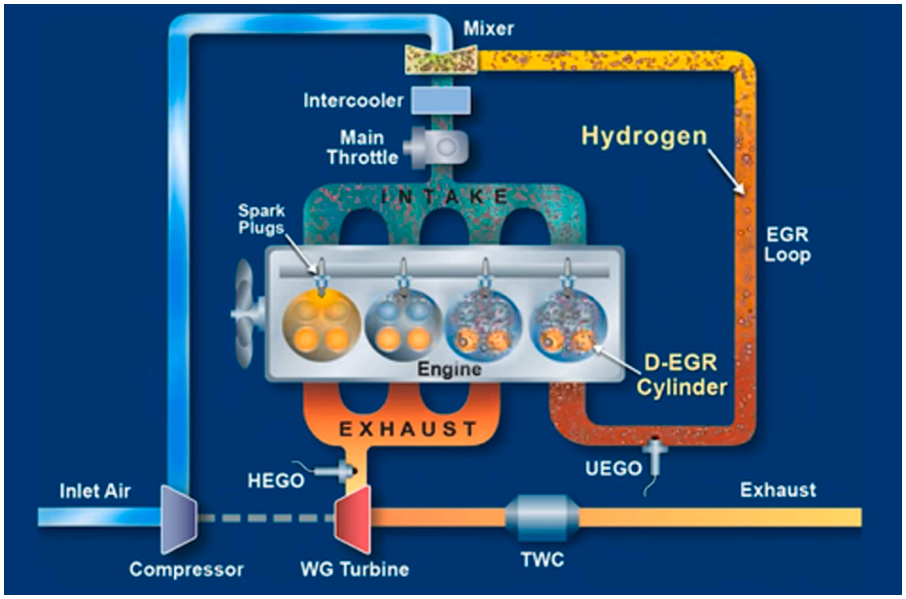

Fig. 58. Schematic of a turbocharged engine in a D-EGR configuration [571].

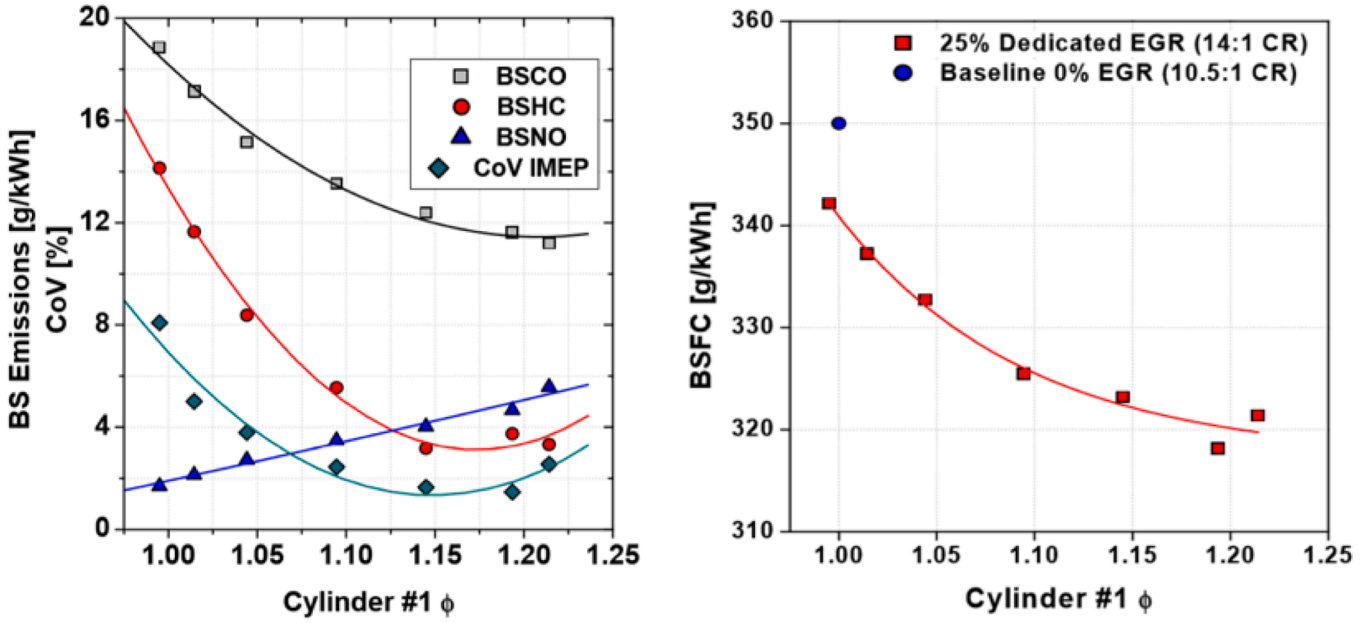

Fig. 60. Engine-out emissions, engine-average CoV (left) and fuel consumption (right) of an engine running 25 % D-EGR at 2000 rpm / 2 bar BMEP [570].

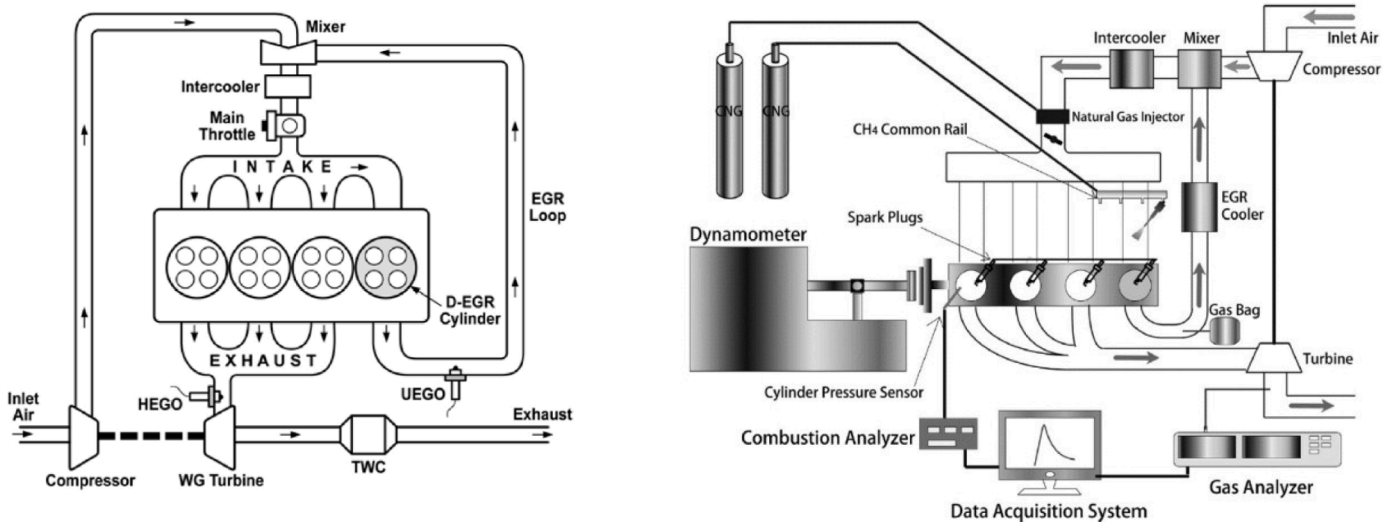

Fig. 61. Schematic of D-EGR [570] (left) and TFR [573] (right) experimental setups.

and engine uniformity by sweeping the equivalence ratio (ϕ) of the TFR cylinder from 1 to 1.4. At ϕ=1.2, where the maximum CO and H_2 concentrations were achieved, an upper limit for stability of the rich-combustion with natural gas fueling in the TFR cylinder was found over a range of low-to-high loads. Therefore, $\varphi_{TFR} = 1$ indicated a constant EGR rate of 25%, and $\varphi_{TFR} = 1.2$ is representative of the same rate but containing reformate gas. Early results indicated that the CoV of IMEP improved by about 65% for low engine loads and engine performance and emissions except that NOx was elevated over the entire load range tested in the case of $\varphi_{TFR} = 1.2$ compared to $\varphi_{TFR} = 1$ (conventional EGR).

New term definition:

From the literature reviewed here cylinder(s) dedicated to run under on-board fuel reforming conditions and rich combustion can be marked as the D-EGR/TFR or rich cylinder(s) and the rest referred to as normal or stoichiometric cylinders. Additional fuel required for performing fuel-rich combustion in the D-EGR cylinder(s) can also be referred to by the over-fueling or reformation ratio, e.g., 30% over-fueling/reformation ratio that means φ_{DEGR}=1.3. The produced reformate is also called D-EGR/TFR gas. Some new terms have also been extracted from the comparison between traditional EGR (inert gases) and D-EGR (EGR + reformate) that are explained in the following.

In this concept, when routing the reformate-enriched EGR (or EGR in D-EGR engine) back to the intake manifold, it is vital to characterize the intake concentrations, since highly reactive species like H_2 in the intake charge could promote backfiring, which can damage the intake system. Moreover, the contributions of isolated reactive species and inert gases from D-EGR in the intake charge are not well-known, and eventually, affect the main combustion. Thus, a new parameter of *total inert dilution ratio (TIDR)* was empirically defined by Alger et al. [574] as a common basis for comparison EGR and D-EGR. The definition is:

$$\mathrm{TIDR} = \frac{X_{N2\_in} + X_{CO_2\_in} + X_{H_2O\_in}}{X_{N2\_in} + X_{CO_2\_in} + X_{H_2O\_in} + X_{O_2\_in}} \quad (7)$$

where the X is mole fraction of intake constituents.

Based on the TIDR definition, a decrease of nearly 2% in the con-

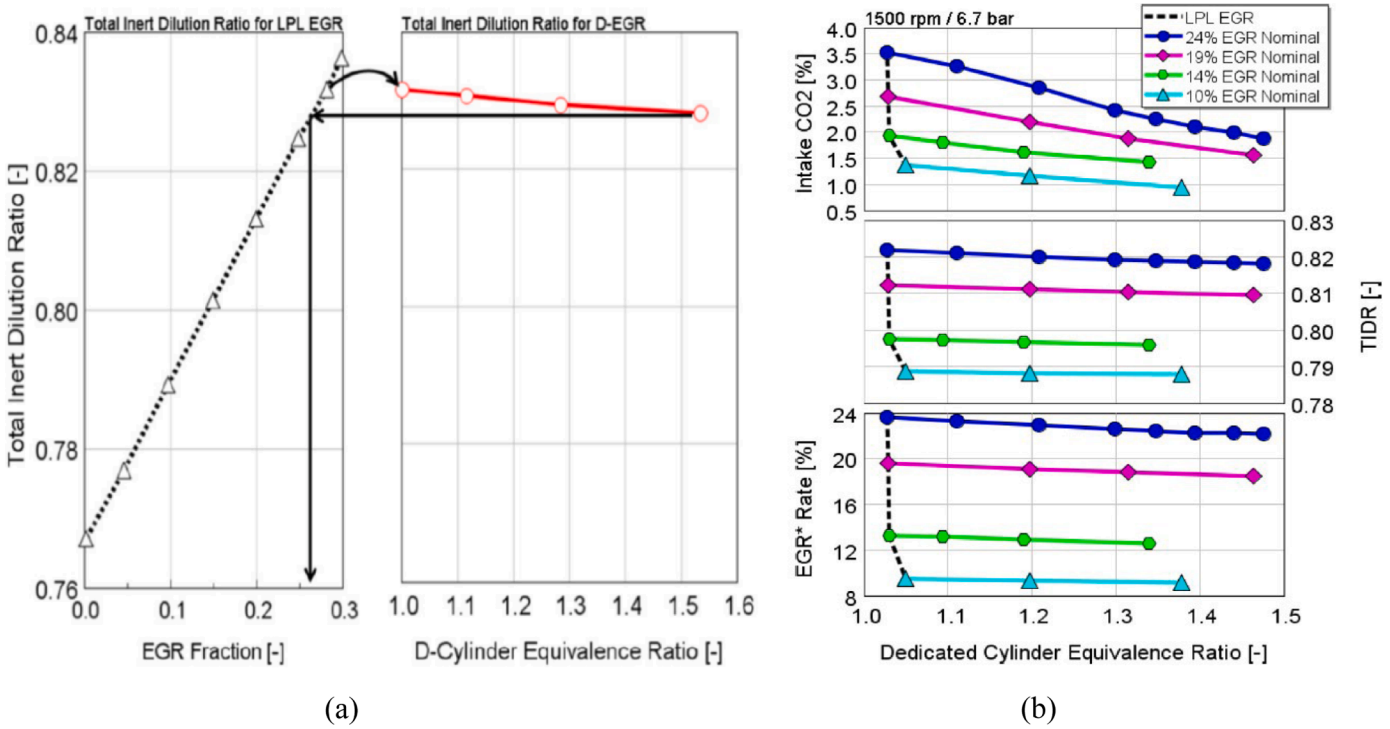

Fig. 62. Total Inert Dilution Ratio (TIDR) comparison between LPL EGR and D-EGR, (a) from simulations and; (b) from engine tests along with measured intake CO_2 and EGR*rate [574].

ventional EGR rate (calculated by the ratio of CO_2 at the intake and exhaust manifold) has been shown when the air-fuel mixture's equivalence ratio in the D-EGR cylinder was swept from 1 to about 1.5. Therefore, this term shows the discrepancy between conventional EGR (i.e., stoichiometric EGR with 100% diluents) and D-EGR (i.e., rich EGR with a mixture of diluents and reactive species). Nevertheless, since TIDR has a slight variation range (0% and 30% EGR rate = 0.77 and 0.83 of TIDR, respectively) and the largest constituent of diluents is N_2, a substitute term named EGR* [575] also is defined to show sufficiently the differences between the nominal rate of conventional EGR (e.g., low-pressure loop EGR) and D-EGR, as shown in Fig. 62, and:

$$EGR^{*}\ [0-1] = \frac{\dot{m}_{EGR} * \left(\frac{m_{inert}}{m_{EGR_t}}\right)}{\dot{m}_{EGR} * \left(\frac{m_{inert}}{m_{EGR_t}}\right) + \dot{m}_{air}}, \quad \frac{m_{inert}}{m_{EGR_t}} = 1 * \phi_{D-EGR}{}^{-0.2501} \qquad (8)$$

where $\dot{m}_{EGR}$ and $\dot{m}_{air}$ are the mass flow rate of EGR and air; m_{inert} and m_{EGR_t} are inert mass and total EGR (inert + reactive species) mass, respectively, and$\varphi_{D\ -\ EGR}$ denotes the fuel/air equivalence ratio of the dedicated cylinder.

Comparison with conventional EGR:

The D-EGR concept was introduced to overcome conventional EGR shortcomings, such as combustion instability and misfiring at a high rate, and inappropriate flow control. Therefore, in most earlier studies, the D-EGR concept was compared to conventional EGR.

In a direct comparison study, Gukelberger et al. [576,577] compared D-EGR with low-pressure loop (LPL) cooled EGR at part- and high-load operation in a turbocharged, 2L PFI SI engine. They found that at low engine load, combustion stability of $\varphi_{D\ -\ EGR}$= 1.45 is comparable with almost 13-14% LPL cooled EGR. Both HC and CO emissions were reduced; however, NOx emissions were increased slightly with D-EGR operation. Generally, at low loads, the findings indicated that the D-EGR engine could withstand higher levels of EGR dilution, allow faster burning speeds, and afford a further improvement in efficiency, and at high loads, provides superior knock tolerance and stability over the LPL

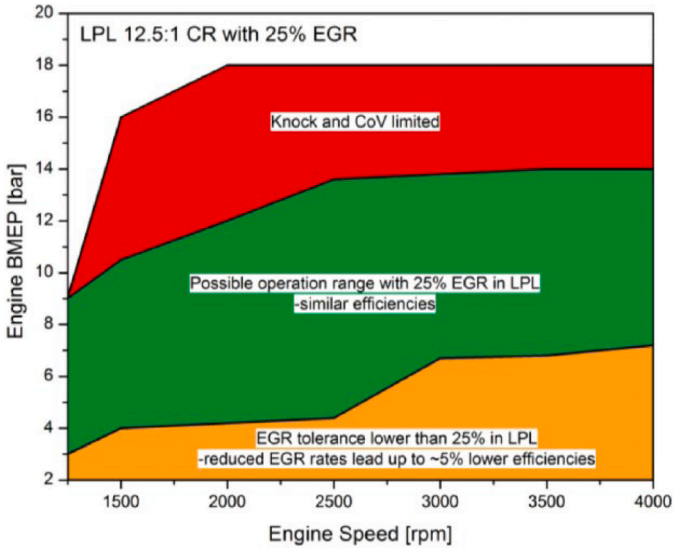

Fig. 63. Engine operating map with 25% LPL EGR [577].

EGR system. It is noteworthy that the D-EGR engine was allowed to operate with higher compression ratios (12.5:1 and 13.5:1 at high load) than the baseline case (9:1). The engine operation map for 25% LPL EGR is demonstrated in Fig. 63. It can be seen that only 25% EGR has comparable performance with D-EGR (with the same nominal EGR rate, i.e., 25%) in the green region. The yellow region could be covered with EGR but at a lower rate of 25% and approximately a 5% increase in BSFC. The region colored red could be covered with D-EGR and an adequate boosting system, but cannot be accessed with the LPL EGR setup due to knocking propensity.

Overall, the D-EGR concept is a revision of conventional EGR (cooled EGR) concepts, and has advantages over those, including eliminating any uncertainty in EGR production and the need for the EGR valve,

providing an easy way for transient control, and increasing the EGR quality by the reformate from in-cylinder fuel reforming. Interestingly, the potential of more than 25% nominal EGR has numerically been explored for a V6 engine modified to run at 50% D-EGR using three of the six cylinders in D-EGR mode [578,579].

Fuel type effects:

The main research related to D-EGR have been carried out on gasoline or natural gas fueled SI engines. Gasoline with various research octane number (RON) or anti-knock indices (RON+MON/2) and with different ethanol blended (E0:100% gasoline [by vol.] and E47: 47% ethanol [by vol.]) [580,581], and natural gas [573] blended with alcohol fuels like ethanol [582], methanol [583–585], propanol isomers [585,586], n-heptane [587,588], iso-octane [588] and propane [589] fuels have been studied so far.

Gasoline fuels with various anti-knock indices (AKI) were selected to examine the relationship between the reformation rate (over-fueling) and octane fuel number [580]. It was shown that a 1.8 AKI increase corresponds to a 10% increase in the reformation rate. As shown in Fig. 64, higher octane fuel would be the same as lower octane fuel at a reformation ratio of 30%. Additionally, more than 30% over-fueling could worsen the IMEP balance between the dedicated cylinder and normal cylinders, resulting in degenerating engine uniformity. Also, it was shown that higher ethanol content in gasoline fuel (e.g., E-47) leads to an apparent increase in hydrogen production through the D-EGR in-cylinder fuel reforming having a higher H/C ratio, but the brake thermal efficiency is virtually independent of that [581] (see Fig. 64 right).

A small amount of alcohol as an enriching fuel can improve fuel reforming due to higher radical production to ease the partial oxidation reactions participating in the in-cylinder fuel reforming process. He et al. [582] experimentally compared natural gas and ethanol enrichment at φ_{TFR}=1.25 and a fixed spark timing of 20° BTDC for a natural gas SI engine. Their results indicated more stable engine operation (i.e., lower cyclic variability, see Fig. 65 (c)), higher engine uniformity (i.e., less IMEP disparity between the TFR cylinder and a normal cylinder, as shown by cylinder2, see Fig. 65 (d)), higher rates of produced H_2 and CO concentrations and also lower unburnt CH_4 fraction in the reformate (i.e., complete in-cylinder TRF, see Fig. 65 (a)), and significantly lower NOx with the case of ethanol enrichment. More reactive species are due to presence of hydroxyl in the structure of ethanol that might potentially lead to higher O, H, OH radicals (see Fig. 65 (a)) and improved fuel oxidation.

Zhu et al. [585] numerically and experimentally showed that methanol enrichment has a great contribution to methane oxidation as compared with ethanol, propanol, ethylene glycol, aiding to the higher formation of H_2 and CO, due to the presence of OH. Thus, methanol is the optimal enrichment fuel for the TFR-cylinder operating on natural gas.

Reformate analysis:

D-EGR reformate gas provided by running fuel-rich combustion depends on how the fuel-air mixture's rich limit behaves under engine-relevant conditions, which itself depends upon the fuel type used. Alger et al. [590] reported that only 0.2% and about 0.4% hydrogen by volume is needed in the intake stream of a SI engine fueled with gasoline and natural gas, respectively, to enhance engine stability significantly. For instance, Fig. 59 and Fig. 65(b) represent the reactive species generated in the D-EGR and TRF concepts, respectively, based on the fuel used.

Liu et al. [591] ran a single-cylinder, natural gas SI engine, retrofitted from a diesel engine, in a fuel-rich combustion mode (as a D-EGR cylinder) to characterize the generated reformate quantitatively by gas chromatography. They found that both H_2 and CO mole fractions were increased linearly from ϕ=1 to ϕ=1.4 by about 8% with a nearly constant H_2/CO ratio (1:1 by vol.). They also employed rapid compression machine (RCM) experiments [592] for the CH_4 ignition at similar conditions. They also examined the effect of 1% (φ_{D-EGR}= 1.2) and 2% (φ_{D-EGR}= 1.4) H_2/CO ratio (by vol.) on stoichiometric natural gas combustion at a part load condition of ~ 6 bar IMEP at two nominal EGR rates of 15% and 20%.

From the literature, φ_{D-EGR} between 1.2-1.4 is a decent range in terms of stability while φ_{D-EGR}>1.4 imposes a rich limit for fuels used. The possibility of φ_{D-EGR} up to 3 and its effects on reformate generation were investigated numerically [579]. Although D-EGR is indeed a non-catalyst fuel reforming technique, catalyst formulation such as the WGS catalyst with Rhodium and Barium was employed in the exhaust stream of the D-EGR cylinder to further boost H_2 generation [593]; it was shown that H_2 generation reaches 7% (by volume) through optimizing the catalyst formulation, though an activity loss was seen after about 12 hours. This imposes durability challenges.

Demonstration of D-EGR vehicle:

As mentioned before, the constraints of a downsized boosted SI engine operating stoichiometric with traditional (cooled or uncooled) EGR pertain to knock limitations, EGR tolerance, and combustion instability, which can be improved using reformate along with EGR. Therefore, the D-EGR concept provides the pathways of achieving high-efficiency SI engines. To better demonstrate an actual D-EGR vehicle, several instruments, including an advanced high-energy dual coil offset (DCO) ignition system [594] for facilitating ignition of dilute mixtures and a

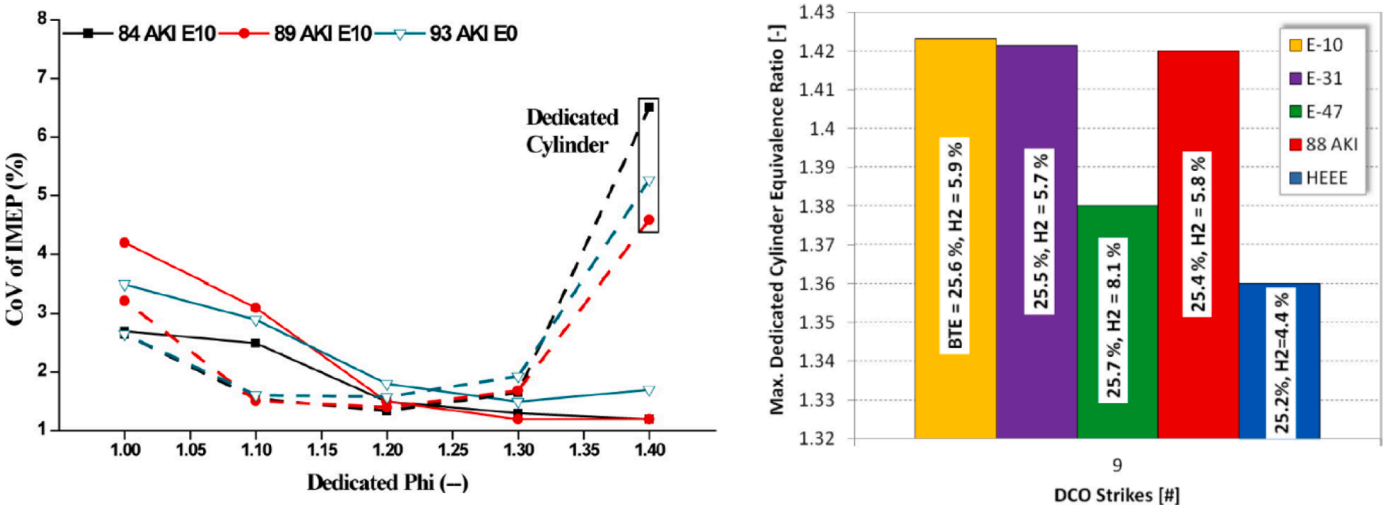

Fig. 64. Engine stability as a function of φ_{D-EGR} in D-EGR cylinder with varying AKI – solid line related to a normal cylinder [580] (left), H_2 concentration and BTE for a specific designed high energy ignition system (DCO) [581] (right), at 2 bar BMEP / 2000 rpm.

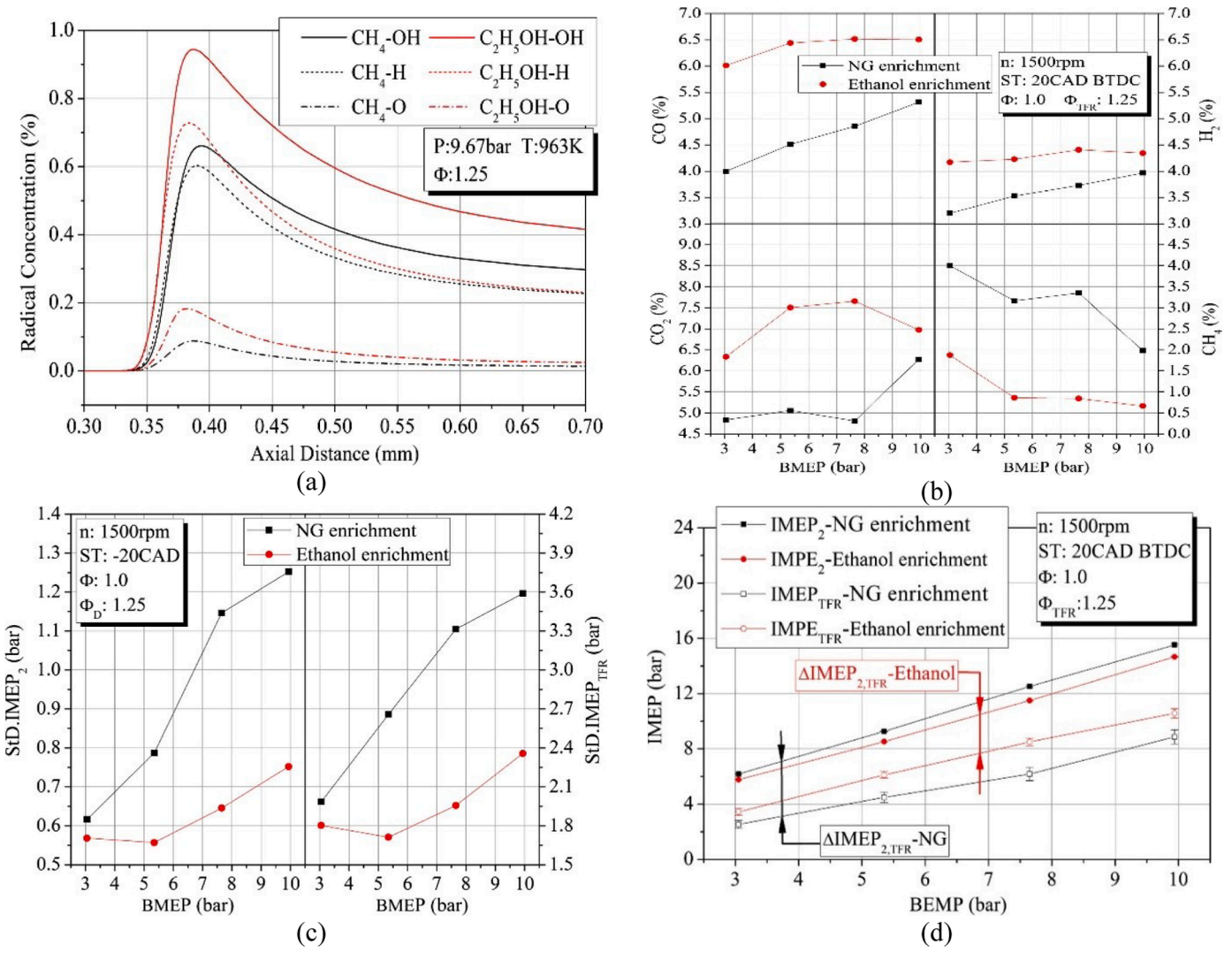

Fig. 65. Comparison natural gas with ethanol enrichment [582], in terms of laminar flame speed from calculation of CH_4-air and C_2H_5OH-air mixtures (a), and reformate production (b), IMEP cyclic variability (c) and IMEP discrepancy (c), from experiment. (With permission of Elsevier).

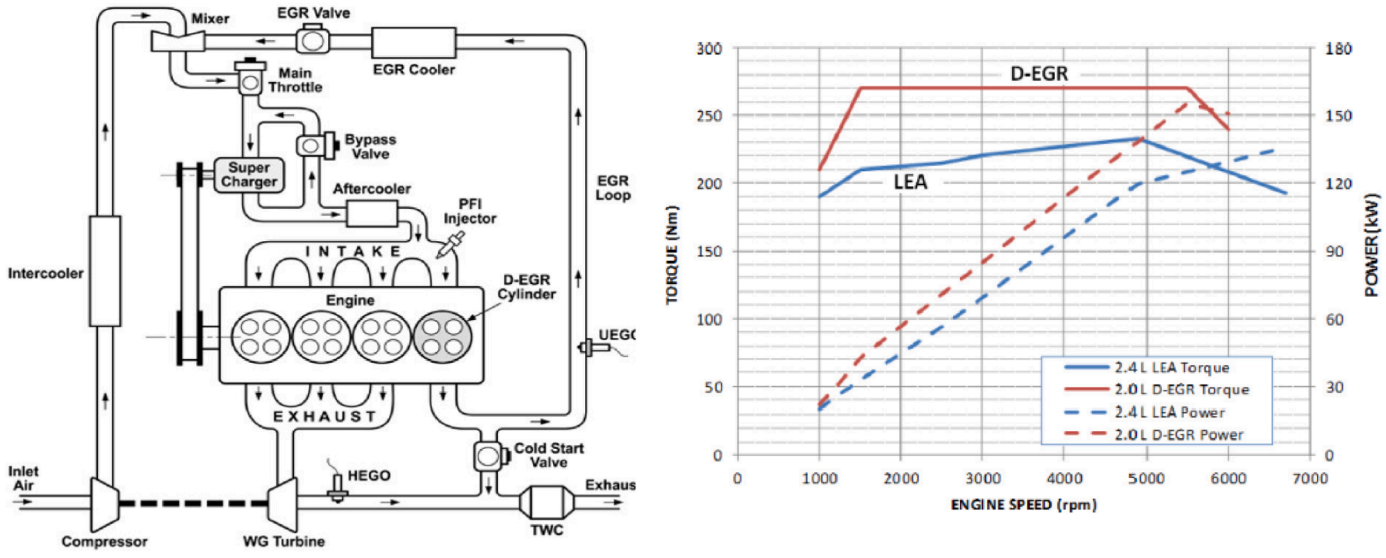

Fig. 66. New designed air handling system for D-EGR engine (left) and D-EGR and LEA power and torque comparisons (right) [571,599].

D-EGR mixer [595] for promoting reformate distribution to suppress sudden imbalances in CoV of IMEP of the normal cylinders, have been developed together with applying improvements in order to increase the reformate yield such as improved injection strategies (more effective with split and late DI than PFI, except at low speed) [596], valve timing (more sensitive to retardation of exhaust valve compared to advance intake valve) [596] and ignition timing based on transient control [597, 598].

Chadwell et al. [571] first successfully replaced a 2.4 L, NA PFI SI engine (LEA, engine produced by GM) with a converted D-EGR, 2 L, TC DISI engine (LHU, engine produced by GM) fueling with Haltermann EEE certification gasoline with an anti-knock index of 92 on a production vehicle (2012 Buick Regal) with a designed air handling system consisting of EGR control, boosting and D-EGR mixing systems, as seen in Fig. 66 (left), and with an increased compression ratio of OEM LHU from 9.3:1 to 11.7:1. The target operating points of torque and power for vehicle-based D-EGR with a nominal EGR ratio of 25% were designed beyond the reference vehicle with GM LEA (see Fig. 66 (right)). It was observed that BSFC is reduced by an average of 10% across most operating points relative to the reference engine. The most considerable reduction occurred at high speeds and high engine loads due to completely removing the over-fueling in the D-EGR cylinder. This fuel economy improvement was attributed primarily to increased compression ratio due to enhanced knock tolerance resulting from the reformate existing in the charge and stoichiometric operation. Also, it was reported that the sufficient hydrogen concentration to stabilize the combustion at low loads was about just 1% by volume. Robertson et al. [599] tested the performance of the same converted D-EGR vehicle on the FTP-75 (for the city) and HWFET (for the highway); compared to the baseline vehicle, they observed that the fuel consumption was reduced by 13% and 9%, NOx was reduced by 85%, non-methane organic gases (NMOG) emissions remained constant and were reduced by 33%, respectively, for the FTP-75 and HWFET.

Also, potential demonstration of D-EGR system in a moderately large displacement (~ 3-4 L) gasoline engine as substitution of a medium-duty diesel truck (~ 6-7 L) was shown using GT-Power simulations, and comparable thermal efficiency and GHC emissions results were noticed [600].

The core aim of the concept is to improve the stoichiometric SI engine's efficiency through extension of its dilution-limit without sacrificing TWC's efficiency or increasing the tailpipe-out emissions of the vehicle by using reformate (syngas)-enriched EGR. Jung and Lee [601] determined computationally the D-EGR potential with a lean SI engine fueled with methane. They founded the highest engine thermal efficiency (η_{th_e}) of 42.9% resulted from a combination of $\varphi_{D-EGR} = 2$ with $\varphi_{Normal} = 0.7$ operation, compared to the maximum η_{th_e} of 39.4% for $\varphi_{D-EGR} = 1.9$ and $\varphi_{Normal} = 1$. Recently, use of an air-assisted pre-chamber in a natural gas fueled six-cylinder D-EGR engine has also been shown to be highly effective in stabilizing the combustion and extending enrichment limits by 11.7% [602]. The leaner mixture permits ignition of the mixture and stabilizes combustion. Therefore, the conventional benefits of the pre-chamber can be utilized for D-EGR applications. Osaka Gas Co. [603] has also considered applying a D-EGR system to a turbocharged lean HCCI engine as a long-term pathway for a high-efficiency small gas engine in power generation applications.

Conclusion:

To sum up, in-cylinder on-board fuel reforming with the D-EGR/TFR concept has been realized in various production vehicle SI engines operating stoichiometric without requiring any external reforming device, while avoiding catalyst-related issues (poisoning and aging) and vast internal engine modifications (excluding potential compression ratio increase due to enhanced knock resistance). However, some devices are required to convert a SI engine to an effective D-EGR one, including a mixer, boosting device, charge air cooler, and suitable ignition system as well as an over-fueling requirement along with supplying injector(s) and delivering the D-EGR loop for the dedicated cylinder. Profound consequences include increased engine efficiency with reduced emissions and increased EGR quality due to reformate presence with reduced/eliminated downside effects of conventional EGR, namely, uncertainty in EGR production and difficulty in transient control and the need for high EGR levels (>15%). Isolated combustion stability of the dedicated cylinder(s) and the balanced IMEP between D-EGR (rich) cylinder(s) and normal (stoichiometric) cylinders (engine uniformity) represent a new trade-off that must also be considered as well as fresh concerns related to fuel selection. D-EGR fueling optimization based on fuel type is of significant importance and has not been well addressed until now. Besides, D-EGR experiments with lean SI engines might be an interesting topic for the future.

We would like to refer the readers to Fig. 47, where they can see all the on-board reforming techniques reviewed in this chapter in detail.

5. Summary and outlook

5.1. Summary

This paper provides a critical comprehensive review on the use of syngas for IC engines over the last few decades, since syngas has become more attractive as an alternative and potentially renewable fuel for IC engines. Generally, engine configurations studied in the literature are considerably different and the results have been rather difficult to compare. An overall observation based on the literature is that the selection of the base fuel for reforming, the syngas production method, its physicochemical properties, engine operating conditions, and the engine design parameters play important roles in dictating the potential advantages of syngas use in IC engines. Some important conclusions from this review are summarized below:

- Variation of the hydrogen fraction in syngas has been a factor, prohibiting its widespread usage. In addition, other gaseous elements such as CO_2, N_2, and CH_4 in the syngas can have adverse effects on engine combustion characteristics. To address these issues, a better understanding of fundamental combustion properties is vital. A large set of experimental data is available for the combustion of syngas with various H_2/CO contents. However, studies related to ignition delay times and laminar flame speeds measurements of syngas mixed with other gases under engine relevant conditions are still limited. Detailed numerical and experimental studies are required to gap the bridge.
- The most important factors that cause power de-rating in an SI engine are the low energy density of syngas/air mixtures and reduced engine volumetric efficiency due to air replacement. With high H_2-content syngas addition to the engine as the secondary fuel, combustion and performance were better than with low H_2-content syngas. Using higher compression ratios in syngas-fueled engines led to reduced power de-rating without any increase in the knock tendency. Power de-rating can also be eliminated by direct injection of syngas, which is a promising solution to avoid problems of reduced volumetric efficiency and unwanted pre-ignition or surface ignition in the intake system.
- Among the different types of engines, syngas as the secondary fuel or blended with other fuels in dual-fuel engines showed very interesting results due to their lower power de-rating capability compared to syngas-fueled SI engines, which have problems running the engine under near stoichiometric conditions and increased PM emissions with 100% syngas. High efficiencies with low emissions can be also obtained in the whole operating range with the use of appropriate strategies in dual-fuel engines. Recently, efforts have been directed towards the optimization of these engines with advanced numerical techniques. However, the presence of two distinct fuel supply lines is a complexity that points out problems related to the storage and the transportation of the fuels.

- Fuel reforming combined with dual-fuel combustion is capable of increasing the global efficiency of the system over conventional diesel combustion. On-board fuel reforming is an attractive method to convert a dual-fuel RCCI combustion strategy into a single-fuel RCCI concept and thus eliminates the need for two fuel lines and fuel tanks, which is one of the important demerits of RCCI combustion. On-board catalytic fuel reforming is also a promising technique for improving efficiency and reducing pollutant emissions from IC engines. Overall, it seems that syngas in a single/dual-fuel engine is a promising technique for controlling both NOx and soot emissions in existing engines, but with slight engine hardware modifications needed.
- In HCCI engines, 100% reformate at higher intake temperature would be a suitable strategy, compared to the 100% reformate, which was more favorable for SI engines at conventional operating conditions. RG blending was found to be an effective method for retarding combustion phasing, since it reduces the heat release at low temperatures, followed by a prolongation of the NTC delay period and a delay in the high-temperature heat release. RG can act like an ignition controller for the main engine fuel and can eliminate the need for preheating the intake charge. The levels of exhaust CO and UHC emissions increase as the RG concentration increases while NOx decreases. The chemical effects of RG on HCCI combustion of PRFs were found to be stronger than thermodynamic effects and dilution.
- Exhaust gas reforming systems are currently being considered in different configurations. Fuel choice dictates which R-EGR method is preferred. Catalytic on-board fuel reforming can be challenging since some hydrocarbon fuels like gasoline require high temperatures to reform, and the sulfur content in some fuels can poison the catalyst. Another drawback of on-board fuel reforming method using the POX method is the reduced LHV of the fuels, thus reducing overall engine efficiency. Catalytic R-EGR results showed that good hydrogen rates could be produced with adequate control of the reaction parameters at temperatures typical of the exhaust gas temperatures of diesel engines operating at part load without any external heat source or air and steam supply requirements. Overall, the use of R-EGR allowed the realization of the benefits of both EGR and waste heat. Moreover, a mixture diluted by R-EGR can reduce the knock tendency compared to EGR dilution cases. With faster laminar burning velocities, the R-EGR technology is a promising approach to support high levels of EGR dilution in advanced SI engines for increased thermal efficiency.
- In-cylinder fuel reforming techniques like D-EGR/TFR are capable of delivering up to 15% more efficient engines than today's mainstream ones, while simultaneously improving engine performance. It allows manufacturers to address future, more aggressive fuel economy standards and meet LEV III/Tier 3 emissions levels [604] cost-effectively. The results reported in this paper indicate that the D-EGR engine can tolerate higher levels of EGR dilution at low loads, allow faster burn speeds, minimize cycle-to-cycle variations, and can further boost performance and emissions. At high loads, the D-EGR technique provides superior knock tolerance and stability over the LPL EGR. Disadvantages of in-cylinder reforming strategies include slow kinetics and limited reforming stoichiometry. Furthermore, homogeneous in-cylinder reforming of heavier fuels like diesel can potentially lead to excessive carbon formation at rich equivalence ratios.

Overall, syngas combustion technology seems to have reached a considerable level of technical development, and the analysis of the literature on syngas combustion in IC engines shows the potential for widespread research and development work on syngas in the automotive industry in future.

5.2. Outlook

Syngas-fueled IC engines with technological advancements are attractive and economically viable and can serve as a future option for power and transportation applications. New measurements of the laminar flame speed of syngas diluted with other gaseous compositions at elevated pressures would help further understand syngas combustion kinetics. The main issue with modelling combustion kinetics is the demand for expert knowledge and optimization against experiments, as well as the lack of understanding of the associated uncertainties. Therefore, data-driven ML approaches that enable efficient discovery and calibration of kinetic models can be employed for syngas combustion modeling in coming years. The ML model can be a promising alternative to time-consuming experimental measurements or numerical calculations.

It is well documented that supplying syngas directly to the intake manifold has several limitations, including backfire, pre-ignition, and power loss through reduced volumetric efficiency. Transient operation is also limited due to the time required for gas to travel through the intake system, depending on where it is mixed. Syngas direct injection technology can eliminates these limitations but requires high-pressure reforming, which could be an area for future study. Numerical models should also account for the intake and exhaust processes, which are usually not considered in the simulations of syngas-fueled PFI engines. Since a considerable fraction of the power derating is related to the decrease of volumetric efficiency, those processes should be included in the simulations. Similar to DI technology, stratified lean-burn combustion is also an effective way of using syngas in modern engines to address problems associated with air-handling at lean stoichiometric air-fuel ratios. However, the required injection durations should be taken due into account. For better performance and emissions, further investigation of the optimization of injection timing, fuel composition, air-fuel ratio, and ignition advance are required.

Studies have shown that single-fuel RCCI combustion can achieve high efficiencies while maintaining low NOx and soot emissions. Conversely, the transient performance of the combustion process alone (i.e., without the reformer) is assumed to be similar to other gaseous dual-fuel engines operating at early direct injection times, which may pose additional challenges in combustion control [605,606] if hydrogen percentages in the reformed fuel are not kept below those resulting in the high-pressure oscillation region. Future work should further analyze reformate concentrations and examine fuel reactivity as a function of reactor stoichiometry and temperature. In addition, matching reformer performance with the engine conditions that enable it to run effectively should also be considered. Such studies would provide invaluable information to more optimally control combustion, and further define the operability range of thermally integrated reforming reactor systems.

To minimize HC and CO emissions, the efficiency of syngas-operated dual-fuel CI engines must be optimized. Moreover, other engine operational parameters should be tuned in addition to the amount of combustible mixture inside the combustion chamber for achieving better combustion characteristics. Based on the present review, detailed numerical and experimental studies with different compositions of the syngas and engine parameters are therefore needed.

Syngas production and combustion research for IC engines have mainly focused on steady-state operating conditions, and very few transient operation studies have been investigated. It is expected that there will be challenges to allow reforming systems to work efficiently over the entire operating load and speed range. The long-term viability of the reforming catalyst and the reforming reaction's response to a variety of fuels should be examined. In-cylinder reforming processes like D-EGR/TFR and NVO are the most promising for on-board syngas production. The products of these processes should be evaluated for controlling combustion phasing and enabling advanced combustion strategies. For D-EGR vehicles, the low exhaust temperatures are a challenge for meeting future emissions regulations because some

catalytic aftertreatment solutions for reducing emissions are not currently feasible due to poor low temperature activity. Hydrocarbon traps are an area of future work for D-EGR- equipped vehicles. The effect of reformate composition on combustion and exhaust emissions can also be studied in future work. The stability and efficiency of combustion in the D-EGR cylinder may be a major concern for D-EGR natural gas engines and optimizing the equivalence ratio of the D-EGR cylinder is crucial for D-EGR in order to improve the overall engine combustion output.

The research aimed at improving IC engine start-up and transient behavior is needed to broaden the range of possible applications. Examination of heat transfer processes is necessary to illustrate the optimum configuration for complex systems, compared to conventional IC engines, including multiple fuel heating, evaporation, and reforming processes when using exhaust gas heat, and refreshing the reforming products before they are delivered to the engine.

Finally, syngas-fueled engines can be optimally designed for hybrid electric vehicle application [607], allowing high efficiency operation at target engine speed and loads. For hybrid configuration research, investigating low-carbon fuels and optimized engines according to upcoming emissions regulations for CO_2 will be of particular interest. In addition, since most literature research has focused on light duty vehicles, multi-mode hybrid powertrains can be investigated for commercial and medium/heavy duty trucks. Thus, there are still numerous issues that require further numerical and experimental investigation, particularly in the field of on-board fuel reforming and fundamental syngas combustion studies in IC engines for transport applications.

Declaration of competing interest

The authors declare that they have no known competing financial interests or personal relationships that could have appeared to influence the work reported in this paper.

Acknowledgments

Firstly, we thank the reviewers for their contributions that significantly improved the manuscript. A. Paykani acknowledges the financial support by the Engineering and Physical Science Research Council (EPSRC) through the grant number EP/T033800/1. T. Alger would like to acknowledge the HEDGE consortium and Southwest Research Institute for providing funding for their work. The authors thank Dr Frouzakis at ETH Zurich for the useful discussion on the fundamentals of the syngas combustion section.

Supplementary materials

Supplementary material associated with this article can be found, in the online version, at doi:10.1016/j.pecs.2022.100995.

References

[1] Kalghatgi G. Is it really the end of internal combustion engines and petroleum in transport? Applied energy 2018;225:965–74.
[2] Leach F, Kalghatgi G, Stone R, Miles P. The scope for improving the efficiency and environmental impact of internal combustion engines. Transportation Engineering 2020:100005.
[3] Reitz H, Ogawa H, Payri R, Fansler T, Kokjohn S, Moriyoshi Y, et al. IJER editorial: The future of the internal combustion engine. London, England: SAGE Publications Sage UK; 2019.
[4] Rogelj J, Den Elzen M, Höhne N, Fransen T, Fekete H, Winkler H, et al. Paris Agreement climate proposals need a boost to keep warming well below 2 C. Nature 2016;534:631.
[5] Tuner M. Review and Benchmarking of Alternative Fuels in Conventional and Advanced Engine Concepts with Emphasis on Efficiency, CO 2, and Regulated Emissions. SAE Technical Paper; 2016.
[6] Bae C, Kim J. Alternative fuels for internal combustion engines. Proceedings of the Combustion Institute 2017;36:3389–413.
[7] Kakaee A-H, Paykani A, Ghajar M. The influence of fuel composition on the combustion and emission characteristics of natural gas fueled engines. Renewable and Sustainable Energy Reviews 2014;38:64–78.
[8] Kakaee A-H, Paykani A. Research and development of natural-gas fueled engines in Iran. Renewable and Sustainable Energy Reviews 2013;26:805–21.
[9] Moriarty P, Honnery D. Prospects for hydrogen as a transport fuel. International Journal of Hydrogen Energy 2019;44:16029–37.
[10] Kobayashi H, Hayakawa A, Somarathne KKA. Okafor EC. Science and technology of ammonia combustion. Proceedings of the Combustion Institute 2019;37:109–33.
[11] Valera-Medina A, Xiao H, Owen-Jones M, David W, Bowen P. Ammonia for power. Progress in Energy and Combustion Science 2018;69:63–102.
[12] Shi Y, Ge H-W, Reitz RD. Computational optimization of internal combustion engines. Springer Science & Business Media; 2011.
[13] Karim GA. Hydrogen as a spark ignition engine fuel. International Journal of Hydrogen Energy 2003;28:569–77.
[14] Akansu SO, Dulger Z, Kahraman N, Veziroğlu TN. Internal combustion engines fueled by natural gas—hydrogen mixtures. International journal of hydrogen energy 2004;29:1527–39.
[15] Dimitriou P, Tsujimura T. A review of hydrogen as a compression ignition engine fuel. International Journal of Hydrogen Energy 2017;42:24470–86.
[16] Venkataraman V, El-Kharouf A, Pandya B, Amakiri E, Steinberger-Wilckens R. Coupling of engine exhaust and fuel cell exhaust with vapour absorption refrigeration/air conditioning systems for transport applications: A review. Thermal Science and Engineering Progress 2020;18:100550.
[17] Acar C, Dincer I. Review and evaluation of hydrogen production options for better environment. Journal of Cleaner Production 2019;218:835–49.
[18] White CM, Steeper RR, Lutz AE. The hydrogen-fueled internal combustion engine: a technical review. International Journal of Hydrogen Energy 2006;31:1292–305.
[19] Verhelst S, Wallner T. Hydrogen-fueled internal combustion engines. Progress in energy and combustion science 2009;35:490–527.
[20] White C, Steeper R, Lutz A. The hydrogen-fueled internal combustion engine: a technical review. International journal of hydrogen energy 2006;31:1292–305.
[21] Babayev R, Andersson A, Dalmau AS, Im HG, Johansson B. Computational characterization of hydrogen direct injection and nonpremixed combustion in a compression-ignition engine. International Journal of Hydrogen Energy 2021;46:18678–96.
[22] Cau G, Cocco D, Serra F. Energy and cost analysis of small-size integrated coal gasification and syngas storage power plants. Energy conversion and management 2012;56:121–9.
[23] Farrell AE, Keith DW, Corbett JJ. A strategy for introducing hydrogen into transportation. Energy Policy 2003;31:1357–67.
[24] Tartakovsky L, Baibikov V, Veinblat M. Comparative performance analysis of SI engine fed by ethanol and methanol reforming products. SAE Technical Paper; 2013.
[25] Houseman J, Hoehn FW. A two-charge engine concept: hydrogen enrichment. SAE Technical Paper; 1974.
[26] Jain I. Hydrogen the fuel for 21st century. International journal of hydrogen energy 2009;34:7368–78.
[27] Boehman AL, Corre OL. Combustion of syngas in internal combustion engines. Combustion Science and Technology 2008;180:1193–206.
[28] Whitty KJ, Zhang HR, Eddings EG. Emissions from syngas combustion. Combustion Science and Technology 2008;180:1117–36.
[29] Lieuwen T, Yang V, Yetter R. Synthesis gas combustion. Fundamentals and Applications. 2010.
[30] Herdin G, Gruber F, Klausner J, Robitschko R, Chvatal D. Hydrogen and Hydrogen Mixtures as Fuel in Stationary Gas Engines. SAE technical paper; 2007.
[31] Shahsavan M, Morovatiyan M, Mack JH. A numerical investigation of hydrogen injection into noble gas working fluids. International Journal of Hydrogen Energy 2018.
[32] Todd DM. In: Gas turbine improvements enhance IGCC viability. Gasification Technologies Conference; 2000.
[33] Tartakovsky L, Sheintuch M. Fuel reforming in internal combustion engines. Progress in Energy and Combustion Science 2018;67:88–114.
[34] Rahnama P, Paykani A, Reitz RD. A numerical study of the effects of using hydrogen, reformer gas and nitrogen on combustion, emissions and load limits of a heavy duty natural gas/diesel RCCI engine. Applied energy 2017;193:182–98.
[35] Larson ED, Kartha S. Expanding roles for modernized biomass energy. Energy for sustainable development 2000;4:15–25.
[36] Johansson TB, Burnham L. Renewable energy: sources for fuels and electricity. Island press; 1993.
[37] Agarwal AK. Biofuels (alcohols and biodiesel) applications as fuels for internal combustion engines. Progress in energy and combustion science 2007;33:233–71.
[38] Demirbas A. Progress and recent trends in biofuels. Progress in energy and combustion science 2007;33:1–18.
[39] Zhang H, Kaczmarek D, Rudolph C, Schmitt S, Gaiser N, Oßwald P, et al. Dimethyl ether (DME) and dimethoxymethane (DMM) as reaction enhancers for methane: Combining flame experiments with model-assisted exploration of a polygeneration process. Combustion and Flame 2022;237:111863.
[40] Wang T, Stiegel GJ. Integrated Gasification Combined Cycle (IGCC) Technologies. Woodhead Publishing; 2016.
[41] Oreggioni GD, Brandani S, Luberti M, Baykan Y, Friedrich D, Ahn H. CO 2 capture from syngas by an adsorption process at a biomass gasification CHP plant: its comparison with amine-based CO 2 capture. International Journal of Greenhouse Gas Control 2015;35:71–81.

[42] Majoumerd MM, De S, Assadi M, Breuhaus P. An EU initiative for future generation of IGCC power plants using hydrogen-rich syngas: simulation results for the baseline configuration. Applied energy 2012;99:280–90.
[43] Xu X, Li P, Shen Y. Small-scale reforming of diesel and jet fuels to make hydrogen and syngas for fuel cells: A review. Applied energy 2013;108:202–17.
[44] CO Colpan, Dincer I, Hamdullahpur F. Thermodynamic modeling of direct internal reforming solid oxide fuel cells operating with syngas. International Journal of Hydrogen Energy 2007;32:787–95.
[45] Choudhary T, Murty P. Parametric analysis of syn-gas fueled SOFC with internal reforming. SAE Technical Paper; 2015.
[46] Brown LF. A comparative study of fuels for on-board hydrogen production for fuel-cell-powered automobiles. International Journal of Hydrogen Energy 2001;26:381–97.
[47] Wilhelm D, Simbeck D, Karp A, Dickenson R. Syngas production for gas-to-liquids applications: technologies, issues and outlook. Fuel processing technology 2001;71:139–48.
[48] Gupta K, Rehman A, Sarviya R. Bio-fuels for the gas turbine: A review. Renewable and Sustainable Energy Reviews 2010;14:2946–55.
[49] Ghenai C. Combustion of syngas fuel in gas turbine can combustor. Advances in Mechanical Engineering 2010.
[50] Gadde S, Wu J, Gulati A, McQuiggan G, Koestlin B, Prade B. Syngas capable combustion systems development for advanced gas turbines. In: ASME Turbo Expo 2006: Power for Land, Sea, and Air. American Society of Mechanical Engineers; 2006. p. 547–54.
[51] Yaliwal V, Banapurmath N, Gireesh N, Tewari P. Production and utilization of renewable and sustainable gaseous fuel for power generation applications: A review of literature. Renewable and Sustainable Energy Reviews 2014;34:608–27.
[52] Reyes SC, Sinfelt JH, Feeley JS. Evolution of processes for synthesis gas production: Recent developments in an old technology. Industrial & Engineering Chemistry Research 2003;42:1588–97.
[53] Choudhary TV, Choudhary VR. Energy-Efficient Syngas Production through Catalytic Oxy-Methane Reforming Reactions. Angewandte Chemie International Edition 2008;47:1828–47.
[54] Narnaware SL, Srivastava N, Vahora S. Gasification: An alternative solution for energy recovery and utilization of vegetable market waste. Waste Management & Research 2017;35:276–84.
[55] Lombardi L, Carnevale E, Corti A. A review of technologies and performances of thermal treatment systems for energy recovery from waste. Waste management 2015;37:26–44.
[56] Bharadwaj S, Schmidt L. Catalytic partial oxidation of natural gas to syngas. Fuel Processing Technology 1995;42:109–27.
[57] Asadullah M. Biomass gasification gas cleaning for downstream applications: A comparative critical review. Renewable and sustainable energy reviews 2014;40:118–32.
[58] Sikarwar VS, Zhao M, Clough P, Yao J, Zhong X, Memon MZ, et al. An overview of advances in biomass gasification. Energy & Environmental Science 2016;9:2939–77.
[59] Hagos FY, Aziz ARA, Sulaiman SA. Trends of syngas as a fuel in internal combustion engines. Advances in Mechanical Engineering 2014;6:401587.
[60] Fiore M, Magi V, Viggiano A. Internal combustion engines powered by syngas: A review. Applied Energy 2020;276:115415.
[61] Heidenreich S, Foscolo PU. New concepts in biomass gasification. Progress in energy and combustion science 2015;46:72–95.
[62] Richardson Y, Blin J, Julbe A. A short overview on purification and conditioning of syngas produced by biomass gasification: catalytic strategies, process intensification and new concepts. Progress in Energy and Combustion Science 2012;38:765–81.
[63] Peña MA, Gómez JP, Fierro JLG. New catalytic routes for syngas and hydrogen production. Applied Catalysis A: General 1996;144:7–57.
[64] Kumar A, Jones DD, Hanna MA. Thermochemical biomass gasification: a review of the current status of the technology. Energies 2009;2:556–81.
[65] Lv P, Yuan Z, Wu C, Ma L, Chen Y, Tsubaki N. Bio-syngas production from biomass catalytic gasification. Energy Conversion and Management 2007;48:1132–9.
[66] Farzad S, Mandegari MA, Görgens JF. A critical review on biomass gasification, co-gasification, and their environmental assessments. Biofuel Research Journal 2016;3:483–95.
[67] Couto N, Rouboa A, Silva V, Monteiro E, Bouziane K. Influence of the biomass gasification processes on the final composition of syngas. Energy Procedia 2013;36:596–606.
[68] Asadullah M. Barriers of commercial power generation using biomass gasification gas: A review. Renewable and Sustainable Energy Reviews 2014;29:201–15.
[69] Shayan E, Zare V, Mirzaee I. Hydrogen production from biomass gasification; a theoretical comparison of using different gasification agents. Energy Conversion and Management 2018;159:30–41.
[70] La Villetta M, Costa M, Cirillo D, Massarotti N, Vanoli L. Performance analysis of a biomass powered micro-cogeneration system based on gasification and syngas conversion in a reciprocating engine. Energy Conversion and Management 2018;175:33–48.
[71] Basu P. Biomass gasification and pyrolysis: practical design and theory. Academic press; 2010.
[72] La Villetta M, Costa M, Massarotti N. Modelling approaches to biomass gasification: A review with emphasis on the stoichiometric method. Renewable and Sustainable Energy Reviews 2017;74:71–88.
[73] Fanelli E, Viggiano A, Braccio G, Magi V. On laminar flame speed correlations for H 2/CO combustion in premixed spark ignition engines. Applied Energy 2014;130:166–80.
[74] Ramasubramanian S, Chandrasekaran M. A statistical analysis on tar reduction in producer gas for IC engine application. International Journal of Ambient Energy 2018:1–7.
[75] Oh G, Ra HW, Yoon SM, Mun TY, Seo MW, Lee J-G, et al. Syngas production through gasification of coal water mixture and power generation on dual-fuel diesel engine. Journal of the Energy Institute 2018.
[76] Göransson K, Söderlind U, He J, Zhang W. Review of syngas production via biomass DFBGs. Renewable and Sustainable Energy Reviews 2011;15:482–92.
[77] Janajreh I, Raza SS, Valmundsson AS. Plasma gasification process: Modeling, simulation and comparison with conventional air gasification. Energy Conversion and Management 2013;65:801–9.
[78] Rutberg PG, Kuznetsov VA, Popov VE, Bratsev AN, Popov SD, Surov AV. Improvements of biomass gasification process by plasma technologies. Pretreatment Techniques for Biofuels and Biorefineries: Springer; 2013. p. 261–87.
[79] Fabry F, Rehmet C, Rohani V-J, Fulcheri L. Waste gasification by thermal plasma: a review. Waste and Biomass Valorization 2013;4:421–39.
[80] Paulino RFS, Essiptchouk AM, Silveira JL. The use of syngas from biomedical waste plasma gasification systems for electricity production in internal combustion. Thermodynamic and economic issues. Energy. 2020:117419.
[81] Freitas A, Guirardello R. Thermodynamic analysis of supercritical water gasification of microalgae biomass for hydrogen and syngas production. Chemical Engineering Transactions 2013.
[82] Freitas A, Guirardello R. Supercritical water gasification of glucose and cellulose for hydrogen and syngas production. Chemical Engineering Transactions 2012.
[83] Wierzbicki TA, Lee IC, Gupta AK. Recent advances in catalytic oxidation and reformation of jet fuels. Applied Energy 2016;165:904–18.
[84] Gallagher MJ, Geiger R, Polevich A, Rabinovich A, Gutsol A, Fridman A. On-board plasma-assisted conversion of heavy hydrocarbons into synthesis gas. Fuel 2010;89:1187–92.
[85] Bell DA, Towler BF, Fan M. Coal gasification and its applications. William Andrew; 2010.
[86] Vernon PD, Green ML, Cheetham AK. Ashcroft AT. Partial oxidation of methane to synthesis gas. Catalysis Letters 1990;6:181–6.
[87] York AP, Xiao T, Green ML. Brief overview of the partial oxidation of methane to synthesis gas. Topics in catalysis 2003;22:345–58.
[88] Cormier JM, Rusu I. Syngas production via methane steam reforming with oxygen: plasma reactors versus chemical reactors. Journal of Physics D: Applied Physics 2001;34:2798.
[89] Van Hook JP. Methane-steam reforming. Catalysis Reviews—Science and Engineering. 1980;21:1–51.
[90] Mokheimer EM, Hussain MI, Ahmed S, Habib MA, Al-Qutub AA. On the modeling of steam methane reforming. Journal of Energy Resources Technology 2015;137:012001.
[91] Khzouz M, Gkanas EI. Experimental and Numerical Study of Low Temperature Methane Steam Reforming for Hydrogen Production. Catalysts 2017;8:5.
[92] Christensen T, Primdahl I. Improve syngas production using autothermal reforming. Hydrocarbon Processing;(United States) 1994:73.
[93] Rowshanzamir S, Eikani M. Autothermal reforming of methane to synthesis gas: Modeling and simulation. international journal of hydrogen energy 2009;34:1292–300.
[94] Aasberg-Petersen K, Christensen TS, Nielsen CS. Dybkjær I. Recent developments in autothermal reforming and pre-reforming for synthesis gas production in GTL applications. Fuel Processing Technology 2003;83:253–61.
[95] Dybkjær I. Tubular reforming and autothermal reforming of natural gas—an overview of available processes. Fuel Processing Technology 1995;42:85–107.
[96] Megaritis A, Tsolakis A, Wyszynski M, Golunski S. Fuel reforming for diesel engines. Advanced Direct Injection Combustion Engine Technologies and Development: Diesel Engines. Elsevier; 2010. p. 543–61.
[97] Zhang Z, Jia P, Zhong G, Liang J, Li G. Numerical study of exhaust reforming characteristics on hydrogen production for a marine engine fueled with LNG. Applied Thermal Engineering 2017;124:241–9.
[98] Elnashaie SSEH, Al-Ubaid AS, Soliman MA. Steam Reforming: Kinetics, Catalyst Deactivation and Reactor Design. editors. In: Bibby DM, Chang CD, Howe RF, Yurchak S, editors. Studies in Surface Science and Catalysis. Elsevier; 1988. p. 89–93.
[99] Gomes SR, Bion N, Blanchard G, Rousseau S, Bellière-Baca V, Harlé V, et al. Thermodynamic and experimental studies of catalytic reforming of exhaust gas recirculation in gasoline engines. Applied Catalysis B: Environmental 2011;102:44–53.
[100] Fennell DA. Exhaust gas fuel reforming for improved gasoline direct injection engine efficiency and emissions. University of Birmingham; 2014.
[101] Holladay JD, Hu J, King DL, Wang Y. An overview of hydrogen production technologies. Catalysis today 2009;139:244–60.
[102] Paykani A, Frouzakis CE, Boulouchos K. Numerical optimization of methane-based fuel blends under engine-relevant conditions using a multi-objective genetic algorithm. Applied Energy 2019;242:1712–24.
[103] Paykani A, Frouzakis CE, Schürch C, Perini F, Boulouchos K. Computational optimization of CH4/H2/CO blends in a spark-ignition engine using quasi-dimensional combustion model. Fuel 2021;303:121281.
[104] Decker K. Wood gas vehicles: firewood in the fuel tank. Low-tech Magazine Barcelona; 2010.
[105] Donath EE. Vehicle gas producers. Fuel Processing Technology 1980;3:141–53.

[106] Breag GR, Chittenden AE. Producer gas: its potential and application in developing countries 1979.
[107] Szybist JP, Busch S, McCormick RL, Pihl JA, Splitter DA, Ratcliff MA, et al. What fuel properties enable higher thermal efficiency in spark-ignited engines? Progress in Energy and Combustion Science 2021;82:100876.
[108] Von Szeszich L. Herstellung von Synthesegas im Otto-Motor bei gleichzeitiger Arbeitsgewinnung. Chemie Ingenieur Technik 1956;28:190–5.
[109] Cruz IE. Producer-gas technology for rural applications: Food & Agriculture Org.; 1985.
[110] Davis SC, Diegel SW, Boundy RG. Transportation energy data book. 2010.
[111] Baratieri M, Baggio P, Bosio B, Grigiante M, Longo G. The use of biomass syngas in IC engines and CCGT plants: a comparative analysis. Applied Thermal Engineering 2009;29:3309–18.
[112] Sánchez D, Chacartegui R, Munoz J, Muñoz A, Sánchez T. Performance analysis of a heavy duty combined cycle power plant burning various syngas fuels. international journal of hydrogen energy 2010;35:337–45.
[113] Munasinghe PC, Khanal SK. Biomass-derived syngas fermentation into biofuels: opportunities and challenges. Bioresource technology 2010;101:5013–22.
[114] Canter N. Biofuel production using syngas fermentation. Tribology & Lubrication Technology 2017;73:14.
[115] Peng X. Analysis of the thermal efficiency limit of the steam methane reforming process. Industrial & Engineering Chemistry Research 2012;51:16385–92.
[116] Golunski S. What is the point of on-board fuel reforming? Energy & Environmental Science 2010;3:1918–23.
[117] Stocky J, Dowdy MW, Vanderbrug T. An examination of the performance of spark ignition engines using hydrogen-supplemented fuels. SAE Technical Paper; 1975.
[118] Newkirk MS, Abel JL. The Boston reformed fuel car. SAE Transactions 1972: 2006–14.
[119] Martin MD. Gaseous automotive fuels from steam reformed liquid hydrocarbons. SAE Technical Paper; 1978.
[120] Houseman J, Cerini DJ. On-board hydrogen generator for a partial hydrogen injection internal combustion engine. SAE Technical Paper; 1974.
[121] Sjöström K. Steam Reforming of n-Heptane at Low Concentration for Hydrogen Injection into Internal Combustion Engines. Industrial & Engineering Chemistry Process Design and Development 1980;19:148–53.
[122] Sjöström K, Eriksson S, Landqvist G. Onboard hydrogen generation for hydrogen injection into internal combustion engines. SAE Technical Paper; 1981.
[123] Lindner B, Sjöström K. Operation of an internal combustion engine: lean conditions with hydrogen produced in an onboard methanol reforming unit. Fuel 1984;63:1485–90.
[124] Jones MR. Feasibility studies of the exhaust-gas reforming of hydrocarbon and alcohol fuels. University of Birmingham; 1992.
[125] Jones M, Wyszynski M. Exhaust-gas reforming of hydrocarbon fuels. SAE Technical Paper; 1993.
[126] Pettersson L, Sjöström K. Decomposed Methanol as a Fuel—A review. Combustion science and technology 1991;80:265–303.
[127] Jamal Y, Wyszynski ML. On-board generation of hydrogen-rich gaseous fuels—a review. International Journal of Hydrogen Energy 1994;19:557–72.
[128] Demirbas A. Biofuels sources, biofuel policy, biofuel economy and global biofuel projections. Energy Conversion and Management 2008;49:2106–16.
[129] Birol F. World energy outlook 2010. International Energy Agency 2010:1.
[130] Van der Drift A, Boerrigter H. Synthesis gas from biomass for fuels and chemicals: ECN Biomass. Coal and Environmental Research; 2006.
[131] Sridhar G, Sridhar H, Dasappa S, Paul P, Rajan N, Mukunda H. Development of producer gas engines. Proceedings of the Institution of Mechanical Engineers, Part D: Journal of Automobile Engineering 2005;219:423–38.
[132] Boloy RAM, Silveira JL, Tuna CE, Coronado CR, Antunes JS. Ecological impacts from syngas burning in internal combustion engine: Technical and economic aspects. Renewable and Sustainable Energy Reviews 2011;15:5194–201.
[133] Sobyanin V, Sadykov V, Kirillov V, Kuzmin V, Kuzin N, Vostrikov Z, et al. Syngas as a fuel for IC and diesel engines: efficiency and harmful emissions cut-off. In: Proceedings of International Hydrogen Energy Congress and Exhibition IHEC; 2005.
[134] Verhelst S, Turner JW, Sileghem L, Vancoillie J. Methanol as a fuel for internal combustion engines. Progress in Energy and Combustion Science 2019;70:43–88.
[135] D'andrea T, Henshaw P, Ting D-K. The addition of hydrogen to a gasoline-fuelled SI engine. International journal of hydrogen energy 2004;29:1541–52.
[136] Bell SR, Gupta M. Extension of the lean operating limit for natural gas fueling of a spark ignited engine using hydrogen blending. Combustion Science and Technology 1997;123:23–48.
[137] Lee H, Jiang L, Mohamad A. A review on the laminar flame speed and ignition delay time of Syngas mixtures. International Journal of Hydrogen Energy 2014; 39:1105–21.
[138] Jithin EV, Raghuram GKS, Keshavamurthy TV, Velamati RK, Prathap C, Varghese RJ. A review on fundamental combustion characteristics of syngas mixtures and feasibility in combustion devices. Renewable and Sustainable Energy Reviews 2021;146:111178.
[139] Speight J. Synthetic fuels handbook: properties, process and performance. 2008.
[140] Zabetakis MG. Flammability characteristics of combustible gases and vapors. Bureau of Mines Washington DC; 1965.
[141] Cecrle E, Depcik C, Guo J, Peltier E. Analysis of the effects of reformate (hydrogen/carbon monoxide) as an assistive fuel on the performance and emissions of used canola-oil biodiesel. international journal of hydrogen energy 2012;37:3510–27.
[142] Hotta SK, Sahoo N, Mohanty K. Ignition advancement study for optimized characteristics of a raw biogas operated spark ignition engine. International Journal of Green Energy 2019;16:101–13.
[143] Porpatham E, Ramesh A, Nagalingam B. Effect of swirl on the performance and combustion of a biogas fuelled spark ignition engine. Energy Conversion and Management 2013;76:463–71.
[144] Brabbs T, Belles F, Brokaw R. Shock-tube measurements of specific reaction rates in the branched-chain H2-CO-O2 system. Symposium (International) on Combustion: Elsevier; 1971. p. 129–36.
[145] Gardiner Jr W, McFarland M, Morinaga K, Takeyama T, Walker BF. Initiation rate for shock-heated hydrogen-oxygen-carbon monoxide-argon mixtures as determined by OH induction time measurements. The Journal of Physical Chemistry 1971;75:1504–9.
[146] Gardiner Jr W, Mallard W, McFarland M, Morinaga K, Owen J, Rawlins W, et al. Elementary reaction rates from post-induction-period profiles in shock-initiated combustion. Symposium (International) on Combustion. Elsevier; 1973. p. 61–75.
[147] Dean A, Steiner D, Wang E. A shock tube study of the H2/O2/CO/Ar and H2/ N2O/CO/Ar Systems: Measurement of the rate constant for H+ N2O= N2+ OH. Combustion and Flame 1978;32:73–83.
[148] Yetter R, Dryer F, Rabitz H. Flow reactor studies of carbon monoxide/hydrogen/ oxygen kinetics. Combustion Science and Technology 1991;79:129–40.
[149] Fotache C, Tan Y, Sung C, Law CK. Ignition of CO/H2/N2 versus heated air in counterflow: experimental and modeling results. Combustion and flame 2000; 120:417–26.
[150] Wierzba I, Kilchyk V. Flammability limits of hydrogen–carbon monoxide mixtures at moderately elevated temperatures. International Journal of Hydrogen Energy 2001;26:639–43.
[151] Davis SG, Joshi AV, Wang H, Egolfopoulos F. An optimized kinetic model of H2/ CO combustion. Proceedings of the combustion Institute 2005;30:1283–92.
[152] Mittal G, Sung CJ, Yetter RA. Autoignition of H2/CO at elevated pressures in a rapid compression machine. International Journal of Chemical Kinetics 2006;38: 516–29.
[153] Mittal G, Sung C, Fairweather M, Tomlin A, Griffiths J, Hughes K. Significance of the HO2+ CO reaction during the combustion of CO+ H2 mixtures at high pressures. Proceedings of the combustion Institute 2007;31:419–27.
[154] Walton S, He X, Zigler B, Wooldridge M. An experimental investigation of the ignition properties of hydrogen and carbon monoxide mixtures for syngas turbine applications. Proceedings of the Combustion Institute 2007;31:3147–54.
[155] Sivaramakrishnan R, Comandini A, Tranter R, Brezinsky K, Davis S, Wang H. Combustion of CO/H2 mixtures at elevated pressures. Proceedings of the Combustion Institute 2007;31:429–37.
[156] Petersen EL, Kalitan DM, Barrett AB, Reehal SC, Mertens JD, Beerer DJ, et al. New syngas/air ignition data at lower temperature and elevated pressure and comparison to current kinetics models. Combustion and Flame 2007;149:244–7.
[157] Chaos M, Dryer FL. Syngas combustion kinetics and applications. Combustion Science and Technology 2008;180:1053–96.
[158] Sung C-J, Law CK. Fundamental combustion properties of H2/CO mixtures: ignition and flame propagation at elevated pressures. Combustion Science and Technology 2008;180:1097–116.
[159] Mansfield AB, Wooldridge MS. High-pressure low-temperature ignition behavior of syngas mixtures. Combustion and flame 2014;161:2242–51.
[160] Kalitan DM, Mertens JD, Crofton MW, Petersen EL. Ignition and oxidation of lean CO/H2 fuel blends in air. Journal of propulsion and power. 2007;23:1291–301.
[161] Krejci MC, Mathieu O, Vissotski AJ, Ravi S, Sikes TG, Petersen EL, et al. Laminar flame speed and ignition delay time data for the kinetic modeling of hydrogen and syngas fuel blends. Journal of Engineering for Gas Turbines and Power 2013;135: 021503.
[162] Krejci M, Vissotski A, Ravi S, Metcalfe W, Keromnes A, Curran H, et al. Laminar flame speed measurements of moist syngas fuel blends at elevated pressures and temperatures. Spring technical meeting of the central states section of the combustion institute2012.
[163] Mathieu O, Kopp M, Petersen E. Shock-tube study of the ignition of multi-component syngas mixtures with and without ammonia impurities. Proceedings of the Combustion Institute 2013;34:3211–8.
[164] Vasu SS, Davidson DF, Hanson RK. Shock tube study of syngas ignition in rich CO2 mixtures and determination of the rate of H+ O2+ CO2→ HO2+ CO2. Energy & Fuels 2011;25:990–7.
[165] Kéromnès A, Metcalfe WK, Heufer KA, Donohoe N, Das AK, Sung C-J, et al. An experimental and detailed chemical kinetic modeling study of hydrogen and syngas mixture oxidation at elevated pressures. Combustion and Flame 2013;160: 995–1011.
[166] Gersen S, Darmeveil H, Levinsky H. The effects of CO addition on the autoignition of H 2, CH 4 and CH 4/H 2 fuels at high pressure in an RCM. Combustion and Flame 2012;159:3472–5.
[167] Gersen S, Anikin N, Mokhov A, Levinsky H. Ignition properties of methane/ hydrogen mixtures in a rapid compression machine. International Journal of Hydrogen Energy 2008;33:1957–64.
[168] Huang J, Hill P, Bushe W, Munshi S. Shock-tube study of methane ignition under engine-relevant conditions: experiments and modeling. Combustion and flame 2004;136:25–42.
[169] Paykani A. Comparative Study on Chemical Kinetics Mechanisms for Methane-Based Fuel Mixtures under Engine-Relevant Conditions. Energies 2021;14:2834.
[170] Lutz AE, Kee RJ, Miller JA. SENKIN: A FORTRAN program for predicting homogeneous gas phase chemical kinetics with sensitivity analysis. Livermore, CA (USA): Sandia National Labs.; 1988.

[171] Mansfield AB, Wooldridge MS. The effect of impurities on syngas combustion. Combustion and Flame 2015;162:2286–95.
[172] Ouyang L, Li H, Sun S, Wang X, Lu X. Auto-ignition of biomass synthesis gas in shock tube at elevated temperature and pressure. Science bulletin 2015;60:1935–46.
[173] Das A, Sung C-J. Ignition delay study of moist syngas/oxidizer and hydrogen/oxidizer mixtures using a rapid compression machine. In: 49th AIAA Aerospace Sciences Meeting including the New Horizons Forum and Aerospace Exposition; 2011. p. 91.
[174] Heywood JB. Internal combustion engine fundamentals. Mcgraw-hill New York; 1988.
[175] Leiker M, K C, W C, Pfeifer U, Rankl M. Evaluation of antiknocking property of gaseous fuels by means of methane number and its practical application to gas engines. Mechanical Engineering. NEW YORK, NY: ASME-AMER SOC MECHANICAL ENG 345 E 47TH ST; 1972. 1001755-&.
[176] Montoya JPG, Amell AA, Olsen DB. Prediction and measurement of the critical compression ratio and methane number for blends of biogas with methane, propane and hydrogen. Fuel 2016;186:168–75.
[177] Díaz GJA, Martinez LMC, Montoya JPG, Olsen DB. Methane number measurements of hydrogen/carbon monoxide mixtures diluted with carbon dioxide for syngas spark ignited internal combustion engine applications. Fuel 2019;236:535–43.
[178] Amador G, Forero JD, Rincon A, Fontalvo A, Bula A, Padilla RV, et al. Characteristics of Auto-ignition in internal combustion engines operated with gaseous fuels of variable methane number. Journal of Energy Resources Technology 2017;139:042205.
[179] Gobbato P, Masi M, De Simio L, Iannaccone S. A method for determining hydrogen–methane–nitrogen mixtures for laboratory tests of syngas-fuelled internal combustion engines. International Journal of Engine Research 2020:1468087420946134.
[180] Avl LG, Avl methane, url:https://www.avl.com/; February 2002.
[181] Euromot.http://www.euromot.eu/mediaandevents/publications/mn WpwaiS.
[182] Malenshek M, Olsen DB. Methane number testing of alternative gaseous fuels. Fuel 2009;88:650–6.
[183] Arunachalam A, Olsen DB. Experimental evaluation of knock characteristics of producer gas. Biomass and bioenergy 2012;37:169–76.
[184] Lechner R, Hornung A, Brautsch M. Prediction of the knock propensity of biogenous fuel gases: Application of the detonation theory to syngas blends. Fuel 2020;267:117243.
[185] Bestel D, Bayliff S, Xu H, Marchese A, Olsen D, Windom B. Investigation of the end-gas autoignition process in natural gas engines and evaluation of the methane number index. Proceedings of the Combustion Institute 2021;38:5839–47.
[186] Ranzi E, Frassoldati A, Grana R, Cuoci A, Faravelli T, Kelley A, et al. Hierarchical and comparative kinetic modeling of laminar flame speeds of hydrocarbon and oxygenated fuels. Progress in Energy and Combustion Science 2012;38:468–501.
[187] Egolfopoulos FN, Hansen N, Ju Y, Kohse-Höinghaus K, Law CK, Qi F. Advances and challenges in laminar flame experiments and implications for combustion chemistry. Progress in Energy and Combustion Science 2014;43:36–67.
[188] McLean IC, Smith DB, Taylor SC. The use of carbon monoxide/hydrogen burning velocities to examine the rate of the CO+OH reaction. Symposium (International) on Combustion 1994;25:749–57.
[189] Hassan M, Aung K, Faeth G. Properties of laminar premixed CO/H/air flames at various pressures. Journal of Propulsion and Power 1997;13:239–45.
[190] Natarajan J, Lieuwen T, Seitzman J. Laminar flame speeds of H 2/CO mixtures: effect of CO 2 dilution, preheat temperature, and pressure. Combustion and flame 2007;151:104–19.
[191] Bouvet N, Chauveau C, Gökalp I, Lee S-Y, Santoro RJ. Characterization of syngas laminar flames using the Bunsen burner configuration. International Journal of Hydrogen Energy 2011;36:992–1005.
[192] Bouvet N, Chauveau C, Gökalp I, Halter F. Experimental studies of the fundamental flame speeds of syngas (H2/CO)/air mixtures. Proceedings of the Combustion Institute 2011;33:913–20.
[193] Singh D, Nishiie T, Tanvir S, Qiao L. An experimental and kinetic study of syngas/air combustion at elevated temperatures and the effect of water addition. Fuel 2012;94:448–56.
[194] Askari O, Moghaddas A, Alholm A, Vien K, Alhazmi B, Metghalchi H. Laminar burning speed measurement and flame instability study of H2/CO/air mixtures at high temperatures and pressures using a novel multi-shell model. Combustion and Flame 2016;168:20–31.
[195] Natarajan J, Lieuwen T, Seitzman J. Laminar flame speeds of H2/CO mixtures: effect of CO2 dilution, preheat temperature, and pressure. Combustion and flame 2007;151:104–19.
[196] Sun H, Yang S, Jomaas G, Law C. High-pressure laminar flame speeds and kinetic modeling of carbon monoxide/hydrogen combustion. Proceedings of the Combustion Institute 2007;31:439–46.
[197] Konnov AA, Mohammad A, Kishore VR, Kim NI, Prathap C, Kumar S. A comprehensive review of measurements and data analysis of laminar burning velocities for various fuel+ air mixtures. Progress in Energy and Combustion Science 2018;68:197–267.
[198] Han W, Dai P, Gou X, Chen Z. A review of laminar flame speeds of hydrogen and syngas measured from propagating spherical flames. Applications in Energy and Combustion Science 2020;1-4:100008.
[199] Kelley AP, Jomaas G, Law CK. Critical radius for sustained propagation of spark-ignited spherical flames. Combustion and Flame 2009;156:1006–13.
[200] Han M, Ai Y, Chen Z, Kong W. Laminar flame speeds of H2/CO with CO2 dilution at normal and elevated pressures and temperatures. Fuel 2015;148:32–8.
[201] Wang S, Wang Z, Han X, Chen C, He Y, Zhu Y, et al. Experimental and numerical study of the effect of elevated pressure on laminar burning velocity of lean H2/CO/O2/diluents flames. Fuel 2020;273:117753.
[202] Vu TM, Park J, Kwon OB, Bae DS, Yun JH, Keel SI. Effects of diluents on cellular instabilities in outwardly propagating spherical syngas–air premixed flames. international journal of hydrogen energy 2010;35:3868–80.
[203] Goswami M, Van Griensven J, Bastiaans R, Konnov AA, De Goey L. Experimental and modeling study of the effect of elevated pressure on lean high-hydrogen syngas flames. Proceedings of the Combustion Institute 2015;35:655–62.
[204] Li J, Zhao Z, Kazakov A, Chaos M, Dryer FL, Scire Jr JJ. A comprehensive kinetic mechanism for CO, CH2O, and CH3OH combustion. International Journal of Chemical Kinetics 2007;39:109–36.
[205] Burke MP, Chaos M, Ju Y, Dryer FL, Klippenstein SJ. Comprehensive H2/O2 kinetic model for high-pressure combustion. International Journal of Chemical Kinetics 2012;44:444–74.
[206] Goswami M, Bastiaans R, Konnov A, De Goey L. Laminar burning velocity of lean H2–CO mixtures at elevated pressure using the heat flux method. International journal of hydrogen energy 2014;39:1485–98.
[207] Zhang W, Gou X, Kong W, Chen Z. Laminar flame speeds of lean high-hydrogen syngas at normal and elevated pressures. Fuel 2016;181:958–63.
[208] Morovatiyan M, Shahsavan M, Baghirzade M, Mack JH. Impact of syngas addition to methane on laminar burning velocity. Journal of Engineering for Gas Turbines and Power 2021;143:051004.
[209] Liu C, Shy S, Chiu C, Peng M, Chung H. Hydrogen/carbon monoxide syngas burning rates measurements in high-pressure quiescent and turbulent environment. international journal of hydrogen energy 2011;36:8595–603.
[210] Askari O, Wang Z, Vien K, Sirio M, Metghalchi H. On the flame stability and laminar burning speeds of syngas/O 2/He premixed flame. Fuel 2017;190:90–103.
[211] Xie Y, Wang J, Cai X, Huang Z. Self-acceleration of cellular flames and laminar flame speed of syngas/air mixtures at elevated pressures. International Journal of Hydrogen Energy 2016;41:18250–8.
[212] Hu Z, Wang Y, Zhang J, Hou X. Experimental study on self-acceleration characteristics of unstable flame of low calorific value gas blended with hydrogen. International Journal of Hydrogen Energy 2019;44:25248–56.
[213] Bradley D, Lawes M, Liu K, Verhelst S, Woolley R. Laminar burning velocities of lean hydrogen–air mixtures at pressures up to 1.0 MPa. Combustion and Flame 2007;149:162–72.
[214] Prathap C, Ray A, Ravi M. Effects of dilution with carbon dioxide on the laminar burning velocity and flame stability of H2–CO mixtures at atmospheric condition. Combustion and flame 2012;159:482–92.
[215] Wang Z, Weng W, He Y, Li Z, Cen K. Effect of H 2/CO ratio and N 2/CO 2 dilution rate on laminar burning velocity of syngas investigated by direct measurement and simulation. Fuel 2015;141:285–92.
[216] Li H-M, Li G-X, Jiang Y-H. Laminar burning velocities and flame instabilities of diluted H2/CO/air mixtures under different hydrogen fractions. International Journal of Hydrogen Energy 2018;43:16344–54.
[217] Prathap C, Ray A, Ravi M. Investigation of nitrogen dilution effects on the laminar burning velocity and flame stability of syngas fuel at atmospheric condition. Combustion and Flame 2008;155:145–60.
[218] Burbano HJ, Pareja J, Amell AA. Laminar burning velocities and flame stability analysis of H2/CO/air mixtures with dilution of N2 and CO2. International journal of hydrogen energy 2011;36:3232–42.
[219] Zhang Y, Shen W, Zhang H, Wu Y, Lu J. Effects of inert dilution on the propagation and extinction of lean premixed syngas/air flames. Fuel 2015;157:115–21.
[220] Shang R, Zhang Y, Zhu M, Zhang Z, Zhang D, Li G. Laminar flame speed of CO2 and N2 diluted H2/CO/air flames. International Journal of Hydrogen Energy 2016;41:15056–67.
[221] Li H-M, Li G-X, Sun Z-Y, Zhou Z-H, Li Y, Yuan Y. Investigation on dilution effect on laminar burning velocity of syngas premixed flames. Energy 2016;112:146–52.
[222] Varghese RJ, Kolekar H, Kumar S. Demarcation of reaction effects on laminar burning velocities of diluted syngas–air mixtures at elevated temperatures. International Journal of Chemical Kinetics 2019;51:95–104.
[223] Xie Y, Wang J, Xu N, Yu S, Huang Z. Comparative study on the effect of CO2 and H2O dilution on laminar burning characteristics of CO/H2/air mixtures. International Journal of Hydrogen Energy 2014;39:3450–8.
[224] Das AK, Kumar K, Sung C-J. Laminar flame speeds of moist syngas mixtures. Combustion and Flame 2011;158:345–53.
[225] Santner J, Dryer FL, Ju Y. The effects of water dilution on hydrogen, syngas, and ethylene flames at elevated pressure. Proceedings of the Combustion Institute 2013;34:719–26.
[226] Zhou Q, Cheung C, Leung C, Li X, Li X, Huang Z. Effects of fuel composition and initial pressure on laminar flame speed of H2/CO/CH4 bio-syngas. Fuel 2019;238:149–58.
[227] Law CK, Kwon OC. Effects of hydrocarbon substitution on atmospheric hydrogen–air flame propagation. International Journal of Hydrogen Energy 2004;29:867–79.
[228] Lapalme D, Seers P. Influence of CO2, CH4, and initial temperature on H2/CO laminar flame speed. International Journal of Hydrogen Energy 2014;39:3477–86.
[229] Liu J, Zhang X, Wang T, Hou X, Zhang J, Zheng S. Numerical study of the chemical, thermal and diffusion effects of H2 and CO addition on the laminar flame speeds of methane–air mixture. International Journal of Hydrogen Energy 2015;40:8475–83.

[230] Xie Y, Wang X, Bi H, Yuan Y, Wang J, Huang Z, et al. A comprehensive review on laminar spherically premixed flame propagation of syngas. Fuel Processing Technology 2018;181:97–114.
[231] Huang Y, Sung C, Eng J. Laminar flame speeds of primary reference fuels and reformer gas mixtures. Combustion and Flame 2004;139:239–51.
[232] Hernandez JJ, Lapuerta M, Serrano C, Melgar A. Estimation of the Laminar Flame Speed of Producer Gas from Biomass Gasification. Energy & Fuels 2005;19:2172–8.
[233] Serrano C, Hernández JJ, Mandilas C, Sheppard CGW, Woolley R. Laminar burning behaviour of biomass gasification-derived producer gas. International Journal of Hydrogen Energy 2008;33:851–62.
[234] Monteiro E, Bellenoue M, Sotton J, Moreira NA, Malheiro S. Laminar burning velocities and Markstein numbers of syngas–air mixtures. Fuel 2010;89:1985–91.
[235] Yan B, Wu Y, Liu C, Yu JF, Li B, Li ZS, et al. Experimental and modeling study of laminar burning velocity of biomass derived gases/air mixtures. International Journal of Hydrogen Energy 2011;36:3769–77.
[236] Tippa M, Akash M, Subbiah S, Prathap C. A comprehensive study on laminar burning velocity and flame stability of oxy-producer gas mixtures. Part-1: Gas mixture composition and flame stability analysis based on Lewis number. Fuel 2021;292:120302.
[237] Tippa M, Akash M, Subbiah S, Prathap C. A comprehensive study on laminar burning velocity and flame stability of oxy-producer gas mixtures. Part-2: Laminar burning velocity and Markstein length analysis. Fuel 2021;292:119982.
[238] Kwon H, Min K. Laminar Flame Speed Characteristics and Combustion Simulation of Synthetic Gas Fueled SI Engine. SAE International; 2008.
[239] Keesee CL, Petersen EL, Zhang K, Curran HJ. Laminar Flame Speed Measurements of Synthetic Gas Blends with Hydrocarbon Impurities. In: ASME Turbo Expo 2015: Turbine Technical Conference and Exposition. American Society of Mechanical Engineers; 2015. V04ATA068-V04AT04A.
[240] Xu H, Liu F, Sun S, Meng S, Zhao Y. A systematic numerical study of the laminar burning velocity of iso-octane/syngas/air mixtures. Chemical Engineering Science 2019;195:598–608.
[241] Askari O, Vien K, Wang Z, Sirio M, Metghalchi H. Exhaust gas recirculation effects on flame structure and laminar burning speeds of H 2/CO/air flames at high pressures and temperatures. Applied Energy 2016;179:451–62.
[242] Morovatiyan M, Shahsavan M, Baghirzade M, Mack JH. Effect of Hydrogen and Carbon Monoxide Addition to Methane on Laminar Burning Velocity. In: Internal Combustion Engine Division Fall Technical Conference: American Society of Mechanical Engineers; 2019. V001T02A6.
[243] Xu H, LaPointe LA, Bremmer RJ. Syngas Laminar Flame Speed Computation and its Application to Gaseous Fueled Spark Ignited Engines Performance Prediction. In: ASME 2016 Internal Combustion Engine Fall Technical Conference: American Society of Mechanical Engineers; 2016. V001T03A16-VT03A16.
[244] Xu H, LaPointe LA. Engine Capability Prediction for Spark Ignited Engine Fueled With Syngas. Journal of Engineering for Gas Turbines and Power 2016;138:102812.
[245] Ravi S, Petersen EL. Laminar flame speed correlations for pure-hydrogen and high-hydrogen content syngas blends with various diluents. International Journal of Hydrogen Energy 2012;37:19177–89.
[246] Shang R, Zhang Y, Zhu M, Zhang Z, Zhang D. Semiempirical Correlation for Predicting Laminar Flame Speed of H2/CO/Air Flames with CO2 and N2 Dilution. Energy & Fuels 2017;31:9957–66.
[247] Halter F, Chauveau C, Djebaili-Chaumeix N, Gökalp I. Characterization of the effects of pressure and hydrogen concentration on laminar burning velocities of methane–hydrogen–air mixtures. Proceedings of the Combustion Institute 2005;30:201–8.
[248] Natarajan J, Nandula S, Lieuwen T, Seitzman J. Laminar flame speeds of synthetic gas fuel mixtures. ASME Turbo Expo 2005: Power for Land, Sea, and Air. American Society of Mechanical Engineers; 2005. p. 677–86.
[249] Bougrine S, Richard S, Nicolle A, Veynante D. Numerical study of laminar flame properties of diluted methane-hydrogen-air flames at high pressure and temperature using detailed chemistry. international journal of hydrogen energy 2011;36:12035–47.
[250] Varghese RJ, Kumar S. Machine learning model to predict the laminar burning velocities of H2/CO/CH4/CO2/N2/air mixtures at high pressure and temperature conditions. International Journal of Hydrogen Energy 2020;45:3216–32.
[251] Frassoldati A, Faravelli T, Ranzi E. The ignition, combustion and flame structure of carbon monoxide/hydrogen mixtures. Note 1: Detailed kinetic modeling of syngas combustion also in presence of nitrogen compounds. International Journal of Hydrogen Energy 2007;32:3471–85.
[252] Abdel-Gayed R, Bradley D, Lawes M. Turbulent burning velocities: a general correlation in terms of straining rates. Proceedings of the Royal Society of London A Mathematical and Physical Sciences 1987;414:389–413.
[253] Lipatnikov A, Chomiak J. Turbulent flame speed and thickness: phenomenology, evaluation, and application in multi-dimensional simulations. Progress in energy and combustion science 2002;28:1–74.
[254] Heywood JB. Internal combustion engine fundamentals: McGraw-Hill Education; 2018.
[255] Venkateswaran P, Marshall A, Shin DH, Noble D, Seitzman J, Lieuwen T. Measurements and analysis of turbulent consumption speeds of H2/CO mixtures. Combustion and Flame 2011;158:1602–14.
[256] Ichikawa Y, Otawara Y, Kobayashi H, Ogami Y, Kudo T, Okuyama M, et al. Flame structure and radiation characteristics of CO/H2/CO2/air turbulent premixed flames at high pressure. Proceedings of the Combustion Institute 2011;33:1543–50.
[257] Daniele S, Jansohn P, Mantzaras J, Boulouchos K. Turbulent flame speed for syngas at gas turbine relevant conditions. Proceedings of the Combustion Institute 2011;33:2937–44.
[258] Lin Y-C, Jansohn P, Boulouchos K. Turbulent flame speed for hydrogen-rich fuel gases at gas turbine relevant conditions. International Journal of Hydrogen Energy 2014;39:20242–54.
[259] Zhang M, Wang J, Chang M, Huang Z. Turbulent flame topology and the wrinkled structure characteristics of high pressure syngas flames up to 1.0 MPa. International Journal of Hydrogen Energy 2018.
[260] Shy S, Liu C, Lin J, Chen L, Lipatnikov A, Yang S. Correlations of high-pressure lean methane and syngas turbulent burning velocities: Effects of turbulent Reynolds, Damköhler, and Karlovitz numbers. Proceedings of the Combustion Institute 2015;35:1509–16.
[261] Chiu C-W, Dong Y-C, Shy SS. High-pressure hydrogen/carbon monoxide syngas turbulent burning velocities measured at constant turbulent Reynolds numbers. International Journal of Hydrogen Energy 2012;37:10935–46.
[262] Liu CC, Shy SS, Chen HC, Peng MW. On interaction of centrally-ignited, outwardly-propagating premixed flames with fully-developed isotropic turbulence at elevated pressure. Proceedings of the Combustion Institute 2011;33:1293–9.
[263] Wang J, Zhang M, Xie Y, Huang Z, Kudo T, Kobayashi H. Correlation of turbulent burning velocity for syngas/air mixtures at high pressure up to 1.0 MPa. Experimental Thermal and Fluid Science 2013;50:90–6.
[264] Venkateswaran P, Marshall A, Seitzman J, Lieuwen T. Pressure and fuel effects on turbulent consumption speeds of H2/CO blends. Proceedings of the Combustion Institute 2013;34:1527–35.
[265] Rabello de Castro R, Brequigny P, Dufitumukiza JP. Mounaïm-Rousselle C. Laminar flame speed of different syngas compositions for varying thermodynamic conditions. Fuel 2021;301:121025.
[266] Sun ZY, Xu C. Turbulent burning velocity of stoichiometric syngas flames with different hydrogen volumetric fractions upon constant-volume method with multi-zone model. International Journal of Hydrogen Energy 2020;45:4969–78.
[267] Venkateswaran P, Marshall A, Seitzman J, Lieuwen T. Scaling turbulent flame speeds of negative Markstein length fuel blends using leading points concepts. Combustion and Flame 2015;162:375–87.
[268] Aspden AJ, Day MS, Bell JB. Turbulence-chemistry interaction in lean premixed hydrogen combustion. Proceedings of the Combustion Institute 2015;35:1321–9.
[269] Ranga Dinesh KKJ, Shalaby H, Luo KH, van Oijen JA, Thévenin D. High hydrogen content syngas fuel burning in lean premixed spherical flames at elevated pressures: Effects of preferential diffusion. International Journal of Hydrogen Energy 2016;41:18231–49.
[270] Ranga Dinesh KKJ, Shalaby H, Luo KH, van Oijen JA, Thévenin D. Heat release rate variations in high hydrogen content premixed syngas flames at elevated pressures: Effect of equivalence ratio. International Journal of Hydrogen Energy 2017;42:7029–44.
[271] Bhide KG, Sreedhara S. A DNS study on turbulence-chemistry interaction in lean premixed syngas flames. International Journal of Hydrogen Energy 2020;45:23615–23.
[272] Mustafi N, Miraglia Y, Raine R, Bansal P, Elder S. Spark-ignition engine performance with 'Powergas' fuel (mixture of CO/H 2): a comparison with gasoline and natural gas. Fuel 2006;85:1605–12.
[273] Caligiuri C, Žvar Baškovič U, Renzi M, Seljak T, Oprešnik SR, Baratieri M, et al. Complementing Syngas with Natural Gas in Spark Ignition Engines for Power Production: Effects on Emissions and Combustion. Energies 2021;14:3688.
[274] Ando Y, Yoshikawa K, Beck M, Endo H. Research and development of a low-BTU gas-driven engine for waste gasification and power generation. Energy 2005;30:2206–18.
[275] Bika AS. Synthesis gas use in internal combustion engines. University of Minnesota; 2010.
[276] Munoz M, Moreno F, Morea-Roy J, Ruiz J, Arauzo J. Low heating value gas on spark ignition engines. Biomass and Bioenergy 2000;18:431–9.
[277] Shah A, Srinivasan R, To SDF, Columbus EP. Performance and emissions of a spark-ignited engine driven generator on biomass based syngas. Bioresource technology 2010;101:4656–61.
[278] Dasappa S, Subbukrishna D, Suresh K, Paul P, Prabhu G. Operational experience on a grid connected 100 kWe biomass gasification power plant in Karnataka, India. Energy for sustainable development 2011;15:231–9.
[279] Tsiakmakis S, Mertzis D, Dimaratos A, Toumasatos Z, Samaras Z. Experimental study of combustion in a spark ignition engine operating with producer gas from various biomass feedstocks. Fuel 2014;122:126–39.
[280] Kravos A, Seljak T, Rodman Oprešnik S, Katrašnik T. Operational stability of a spark ignition engine fuelled by low H2 content synthesis gas: Thermodynamic analysis of combustion and pollutants formation. Fuel 2020;261:116457.
[281] Arroyo J, Moreno F, Munoz M, Monne C. Efficiency and emissions of a spark ignition engine fueled with synthetic gases obtained from catalytic decomposition of biogas. international journal of hydrogen energy 2013;38:3784–92.
[282] Ran Z, Hariharan D, Lawler B, Mamalis S. Experimental study of lean spark ignition combustion using gasoline, ethanol, natural gas, and syngas. Fuel 2019;235:530–7.
[283] Kan X, Zhou D, Yang W, Zhai X, Wang C-H. An investigation on utilization of biogas and syngas produced from biomass waste in premixed spark ignition engine. Applied Energy 2018;212:210–22.
[284] Sridhar G, Paul P, Mukunda H. Biomass derived producer gas as a reciprocating engine fuel—an experimental analysis. Biomass and Bioenergy 2001;21:61–72.
[285] Sridhar G, Yarasu RB. Facts about producer gas engine. Paths to Sustainable Energy 2010. InTech.

[286] Homdoung N, Tippayawong N, Dussadee N. Performance and emissions of a modified small engine operated on producer gas. Energy Conversion and Management 2015;94:286–92.
[287] Homdoung N, Tippayawong N, Dussadee N. Performance investigation of a modified small engine fueled with producer gas. Maejo International Journal of Science and Technology 2015;9:10.
[288] Sridhar G, Paul P, Mukunda H. Zero-dimensional modelling of a producer gas-based reciprocating engine. Proceedings of the Institution of Mechanical Engineers, Part A: Journal of Power and Energy 2006;220:923–31.
[289] Raman P, Ram N. Performance analysis of an internal combustion engine operated on producer gas, in comparison with the performance of the natural gas and diesel engines. Energy 2013;63:317–33.
[290] Park H, Lee J, Jamsran N, Oh S, Kim C, Lee Y, et al. Comparative assessment of stoichiometric and lean combustion modes in boosted spark-ignition engine fueled with syngas. Energy Conversion and Management 2021;239:114224.
[291] Hagos F. Combustion, Performance and Emissions Characteristics of Imitated Syngases in Direct-injection Sparkigntion Engine. PhD, Department of Mechanical Engineering. Seri Iskandar, Malaysia: Universiti Teknologi PETRONAS; 2013.
[292] Hagos FY, Aziz ARA, Sulaiman SA. Syngas (H 2/CO) in a spark-ignition direct-injection engine. Part 1: Combustion, performance and emissions comparison with CNG. International Journal of Hydrogen Energy 2014;39:17884–95.
[293] Hagos FY, Aziz ARA, Sulaiman SA. Effect of injection timing on combustion, performance and emissions of lean-burn syngas (H2/CO) in spark-ignition direct-injection engine. International Journal of Engine Research 2016;17:921–33.
[294] Hagos FY, Aziz ARA, Sulaiman SA. Methane enrichment of syngas (H 2/CO) in a spark-ignition direct-injection engine: combustion, performance and emissions comparison with syngas and compressed natural gas. Energy 2015;90:2006–15.
[295] Hagos FY, Aziz ARA, Sulaiman SA, Mamat R. Effect of fuel injection timing of hydrogen rich syngas augmented with methane in direct-injection spark-ignition engine. International Journal of Hydrogen Energy 2017.
[296] Hagos FY, Aziz ARA, Sulaiman SA, Mamat R. Engine speed and air-fuel ratio effect on the combustion of methane augmented hydrogen rich syngas in DI SI engine. International Journal of Hydrogen Energy 2019;44:477–86.
[297] Fiore M, Viggiano A, Fanelli E, Braccio G, Magi V. Influence of piston shape and injector geometry on combustion and emission characteristics of syngas in direct-injection spark-ignition engine. Energy Procedia 2018;148:392–9.
[298] Velji A, Yeom K, Wagner U, Spicher U, Roßbach M, Suntz R, et al. Investigations of the formation and oxidation of soot inside a direct injection spark ignition engine using advanced laser-techniques. SAE Technical Paper; 2010.
[299] Raza M, Chen L, Leach F, Ding S. A review of particulate number (PN) emissions from gasoline direct injection (GDI) engines and their control techniques. Energies 2018;11:1417.
[300] Thawko A, Yadav H, Eyal A, Shapiro M, Tartakovsky L. Particle emissions of direct injection internal combustion engine fed with a hydrogen-rich reformate. International Journal of Hydrogen Energy 2019;44:28342–56.
[301] Bogarra M, Herreros J, Tsolakis A, York A, Millington P. Study of particulate matter and gaseous emissions in gasoline direct injection engine using on-board exhaust gas fuel reforming. Applied Energy 2016;180:245–55.
[302] Gerty MD, Heywood JB. An Investigation of Gasoline Engine Knock Limited Performance and the Effects of Hydrogen Enhancement. SAE International; 2006.
[303] Ayala FA, Gerty MD, Heywood JB. Effects of combustion phasing, relative air-fuel ratio, compression ratio, and load on SI engine efficiency. SAE Technical Paper; 2006.
[304] Ivanič Ž, Ayala F, Goldwitz J, Heywood JB. Effects of hydrogen enhancement on efficiency and NOx emissions of lean and EGR-diluted mixtures in a SI engine. SAE Technical Paper; 2005.
[305] Ayala FA, Heywood JB. Lean SI engines: the role of combustion variability in defining lean limits. SAE Technical Paper; 2007.
[306] Smith JA, Bartley GJ. Stoichiometric operation of a gas engine utilizing synthesis gas and EGR for NOx control. Journal of engineering for gas turbines and power 2000;122:617–23.
[307] Cha H, Eom T, Song S, Chun KM. An experimental study on the fuel conversion efficiency and NO x emissions of a spark-ignition gas engine for power generation by fuel mixture of methane and model syngas (H 2/CO). Journal of Natural Gas Science and Engineering 2015;23:517–23.
[308] Conte E, Boulouchos K. Experimental investigation into the effect of reformer gas addition on flame speed and flame front propagation in premixed, homogeneous charge gasoline engines. Combustion and Flame 2006;146:329–47.
[309] Papagiannakis R, Rakopoulos C, Hountalas D, Giakoumis E. Study of the performance and exhaust emissions of a spark-ignited engine operating on syngas fuel. International Journal of Alternative Propulsion 2007;1:190–215.
[310] Rakopoulos C, Michos C. Development and validation of a multi-zone combustion model for performance and nitric oxide formation in syngas fueled spark ignition engine. Energy Conversion and management 2008;49:2924–38.
[311] Arroyo J, Moreno F, Muñoz M, Monné C, Bernal N. Combustion behavior of a spark ignition engine fueled with synthetic gases derived from biogas. Fuel 2014;117:50–8.
[312] Arroyo J, Moreno F, Muñoz M, Monné C. Experimental study of ignition timing and supercharging effects on a gasoline engine fueled with synthetic gases extracted from biogas. Energy Conversion and Management 2015;97:196–211.
[313] Ran Z, Hariharan D, Lawler B, Mamalis S. Exploring the potential of ethanol, CNG, and syngas as fuels for lean spark-ignition combustion-An experimental study. Energy 2020;191:116520.
[314] Gamiño B, Aguillón J. Numerical simulation of syngas combustion with a multi-spark ignition system in a diesel engine adapted to work at the Otto cycle. Fuel 2010;89:581–91.
[315] Ulfvik J, Achilles M, Tuner M, Johansson B, Ahrenfeldt J, Schauer FX, et al. SI Gas Engine: Evaluation of Engine Performance, Efficiency and Emissions Comparing Producer Gas and Natural Gas. SAE International Journal of Engines 2011;4:1202–9.
[316] Shivapuji AM, Dasappa S. Selection and thermodynamic analysis of a turbocharger for a producer gas-fuelled multi-cylinder engine. Proceedings of the Institution of Mechanical Engineers, Part A: Journal of Power and Energy 2014;228:340–56.
[317] Shivapuji AM, Dasappa S. Influence of fuel hydrogen fraction on syngas fueled SI engine: Fuel thermo-physical property analysis and in-cylinder experimental investigations. international journal of hydrogen energy 2015;40:10308–28.
[318] Kim S, Kim J. Feasibility assessment of hydrogen-rich syngas spark-ignition engine for heavy-duty long-distance vehicle application. Energy Conversion and Management. 2021:115048.
[319] Yao M, Zheng Z, Liu H. Progress and recent trends in homogeneous charge compression ignition (HCCI) engines. Progress in energy and combustion science 2009;35:398–437.
[320] Saxena S, Bedoya ID. Fundamental phenomena affecting low temperature combustion and HCCI engines, high load limits and strategies for extending these limits. Progress in Energy and Combustion Science 2013;39:457–88.
[321] Stenlåås O, Christensen M, Egnell R, Tunestål P, Johansson B, Mauss F. Reformed methanol gas as homogeneous charge compression ignition engine fuel. SAE Technical Paper; 2004.
[322] Stenlåås O, Christensen M, Egnell R, Johansson B, Mauss F. Hydrogen as homogeneous charge compression ignition engine fuel. SAE transactions 2004:1317–26.
[323] Bika AS, Franklin L, Kittelson DB. Homogeneous charge compression ignition engine operating on synthesis gas. international journal of hydrogen energy 2012;37:9402–11.
[324] Kozlov V, Chechet I, Matveev S, Titova N, Starik A. Modeling study of combustion and pollutant formation in HCCI engine operating on hydrogen rich fuel blends. International Journal of Hydrogen Energy 2016;41:3689–700.
[325] Starik A, Korobov A, Titova N. Combustion improvement in HCCI engine operating on synthesis gas via addition of ozone or excited oxygen molecules to the charge: Modeling study. International Journal of Hydrogen Energy 2017;42:10475–84.
[326] Yamasaki Y, Kaneko S. Prediction of Ignition and Combustion Development in an HCCI Engine Fueled by Syngas. SAE Technical Paper; 2014.
[327] Maurya RK, Saxena MR, Yadav R, Rathore A. Numerical Investigation of Syngas Fueled HCCI Engine Using Stochastic Reactor Model with Detailed Kinetic Mechanism. SAE Technical Paper; 2018.
[328] Przybyla G, Szlek A, Haggith D, Sobiesiak A. Fuelling of spark ignition and homogenous charge compression ignition engines with low calorific value producer gas. Energy 2016;116:1464–78.
[329] Bhaduri S, Contino F, Jeanmart H, Breuer E. The effects of biomass syngas composition, moisture, tar loading and operating conditions on the combustion of a tar-tolerant HCCI (Homogeneous Charge Compression Ignition) engine. Energy 2015;87:289–302.
[330] Bhaduri S, Berger B, Pochet M, Jeanmart H, Contino F. HCCI engine operated with unscrubbed biomass syngas. Fuel Processing Technology 2017;157:52–8.
[331] Bhaduri S, Jeanmart H, Contino F. Tar Tolerant HCCI Engine Fuelled with Biomass Syngas: Combustion Control Through EGR. Energy Procedia 2017;105:1764–70.
[332] Bhaduri S, Jeanmart H, Contino F. EGR control on operation of a tar tolerant HCCI engine with simulated syngas from biomass. Applied Energy 2018;227:159–67.
[333] Iverson RJ, Herold RE, Augusta R, Foster DE, Ghandhi JB, Eng JA, et al. The effects of intake charge preheating in a gasoline-fueled HCCI engine. SAE transactions 2005:1566–74.
[334] Sjöberg M, Dec JE, Hwang W. Thermodynamic and chemical effects of EGR and its constituents on HCCI autoignition. SAE Transactions 2007:271–89.
[335] Sjöberg M, Dec JE. Effects of EGR and its constituents on HCCI autoignition of ethanol. Proceedings of the Combustion Institute 2011;33:3031–8.
[336] Olsson J-O, Tunestål P, Johansson B. Boosting for high load HCCI. SAE transactions 2004:579–88.
[337] Silke EJ, Pitz WJ, Westbrook CK, Sjöberg M, Dec JE. Understanding the chemical effects of increased boost pressure under HCCI conditions. SAE International Journal of Fuels and Lubricants 2009;1:12–25.
[338] Shibata G, Oyama K, Urushihara T, Nakano T. The effect of fuel properties on low and high temperature heat release and resulting performance of an HCCI engine. SAE Technical Paper; 2004.
[339] Bessonette PW, Schleyer CH, Duffy KP, Hardy WL, Liechty MP. Effects of fuel property changes on heavy-duty HCCI combustion. SAE Transactions 2007:242–54.
[340] Agarwal AK, Singh AP, Maurya RK. Evolution, challenges and path forward for low temperature combustion engines. Progress in energy and combustion science 2017;61:1–56.
[341] Duan X, Lai M-C, Jansons M, Guo G, Liu J. A review of controlling strategies of the ignition timing and combustion phase in homogeneous charge compression ignition (HCCI) engine. Fuel 2021;285:119142.
[342] Shibata G, Oyama K, Urushihara T, Nakano T. Correlation of low temperature heat release with fuel composition and HCCI engine combustion. SAE Technical Paper; 2005.
[343] Eng J, Leppard W, Sloane T. The Effect of POx on the Autoignition Chemistry of n-Heptane and Isooctane in an HCCI Engine. SAE Transactions 2002:1881–95.

[344] Fleisch T, McCarthy C, Basu A, Udovich C, Charbonneau P, Slodowske W, et al. A new clean diesel technology: demonstration of ULEV emissions on a Navistar diesel engine fueled with dimethyl ether. SAE transactions 1995:42–53.
[345] Semelsberger TA, Borup RL, Greene HL. Dimethyl ether (DME) as an alternative fuel. Journal of power sources 2006;156:497–511.
[346] Shudo T, Ono Y. HCCI combustion of hydrogen, carbon monoxide and dimethyl ether. SAE Transactions 2002:459–64.
[347] Shudo T, Ono Y, Takahashi T. Influence of hydrogen and carbon monoxide on HCCI combustion of dimethyl ether. SAE Transactions 2002:1784–93.
[348] Shudo T, Takahashi T. Influence of reformed gas composition on HCCI combustion of onboard methanol-reformed gases. SAE Technical Paper; 2004.
[349] Shudo T, Yamada H. Hydrogen as an ignition-controlling agent for HCCI combustion engine by suppressing the low-temperature oxidation. International Journal of Hydrogen Energy 2007;32:3066–72.
[350] Shudo T. Influence of gas composition on the combustion and efficiency of a homogeneous charge compression ignition engine system fuelled with methanol reformed gases. International Journal of Engine Research 2008;9:399–408.
[351] Shudo T, Shima Y, Fujii T. Production of dimethyl ether and hydrogen by methanol reforming for an HCCI engine system with waste heat recovery–Continuous control of fuel ignitability and utilization of exhaust gas heat. International journal of hydrogen energy 2009;34:7638–47.
[352] Shudo T, Ono Y, Takahashi T. Ignition control by DME-reformed gas in HCCI combustion of DME. SAE transactions 2003:1195–202.
[353] Shudo T, Suzuki H. Applicability of heat transfer equations to hydrogen combustion. JSAE review 2002;23:303–8.
[354] Peucheret S, Wyszyn´ski M. Exhaust-gas reforming of methane to aid natural gas HCCI combustion: experimental results of open loop hydrogen production and basic thermodynamic analysis. Engineering Systems Design and Analysis 2004: 453–60.
[355] Peucheret S, Wyszyński M, Lehrle R, Golunski S, Xu H. Use of catalytic reforming to aid natural gas HCCI combustion in engines: experimental and modelling results of open-loop fuel reforming. International journal of hydrogen energy 2005;30:1583–94.
[356] Yap D, Peucheret S, Megaritis A, Wyszynski M, Xu H. Natural gas HCCI engine operation with exhaust gas fuel reforming. International Journal of Hydrogen Energy 2006;31:587–95.
[357] Xu H, Wyszynski M, Megaritis A, Yap D, Wilson T, Qiao J, et al. Research on expansion of operating windows of controlled homogeneous auto-ignition engines. International journal of engine research 2007;8:29–40.
[358] Hosseini V, Checkel MD. Effect of reformer gas on HCCI combustion-Part I: High Octane Fuels. SAE Technical Paper; 2007.
[359] Hosseini V, Checkel MD. Effect of Reformer Gas on HCCI Combustion - Part II: Low Octane Fuels. SAE International; 2007.
[360] Hosseini V, Checkel MD. Using reformer gas to enhance HCCI combustion of CNG in a CFR engine. SAE Technical Paper; 2006.
[361] Hosseini V, Checkel MD. Reformer gas composition effect on HCCI combustion of n-heptane, iso-octane, and natural gas. SAE Technical Paper; 2008.
[362] Hosseini V, Checkel MD. Alternate Modes Combustion Study: HCCI Fueled with Heptane and Spark Ignition Fueled with Reformer Gas. Internal Combustion Engine Division Fall Technical Conference2005. p. 253-64.
[363] Neshat E, Saray RK, Parsa S. Numerical analysis of the effects of reformer gas on supercharged n-heptane HCCI combustion. Fuel 2017;200:488–98.
[364] Guo H, Hosseini V, Neill WS, Chippior WL, Dumitrescu CE. An experimental study on the effect of hydrogen enrichment on diesel fueled HCCI combustion. international journal of hydrogen energy 2011;36:13820–30.
[365] Guo H, Neill WS. The effect of hydrogen addition on combustion and emission characteristics of an n-heptane fuelled HCCI engine. International journal of hydrogen energy 2013;38:11429–37.
[366] Kongsereeparp P, Checkel MD. Investigating the effects of reformed fuel blending in a methane-or n-heptane-HCCI engine using a multi-zone model. SAE Technical Paper; 2007.
[367] Kongsereeparp P, Checkel MD. Study of reformer gas effects on n-heptane HCCI combustion using a chemical kinetic mechanism optimized by genetic algorithm. SAE Technical Paper; 2008.
[368] Neshat E, Saray RK, Hosseini V. Effect of reformer gas blending on homogeneous charge compression ignition combustion of primary reference fuels using multi zone model and semi detailed chemical-kinetic mechanism. Applied Energy 2016; 179:463–78.
[369] Neshat E, Saray RK, Hosseini V. Investigation of the effect of reformer gas on PRFs HCCI combustion based on exergy analysis. International Journal of Hydrogen Energy 2016;41:4278–95.
[370] Reyhanian M, Hosseini V. Various effects of reformer gas enrichment on natural-gas, iso-octane and normal-heptane HCCI combustion using artificial inert species method. Energy Conversion and Management 2018;159:7–19.
[371] Hosseini V, Neill WS, Checkel MD. Controlling n-heptane HCCI combustion with partial reforming: experimental results and modeling analysis. Journal of engineering for gas turbines and power. 2009:131.
[372] Voshtani S, Reyhanian M, Ehteram M, Hosseini V. Investigating various effects of reformer gas enrichment on a natural gas-fueled HCCI combustion engine. international journal of hydrogen energy 2014;39:19799–809.
[373] Zheng Z, Liu C, Zhang X. Numerical study of effects of reformed exhaust gas recirculation (REGR) on dimethyl ether HCCI combustion. International Journal of Hydrogen Energy 2014;39:8106–17.
[374] Kozlov V, Titova N, Chechet I. Modeling study of hydrogen or syngas addition on combustion and emission characteristics of HCCI engine operating on iso-octane. Fuel 2018;221:61–71.
[375] Achilles M, Ulfvik J, Tuner M, Johansson B, Ahrenfeldt J, Henriksen U, et al. HCCI Gas Engine: Evaluation of Engine Performance, Efficiency and Emissions-Comparing Producer Gas and Natural Gas. SAE Technical Paper; 2011.
[376] Bhaduri S, Jeanmart H, Contino F. EGR control on operation of a tar tolerant HCCI engine with simulated syngas from biomass. Applied Energy. 2017.
[377] Starik A, Korobov A, Titova N. Combustion improvement in HCCI engine operating on synthesis gas via addition of ozone or excited oxygen molecules to the charge: Modeling study. International Journal of Hydrogen Energy 2017.
[378] Jamsran N, Park H, Lee J, Oh S, Kim C, Lee Y, et al. Influence of syngas composition on combustion and emissions in a homogeneous charge compression ignition engine. Fuel 2021;306:121774.
[379] Liu Z, Karim G. Simulation of combustion processes in gas-fuelled diesel engines. Proceedings of the Institution of Mechanical Engineers, Part A: Journal of Power and Energy 1997;211:159–69.
[380] Paykani A, Kakaee A-H, Rahnama P, Reitz RD. Progress and recent trends in reactivity-controlled compression ignition engines. International Journal of Engine Research 2016;17:481–524.
[381] Paykani A, Garcia A, Shahbakhti M, Rahnama P, Reitz RD. Reactivity controlled compression ignition engine: Pathways towards commercial viability. Applied Energy 2021;282:116174.
[382] Wagemakers A, Leermakers C. Review on the effects of dual-fuel operation, using diesel and gaseous fuels, on emissions and performance. SAE Technical Paper; 2012.
[383] Wei L, Li X, Yang W, Dai Y, Wang C-H. Optimization of operation strategies of a syngas-fueled engine in a distributed gasifier-generator system driven by horticulture waste. Energy Conversion and Management 2020;208:112580.
[384] Singh P, Kumar R, Sharma S, Kumar S. Effect of Engine Parameters on the Performance of Dual-Fuel CI Engines with Producer Gas—A Review. Energy & Fuels 2021;35:16377–402.
[385] Garnier C, Bilcan A, Le Corre O, Rahmouni C. Characterisation of a syngas-diesel fuelled CI engine. SAE Technical Paper; 2005.
[386] Sahoo BB, Sahoo N, Saha UK. Assessment of a syngas-diesel dual fuelled compression ignition engine. Energy Sustainability2010. p. 515-22.
[387] Sahoo B, Saha U, Sahoo N. Effect of load level on the performance of a dual fuel compression ignition engine operating on syngas fuels with varying h2/co content. Journal of engineering for gas turbines and power. 2011:133.
[388] Sahoo BB, Sahoo N, Saha UK. Effect of H2: CO ratio in syngas on the performance of a dual fuel diesel engine operation. Applied Thermal Engineering 2012;49: 139–46.
[389] Sahoo BB, Saha UK, Sahoo N. Theoretical performance limits of a syngas–diesel fueled compression ignition engine from second law analysis. Energy 2011;36: 760–9.
[390] Bika AS, Franklin L, Kittelson D. Cycle efficiency and gaseous emissions from a diesel engine assisted with varying proportions of hydrogen and carbon monoxide (synthesis gas). SAE Technical Paper; 2011.
[391] Sahoo B, Sahoo N, Saha U. Effect of engine parameters and type of gaseous fuel on the performance of dual-fuel gas diesel engines—A critical review. Renewable and Sustainable Energy Reviews 2009;13:1151–84.
[392] Wei L, Geng P. A review on natural gas/diesel dual fuel combustion, emissions and performance. Fuel Processing Technology 2016;142:264–78.
[393] Antunes JG, Mikalsen R, Roskilly A. An experimental study of a direct injection compression ignition hydrogen engine. International journal of hydrogen energy 2009;34:6516–22.
[394] Boretti A. Advantages of the direct injection of both diesel and hydrogen in dual fuel H2ICE. international journal of hydrogen energy 2011;36:9312–7.
[395] Tomita E, Fukatani N, Kawahara N, Maruyama K, Komoda T. Combustion in a supercharged biomass gas engine with micro-pilot ignition-Effects of injection pressure and amount of diesel fuel. Journal of KONES 2007;14:513–20.
[396] Roy MM, Tomita E, Kawahara N, Harada Y, Sakane A. Effect of fuel injection parameters on engine performance and emissions of a supercharged producer gas-diesel dual fuel engine. SAE Technical Paper; 2009.
[397] Roy MM, Tomita E, Kawahara N, Harada Y. Sakane A. Performance and emission comparison of a supercharged dual-fuel engine fueled by producer gases with varying hydrogen content. International Journal of Hydrogen Energy 2009;34: 7811–22.
[398] Roy MM, Tomita E, Kawahara N, Harada Y, Sakane A. Performance and emissions of a supercharged dual-fuel engine fueled by hydrogen-rich coke oven gas. International journal of hydrogen energy 2009;34:9628–38.
[399] Roy MM, Tomita E, Kawahara N, Harada Y, Sakane A. An experimental investigation on engine performance and emissions of a supercharged H2-diesel dual-fuel engine. International Journal of Hydrogen Energy 2010;35:844–53.
[400] Roy MM, Tomita E, Kawahara N, Harada Y. Sakane A. Comparison of performance and emissions of a supercharged dual-fuel engine fueled by hydrogen and hydrogen-containing gaseous fuels. International Journal of Hydrogen Energy 2011;36:7339–52.
[401] Azimov U, Tomita E, Kawahara N, Harada Y. Effect of syngas composition on combustion and exhaust emission characteristics in a pilot-ignited dual-fuel engine operated in PREMIER combustion mode. international journal of hydrogen energy 2011;36:11985–96.
[402] Azimov U, Okuno M, Tsuboi K, Kawahara N, Tomita E. Multidimensional CFD simulation of syngas combustion in a micro-pilot-ignited dual-fuel engine using a constructed chemical kinetics mechanism. international journal of hydrogen energy 2011;36:13793–807.
[403] Azimov U, Tomita E, Kawahara N, Harada Y. Premixed mixture ignition in the end-gas region (PREMIER) combustion in a natural gas dual-fuel engine:

operating range and exhaust emissions. International Journal of Engine Research 2011;12:484–97.
[404] Spaeth CT. Performance characteristics of a diesel fuel piloted syngas compression ignition engine: Queen's University (Canada); 2012.
[405] Ramadhas A, Jayaraj S, Muraleedharan C. Power generation using coir-pith and wood derived producer gas in diesel engines. Fuel processing technology 2006;87:849–53.
[406] Singh R, Singh S, Pathak B. Investigations on operation of CI engine using producer gas and rice bran oil in mixed fuel mode. Renewable Energy 2007;32:1565–80.
[407] Ramadhas A, Jayaraj S, Muraleedharan C. Dual fuel mode operation in diesel engines using renewable fuels: Rubber seed oil and coir-pith producer gas. Renewable Energy 2008;33:2077–83.
[408] Das D, Dash S, Ghosal M. Performance evaluation of a diesel engine by using producer gas from some under-utilized biomass on dual-fuel mode of diesel cum producer gas. Journal of Central South University 2012;19:1583–9.
[409] Dhole A, Yarasu R, Lata D, Priyam A. Effect on performance and emissions of a dual fuel diesel engine using hydrogen and producer gas as secondary fuels. International Journal of Hydrogen Energy 2014;39:8087–97.
[410] Dhole A, Yarasu R, Lata D. Investigations on the combustion duration and ignition delay period of a dual fuel diesel engine with hydrogen and producer gas as secondary fuels. Applied Thermal Engineering 2016;107:524–32.
[411] Dhole A, Lata D, Yarasu R. Effect of hydrogen and producer gas as secondary fuels on combustion parameters of a dual fuel diesel engine. Applied Thermal Engineering 2016;108:764–73.
[412] Lata D, Misra A, Medhekar S. Effect of hydrogen and LPG addition on the efficiency and emissions of a dual fuel diesel engine. International Journal of Hydrogen Energy 2012;37:6084–96.
[413] Kokjohn SL, Hanson RM, Splitter D, Reitz R. Fuel reactivity controlled compression ignition (RCCI): a pathway to controlled high-efficiency clean combustion. International Journal of Engine Research 2011;12:209–26.
[414] Reitz RD, Duraisamy G. Review of high efficiency and clean reactivity controlled compression ignition (RCCI) combustion in internal combustion engines. Progress in Energy and Combustion Science 2015;46:12–71.
[415] Mohammadian A, Chehrmonavari H, Kakaee A, Paykani A. Effect of injection strategies on a single-fuel RCCI combustion fueled with isobutanol/isobutanol + DTBP blends. Fuel 2020;278:118219.
[416] Chuahy FD, Kokjohn SL. Effects of reformed fuel composition in "single" fuel reactivity controlled compression ignition combustion. Applied Energy 2017;208:1–11.
[417] Chuahy FD, Kokjohn SL. High efficiency dual-fuel combustion through thermochemical recovery and diesel reforming. Applied Energy 2017;195:503–22.
[418] Rahnama P, Paykani A, Bordbar V, Reitz RD. A numerical study of the effects of reformer gas composition on the combustion and emission characteristics of a natural gas/diesel RCCI engine enriched with reformer gas. Fuel 2017;209:742–53.
[419] Xu Z, Jia M, Li Y, Chang Y, Xu G, Xu L, et al. Computational optimization of fuel supply, syngas composition, and intake conditions for a syngas/diesel RCCI engine. Fuel 2018;234:120–34.
[420] Xu Z, Jia M, Xu G, Li Y, Zhao L, Xu L, et al. Potential for reducing emissions in reactivity-controlled compression ignition engines by fueling syngas and diesel. Energy & Fuels 2018;32:3869–82.
[421] Hariharan D, Boldaji MR, Yan Z, Mamalis S, Lawler B. Single-fuel reactivity controlled compression ignition through catalytic partial oxidation reformation of diesel fuel. Fuel 2020;264:116815.
[422] Kousheshi N, Yari M, Paykani A, Saberi Mehr A, de la Fuente GF. Effect of Syngas Composition on the Combustion and Emissions Characteristics of a Syngas/Diesel RCCI Engine. Energies 2020;13:212.
[423] Jafari B, Seddiq M, Mirsalim SM. Impacts of diesel injection timing and syngas fuel composition in a heavy-duty RCCI engine. Energy Conversion and Management 2021;247:114759.
[424] Olanrewaju FO, Li H, Aslam Z, Hammerton J, Lovett JC. Analysis of the effect of syngas substitution of diesel on the Heat Release Rate and combustion behaviour of Diesel-Syngas dual fuel engine. Fuel 2022;312:122842.
[425] Zhong S, Xu S, Bai X-S, Peng Z, Zhang F. Large eddy simulation of n-heptane/syngas pilot ignition spray combustion: ignition process, liftoff evolution and pollutant emissions. Energy 2021:121080.
[426] Chuahy FDF, Kokjohn S. System and Second Law Analysis of the Effects of Reformed Fuel Composition in "Single" Fuel RCCI Combustion. SAE International Journal of Engines 2018;11:861–78.
[427] Hwang JT, Kane SP, Northrop WF. Demonstration of Single-Fuel Reactivity Controlled Compression Ignition Using Reformed Exhaust Gas Recirculation. SAE Technical Paper; 2018.
[428] Agarwal D, Kumar L, Agarwal AK. Performance evaluation of a vegetable oil fuelled compression ignition engine. Renewable energy 2008;33:1147–56.
[429] Banapurmath N, Tewari P, Hosmath R. Experimental investigations of a four-stroke single cylinder direct injection diesel engine operated on dual fuel mode with producer gas as inducted fuel and Honge oil and its methyl ester (HOME) as injected fuels. Renewable Energy 2008;33:2007–18.
[430] Banapurmath N, Tewari P. Comparative performance studies of a 4-stroke CI engine operated on dual fuel mode with producer gas and Honge oil and its methyl ester (HOME) with and without carburetor. Renewable Energy 2009;34:1009–15.
[431] Banapurmath N, Tewari P, Yaliwal V, Kambalimath S, Basavarajappa Y. Combustion characteristics of a 4-stroke CI engine operated on Honge oil, Neem and Rice Bran oils when directly injected and dual fuelled with producer gas induction. Renewable energy 2009;34:1877–84.
[432] Banapurmath N, Yaliwal V, Hosmath R, Tewari P. Life improvement programme of producer gas–biodiesel operated dual fuel engines. International Journal of Sustainable Engineering 2012;5:350–6.
[433] Yaliwal V, Banapurmath N, Tewari P, Adaganti S. Fuel efficiency improvement of a dual-fuel engine fuelled with Honge oil methyl ester (HOME)–bioethanol and producer gas. International Journal of Sustainable Engineering 2014;7:269–82.
[434] Yaliwal V, Nataraja K, Banapurmath N, Tewari P. Honge oil methyl ester and producer gas-fuelled dual-fuel engine operated with varying compression ratios. International Journal of Sustainable Engineering 2014;7:330–40.
[435] Yaliwal V, Banapurmath N, Tewari P. Performance, combustion and emission characteristics of a single-cylinder, four-stroke, direct injection diesel engine operated on a dual-fuel mode using Honge oil methyl ester and producer gas derived from biomass feedstock of different origin. International Journal of Sustainable Engineering 2014;7:253–68.
[436] Yaliwal V, Banapurmath N, Gireesh N, Hosmath R, Donateo T, Tewari P. Effect of nozzle and combustion chamber geometry on the performance of a diesel engine operated on dual fuel mode using renewable fuels. Renewable Energy 2016;93:483–501.
[437] Yaliwal V, Banapurmath N, Hosmath R, Khandal S, Budzianowski WM. Utilization of hydrogen in low calorific value producer gas derived from municipal solid waste and biodiesel for diesel engine power generation application. Renewable Energy 2016;99:1253–61.
[438] Yaliwal V, Banapurmath N, Gaitonde V, Malipatil M. Simultaneous optimization of multiple operating engine parameters of a biodiesel-producer gas operated compression ignition (CI) engine coupled with hydrogen using response surface methodology. Renewable Energy 2019;139:944–59.
[439] Banapurmath N, Yaliwal V, Hosmath R, Indudhar M, Guluwadi S, Bidari S. Dual fuel engines fueled with three gaseous and biodiesel fuel combinations. Biofuels 2018;9:75–87.
[440] Carlucci A, Ficarella A, Laforgia D. Potentialities of a common rail injection system for the control of dual fuel biodiesel-producer gas combustion and emissions. Journal of Energy Engineering 2014;140:A4014011.
[441] Carlucci A, Colangelo G, Ficarella A, Laforgia D, Strafella L. Improvements in dual-fuel biodiesel-producer gas combustion at low loads through pilot injection splitting. Journal of Energy Engineering 2015;141:C4014006.
[442] Carlucci A, Ficarella A, Laforgia D, Strafella L. Improvement of dual-fuel biodiesel-producer gas engine performance acting on biodiesel injection parameters and strategy. Fuel 2017;209:754–68.
[443] Kan X, Wei L, Li X, Li H, Zhou D, Yang W, et al. Effects of the three dual-fuel strategies on performance and emissions of a biodiesel engine. Applied Energy 2020;262:114542.
[444] Christodoulou F, Megaritis A. The effect of reformer gas mixture on the performance and emissions of an HSDI diesel engine. international journal of hydrogen energy 2014;39:9798–808.
[445] Rinaldini CA, Allesina G, Pedrazzi S, Mattarelli E, Savioli T, Morselli N, et al. Experimental investigation on a Common Rail Diesel engine partially fuelled by syngas. Energy Conversion and Management 2017;138:526–37.
[446] Balakrishnan N, Mayilsamy K. Effect of compression ratio on compression ignition engine performance with biodiesel and producer gas in mixed fuel mode. Journal of Renewable and Sustainable Energy 2014;6:023103.
[447] Balakrishnan N, Mayilsamy K, Nedunchezhian N. An Investigation of the Performance, Combustion, and Emission Characteristics of a CI Engine Fueled with Used Vegetable Oil Methyl Ester and Producer Gas. International Journal of Green Energy 2015;12:506–14.
[448] Yaliwal VS, Banapurmath NR, Gaddigoudar P, Patil ND, Harari PA. Performance and emission characteristics of a diesel engine operated on diverse modes using renewable and sustainable fuels derived from dairy scum and municipal solid waste. In: Materials Today: Proceedings; 2021.
[449] Costa M, La Villetta M, Massarotti N, Piazzullo D, Rocco V. Numerical analysis of a compression ignition engine powered in the dual-fuel mode with syngas and biodiesel. Energy. 2017.
[450] Krishnamoorthi M, Sreedhara S, Duvvuri PP. Experimental, numerical and exergy analyses of a dual fuel combustion engine fuelled with syngas and biodiesel/diesel blends. Applied Energy 2020;263:114643.
[451] Chan WP, Yusoff SAMB, Veksha A, Giannis A, Lim T-T, Lisak G. Analytical assessment of tar generated during gasification of municipal solid waste: Distribution of GC–MS detectable tar compounds, undetectable tar residues and inorganic impurities. Fuel 2020;268:117348.
[452] Woolcock PJ, Brown RC. A review of cleaning technologies for biomass-derived syngas. Biomass and bioenergy 2013;52:54–84.
[453] Sikarwar VS, Zhao M, Fennell PS, Shah N, Anthony EJ. Progress in biofuel production from gasification. Progress in Energy and Combustion Science 2017;61:189–248.
[454] Abdoulmoumine N, Adhikari S, Kulkarni A, Chattanathan S. A review on biomass gasification syngas cleanup. Applied Energy. 2015;155:294–307.
[455] Mendiburu AZ, Roberts JJ, Carvalho Jr JA, Silveira JL. Thermodynamic analysis and comparison of downdraft gasifiers integrated with gas turbine, spark and compression ignition engines for distributed power generation. Applied Thermal Engineering 2014;66:290–7.
[456] Andriatoavina DAS, Fakra DAH, Razafindralambo NAMN, Praene JP, Andriamampianina JMM. Potential of fueling spark-ignition engines with syngas or syngas blends for power generation in rural electrification: A short review and S.W.O.T. analysis. Sustainable Energy Technologies and Assessments 2021;47:101510.

[457] Hagos FY, Aziz ARA, Sulaiman SA. Investigation of deposit formation in direct-injection spark-ignition engine powered on syngas. International Journal of Automotive Technology 2015;16:479–85.
[458] Ahrenfeldt J, Henriksen U, Schramm J, Jensen TK, Egsgaard H. Combustion chamber deposits and PAH formation in SI engines fueled by producer gas from biomass gasification. SAE Technical Paper; 2003.
[459] Yang P, Columbus E, Wooten J, Batchelor W, Buchireddy P, Ye X, et al. Evaluation of syngas storage under different pressures and temperatures. Applied Engineering in Agriculture 2009;25:121–8.
[460] Posada F, Bedick C, Clark N, Kozlov A, Linck M, Boulanov D, et al. Low Temperature Combustion with Thermo-Chemical Recuperation. SAE Technical Paper; 2007.
[461] Chakravarthy VK, Daw CS, Pihl JA, Conklin JC. Study of the theoretical potential of thermochemical exhaust heat recuperation for internal combustion engines. Energy & Fuels 2010;24:1529–37.
[462] Tartakovsky L, Baibikov V, Gutman M, Poran A, Veinblat M. Thermo-Chemical Recuperation as an Efficient Way of Engine's Waste Heat Recovery. Applied Mechanics and Materials: Trans Tech Publ; 2014:256–61.
[463] Saidur R, Rezaei M, Muzammil WK, Hassan M, Paria S, Hasanuzzaman M. Technologies to recover exhaust heat from internal combustion engines. Renewable and sustainable energy reviews 2012;16:5649–59.
[464] Isherwood KD, Linna J-R, Loftus PJ. Using on-board fuel reforming by partial oxidation to improve SI engine cold-start performance and emissions. SAE transactions 1998:411–9.
[465] Kirwan JE, Quader AA, Grieve MJ. Fast start-up on-board gasoline reformer for near zero emissions in spark-ignition engines. SAE Transactions 2002:1722–33.
[466] LQd Almeida, Sales LCM, Sodré JR. Fuel consumption and emissions from a vehicle operating with ethanol, gasoline and hydrogen produced on-board. International Journal of Hydrogen Energy 2015;40:6988–94.
[467] Horng R-F, Chang Y-P, Wu S-C. Investigation on the production of hydrogen rich gas in a plasma converter for motorcycle applications. Energy Conversion and Management 2006;47:2155–66.
[468] Chao Y, Lee H-M, Chen S-H, Chang M-B. Onboard motorcycle plasma-assisted catalysis system – Role of plasma and operating strategy. International Journal of Hydrogen Energy 2009;34:6271–9.
[469] Bromberg L, Crane S, Rabinovich A, Kong Y, Cohn D, Heywood J. Hydrogen generation from plasmatron reformers: A promising technology for Nox adsorber regeneration and other automotive applications. MIT PSFC (US); ArvinMeritor. MIT Mech. Eng. Department; Baikov Inst 2003.
[470] Bromberg L, Cohn D, Rabinovich A, Heywood J. Emissions reductions using hydrogen from plasmatron fuel converters. International Journal of Hydrogen Energy 2001;26:1115–21.
[471] Cohn D, Rabinovich A, Titus C, Bromberg L. Near-term possibilities for extremely low emission vehicles using onboard plasmatron generation of hydrogen. International Journal of Hydrogen Energy 1997;22:715–23.
[472] Rabinovich A, Cohn DR, Bromberg L. Plasmatron internal combustion engine system for vehicle pollution reduction. International Journal of Vehicle Design 1994;15:234–42.
[473] Gallagher Jr MJ, Fridman A. Plasma reforming for H2-rich synthesis gas. Fuel cells: Technologies for fuel processing. Elsevier; 2011. p. 223–59.
[474] Rabinovich A, Bromberg L, Cohn D, Surma J, Virden J. Onboard plasmatron reforming of biofuels, gasoline and diesel fuel. SAE Technical Paper; 1998.
[475] Bromberg L, Cohn D, Rabinovich A, O'brie C, Hochgreb S. Plasma reforming of methane. Energy & fuels 1998;12:11–8.
[476] Green Jr J, Domingo N, Storey J, Wagner R, Armfield J, Bromberg L, et al. Experimental evaluation of SI engine operation supplemented by hydrogen rich gas from a compact plasma boosted reformer. SAE transactions 2000:1875–82.
[477] Virden JW, Surma JE, Bromberg L, Rabinovich A, Cohn D, Armfield J. A Feasibility Evaluation of a Thermal Plasma Fuel Reformer for Supplemental Hydrogen Addition to Internal Combustion Engines. SAE Technical Paper; 1999.
[478] Chen F, Huang X, Cheng D-g, Zhan X. Hydrogen production from alcohols and ethers via cold plasma: A review. International journal of hydrogen energy 2014;39:9036–46.
[479] Bromberg L, Hadidi K, Cohn DR. Plasmatron reformation of renewable fuels. 2005.
[480] Starikovskiy A, Aleksandrov N. Plasma-assisted ignition and combustion. Progress in Energy and Combustion Science 2013;39:61–110.
[481] Ju Y, Sun W. Plasma assisted combustion: Dynamics and chemistry. Progress in Energy and Combustion Science 2015;48:21–83.
[482] Tully EJ, Heywood JB. Lean-Burn Characteristics of a Gasoline Engine Enriched with Hydrogen from a Plasmatron Fuel Reformer. SAE Transactions 2003;112:851–64.
[483] Ivanič Ž, Ayala F, Goldwitz J, Heywood JB. Effects of Hydrogen Enhancement on Efficiency and NOx Emissions of Lean and EGR-Diluted Mixtures in a SI Engine. SAE Transactions 2005;114:138–49.
[484] Leung P, Tsolakis A, Rodríguez-Fernández J, Golunski S. Raising the fuel heating value and recovering exhaust heat by on-board oxidative reforming of bioethanol. Energy & Environmental Science 2010;3:780–8.
[485] Ashida K, Maeda H, Araki T, Hoshino M, Hiraya K, Izumi T, et al. Study of an on-board fuel reformer and hydrogen-added EGR combustion in a gasoline engine. SAE International Journal of Fuels and Lubricants 2015;8:358–66.
[486] Chang Y, Szybist JP, Pihl JA, Brookshear DW. Catalytic exhaust gas recirculation-loop reforming for high efficiency in a stoichiometric spark-ignited engine through thermochemical recuperation and dilution limit extension, part 2: engine performance. Energy & Fuels 2018;32:2257–66.
[487] Hwang JT, Kane SP, Northrop WF. Hydrous Ethanol Steam Reforming and Thermochemical Recuperation to Improve Dual-Fuel Diesel Engine Emissions and Efficiency. Journal of Energy Resources Technology 2019:141.
[488] Sall ED, Morgenstern DA, Fornango JP, Taylor JW, Chomic N, Wheeler J. Reforming of ethanol with exhaust heat at automotive scale. Energy & fuels 2013;27:5579–88.
[489] Jamal Y, Wagner T, Wyszynski M. Exhaust gas reforming of gasoline at moderate temperatures. International Journal of Hydrogen Energy 1996;21:507–19.
[490] Gomes SR, Bion N, Blanchard G, Rousseau S, Bellière-Baca V, Harlé V, et al. Thermodynamic and experimental studies of catalytic reforming of exhaust gas recirculation in gasoline engines. Applied Catalysis B: Environmental 2011;102:44–53.
[491] Gomes SR, Bion N, Blanchard G, Rousseau S, Duprez D, Epron F. Study of the main reactions involved in reforming of exhaust gas recirculation (REGR) in gasoline engines. RSC advances 2011;1:109–16.
[492] Fennell D, Herreros Arellano JM, Tsolakis A, Wyszynski M, Cockle K, Pignon J, et al. On-board thermochemical energy recovery technology for low carbon clean gasoline direct injection engine powered vehicles. Proceedings of the Institution of Mechanical Engineers, Part D: Journal of Automobile Engineering 2018;232:1079–91.
[493] Edwards N, Ellis SR, Frost JC, Golunski SE, van Keulen AN, Lindewald NG, et al. On-board hydrogen generation for transport applications: the HotSpot™ methanol processor. Journal of power sources 1998;71:123–8.
[494] Wang W. The effect of internal air bleed on CO poisoning in a proton exchange membrane fuel cell. Journal of Power Sources 2009;191:400–6.
[495] Tsolakis A, Megaritis A, Wyszynski M. Application of exhaust gas fuel reforming in compression ignition engines fueled by diesel and biodiesel fuel mixtures. Energy & fuels 2003;17:1464–73.
[496] Tsolakis A, Megaritis A, Wyszynski M. Low temperature exhaust gas fuel reforming of diesel fuel. Fuel 2004;83:1837–45.
[497] Tsolakis A, Megaritis A. Catalytic exhaust gas fuel reforming for diesel engines—effects of water addition on hydrogen production and fuel conversion efficiency. International Journal of Hydrogen Energy 2004;29:1409–19.
[498] Tsolakis A, Megaritis A, Yap D, Abu-Jrai A. Combustion characteristics and exhaust gas emissions of a diesel engine supplied with reformed EGR. SAE Technical Paper; 2005.
[499] Tsolakis A, Torbati R, Megaritis A, Abu-Jrai A. Low-load dual-fuel compression ignition (CI) engine operation with an on-board reformer and a diesel oxidation catalyst: effects on engine performance and emissions. Energy & fuels 2010;24:302–8.
[500] Megaritis A, Tsolakis A, Wyszynski M, Golunski S. Advanced direct injection combustion engine technologies and development. Fuel reforming for diesel engines. Elsevier; 2010. p. 543–61.
[501] Lau C, Allen D, Tsolakis A, Golunski SE, Wyszynski M. Biogas upgrade to syngas through thermochemical recovery using exhaust gas reforming. Biomass and bioenergy 2012;40:86–95.
[502] Abu-Jrai A, Tsolakis A, Theinnoi K, Megaritis A, Golunski SE. Diesel exhaust-gas reforming for H2 addition to an aftertreatment unit. Chemical Engineering Journal 2008;141:290–7.
[503] Tsolakis A, Megaritis A, Yap D. Application of exhaust gas fuel reforming in diesel and homogeneous charge compression ignition (HCCI) engines fuelled with biofuels. Energy 2008;33:462–70.
[504] Tsolakis A, Megaritis A. Partially premixed charge compression ignition engine with on-board H2 production by exhaust gas fuel reforming of diesel and biodiesel. International Journal of Hydrogen Energy 2005;30:731–45.
[505] Fennell D, Herreros JM, Tsolakis A, Xu H, Cockle K, Millington P. GDI engine performance and emissions with reformed exhaust gas recirculation (REGR). SAE Technical Paper; 2013.
[506] Fennell D, Herreros J, Tsolakis A. Improving gasoline direct injection (GDI) engine efficiency and emissions with hydrogen from exhaust gas fuel reforming. International journal of hydrogen energy 2014;39:5153–62.
[507] Fennell D, Herreros J, Tsolakis A, Cockle K, Pignon J, Millington P. Thermochemical recovery technology for improved modern engine fuel economy–part 1: analysis of a prototype exhaust gas fuel reformer. RSC Advances 2015;5:35252–61.
[508] Bogarra M, Herreros JM, Tsolakis A, York A, Millington P. Study of particulate matter and gaseous emissions in gasoline direct injection engine using on-board exhaust gas fuel reforming. Applied Energy 2016;180:245–55.
[509] Bogarra M, Herreros JM, Tsolakis A, York A, Millington P, Martos F. Impact of exhaust gas fuel reforming and exhaust gas recirculation on particulate matter morphology in gasoline direct injection engine. Journal of Aerosol Science 2017;103:1–14.
[510] Bogarra M, Herreros J, Tsolakis A, York A, Millington P, Martos F. Influence of on-board produced hydrogen and three way catalyst on soot nanostructure in Gasoline Direct Injection engines. Carbon 2017;120:326–36.
[511] Chang Y, Szybist JP, Pihl JA, Brookshear DW. Catalytic Exhaust Gas Recirculation-Loop Reforming for High Efficiency in a Stoichiometric Spark-Ignited Engine through Thermochemical Recuperation and Dilution Limit Extension, Part 1: Catalyst Performance. Energy & Fuels 2018;32:2245–56.
[512] Sengodan S, Lan R, Humphreys J, Du D, Xu W, Wang H, et al. Advances in reforming and partial oxidation of hydrocarbons for hydrogen production and fuel cell applications. Renewable and Sustainable Energy Reviews 2018;82:761–80.
[513] Ashida K, Hoshino M, Maeda H, Araki T, Hiraya K, Yasuoka M. Study of Reformate Hydrogen-Added Combustion in a Gasoline Engine. SAE Technical Paper; 2015.

[514] Hoshino M, Izumi T, Akama H, Zaima M, Hiraya K, Ashida K, et al. Development of an On-Board Fuel Reforming Catalyst for a Gasoline Engine. SAE Technical Paper; 2015.
[515] Brookshear DW, Pihl JA, Szybist JP. Catalytic Steam and Partial Oxidation Reforming of liquid fuels for application in improving the efficiency of internal combustion engines. Energy & Fuels 2018;32:2267–81.
[516] Hwang J, Li X, Northrop W. Exploration of Dual Fuel Diesel Engine Operation with On-Board Fuel Reforming. SAE Technical Paper; 2017.
[517] Tsolakis A, Abu-Jrai A, Theinnoi K, Wyszynski M, Xu H, Megaritis A, et al. Exhaust gas fuel reforming for IC Engines using diesel type fuels. SAE Transactions 2007:720–5.
[518] Ali K, Kim C, Lee Y, Oh S, Kim K. A Numerical Study to Control the Combustion Performance of a Syngas-Fueled HCCI Engine at Medium and High Loads Using Different Piston Bowl Geometry and Exhaust Gas Recirculation. Journal of Energy Resources Technology 2020:143.
[519] Tsolakis A, Megaritis A, Golunski S. Reaction profiles during exhaust-assisted reforming of diesel engine fuels. Energy & fuels 2005;19:744–52.
[520] Lau C, Tsolakis A, Wyszynski M. Biogas upgrade to syn-gas (H2–CO) via dry and oxidative reforming. International Journal of Hydrogen Energy 2011;36:397–404.
[521] Hamedi M, Tsolakis A, Lau C. Biogas upgrading for on-board hydrogen production: reforming process CFD modelling. International Journal of Hydrogen Energy 2014;39:12532–40.
[522] Wheeler JC, Stein RA, Morgenstern DA, Sall ED, Taylor JW. Low-temperature ethanol reforming: a multi-cylinder engine demonstration. SAE Technical Paper; 2011.
[523] Fowler J, Morgenstern D, Sall E, Veinbergs ME. Integration of an E85 reforming system into a vehicle-ready package and project results. SAE Technical Paper; 2014.
[524] Ji C, Dai X, Ju B, Wang S, Zhang B, Liang C, et al. Improving the performance of a spark-ignited gasoline engine with the addition of syngas produced by onboard ethanol steaming reforming. International Journal of Hydrogen Energy 2012;37:7860–8.
[525] Casanovas A, Divins NJ, Rejas A, Bosch R, Llorca J. Finding a suitable catalyst for on-board ethanol reforming using exhaust heat from an internal combustion engine. International Journal of Hydrogen Energy 2017;42:13681–90.
[526] Herreros J, Gill S, Lefort I, Tsolakis A, Millington P, Moss E. Enhancing the low temperature oxidation performance over a Pt and a Pt–Pd diesel oxidation catalyst. Applied Catalysis B: Environmental 2014;147:835–41.
[527] Sittichompoo S, Nozari H, Herreros J, Serhan N, da Silva J, York A, et al. Exhaust energy recovery via catalytic ammonia decomposition to hydrogen for low carbon clean vehicles. Fuel 2021;285:119111.
[528] Al-Harbi AA, Alabduly AJ, Alkhedhair AM, Alqahtani NB, Albishi MS. Effect of operation under lean conditions on NOx emissions and fuel consumption fueling an SI engine with hydrous ethanol–gasoline blends enhanced with synthesis gas. Energy 2022;238:121694.
[529] Li G, Zhang Z, You F, Pan Z, Zhang X, Dong J, et al. A novel strategy for hydrous-ethanol utilization: Demonstration of a spark-ignition engine fueled with hydrogen-rich fuel from an onboard ethanol/steam reformer. International journal of hydrogen energy 2013;38:5936–48.
[530] Poran A, Artoul M, Sheintuch M, Tartakovsky L. Modeling internal combustion engine with thermo-chemical recuperation of the waste heat by methanol steam reforming. SAE International Journal of Engines 2014;7:234–42.
[531] Tartakovsky L, Amiel R, Baibikov V, Fleischman R, Gutman M, Poran A, et al. SI Engine with Direct Injection of Methanol Reforming Products - First Experimental Results. Society of Automotive Engineers of Japan; 2015.
[532] Poran A, Tartakovsky L. Energy efficiency of a direct-injection internal combustion engine with high-pressure methanol steam reforming. Energy 2015;88:506–14.
[533] Poran A, Tartakovsky L. Performance and emissions of a direct injection internal combustion engine devised for joint operation with a high-pressure thermochemical recuperation system. Energy 2017;124:214–26.
[534] Poran A, Tartakovsky L. Influence of methanol reformate injection strategy on performance, available exhaust gas enthalpy and emissions of a direct-injection spark ignition engine. International Journal of Hydrogen Energy 2017;42:15652–68.
[535] Poran A, Thawko A, Eyal A, Tartakovsky L. Direct injection internal combustion engine with high-pressure thermochemical recuperation–Experimental study of the first prototype. International Journal of Hydrogen Energy 2018;43:11969–80.
[536] Liao C-H, Horng R-F. Investigation on the hydrogen production by methanol steam reforming with engine exhaust heat recovery strategy. International Journal of Hydrogen Energy 2016;41:4957–68.
[537] Nguyen D-K, Sileghem L, Verhelst S. Exploring the potential of reformed-exhaust gas recirculation (R-EGR) for increased efficiency of methanol fueled SI engines. Fuel 2019;236:778–91.
[538] Zamfirescu C, Dincer I. Ammonia as a green fuel and hydrogen source for vehicular applications. Fuel processing technology 2009;90:729–37.
[539] Zamfirescu C, Dincer I. Utilization of hydrogen produced from urea on board to improve performance of vehicles. International journal of hydrogen energy 2011;36:11425–32.
[540] Yin S, Xu B, Zhou X, Au C. A mini-review on ammonia decomposition catalysts for on-site generation of hydrogen for fuel cell applications. Applied Catalysis A: General 2004;277:1–9.
[541] Wang W, Herreros JM, Tsolakis A, York AP. Ammonia as hydrogen carrier for transportation; investigation of the ammonia exhaust gas fuel reforming. International journal of hydrogen energy 2013;38:9907–17.
[542] Sittichompoo S, Nozari H, Herreros JM, Serhan N, da Silva JAM, York APE, et al. Exhaust energy recovery via catalytic ammonia decomposition to hydrogen for low carbon clean vehicles. Fuel 2021;285:119111.
[543] Willand J, Nieberding R-G, Vent G, Enderle C. The knocking syndrome-its cure and its potential. SAE transactions 1998:1122–9.
[544] Wolk B, Ekoto I, Northrop WF, Moshammer K, Hansen N. Detailed speciation and reactivity characterization of fuel-specific in-cylinder reforming products and the associated impact on engine performance. Fuel 2016;185:348–61.
[545] Urushihara T, Hiraya K, Kakuhou A, Itoh T. Expansion of HCCI operating region by the combination of direct fuel injection, negative valve overlap and internal fuel reformation. SAE transactions 2003:1092–100.
[546] Koopmans L, Ogink R, Denbratt I. Direct Gasoline Injection in the Negative Valve Overlap of a Homogeneous Charge Compression Ignition Engine. SAE International; 2003.
[547] Waldman J, Nitz D, Aroonsrisopon T, Foster DE, Iida M. Experimental investigation into the effects of direct fuel injection during the negative valve overlap period in an gasoline fueled HCCI engine. SAE Technical Paper; 2007.
[548] Aroonsrisopon T, Nitz DG, Waldman JO, Foster DE, Iida M. A computational analysis of direct fuel injection during the negative valve overlap period in an iso-octane fueled HCCI engine. SAE Technical Paper; 2007.
[549] Borgqvist P, Tuner M, Mello A, Tunestal P, Johansson B. The usefulness of negative valve overlap for gasoline partially premixed combustion, PPC. SAE Technical Paper; 2012.
[550] Chang Y, Wooldridge M, Bohac SV. Extending the dilution limit of spark ignition combustion via fuel injection during negative valve overlap. SAE Technical Paper; 2016.
[551] Rodriguez JF, Cheng WK. Potential of Negative Valve Overlap for Part-Load Efficiency Improvement in Gasoline Engines. SAE International Journal of Engines 2018;11:657–68.
[552] Kuzuoka K, Kondo T, Kudo H, Taniguchi H, Chishima H, Hashimoto K. Controlling combustion with negative valve overlap in a gasoline–diesel dual-fuel compression ignition engine. International Journal of Engine Research 2016;17:354–65.
[553] Mikulski M, Balakrishnan PR, Hunicz J. Natural gas-diesel reactivity controlled compression ignition with negative valve overlap and in-cylinder fuel reforming. Applied Energy 2019;254:113638.
[554] Song H, Edwards C. Understanding chemical effects in low-load-limit extension of homogeneous charge compression ignition engines via recompression reaction. International Journal of Engine Research 2009;10:231–50.
[555] Szybist JP, Steeper RR, Splitter D, Kalaskar VB, Pihl J, Daw C. Negative valve overlap reforming chemistry in low-oxygen environments. SAE International Journal of Engines 2014;7:418–33.
[556] Fitzgerald RP, Steeper R, Snyder J, Hanson R, Hessel R. Determination of cycle temperatures and residual gas fraction for HCCI negative valve overlap operation. SAE International Journal of Engines 2010;3:124–41.
[557] Fitzgerald RP, Steeper R. Thermal and chemical effects of NVO fuel injection on HCCI combustion. SAE international journal of engines 2010;3:46–64.
[558] Arning J, Ramsander T, Collings N. Analysis of in-cylinder hydrocarbons in a multi-cylinder gasoline HCCI engine using gas chromatography. SAE International Journal of Engines 2010;2:141–9.
[559] Yu W, Xie H, Chen T, Li L, Song K, Zhao H. Effects of active species in residual gas on auto-ignition in a HCCI gasoline engine. SAE Technical Paper; 2012.
[560] Kalaskar VB, Szybist JP, Splitter DA, Pihl JA, Gao Z, Daw CS. In-cylinder reaction chemistry and kinetics during negative valve overlap fuel injection under low-oxygen conditions. In: Internal Combustion Engine Division Fall Technical Conference: American Society of Mechanical Engineers; 2013. V002T02A17.
[561] Steeper RR, Davisson ML. Analysis of gasoline negative-valve-overlap fueling via dump sampling. SAE International Journal of Engines 2014;7:762–71.
[562] Szybist JP, Steeper RR, Splitter D, Kalaskar VB, Pihl J, Daw C. Negative valve overlap reforming chemistry in low-oxygen environments. SAE International Journal of Engines 2014;7:418–33.
[563] Ekoto I, Peterson B, Szybist J, Northrop W. Analysis of Thermal and Chemical Effects on Negative Valve Overlap Period Energy Recovery for Low-Temperature Gasoline Combustion. SAE International Journal of Engines 2015;8:2227–39.
[564] Peterson B, Ekoto I, Northrop W. Investigation of negative valve overlap reforming products using gas sampling and single-zone modeling. SAE International Journal of Engines 2015;8:747–57.
[565] Wolk B, Ekoto I, Northrop W. Investigation of fuel effects on in-cylinder reforming chemistry using gas chromatography. SAE International Journal of Engines 2016;9:964–78.
[566] Ekoto IW, Wolk BM, Northrop WF, Hansen N. Moshammer K. Tailoring charge reactivity using in-cylinder generated reformate for gasoline compression ignition strategies. Journal of Engineering for Gas Turbines and Power 2017:139.
[567] Kane S, Li X, Wolk B, Ekoto I, Northrop WF. Investigation of species from negative valve overlap reforming using a stochastic reactor model. SAE Technical Paper; 2017.
[568] Ekoto I, Wolk B, Northrop W. Energy analysis of low-load low-temperature gasoline combustion with auxiliary-fueled negative valve overlap. SAE International Journal of Engines 2017;10:1238–55.
[569] Meyers D, Kubesh J. The hybrid rich-burn/lean-burn engine. 1997.
[570] Alger T, Mangold B. Dedicated EGR: a new concept in high efficiency engines. SAE international journal of engines 2009;2:620–31.
[571] Chadwell C, Alger T, Zuehl J, Gukelberger R. A demonstration of dedicated EGR on a 2.0 L GDI engine. SAE International Journal of Engines 2014;7:434–47.
[572] Alger T, Mangold B. Dedicated EGR: a new concept in high efficiency engines. SAE international journal of engines 2009;2:620–31.

[573] Zhu L, He Z, Xu Z, Lu X, Fang J, Zhang W, et al. In-cylinder thermochemical fuel reforming (TFR) in a spark-ignition natural gas engine. Proceedings of the Combustion Institute 2017;36:3487–97.
[574] Alger T, Gukelberger R, Gingrich J. Impact of EGR quality on the total inert dilution ratio. SAE International Journal of Engines 2016;9:796–806.
[575] Alger T, Gukelberger R, Gingrich J. Impact of EGR Quality on the Total Inert Dilution Ratio. SAE International Journal of Engines 2016;9:796–806.
[576] Gukelberger R, Gingrich J, Alger T, Almaraz S, Denton B. LPL EGR and D-EGR® engine concept comparison part 1: part load operation. SAE International Journal of Engines 2015;8:570–82.
[577] Gukelberger R, Gingrich J, Alger T, Almaraz S. LPL EGR and D-EGR® Engine Concept Comparison Part 2: High Load Operation. SAE International Journal of Engines 2015;8:547–56.
[578] Gingrich JW, Mehta D, Alger T, Czekala M, Shelby MH. OS1-1 Application of a Dedicated EGR Configuration to a V6 Engine : A novel concept for high efficiency gasoline engines(OS1: Ultimate thermal efficiency,Organized Session Papers). 2012.
[579] Lee S, Ozaki K, Iida N, Sako T. A Potentiality of Dedicated EGR in SI Engines Fueled by Natural Gas for Improving Thermal Efficiency and Reducing NOx Emission. SAE International Journal of Engines 2015;8:238–49.
[580] Alger T, Walls M, Chadwell C, Joo S, Denton B, Kleinow K, et al. The interaction between fuel anti-knock index and reformation ratio in an engine equipped with dedicated EGR. SAE International Journal of Engines 2016;9:786–95.
[581] Gukelberger R, Robertson D, Alger T, Almaraz S, Gingrich J, Mohan V. Alternative Fuel Testing on a Port Fuel Injected LPL EGR and D-EGR® Engine. SAE Technical Paper; 2016.
[582] He Z, Zhu L, Xu Z, Kaario O, Li A, Huang Z. Effects of ethanol enrichment on in-cylinder thermochemical fuel reforming (TFR) spark ignition natural gas engine. Fuel 2017;197:334–42.
[583] Randolph E, Gukelberger R, Alger T, Briggs T, Chadwell C, Bosquez Jr A. Methanol fuel testing on port fuel injected internal-only EGR, HPL-EGR and D-EGR® engine configurations. SAE International Journal of Fuels and Lubricants 2017;10:718–27.
[584] Shao Y, Sun Q, Li A, He Z, Xu Z, Qian Y, et al. Effects of natural gas, ethanol, and methanol enrichment on the performance of in-cylinder thermochemical fuel reforming (TFR) spark-ignition natural gas engine. Applied Thermal Engineering 2019;159:113913.
[585] Zhu L, Li A, Zhang Z, Li B, Ma C, Cheng X, et al. Effects of alcohol enrichment on thermochemical fuel reforming (TFR): Insights from chemical kinetics. International Journal of Hydrogen Energy 2020.
[586] Li B, Sun Q, Li A, Shao Y, He Z, Lu X, et al. Effects of propanol isomers enrichment on in-cylinder thermochemical fuel reforming (TFR) in spark ignition natural gas engine. International Journal of Hydrogen Energy 2020.
[587] He Z, Wang J, Li B, Zhu L, Qian Y, Lu X, et al. Effects of n-heptane enrichment on in-cylinder thermochemical fuel reforming (TFR) characteristics and performances of spark ignition natural gas engine: A comparison with natural gas and methanol enrichment. Fuel 2020;271:117531.
[588] Sun Q, Li B, Li A, Shao Y, He Z, Lu X, et al. Insight into fuel reactivity effects on thermochemical fuel reforming (TFR). International Journal of Hydrogen Energy 2020.
[589] Lee S, Iida N, Sako T. Numerical Investigation of a Potential of Dedicated EGR System for Increasing Thermal Efficiency of SI Engines Fueled with Methane and Propane. SAE Technical Paper; 2015.
[590] Alger T, Gingrich J, Mangold B. The effect of hydrogen enrichment on EGR tolerance in spark ignited engines. SAE Technical Paper; 2007.
[591] Liu C, Wang Z, Song H, Qi Y, Li Y, Li F, et al. Experimental and numerical investigation on H2/CO formation and their effects on combustion characteristics in a natural gas SI engine. Energy 2018;143:597–605.
[592] Liu C, Song H, Zhang P, Wang Z, Wooldridge MS, He X, et al. A rapid compression machine study of autoignition, spark-ignition and flame propagation characteristics of H2/CH4/CO/air mixtures. Combustion and Flame 2018;188:150–61.
[593] Gukelberger R, Bartley GJ, Gingrich J, Alger T, Almaraz S, Buckingham J, et al. Water-Gas-Shift Catalyst Development and Optimization for a D-EGR® Engine. SAE Technical Paper; 2015.
[594] Alger T, Gingrich J, Roberts C, Mangold B, Sellnau M. A high-energy continuous discharge ignition system for dilute engine applications. SAE Technical Paper; 2013.
[595] Denton B, Chadwell C, Gukelberger R, Alger T. Design and Implementation of a D-EGR® Mixer for Improved Dilution and Reformate Distribution. SAE International Journal of Engines 2017;10:892–7.
[596] Kalaskar VB, Gukelberger R, Denton B, Briggs T. The impact of engine operating conditions on reformate production in a D-EGR engine. SAE Technical Paper; 2017.
[597] Sarlashkar J, Rengarajan S, Roecker R. Transient Control of a Dedicated EGR Engine. SAE Technical Paper; 2016.
[598] Rengarajan SB, Sarlashkar J, Roecker R, Anderson G. Estimation of Intake Oxygen Mass Fraction for Transient Control of EGR Engines. SAE Technical Paper; 2018.
[599] Robertson D, Chadwell C, Alger T, Zuehl J, Gukelberger R, Denton B, et al. Dedicated EGR vehicle demonstration. SAE International Journal of Engines 2017;10:898–907.
[600] Reinhart T, Megel M. An Efficient, Durable Vocational Truck Gasoline Engine. SAE International Journal of Engines 2016;9:1437–48.
[601] Jung D, Lee S. An investigation on the potential of dedicated exhaust gas recirculation for improving thermal efficiency of stoichiometric and lean spark ignition engine operation. Applied Energy 2018;228:1754–66.
[602] Wang Y, Shah B, Conway G, Williams DR, Chadwell C. Combustion Stabilization for Enriched D-EGR Applications via Air-Assisted Pre-Chambers. SAE International; 2021.
[603] Takashima Y, Katayama S, Sako T, Furutani M. Activities for high-efficiency small gas engines. Applied Thermal Engineering 2017;114:1372–7.
[604] Johnson T, Joshi A. Review of vehicle engine efficiency and emissions. SAE International Journal of Engines 2018;11:1307–30.
[605] Wang X, Khameneian A, Dice P, Chen B, Shahbakhti M, Naber JD, et al. Model-based combustion duration and ignition timing prediction for combustion phasing control of a spark-ignition engine using in-cylinder pressure sensors. In: International Design Engineering Technical Conferences and Computers and Information in Engineering Conference: American Society of Mechanical Engineers; 2019. V009T12A33.
[606] Khameneian A, Wang X, Dice P, Shahbakhti M, Naber JD, Archer C, et al. Model-Based Dynamic In-Cylinder Air Charge, Residual Gas and Temperature Estimation for a GDI Spark Ignition Engine Using Cylinder, Intake and Exhaust Pressures. In: Dynamic Systems and Control Conference: American Society of Mechanical Engineers; 2020. V002T26A.
[607] Senecal P, Leach F. Diversity in transportation: Why a mix of propulsion technologies is the way forward for the future fleet. Results in Engineering 2019;4:100060.

Dr Amin Paykani is a Senior Lecturer and Climate Mitigation Solutions (CMS) research group co-leader at the Department of Engineering, University of Hertfordshire. He received his PhD in Automotive Engineering from Iran University of Science and Technology. Prior to joining the University of Hertfordshire, he was a postdoctoral researcher at the Swiss Federal Institute of Technology in Zurich (ETH). He is currently the PI of an EPSRC project under the new investigator award scheme to work on high-efficiency low emission ammonia fuelled thermal propulsion systems. He has been recognised as a "Global Talent" by the Royal Academy of Engineering in the field of Transport and Mechanical. His areas of interest include computational modelling and optimisation of combustion-based propulsion systems with the aim of decarbonisation of the transport.

Mr Hamed Chehrmonavari is currently a PhD student at the School of Automotive Engineering, Iran University of Science and Technology (IUST). He was a visiting researcher at the Department of Engineering of University of Hertfordshire. His doctoral work explores the way of increasing the efficiency of internal combustion engines through thermochemical recuperation and integrated systems with high-temperature fuel cells. He holds a master's degree in Automotive engineering from IUST, working on direct dual fuel stratification (DDFS) and reactivity controlled compression ignition (RCCI) combustion regimes. His research interests mainly include clean energy conversion devices, advanced combustion strategies, alternative fuels, and artificial intelligence applications in energy systems.

Prof Athanasios Tsolakis is the Chair in Thermodynamics and Director of Research and Knowledge Transfer for the School of Engineering at University of Birmingham. Thanos obtained BEng in Manufacturing Engineering from Technological Education Institute of Piraeus in Greece in 1999 and BEng in Mechanical Engineering in 2001 from the University of Birmingham in the UK. He obtained his PhD from the University of Birmingham in 2004. From Birmingham, Thanos moved to Johnson Matthey plc, where he was a Research Scientist (2004-2005), and worked at their Technology Centre on R&D projects for their catalytic technologies. In October 2005, he joined the University of Birmingham as a Lecturer 2005- 2010, Senior Lecturer (2010- 2012), Reader of Thermodynamics (2012 – 2016). Thanos has published over 150 research papers in scientific journals and conference proceedings in the areas of fuel reforming, low carbon and carbon free energy carriers, combustion and vehicle emissions control technologies such as environmental catalysts and aftertreatment systems. His research covers both fundamentals and industrial applications and he has received funding awards from Research Councils UK, Innovate UK, Horizon2020 in collaboration with industry.

Dr Terry Alger is the Director of Engine & Vehicle R&D at Southwest Research Institute® (SwRI®). Alger holds doctorate and master's degrees in mechanical engineering from UT Austin, a master's degree in business administration from The University of Texas at San Antonio and a bachelor's degree in mechanical engineering from the United States Military Academy. Alger joined the SwRI staff in 2003 following employment at the Ford Motor Company. Alger specializes in combustion research and optical diagnostics. His current research concerns improving engine efficiency and emissions through in-cylinder combustion processes and advanced engine technologies. He also manages SwRI's HEDGE® II Consortium, which focuses on improving gasoline engine efficiency through the use of cooled EGR, advanced ignition systems and other technologies. Alger is one of the inventors of SwRI's DCO® (Dual Coil Offset) Ignition system and the D-EGR® engine, both winners of R&D 100 Awards. Alger is a Fellow of the Society of Automotive Engineers. He has been selected to receive the Forest R. McFarland Award. He has been awarded 23 patents and published over 50 papers on topics covering engine efficiency and emissions. Alger has been inducted into the Mechanical Engineering Academy of Distinguished Alumni.

Dr William Northrop is an Associate Professor in mechanical engineering and the director of the Thomas E Murphy Engine Research Laboratory at the University of Minnesota. Northrop received a bachelor's degree in mechanical engineering from Carnegie Mellon in 1997 and M.S. and Ph.D. degrees in mechanical engineering from University of Michigan in 2004 and 2009, respectively. After receiving his doctorate, he held the position of senior researcher at General Motors R&D, where he worked in the Propulsion Systems Research Laboratory. Northrop's research interests are in the area of internal combustion engines and energy conversion. His work involves fundamental combustion research, emissions characterization, novel engine cycle development, and alternative fuel use. He is leading projects to characterize and reduce harmful emissions from combustion-powered devices and to reduce fuel consumption from engines used primarily in transportation applications.

Prof Rolf D. Reitz is an emeritus professor at the University of Wisconsin-Madison and currently Senior Partner at Wisconsin Engine Research Consultants. His research interest is in the area of internal combustion engines. His recent work on diesel/gasoline dual-fuel reactivity controlled compression ignition (RCCI) has demonstrated dramatic improvements in fuel economy while meeting stringent emissions mandates, reducing the need for NOx and particulate (soot) after-treatment. His spray research has revealed new understandings about atomization mechanisms. Prof. Reitz has authored and co-authored more than 500 journal publications and he has 5 patents. He has lectured widely and has won major research awards, including the Soichiro Honda medal. He is co-founding editor (Americas) of the International Journal of Engine Research, and serves as an industry consultant. He has served on the executive board of the Institute of Liquid Atomization and Spraying Systems and is director of the UW-Madison Mechanical Engineering Department's Engine Research Center. Before joining the university in 1989, Reitz spent six years at the General Motors Research Laboratories, three years as a research staff member at Princeton University, and two years as a research scientist at the Courant Institute of Mathematical Sciences, New York University. He received the PhD degree from Princeton University in 1978.